CANADIAN THESES

THÈSES CANADIENNES

NOTICE

The quality of this microfiche is heavily dependent upon the quality of the original thesis submitted for microfilming. Every effort has been made to ensure the highest quality of reproduction possible.

If pages are missing, contact the university which granted the degree.

Some pages may have indistinct print especially if the original pages were typed with a poor typewriter ribbon or if the university sent us an inferior photocopy.

Previously copyrighted materials (journal articles, published tests, etc.) are not filmed.

Reproduction in full or in part of this film is governed by the Canadian Copyright Act, R.S.C. 1970, c. C-30.

AVIS

La qualité de cette microfiche dépend grandement de la qualité de la thèse soumise au microfilmage. Nous avons tout fait pour assurer une qualité supérieure de reproduction.

S'il manque des pages, veuillez communiquer avec l'université qui a conféré le grade.

La qualité d'impression de certaines pages peut laisser à désirer, surtout si les pages originales ont été dactylographiées à l'aide d'un ruban usé ou si l'université nous a fait parvenir une photocopie de qualité inférieure.

Les documents qui font déjà l'objet d'un droit d'auteur (articles de revue, examens publiés, etc.) ne sont pas microfilmés.

La reproduction, même partielle, de ce microfilm est soumise à la Loi canadienne sur le droit d'auteur, SRC 1970, c. C-30.

THIS DISSERTATION HAS BEEN MICROFILMED EXACTLY AS RECEIVED

LA THÈSE A ÉTÉ MICROFILMÉE TELLE QUE NOUS L'AVONS REÇUE

THE UNIVERSITY OF ALBERTA

Isotopic and Geochemical Studies of Terrane I, South-Central British Columbia

by

Alan D. Smith

A THESIS

SUBMITTED TO THE FACULTY OF GRADUATE STUDIES AND RESEARCH

IN PARTIAL FULFILMENT OF THE REQUIREMENTS FOR THE DEGREE

OF Doctor of Philosophy

Department of Geology

EDMONTON, ALBERTA

Fall 1986

ISBN 0-315-32528-3

THE UNIVERSITY OF ALBERTA

RELEASE FORM

NAME OF AUTHOR Alan D. Smith

TITLE OF THESIS Isotopic and Geochemical Studies of Terrane I, South-Central British Columbia

DEGREE FOR WHICH THESIS WAS PRESENTED Doctor of Philosophy

YEAR THIS DEGREE GRANTED Fall 1986

Permission is hereby granted to THE UNIVERSITY OF ALBERTA LIBRARY to reproduce single copies of this thesis and to lend or sell such copies for private, scholarly or scientific research purposes only.

The author reserves other publication rights, and neither the thesis nor extensive extracts from it may be printed or otherwise reproduced without the author's written permission.

(SIGNED) Alan D. Smith

PERMANENT ADDRESS:

OAKDENE, 79 HARDHORN Rd

POULTON-LE-FYLDE

LANCASHIRE, ENGLAND

DATED 19 June 1986

THE UNIVERSITY OF ALBERTA

FACULTY OF GRADUATE STUDIES AND RESEARCH

The undersigned certify that they have read, and recommend to the Faculty of Graduate Studies and Research, for acceptance, a thesis entitled Isotopic and Geochemical Studies of Terrane I, South-Central British Columbia submitted by Alan D. Smith in partial fulfilment of the requirements for the degree of Doctor of Philosophy.

R. I. J. Lambert
.....

Supervisor

D. J. Tough
.....

H. Baadsgaard
.....

[illegible]
.....

Donald J. DePaolo
.....

External Examiner

Date 19 June 86

Abstract

Isotopic and geochemical studies of Terrane I, British Columbia have defined the nature of crust added to western North America by accretion tectonics, and of the subadjacent mantle.

Kaersutite-bearing Pennsylvanian to Permian metabasalts of the Slide Mountain terrane have ϵ_{Nd} values of +7.7 to +10.1, Sm/Nd >0.3, Zr/Nb ≃17, Zr/Y 3-3.5, and comprise a back-arc ridge assemblage. Contemporaneous basalts of the Cache Creek terrane have ϵ_{Nd} values of +4.5 to +6, Sm/Nd <0.26, Zr/Nb ≃8, Zr/Y 3-9, and represent an ocean island tholeiitic suite. Late Triassic volcanics of the Nicola Group represent an arc assemblage formed above a westward dipping subduction zone which consumed the Slide Mountain terrane, thus accreting Terrane I to North America.

The Nicola volcanics along with the mid-Cretaceous Spences Bridge Group and Eocene Kamloops Group, define a succession of arcs of increasing continental character within Terrane I. The Nicola volcanics show the greatest tholeiitic affinity and have ϵ_{Nd} values from +5 to +8 and $^{87}Sr/^{86}Sr$ ratios from 0.7031 to 0.7036 . In contrast, the Kamloops volcanics are K- rich and have isotopic compositions approaching the bulk Earth value. The trend toward increased incompatible element content and more enriched isotopic compositions shown by the arcs, cannot result from crustal contamination since the underlying terrane material has a depleted isotopic signature characteristic of its oceanic origin. The trends must, therefore, reflect enrichment of the mantle source region over time by continuing subduction processes.

Plateau basalts of the Chilcotin Group erupted throughout Terrane I in the late Tertiary are divided into three groups: A (alkaline), B

(transitional), C (tholeiitic). Group A basalts have $^{143}Nd/^{144}Nd$ >0.51310, $^{87}Sr/^{86}Sr$ <0.7028 and trace element abundances requiring derivation from oceanic mantle garnet lherzolite. Groups B and C result from contamination of a group A melt with spinel lherzolite such as that tapped in the genesis of the preceding calc-alkaline volcanics.

Spinel lherzolite xenoliths from central British Columbia have $^{143}Nd/^{144}Nd$ ratios from 0.51160 to 0.51275 and $^{87}Sr/^{86}Sr$ ratios from 0.7040 to 0.7102, confirming the existence of isotopically enriched mantle beneath western North America. Sm-Nd model ages of 1.6 to 1.5 and 0.7 to 0.1 Ga for derivation from a MORB reservoir, correspond to periods of tectonic activity along the continental margin. Low Rb/Sr ratios contrast the elevated $^{87}Sr/^{86}Sr$ ratios of the xenoliths and require a multi-stage evolution involving (1) equilibration with a slab/sediment- derived fluid (2) depletion by melt extraction, confirming the mantle processes postulated from the volcanic record.

Crust added to the continents by terrane accretion includes a significant proportion of ocean floor and ocean island material in addition to island arc assemblages. Subduction processes accompanying the terrane accretion produce a heterogenous subcontinental mantle characterised by isotopic and incompatible element enrichment.

Acknowledgements

I wish to thank my supervisor, Dr. Richard Lambert, for guidance, encouragement and financial support throughout the study. Dr. Halfdan Baadsgaard gave invaluable advice on the chemical procedures and kindly allowed the use of his laboratory facilities during the first two years of the study. Mass spectrometry facilities were ably cared for by Hugh McCulloch, Dragan Krstic and Paul Wagner. The Rare earth element analyses could not have been performed without the assistance of John Duke, whose interest and efforts in the project were largely responsible for the development of the combined neutron activation-mass spectrometry technique. Dr. L. G. Stephens-Newsham allowed me to use the University of Alberta SLOWPOKE Facility, and the assistance of the staff there, Pete Ford and Dennis Ng, is gratefully acknowledged. Dr Grenville Holland is thanked for XRF analyses, and Mark Brearley for donating the spinel lherzolite samples.

Several of the ideas presented here have evolved from discussions with friends and colleagues, notably Cathy Hickson, Paul Metcalfe and Dr. Takeru Yanagi. Derek Thorkelson is thanked for providing copies of his work on the Spences Bridge Group, and for a review of Chapter 5. An earlier version of the manuscript was considerably improved by the comments of Paul Metcalfe. Financial support during the study was provided by Department of Geology teaching and research assistantships, and by University of Alberta bursaries.

Table of Contents

List of Tables

List of Figures

Constants

Nd isotopic ratios are reported normalised to $^{146}Nd/^{144}Nd = 0.7219$,

Sr isotopic ratios to $^{86}Sr/^{88}Sr = 0.1194$.

Bulk Earth constants:

$^{143}Nd/^{144}Nd = 0.512636$, $^{147}Sm/^{144}Nd = 0.1967$ (Jacobsen and Wasserburg 1984).

$^{87}Sr/^{86}Sr = 0.70478$, Rb/Sr = 0.031 (Allegre et al. 1979).

Abbreviations

BV	Bakerville terrane
CC	Cache Creek terrane
CCB	Bonaparte subterrane of the Cache Creek terrane
CCM	Marble Range subterrane of the Cache Creek terrane
CCP	Pavillion subterrane of the Cache Creek terrane
CCR	Canadian Cordilleran regional conductor
DM	depleted mantle
DMS	Depleted Mantle Schematic: growth curve for the evolution of a mantle reservoir with present day ϵNd of +12
EM	enriched mantle
Eu/Eu*	ratio of measured Eu to theoretical Eu
KO	Kootenay terrane
(La/Yb)n	ratio of chondrite normalised La and Yb values
LDMS	Lower Depleted Mantle Schematic: growth curve for the evolution of a mantle reservoir with present day ϵNd of +8
LIL	large ion lithophile
MO	Monashee terrane

QN	Quesnel terrane
QH	Harper Ranch subterrane of the Quesnel terrane
SM	Slide Mountain terrane
ST	Stikine terrane

I. Introduction

Isotopic studies have shown that the continental crust has grown in a quasi-continuous manner since approximately 3.8 Ga (DePaolo and Wasserburg 1976, McCulloch and Wasserburg 1978, Patchett et al. 1981). This growth is assumed to take place by addition of igneous material above subduction zones at the continental margins (Moorbath 1978) or at island arcs (McCulloch and Wasserburg 1978). Other forms of continental igneous activity such as flood basalt volcanism, may also contribute to the process. The recognition that much of the continental margins comprise prefabricated blocks of material or 'terranes' that were formed separately from the continents, has shifted the focus of attention in studies of crustal evolution from the continents to the ocean basins. The western margin of North America from Baja California to the tip of Alaska, extending an average of 500 km inland (Jones et al. 1982), is composed of a series of terranes which were accreted to the continent since the mid-Mesozoic. This material is at least 30 km thick; therefore, the amount of crust added over the period of accretion (approximately 200 Ma), by volcanic arcs built on the continent or by other types of interior volcanism, is small compared to that added by terrane accretion. The terrane material need not necessarily be of arc origin; ridges, seamounts, and oceanic plateaux, with associated sediments comprise approximately 10% of the ocean floor and are all potential candidates for accretion (Avraham and Nur 1983).

The characterisation of the terrane material is necessary for an understanding of the composition and evolution of the continental crust. However, the original features of this material are invariably obscured by metamorphic events accompanying the accretion of the terrane to the

continent. The first part of this study demonstrates the combined use of the Sm-Nd and Rb-Sr isotopic systems in the characterisation of such terrane material. The Rb-Sr system is sensitive to low grade metamorphism whilst the Sm-Nd system is far less affected. When combined, the two systems provide a means for the characterisation of the original terrane material and of the alteration processes.

The growth of the continents by accretion tectonics also has important implications for mantle evolution. Whilst voluminous basalts produced at ocean ridges, namely MORB, have isotopic signatures indicating derivation from depleted mantle (O'Nions et al. 1977, White and Hofmann 1982), their continental counterparts, flood basalts, are generally more iron-rich and have isotopic compositions close to that of the bulk Earth (DePaolo 1981, 1983). For several of the continental basalt provinces these features may be caused by large amounts of crystal fractionation combined with contamination by continental crust (Carlson 1984, Menzies et al. 1984). For basalts erupted through young terrane material, the chemical and isotopic variations are not explained by crustal contamination because terrane material of oceanic origin would normally have depleted isotopic signatures. Accretion of the terranes to the continents takes place by the removal of the intervening oceanic crust by subduction. Production of enriched mantle by subduction processes is suggested by the moderately depleted to enriched isotopic compositions of arc volcanics (Hawkesworth et al. 1982). The comparatively enriched isotopic signatures of the continental basalts suggest that the process of terrane accretion serves to produce a fertile and isotopically enriched young subcontinental mantle.

The amount of mantle root adhering to the terranes on accretion is unknown. A probable zone of decoupling of the terranes and the upper mantle would be the asthenosphere. The overlying mantle would be of cumulate origin, and be relatively iron-rich compared to the parent lherzolite. In an oceanic environment such lithosphere would play no further part in magma genesis. However, after accretion of the terrane, this material in a subcontinental environment could be rendered fertile, hence accounting for the iron-rich nature of many continental volcanics. The second part of this study concentrates on the post-accretional volcanic history of the terrane material as a means of studying the evolution of the young subcontinental mantle.

Regional Characteristics of the Canadian Cordillera

Over 50 terranes have been recognised in western North America. The Canadian Cordillera, however, is comprised mainly of two superterranes, or microcontinents, Terrane I and Terrane II, that were accreted to the continental margin in the mid- to late Mesozoic.

Terrane I comprises the Slide Mountain, Quesnel, Cache Creek and Stikine terranes (Fig. 1). These terranes were amalgamated during the late Triassic prior to accretion to the continent in the mid-Jurassic (Monger et al. 1982). Terrane II comprises the Alexander and Wrangell terranes, which are both of arc origin. These were amalgamated in the early Cretaceous prior to accretion to the western margin of Terrane I in the late Cretaceous. Palaeomagnetic and faunal evidence suggest that both Terranes I and II originated and were accreted at latitudes close to the equator, and have reached their present position by right-lateral strike-slip movement (Coney et al. 1980), or by oblique subduction

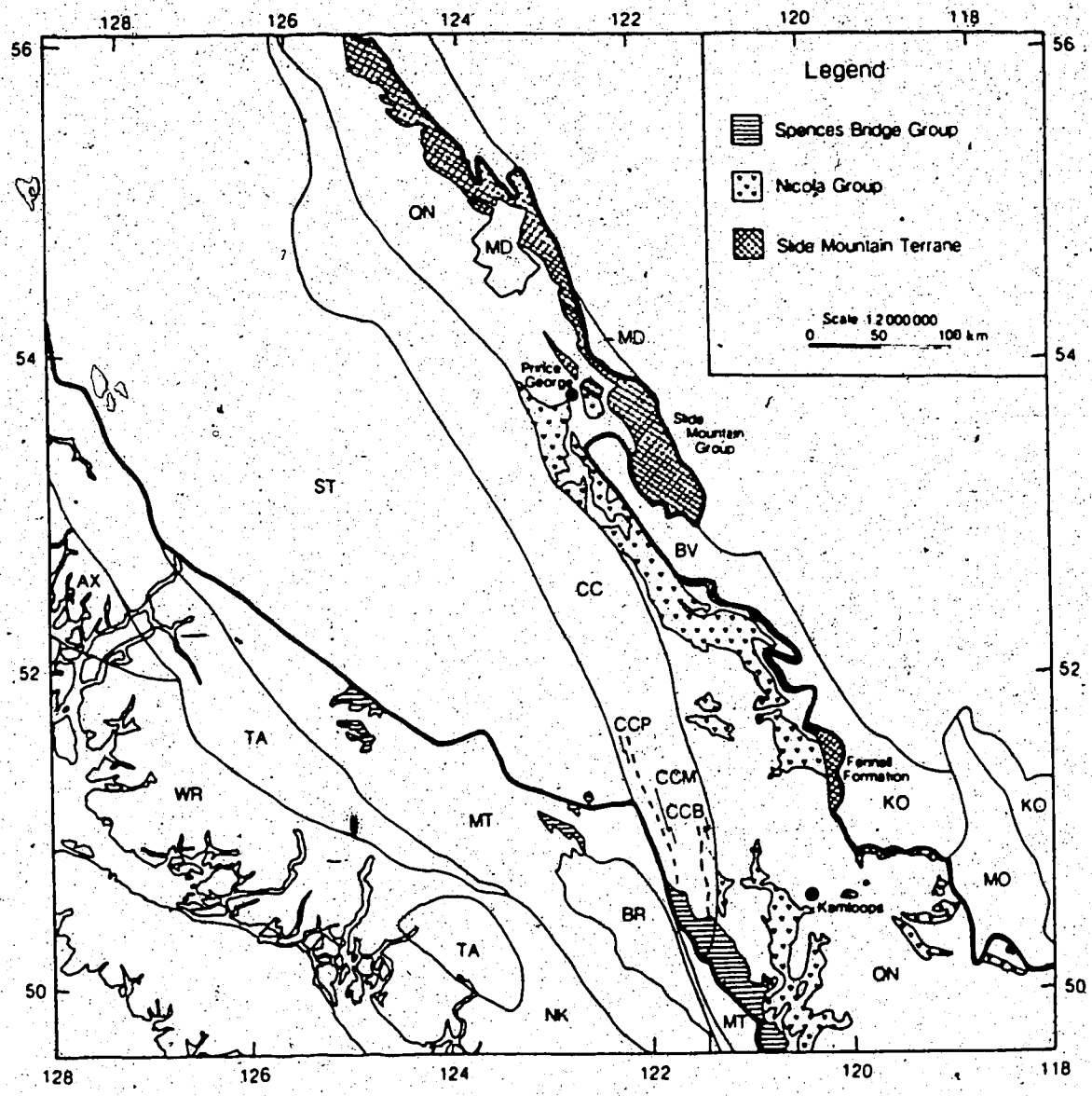

Fig. 1. Terrane map showing the distribution of Nicola and Spences Bridge Group rocks in southern British Columbia (after Tipper et al. 1981, Monger and Berg 1984). Terrane I (shown in bold outline) comprises the Slide Mountain (SM), Quesnel (QN), Cache Creek (CC) and Stikine (ST) terranes. The Cache Creek terrane is further divided into the Bonaparte (CCB), Marble Range (CCM) and Pavillion (CCP) subterranes. To the east of Terrane I lies the McLeod (MD), Bakerville (BV), Kootenay (KO) and Monashee (MO) terranes which consist predominantly of metamorphosed Upper Proterozoic to Lower Palaeozoic strata to which Terrane I was accreted during the mid-Jurassic. To the west of Terrane I, the Methow-Tyaughton (MT) terrane includes strata derived in part from Terrane I during the early Cretaceous. The Wrangell (WR) and Alexander (AX) terranes comprising superterrane, Terrane II, along with the Bridge River (BR), Nootsack (NK) and Tracy Arm (TA) terranes , formed removed from North America and were accreted to Terrane I during the late Cretaceous.

(Chamberlain and Lambert 1985).

Terrane I has been chosen as the focus of this study because of the variation and enigmatic origin of its components: the Cache Creek and Slide Mountain terranes are considered to represent ocean floor assemblages of ridge or seamount affinity, whilst the Quesnel and Stikine terranes are of arc origin. In addition, the earlier accretion of Terrane I to the continental margin allows a more complete study of the evolution of the subcontinental mantle.

The part of Terrane I chosen for study is the area around Kamloops between 120°W 50°N, 120°W 52°N, 122°W 50°N and 122°W 52°N. The region has been mapped at the 1:250 000 (Cockfield 1947, Campbell and Tipper 1971) and 1:125 000 (Monger and McMillan 1984) scales. Geological maps and sample locations are presented in Appendix 1.

II. Slide Mountain and Cache Creek Terranes

Introduction

The Slide Mountain terrane (essentially equivalent to the Eastern terrane of Monger 1977) consists of the Anvil, Sylvester, Nina Creek, Slide Mountain, Fennell, and Milford-Kaslo subterranes at the eastern edge of Terrane I (Fig. 1). The subterranes range in age from late Pennsylvanian to late Permian (Monger 1977) and have been subjected to lower greenschist facies metamorphism. Although the subterranes are isolated from one another they display a similar stratigraphy comprising a mainly sedimentary lower sequence and a mainly volcanic upper sequence. The lower sequence which comprises chert, argillite, sandstone, conglomerate, minor carbonates, and local mafic flows, has been interpreted as forming in a basin environment (Monger and Price 1979). The relationship of this sequence to the overlying volcanics, which include basalt, gabbro, alpine ultramafics and chert, is variable throughout the subterranes. An overthrust relationship was demonstrated in the Anvil subterrane (Tempelman-Kluit et al. 1976) indicating that the volcanic sequence represents obducted oceanic crust (Monger et al. 1972, Hall-Beyer 1976). However, in the Nina Creek subterrane, the sequences are in stratigraphic continuity, suggesting a seamount origin (Monger 1977). The presence of kaersutite in basalts from the Fennell subterrane (Aggarwal et al. 1984), and high K_2O contents (as much as 0.7%) in the Sylvester subterrane (Monger 1977) have been cited in support of an ocean island origin. Alternatively, Monger and Price (1979) suggest the volcanics represent a ridge that developed in a back-arc or marginal basin.

The Cache Creek terrane has been divided into western, central, and eastern belts (Fig. 1). Each belt contains a slightly different lithology, although all belong to an oceanic environment (Monger 1981, Shannon 1981, Monger and Berg 1984), and like the Slide Mountain terrane have been subjected to lower greenschist facies metamorphism. In the study area, the eastern belt or Bonaparte subterrane contains basalt, volcaniclastics, gabbro and serpentinite (Grette 1979, Shannon 1981). Palaeolontological evidence indicates an age range from late Pennsylvanian to late Triassic for the strata. The central belt, the Marble Range subterrane, contains mostly mid- to late Permian carbonates with minor chert, argillite, tuff and basalt. The western belt, the Pavillion subterrane, contains mainly silicified argillite, siltstone, chert and minor limestones. The strata are of Triassic age and rest with a thrust contact on the Marble Range subterrane (Monger 1981). Deformation is most intense in the Bonaparte subterrane, which may represent a subduction complex related to the late Triassic Nicola arc on the Quesnel terrane to the east (Travers 1978).

Sampling

The Fennell subterrane (Fig. 1) was chosen to represent the Slide Mountain terrane in this study because of the conflicting views that the subterrane represents ocean island (Aggarwal et al. 1984) or ocean ridge material (Hall-Beyer 1976). Samples were collected from two localities, one in the north of the subterrane (samples 2-2 to 2-5), the other in the south (samples 1-7A to 1-8). Eight samples studied by Aggarwal et al. (1984) from the vicinity of the Chu-Chua massive sulphide deposit, were also analysed. The Cache Creek samples are entirely from the

Bonaparte subterrane

Mineralogy

Typical mineralogy of the Fennell Formation consists of relict microphenocrysts of augite and plagioclase comprising 25 to 40% of the rock, in a groundmass of similar composition, although this is commonly altered to actinolite, chlorite and epidote. Olivine is rare or absent. Plagioclase compositions are often close to albite and indicate that the basalts have undergone considerable spilitisation. Primary amphibole, originally described as hornblende (Campbell and Tipper 1971, Hall-Beyer 1976) but later identified as kaersutite (Aggarwal et al. 1984), is present in 20% of the samples. This mineral may constitute as much as 50% of the microphenocryst assemblage. The basalts thus differ considerably from modern MORB, where olivine is common and augite is rare. Most of the Cache Creek basalts exhibit a comparable mineralogy of augite and sodic feldspar microphenocrysts within a groundmass which has largely been altered to actinolite, chlorite and epidote. Several of the samples lack a phenocryst assemblage and consist of fine grained chlorite, plagioclase and actinolite, often with a distinct schistose fabric.

Major Element Chemistry

Silica ranges from 47 to 53% in the Fennell Formation (Table 1), compared to the uniformly low contents of 44.5 to 47.5% in the Cache Creek samples (Table 2). Fennell Formation samples with as little as 38% silica were classified as komatiites by Hall-Beyer (1976); however, from their mineralogy and chemical composition these are undoubtedly

Table 1.

Major and trace element compositions of Fennell Formation basalts.

	2715	110	36194	1596	1893	17100	3893	2551
SiO_2	50.47	49.45	50.92	50.82	51.10	51.83	49.90	47.87
Al_2O_3	13.78	13.56	13.97	14.78	13.05	13.56	12.23	13.33
Fe_2O_3	12.93	12.99	12.07	11.40	12.57	12.51	13.82	14.30
MgO	7.78	6.86	7.53	7.40	7.17	7.24	7.80	7.18
CaO	9.81	9.88	9.61	10.25	9.24	9.33	10.57	11.47
Na_2O	2.80	4.79	3.43	3.23	4.22	3.52	3.38	3.13
K_2O	0.17	0.00	0.34	0.17	0.00	0.00	0.00	0.24
TiO_2	1.86	1.62	1.70	1.50	1.93	1.60	1.85	1.94
P_2O_5	0.16	0.19	0.16	0.18	0.20	0.14	0.16	0.16
S	0.02	0.27	0.06	0.07	0.29	0.07	0.05	0.05
MnO	0.20	0.19	0.19	0.18	0.19	0.19	0.22	0.22
Ba	45	211	3603	2587	184	239	53	1259
Nb	7	7	6	7	7	8	8	7
Zr	153	142	141	129	146	139	152	140
Y	46	42	42	37	45	40	44	40
Rb	4.15	0.50	10.1	4.34	0.29	2.06	7.15	2.00
Sr	136	175	258	239	125	135	287	158
Zn	91	75	77	67	120	81	76	99
Cu	47	53	56	48	39	61	77	78
Ni	86	46	84	66	46	52	90	66

	1-7A	1-8	2-2	2-6	2-4	2-5
SiO_2	50.66	49.05	52.05	52.92	51.14	50.86
Al_2O_3	12.27	13.25	13.07	13.77	13.56	13.35
Fe_2O_3	12.18	12.90	12.82	12.32	12.01	10.69
MgO	8.61	8.46	7.72	8.36	7.79	10.05
CaO	10.34	9.46	8.68	6.84	8.67	9.86
Na_2O	3.42	4.27	3.51	3.19	4.21	3.58
K_2O	0.09	0.01	0.36	0.88	0.50	0.00
TiO_2	1.82	1.95	1.39	1.38	1.74	1.34
P_2O_5	0.17	0.21	0.17	0.12	0.14	0.09
S	0.21	0.21	0.03	0.02	0.03	0.04
MnO	0.24	0.23	0.20	0.19	0.20	0.16
Ba	50	32	163	641	121	22
Nb	6	5	6	6	8	6
Zr	130	138	106	113	147	102
Y	50	51	36	37	44	30
Rb	4.80	2.15	10	19	10	1
Sr	176	282	131	116	117	115
Zn	78	89	66	90	87	69
Cu	44	59	72	57	58	71
Ni	108	111	34	27	72	97

Major elements recalculated to 100% on a volatile-free basis.
Trace elements in ppm.

Table 2.

Major and trace element compositions of the Cache Creek basalts.

	2-39A	2-39B	2-46	2-58	2-59	2-68A	2-68B
SiO_2	48.53	47.62	44.57	57.15	45.84	46.46	45.16
Al_2O_3	9.43	13.44	15.21	17.09	11.88	11.87	13.02
Fe_2O_3	12.38	13.57	15.70	5.26	14.17	13.11	13.67
MgO	19.55	7.41	8.01	5.78	16.11	11.41	9.20
CaO	8.18	10.71	9.69	8.09	6.34	12.37	12.82
Na_2O	0.33	3.55	2.42	5.62	1.42	2.20	2.56
K_2O	0.00	0.60	0.53	0.00	0.98	0.45	0.00
TiO_2	1.29	2.61	3.28	0.36	2.79	1.81	1.97
P_2O_5	0.12	0.26	0.32	0.08	0.22	0.15	0.17
S	0.04	0.04	0.06	0.49	0.07	0.01	0.02
MnO	0.17	0.18	0.21	0.07	0.18	0.16	0.17
Ba	39	235	174	38	508	103	38
Nb	16	26	32	4	29	16	15
Zr	114	198	246	69	226	133	143
Y	16	28	36	8	27	23	26
Sr	169	286	176	109	106	321	187
Rb	2	8	7.68	1	25.9	8	1
Zn	84	85	104	16	97	79	90
Cu	63	102	97	27	93	43	100
Ni	589	70	81	27	309	299	155

Major element abundances recalculated to 100% on a volatile-free basis
Trace element abundances in ppm.

spilitised equivalents of the basalts in Table 1.

Moderate to high Na_2O concentrations (as much as 4.3%) combined with low (0 to 0.35%) K_2O contents suggest that this process has affected the whole of the Fennell Formation. The Cache Creek samples have lower Na_2O concentrations (1.4 to 3.5%) but higher K_2O (0.45 to 1.0%). The Fennell Formation thus have Na_2O/K_2O ratios greater than 10 , similar to normal MORB, whilst the Cache Creek samples have Na_2O/K_2O ratios from 1.5 to 6.0 , more akin to ocean island basalts. On a silica versus alkalis diagram (Fig. 2) the Fennell Formation lie mostly in the tholeiitic field, although those with low silica contents lie in the alkaline field as a result of more extensive alteration. In contrast, the Cache Creek basalts lie mostly within the alkaline field. A similar grouping is noted on an AFM plot (Fig. 3).

The average MgO in both groups is 8%, although a greater range (7.4 to 16%) is shown by the Cache Creek samples. Moderate CaO contents (6 to 12%) in both groups suggests that the samples have not been severely affected by calcitisation. TiO_2 and P_2O_5 contents (1.8% and 0.22% respectively) are low in the Fennell Formation. TiO_2/P_2O_5 ratios are close to 8 in both the Fennell Formation and Cache Creek basalts. No major element differences between the kaersutite and non-kaersutite bearing basalts of the Fennell Formation are noted.

Nd-Sr Isotopic Composition

Nd and Sr isotopic data for Fennell Formation and Cache Creek basalts are presented in Table 3. The $^{87}Sr/^{86}Sr$ data for the Fennell Formation show a broad negative correlation with Rb/Sr. Samples with high $^{87}Sr/^{86}Sr$ have very low Rb/Sr ratios of 0.002 to 0.015, indicative

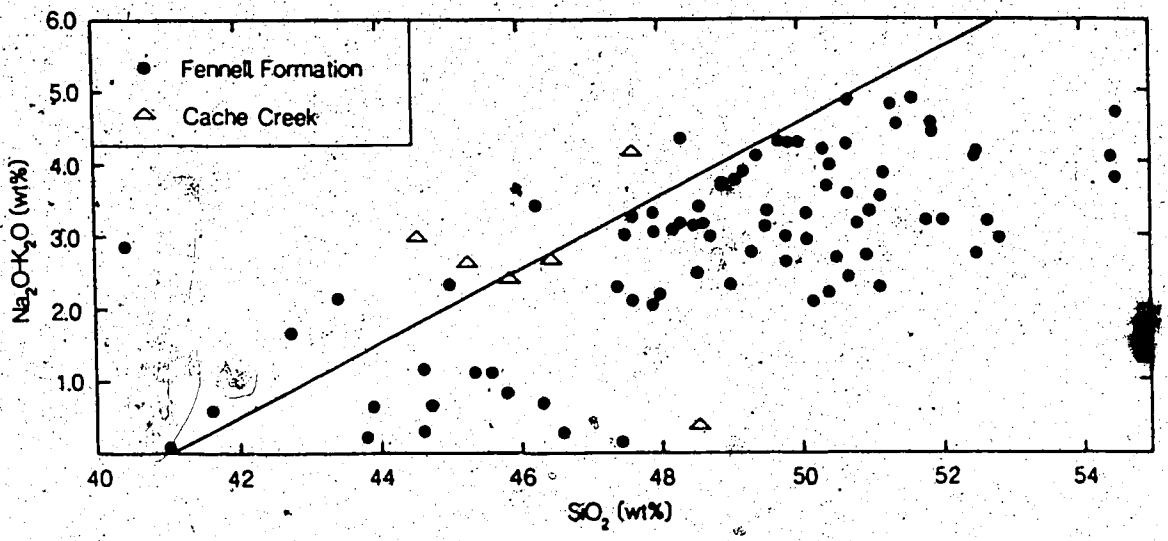

Fig. 2. Alkalis versus silica diagram for the Fennell Formation and Cache Creek basalts. Fennell Formation data includes the undivided analyses of Hall-Beyer (1976). Alkaline-subalkaline field dividing line is from Irvine and Barager (1971).

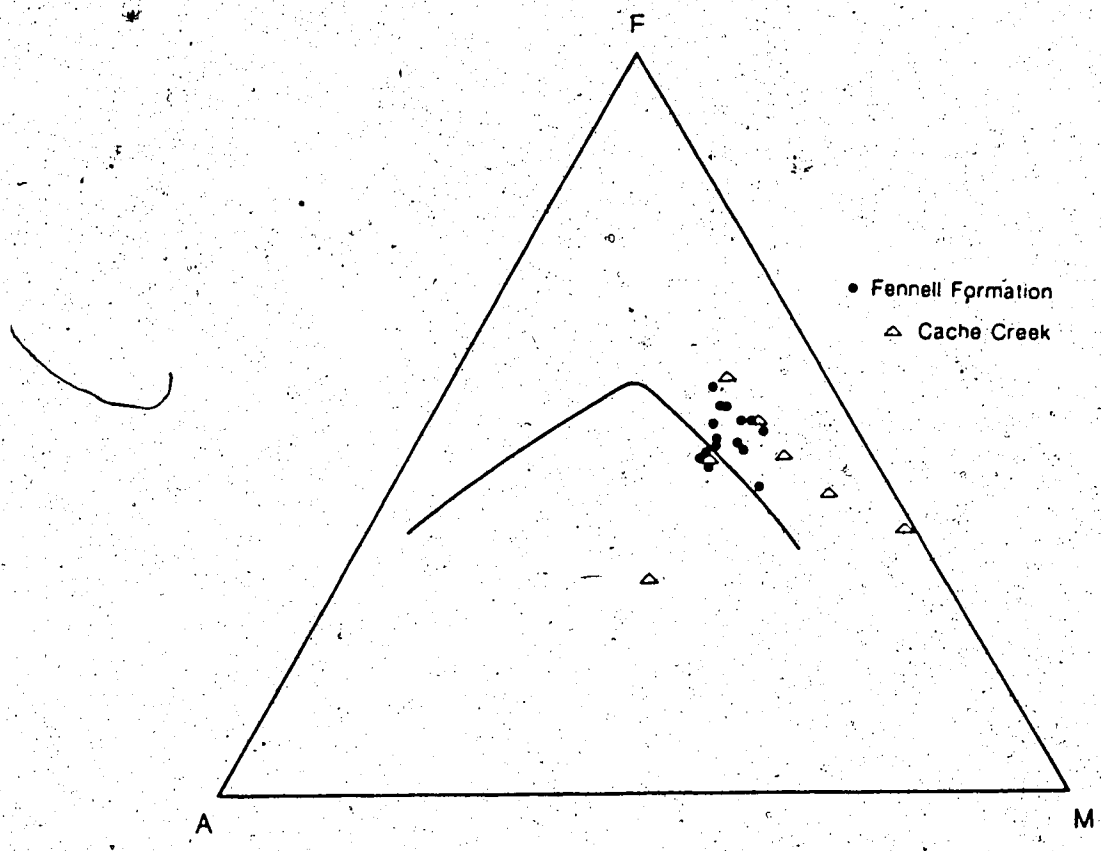

Fig. 3. AFM diagram for Fennell Formation and Cache Creek basalts. $A=Na_2O+K_2O$, $F=FeO+0.8998Fe_2O_3$, $M=MgO$. Symbols as for Fig. 2.

Table 3.

Nd and Sr isotopic compositions of Fennell Formation and Cache Creek basalts.

	Rb/Sr	$^{87}Sr/^{86}Sr$ m	$^{87}Sr/^{86}Sr$ c	Sm (ppm)	Nd (ppm)	Sm/Nd	$^{143}Nd/^{144}Nd$ m	$^{143}Nd/^{144}Nd$ c	ϵNd
Fennell Formation									
2715	0.030	0.70292±3	0.70255	5.38	16.0	0.336	0.513118±22	0.512726	+9.3
110	0.003	0.70425±3	0.70421	4.44	14.3	0.311	0.513089±13	0.512726	+9.3
36194	0.004	0.70370±4	0.70322	4.34	13.3	0.327	0.513138±17	0.512757	+9.9
1596	0.018	0.70394±3	0.70371	3.86	11.8	0.328	0.513120±13	0.512738	+9.5
1893	0.002	0.70388±4	0.70385	4.46	13.1	0.339	0.513129±28	0.512734	+9.5
17100	0.015	0.70350±3	0.70331	3.99	12.4	0.321	0.513141±18	0.512767	+10.1
3893	0.025	0.70310±3	0.70280	4.66	13.8	0.337	0.513043±18	0.512650	+7.8
2551	0.013	0.70397±3	0.70382	4.31	13.0	0.330	0.513025±11	0.512638	+7.6
1-7A	0.027	0.70329±3	0.70295	4.66	14.1	0.331	0.513064±21	0.512679	+8.4
1-8	0.008	0.70345±3	0.70336	4.90	15.0	0.326	0.513037±24	0.512657	+7.9
Cache Creek									
2-46	0.044	0.70450±4	0.70405			0.215	0.512733±28	0.512482	+4.5
2-59	0.244	0.70780±4	0.70529	6.48	24.7	0.262	0.512861±20	0.512556	+6.0

( )m measured isotopic ratio.

( )c isotopic ratio corrected to an age of 300 Ma.

of Rb loss or Sr gain, as could be produced by seawater alteration. Clearly no age can be interpreted from this data; a similar conclusion being reached from the Sm-Nd data on account of the small variation in Sm/Nd (0.31 to 0.34). The measured $^{143}Nd/^{144}Nd$ and $^{87}Sr/^{86}Sr$ ratios have, therefore, been corrected to an age of 300 Ma, this being the average of estimates from palaeolontological evidence. On a Nd-Sr isotopic diagram (Fig. 4) the data show a trend toward high $^{87}Sr/^{86}Sr$ away from the mantle array, consistent with the interpretation of seawater alteration. $^{87}Sr/^{86}Sr$ ratios of 0.7025 to 0.7030 shown by samples 2715, 1-7A and 3893, appear closest to the original values. ϵNd ranges from +7.6 to +10.1 , overlapping the values for MORB from the Mid-Atlantic Ridge and East Pacific Rise (Cohen and O'Nions 1982, White and Hofmann 1982) whilst the lower values lie within the range (ϵNd 7.9 to 8.3) for the Scotia sea back-arc ridge basalts (Hawkesworth et al. 1977).

The Cache Creek data have also been corrected for an age of 300 Ma. The basalts have ϵNd values from +4.5 to +6.0 and $^{87}Sr/^{86}Sr$ ratios from 0.7039 to 0.7048 . Sm/Nd ratios (0.21 to 0.26) are significantly lower than in the Fennell Formation, and suggest that the basalts are LREE enriched. The mobility of the LREE during prehnite-pumpellyite to greenschist facies metamorphism in the oceanic environment has been a topic of considerable debate: Hellman and Henderson (1977) have shown that the LREE content is increased during such alteration, whilst Ludden et al. (1979) have shown that such effects are not ubiquitous. Equilibration with seawater Nd, which has moderately negative ϵNd (present day seawater has ϵNd from -3 to -12 depending on the ocean in question (Piepgras et al. 1979)) could have lowered the $^{143}Nd/^{144}Nd$ and

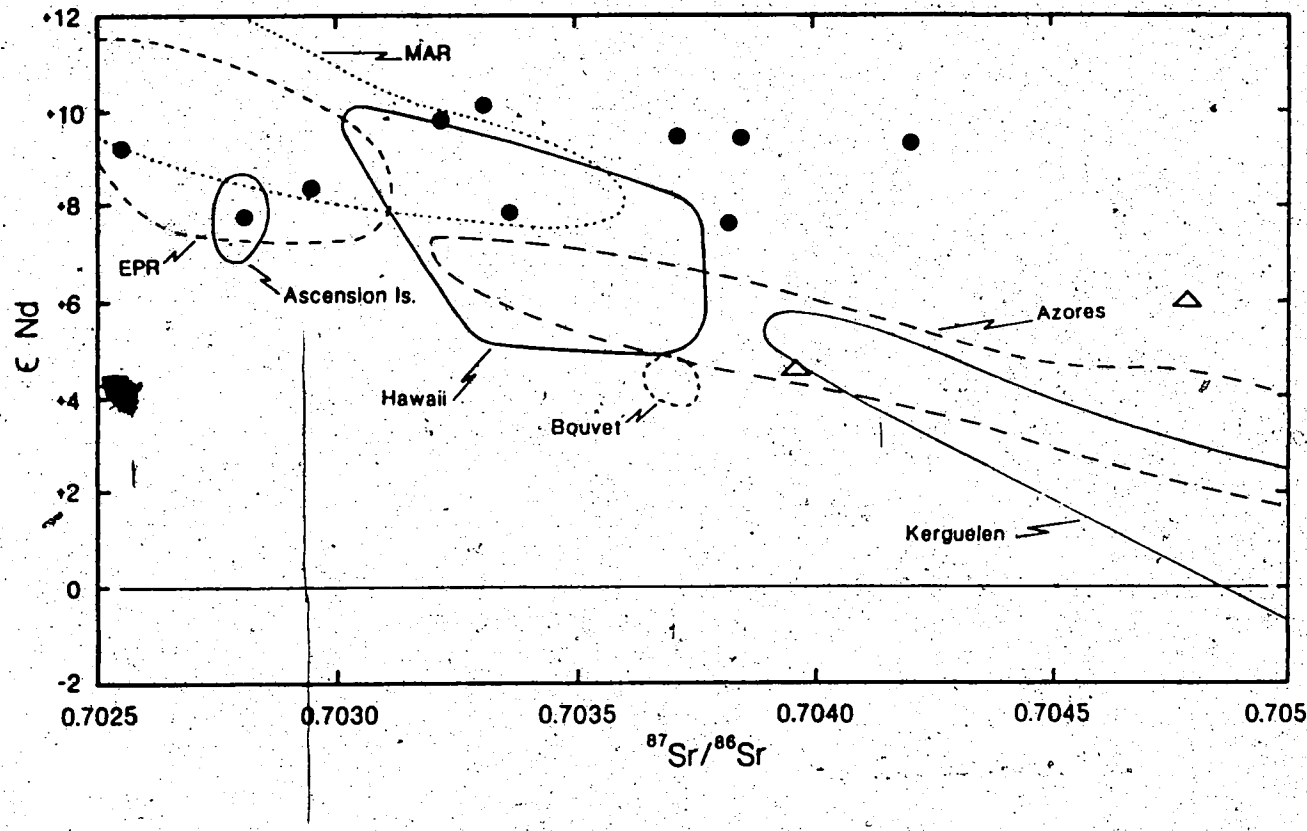

Fig. 4. Nd-Sr isotopic diagram for the Fennell Formation and Cache Creek basalts. Also shown are the fields for the Mid-Atlantic Ridge (MAR) (O'Nions et al. 1977, White and Hofmann 1982), East Pacific Rise (EPR) (Zindler et al. 1984), Hawaii (O'Nions et al. 1977, Chen and Frey 1983, Stille et al. 1983), Ascension Island, Bouvet, Kerguelen and the Azores (O'Nions et al. 1977).

Sm/Nd ratios of the Cache Creek basalts. Such a possibility is considered unlikely because sample 2-46 which has the lowest $^{143}Nd/^{144}Nd$ and Sm/Nd ratios, shows little deviation from the mantle array. Furthermore, the Rb-Sr system shows the Cache Creek basalts to have suffered no more alteration than the Fennell Formation which have consistently high $^{143}Nd/^{144}Nd$ and Sm/Nd ratios.

The ϵNd of the Cache Creek samples is similar to that of ocean island basalts from Hawaii (Stille et al. 1983) and Bouvet Island (O'Nions et al. 1977) (Fig. 4). It is stressed that the difference in ϵNd between the Fennell Formation and Cache Creek basalts is significant no matter what age within the range of the palaeolontological evidence is chosen for the two terranes. The Fennell Formation have Sm/Nd sufficiently close to the bulk Earth value such that their ϵNd does not change significantly over this time interval. In contrast, the low Sm/Nd ratios of the Cache Creek basalts results in their ϵNd decreasing toward the present. The assumed age for these samples is close to the oldest estimates from the palaeolontological evidence and thus the ϵNd values in Table 3 can be considered a maximum for these rocks.

Trace Element Chemistry and Discussion

Because of their immobility, the elements Ti, Nb, Zr, Y and P, have been used in several classification schemes for altered or metamorphosed igneous rocks (Pearce and Cann 1973, Floyd and Winchester 1975, Winchester and Floyd 1976, Pearce and Cann 1979). The use of these elements as absolute discriminants has met only with limited success, partially because of interlaboratory bias in their measurement at low concentrations. The trace element abundances reported here are directly

comparable to the results of Hall-Beyer (1976) having been analysed by the same laboratory. However, the Y concentrations reported here are some 30 to 40% higher, the Zr concentrations 10% higher, and the Nb concentrations some 20% lower than the results of Aggarwal et al. (1984) for the same samples. The consistency of the trace element analyses were determined by reference to an internal standard analysed by four other laboratories. The Y values reported here fall within 4% of the mean of the four other laboratories. The Nb concentrations are 7% higher than the mean which suggests that the results of Aggarwal et al. (1984) are further in error. Zr was found to be 10% high and it is conceded that for this element the results of Aggarwal et al. (1984) may be more accurate. Where this discrepancy results in ambiguity in the data interpretation both sets of Zr results have been considered.

The classification of oceanic basalts is complicated by the existence of a compositional and isotopic range from normal, or N-type MORB, to ocean island tholeiites which may result where a ridge lies in close proximity to an ocean island fed by a mantle plume (LeRoex et al. 1983, Humphries et al. 1985). In such an environment, the ridge basalts may have major element compositions comparable to N-type MORB, but incorporation of the ocean island basalt source material into the MORB source leads to more enriched isotopic ratios and higher incompatible element abundances. LeRoex et al. (1983) recognised three types of oceanic tholeiite, normal (N-type), transitional (T-type) and plume (P-type), reflecting increased contribution from an enriched mantle component:

(1) N-type MORB-derived from normal 'depleted' oceanic mantle, and characterised by Zr/Nb >17 , Y/Nb >8 , $^{143}Nd/^{144}Nd$ ratios from 0.51312

to 0.51302 and $^{87}Sr/^{86}Sr$ ratios from 0.7027 to 0.7030 .

(2) P-type MORB-derived from an enriched source, possibly related to an upwelling mantle plume, and characterised by Zr/Nb 5.6 to 6.8 , Y/Nb 0.9 to 0.12 , $^{143}Nd/^{144}Nd$ ratios from 0.51295 to 0.51286 and $^{87}Sr/^{86}Sr$ ratios from 0.7035 to 0.7037 .

(3) T-type MORB-transitional between N-, and P-types, and characterised by Zr/Nb 7.7 to 11.8 , Y/Nb 1.3 to 3.0 , $^{143}Nd/^{144}Nd$ ratios from 0.51301 to 0.51284 and $^{87}Sr/^{86}Sr$ ratios from 0.7029 to 0.7037 .

A plot of TiO_2 versus Zr (Fig. 5a) shows that both the Fennell Formation and Cache Creek basalts lie on a line of Ti/Zr =80 . Using the Zr values of Aggarwal et al. (1984) this ratio is elevated to 100 , closer to the average for ocean ridge basalts (Basaltic Volcanism Study Project 1981). No matter which Zr values are used, the Fennell Formation lie within the field for ocean floor basalts on this diagram. The Cache Creek basalts overlap this field, but have higher Ti and Zr contents which result in their lying predominantly within the ocean island tholeiite intrusion into the oceanic island alkali basalt field (as defined by Floyd and Winchester (1975)). The plot of Nb against Zr (Fig. 5b) has been widely used to distinguish ocean ridge and island basalts (Basaltic Volcanism Study Project 1981). The data presented here and that of Hall-Beyer (1976) indicate a Zr/Nb ratio of 30 for the Fennell Formation, similar to N-type MORB. The large degree of scatter in Fig. 5b arises mainly from variation in the Zr content, and indicates source region heterogeneity. Using the data of Aggarwal et al. (1984) the Zr/Nb ratio is lowered to 17 , which is still characteristic of N-type MORB. Particularly significant is the separation of the Fennell Formation and Cache Creek basalts on this plot. Although two Cache Creek samples have

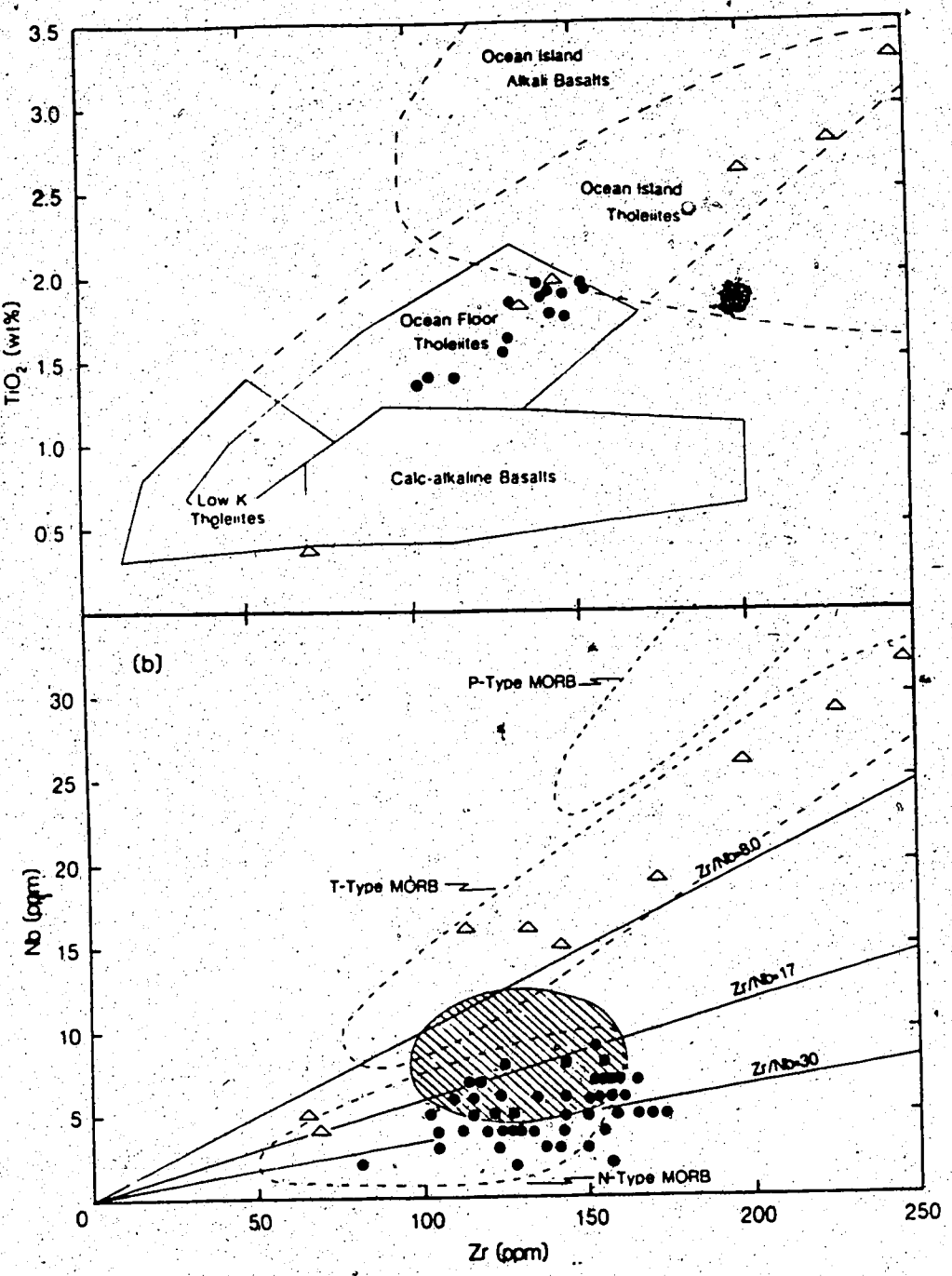

Fig. 5. Fennell Formation and Cache Creek basalts plotted on (a) Ti-Zr discrimination diagram of Pearce and Cann (1973). Fields for ocean island alkali basalts and ocean island tholeiites from Floyd and Winchester (1975). (b) Nb versus Zr diagram. Symbols as for Fig 2. Additional data for the Fennell Formation from Hall-Beyer (1976). Hatched area shows field of Fennell Formation basalts using the data of Aggarwal et al. (1984). Basalts from ridges have Zr/Nb ≃30, whilst those erupted along topographic highs adjacent to ocean islands or platforms, have Zr/Nb ≃10 . Fields for N-, T-, P- type MORB are from LeRoex et al. (1983). The Fennell Formation resemble N-type MORB whichever data set is used.

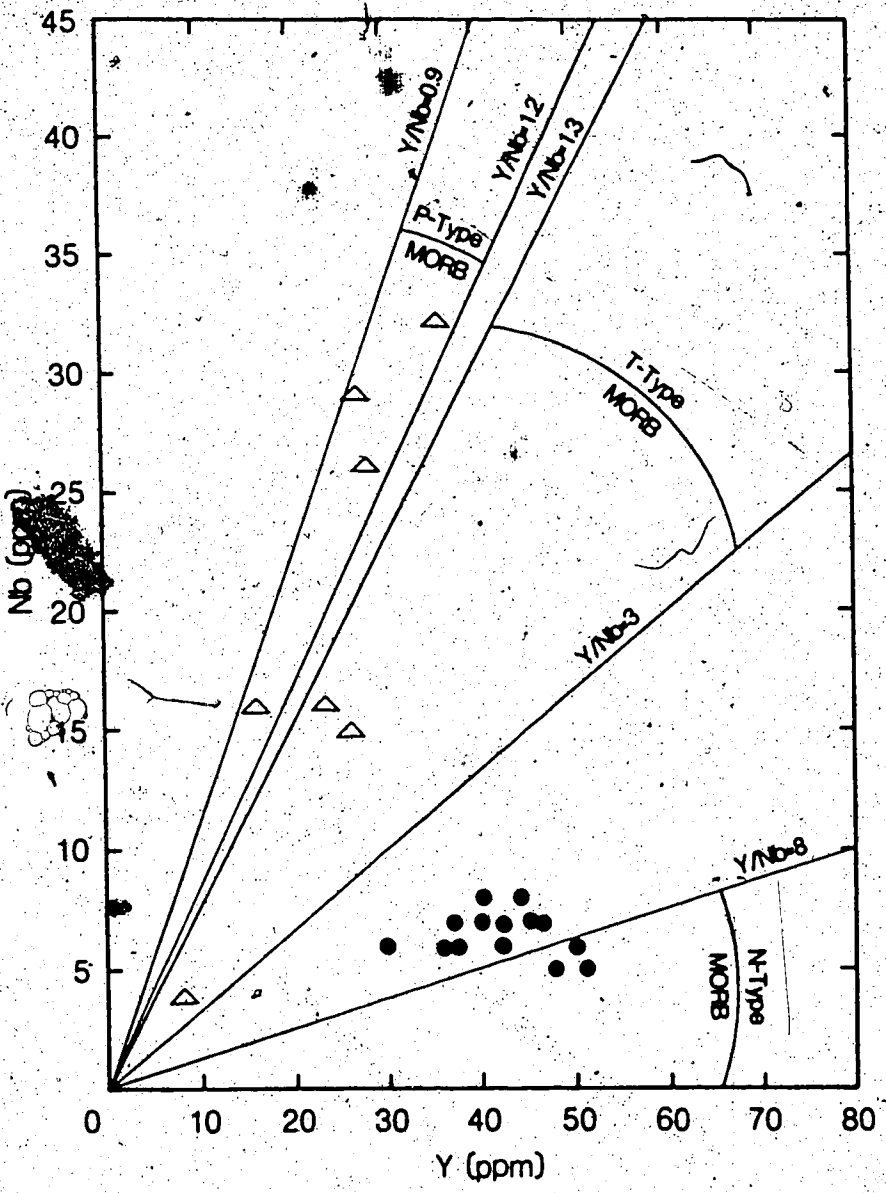

Fig. 6. Nb versus Y diagram for the Fennell Formation and Cache Creek basalts. Y/Nb ratios for N-, T-, P- type MORB are from LeRoex et al. (1983). Symbols as for Fig. 2.

Zr/Nb =15 , similar to the lower ratios of the Fennell Formation, the majority have Zr/Nb less than 8 and fall in the field of T-type MORB. Clear separation of the Fennell Formation and Cache Creek basalts also occurs on a plot of Nb against Y (Fig. 6). The high Y contents of the Fennell Formation (30 to 50 ppm) give Y/Nb ratios from 7 to 7.5. In contrast, the Cache Creek basalts contain 16 to 36 ppm Y, and have Y/Nb ratios from 0.9 to 2.0 , within the range of P-type and T-type basalts. Only one of the two Cache Creek basalts with Zr/Nb similar to the Fennell Formation shows the same affiliation on this diagram. Fig. 7 shows the variation of Zr/Y and Zr/Nb as used by Humphries et al. (1985) to distinguish between ocean ridge and island basalts. The Fennell Formation show a similar range of Zr/Y to the N-type MORB of the Mid-Atlantic ridge. Some regional variation may also be evident as suggested by the lower Zr/Y ratios (2.5 to 3) of samples 1-7A, 1-7C, and 1-8 . The Cache Creek samples show more variation in Zr/Y than Zr/Nb and trend toward the field for Tristan da Cunha whilst overlapping the fields for the P-, and T-type basalts from the Indian Ocean (LeRoex et al. 1983).

The Fennell Formation and Cache Creek basalts have similar low Rb, Sr and Ba contents. (less than 10, 320, and 240 ppm, respectively), characteristic of tholeiitic rather than alkaline suites. However, only two samples, 1-15 and 1-7A, from the Fennell Formation have Ba/Rb close to the mantle ratio of 11.3 (Hofmann and White 1983) and thus may be little altered. Both these samples have $^{87}Sr/^{86}Sr$ ratios less than 0.7030 . Ba/Rb ratios of 13 to 30 in the Cache Creek basalts indicate less alteration than for the Fennell Formation.

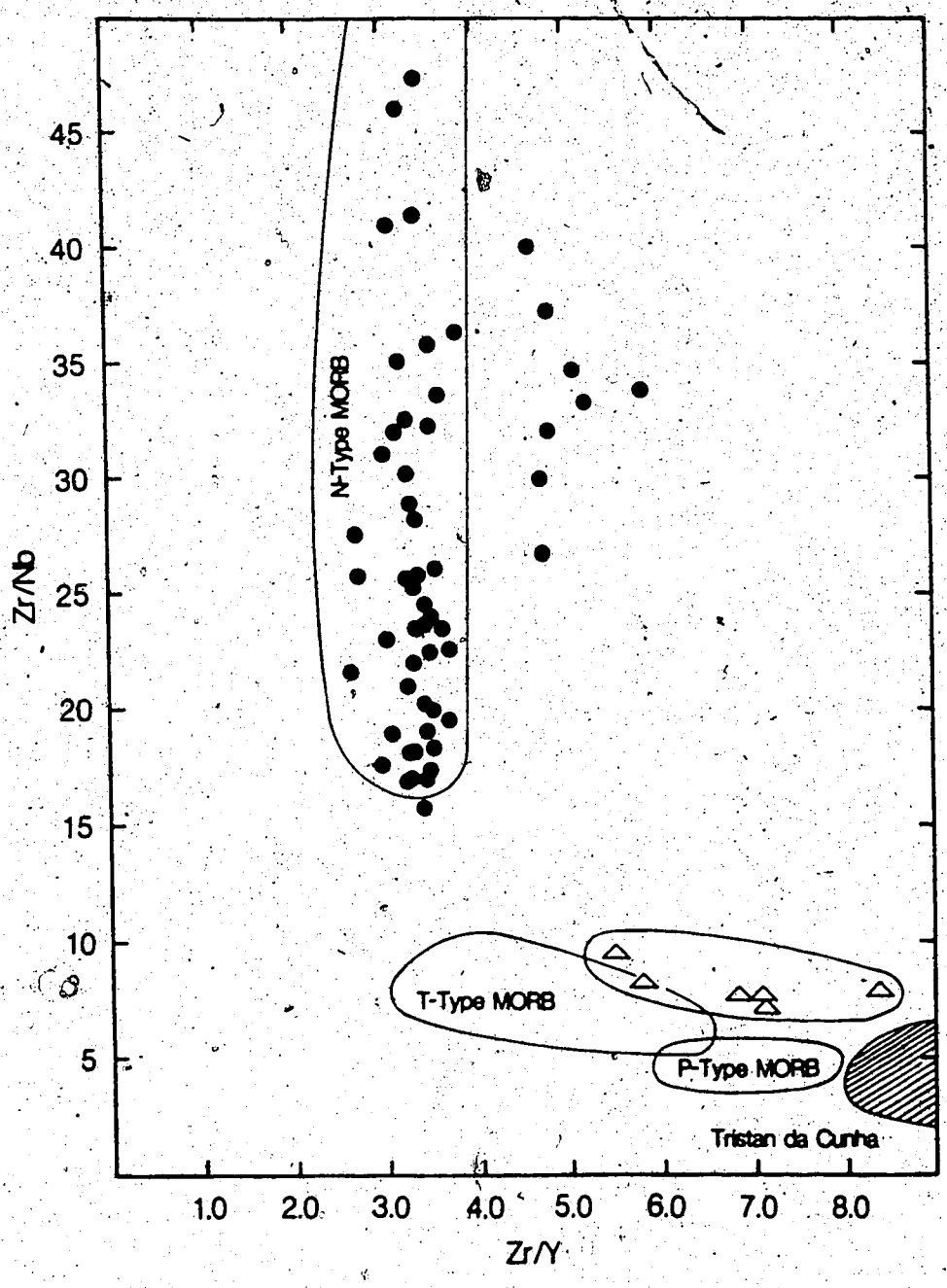

Fig. 7. Zr/Y variation with Zr/Nb ratio in the Fennell Formation and Cache Creek basalts. Additional data for the Fennell Formation from Hall-Beyer (1976). Fields for N-, T-, P- type MORB from LeRoex et al. (1983). Symbols as for Fig. 2.

Ni contents are uniformly higher and show a greater range in the Cache Creek samples (70 to 300 ppm) compared to the Fennell Formation (30 to 130 ppm), consistent with the generally higher MgO of the Cache Creek basalts. Low Ni contents of less than 50 ppm in the Fennell Formation samples classified as komatiites by Hall-Beyer (1976), are one of the principal objections against such an interpretation.

Tectonic Setting

Ocean island basalts may be interpreted as the result of mixing of melt derived from a LIL-depleted MORB-source mantle reservoir and melt from an upwelling mantle plume which is geochemically distinct from MORB (Chen and Frey 1983, 1985). The influence of the plume results in lower $^{143}Nd/^{144}Nd$ and higher $^{87}Sr/^{86}Sr$ ratios, and higher trace element abundances than observed in basalts from other oceanic settings. The similarity of the Cache Creek basalts to T- and P-type MORB in trace element chemistry and isotopic composition strongly suggests an ocean island origin. The basalts are assigned to a tholeiitic suite from their major element chemistry, constant Ti/Zr ratio and low P and Ba abundances.

The presence of small scale (tens of metres to kilometers size) mantle heterogeneities within the upper mantle source region of oceanic basalts has been proposed to provide alternative mixing components to the plume model (Zindler et al. 1984). Suitable candidates for the relatively enriched (compared to MORB-source) material includes ancient segregations of basaltic melt, incompletely mixed remnants of subducted ocean crust, and metasomatised peridotite (ibid.).

The similarity of the Fennell Formation to N-type MORB in major and trace element chemistry and isotopic composition indicates a ridge origin rather than an ocean island setting. However, the mineralogy of the Fennell Formation, in particular the presence of kaersutite, is significantly different from that of ocean ridge basalts. Kaersutite is generally found in alkalic rocks of arc association, but may also be found in basalts of ocean island, seamount, or back-arc ridge affinity (Dick 1982). The contribution to a MORB melt from either a subducted slab-sediment component, similar to the source material of island arc basalts, or metasomatised peridotite, would impart the hydrous nature of the melt required by the presence of kaersutite. As no differences in trace element chemistry or isotopic composition are noted between the kaersutite- and non-kaersutite-bearing Fennell Formation basalts, the contribution of the enriched component must be very small. Subducted slab-sediment material is considered more suitable for this component because no enrichment in Ti, P, Zr and Nb as might be expected from metasomatised peridotite, is observed in the Fennell Formation. This in turn suggests a back-arc setting for the Fennell Formation. The larger, more thoroughly mixed source region of a back-arc ridge compared to a seamount, would account for the uniform chemical composition of the Fennell Formation. Furthermore, P- and T-type MORB which may occur as late stage products in seamount volcanism as a result of the influence of local heterogeneities on the restricted source region, are not observed in the Fennell Formation.

III. Nicola Group

Introduction

Volcanic and sedimentary rocks of the Nicola Group comprise the oldest exposed sequences in the Quesnel terrane (Fig. 1). Palaeolontological evidence (Travers 1978, Grette 1979) and the 205 Ma age of the intruding Guichon Creek batholith (Preto et al. 1979)constrain the age of the Nicola Group to between 230 and 205 Ma (late Triassic). The Nicola Group is equivalent to the Takla and Stuhini Groups of central and northern British Columbia, and the Lewis River Group of the Yukon, and thus comprises part of an extensive belt of early Mesozoic volcanism marking the amalgamation of Terrane I (Souther 1977).

The Nicola Group has been subjected to metamorphism ranging in intensity from prehnite-pumpellyite to lower greenschist facies, along with considerable calcite veining. This alteration has resulted in their interpretation both as a calc-alkaline island arc sequence (Schau 1968, 1970) or as alkaline rift volcanics (Preto 1977). Evidence from associated sediments, which include breccias, conglomerates, greywacke and reef limestones, has not resolved this uncertainty. An origin intermediate between these two extremes, involving rifting associated with oblique subduction, has also been proposed (Souther 1977).

Sampling

The type-locality of the Nicola Group at Nicola Lake has been described in detail by Schau (1968) who divided the succession into lower feldspathic (P) and upper augitic (A) cycles from the dominant

phenocryst phase in the volcanics. Both cycles are further divided into lower, mainly volcanic (P_1 and A_1) and upper, mainly sedimentary (P_2 and A_2) assemblages. Schau (1968) estimated the thickness of the Nicola Group at Nicola Lake to be in excess of 7000 m, although the contact with the underlying strata is not exposed. To the east of Nicola Lake the Nicola Group rests unconformably (Cockfield 1947), or with fault contact (Schau 1968) on phyllitic argillites of the Harper Ranch subterrane. Further north, around Kamloops, the Harper Ranch subterrane (equivalent to the Thompson assemblage of Monger (1977)) includes Permian to late Triassic clastic sediments, carbonates, and rare volcanics (sample 2-108) (Monger 1977, Monger and Berg 1984). These may be partial facies equivalents of, and in part older than the Nicola Group, from the occurrence of augite porphyries similar to the A_1 assemblage interbedded with the sediments (Monger 1982).

Preto (1977) divided the Nicola Group south of Nicola Lake into three northerly trending belts. The boundaries between the belts were interpreted as an old rift system which controlled the distribution of the volcanics. Each belt is characterised by a particular volcanic assemblage: andesite, dacite and tuffs of tholeiitic affinity in the western belt, andesite and basalt of calc-alkaline and alkaline affinity in the central belt, and mostly sedimentary material with rarer, increasingly alkaline volcanics in the eastern belt. This division has not been extended to this study, which has included the Nicola Lake type-section, and the exposures around Kamloops Lake and Canim Lake which were previously described by Cockfield (1947) and Campbell and Tipper (1971). Sampling also included the Copper Creek exposures north of Kamloops Lake which were originally mapped as Cretaceous or Tertiary

(Cockfield 1947). In view of the structural continuity of these rocks with the Nicola Group (Monger 1982) it is proposed that the Nicola Group be expanded to include these strata, renamed the Copper Creek Formation, as the uppermost unit.

Mineralogy

The Nicola volcanics generally contain either abundant plagioclase or augite phenocrysts in a fine grained groundmass of plagioclase and pyroxene. Quartz and phenocrysts of hornblende occur infrequently. Despite the conspicuous absence of orthopyroxene, high normative percentages of this mineral suggest its occurrence in the groundmass. Nepheline and olivine occur in the normative mineralogy but are not present in thin section, although relict olivine has been reported in basalts of the augite cycle (Schau 1968, 1970). Analcite has also been reported in the exposures to the south of the study area (Preto 1977, 1979).

The majority of the samples show considerable alteration: augite is replaced by chlorite, green biotite, or more rarely uralite. Plagioclase, originally labradorite or andesine (Schau 1970, Grette 1979), is in many cases completely albitised. Calcite is present both in fractures and in aggregates in many samples. Epidote, pumpellyite, and rarely prehnite also occur.

Major Element Chemistry

The major element chemistry of the Nicola Group (Table 4a) is characterised by silica contents between 46 and 54% combined with variable, usually high, alkali contents. K_2O ranges from 0.2 to 5% with

Table 4.

(a) Major and trace element chemistry of the Nicola Group.

(i) Calc-alkaline Series.

	2-92B	2-35	2-12	2-15B	2-92A	2-87E	2-16	2-82
SiO_2	49.33	50.66	53.42	49.89	50.03	50.39	62.49	62.05
Al_2O_3	16.10	15.11	14.20	13.00	16.03	18.45	16.05	16.77
Fe_2O_3	11.45	9.52	12.00	12.50	11.04	12.53	6.69	5.34
MgO	9.99	7.29	10.18	10.02	9.35	8.04	3.32	2.87
CaO	7.23	11.24	4.49	9.09	6.71	4.71	4.00	5.70
Na_2O	3.81	2.96	2.24	2.64	3.35	3.39	3.95	3.83
K_2O	0.78	1.42	1.70	1.56	1.91	0.98	1.23	2.31
TiO_2	0.77	0.80	0.97	0.77	0.86	0.98	0.77	0.61
P_2O_5	0.35	0.81	0.25	0.32	0.45	0.15	0.17	0.21
S	0.02	0.01	0.45	0.05	0.06	0.02	1.21	0.13
MnO	0.18	0.18	0.10	0.17	0.21	0.36	0.12	0.18
Ba	499	901	1232	596	814	92	555	1808
Nb	4	4	5	5	4	5	6	6
Zr	60	82	93	68	68	67	116	136
Y	16	17	17	19	18	23	28	21
Sr	532	1138	847	408	382	136	294	813
Rb	13	10	31	35	26	14	23	59
Zn	49	84	84	95	182	293	65	61
Cu	42	1420	42	90	165		24	18
Ni	33	22	43	95	18	9	5	4

(ii) Tholeiitic Series.

	2-84	2-86	2-21B	2-20A	2-87D	2-87C	2-87B
SiO_2	46.20	46.94	44.76	46.05	50.45	50.64	51.71
Al_2O_3	16.56	17.20	17.73	16.77	16.19	16.57	16.19
Fe_2O_3	11.33	12.28	15.84	12.94	13.07	12.17	12.52
MgO	15.09	9.59	12.23	8.92	6.75	5.83	5.92
CaO	7.03	10.41	10.34	10.08	6.74	8.22	6.75
Na_2O	1.96	1.84	2.05	3.43	4.69	4.89	5.03
K_2O	0.00	0.39	0.22	0.18	0.34	0.13	0.21
TiO_2	1.35	1.00	1.28	0.95	1.28	1.10	1.12
P_2O_5	0.29	0.14	0.29	0.12	0.23	0.22	0.25
S	0.04	0.02	0.04	0.37	0.02	0.02	0.05
MnO	0.15	0.20	0.22	0.21	0.23	0.22	0.23
Ba	338	180	226	121	201	98	305
Nb	11	6	7	5	6	5	6
Zr	121	53	86	59	108	78	114
Y	19	18	19	19	34	26	31
Sr	328	322	518	222	520	475	1450
Rb	3	7	5	6	6	4	4
Zn	70	67	114	74	84	77	88
Cu	113	44	238	82	45	29	17
Ni	237	21	123	46	8	4	6

Table 4. contd.

(iii) Calcalkaline low-Al Augite Porphyries.
(iv) Alkaline series.
(v) Shoshonite series

	(iii)				(v)			(v)	
	2-97B	2-97E	2-97F	2-97D	2-79	2-100	2-19	2-208	2-13
SiO_2	50.96	50.31	53.68	50.11	47.47	44.90	48.34	52.77	48.23
Al_2O_3	6.97	8.94	7.97	10.71	14.67	17.61	15.64	14.57	12.23
Fe_2O_3	10.44	11.04	9.22	11.71	14.51	13.17	12.92	10.12	13.01
MgO	15.43	11.07	11.47	12.68	5.14	10.28	8.21	5.88	8.08
CaO	13.27	14.45	13.38	9.74	10.15	5.80	8.73	8.99	12.27
Na_2O	1.05	1.47	1.09	2.57	3.36	4.72	2.54	2.82	2.17
K_2O	0.64	1.22	1.82	0.86	2.52	1.36	1.36	3.40	2.72
TiO_2	0.80	1.01	0.84	1.06	1.53	1.84	1.43	0.75	0.72
P_2O_5	0.17	0.27	0.28	0.29	0.52	0.16	0.37	0.50	0.34
S	0.01	0.00	0.00	0.00	0.02	0.00	0.21	0.18	0.06
MnO	0.24	0.23	0.24	0.26	0.13	0.16	0.24	0.02	0.17
Ba	301	456	807	297	707	298	344	1058	1076
Nb	2	3	4	5	16	6	9	8	4
Zr	45	54	49	63	183	110	135	104	60
Y	19	22	18	23	24	18	26	21	16
Sr	318	764	684	635	597	71	710	722	609
Rb	15	18	23	17	48	28	53	93	58
Zn	82	67	71	99	78	200	73	66	88
Cu	15	50	203	59	120		125	169	69
Ni	91	30	48	30	21	120	37	37	71

(b) Major and trace element chemistry of the Copper Creek Formation and Thompson Assemblage (TA) basalts.

	Copper Creek Formation					TA
	2-91A	2-91B	2-91C	2-91D	1-22	2-108
SiO_2	48.13	47.59	49.27	50.30	45.77	49.83
Al_2O_3	13.68	13.15	13.27	15.06	3.19	15.1
Fe_2O_3	11.85	9.59	9.05	11.14	8.85	13.2
MgO	10.20	15.36	13.31	7.52	35.69	7.60
CaO	9.59	8.79	9.21	8.84	3.97	8.01
Na_2O	4.09	1.70	2.32	5.42	0.01	1.92
K_2O	0.79	2.54	2.32	0.11	1.88	2.33
TiO_2	1.10	0.85	0.83	1.05	0.28	1.24
P_2O_5	0.36	0.26	0.25	0.37	0.08	0.3
S	0.04	0.01	0.01	0.01	0.12	0.01
MnO	0.16	0.16	0.15	0.19	0.16	0.20
Ba	280	638	375	108	265	1386
Nb	6	5	4	6	2	6
Zr	77	70	69	85	10	91
Y	22	21	20	23	5	25
Sr	283	484	602	746	246	633
Rb	13	33	25	2	32	50
Zn	71	78	71	80	54	93
Cu	117	17	11	136	52	104
Ni	40	259	220	33	1189	20

Major elements recalculated to 100% on a volatile-free basis.
Trace elements in ppm.

the result that all four suites, tholeiitic, calc-alkaline, high K and shoshonite, are represented on a K_2O versus silica classification diagram (Fig. 8). A comparable range of Na_2O results in Na_2O/K_2O ratios ranging from 0.5 to 110 . Approximately half of the samples in Table 4a would be classified as alkaline based on total alkali content, although at silica contents greater than 56% the Nicola volcanics are invariably subalkaline (Souther 1977).

Almost half the samples plot within the tholeiitic field on an AFM diagram (Fig. 9). Most of these lie to the right of, rather than above the tholeiitic-calc-alkaline boundary, indicating low iron enrichment. The analyses of Preto (1977), recalculated to 100% on a volatile-free basis, all lie well within the calc-alkaline field with the exception of the western belt samples (c.f. Fig. 6a, ibid.). A similar distribution, which at first approximation could be termed alkaline, is noted on the FeO^*/MgO-silica discrimination diagram (Fig. 10). The distribution on this diagram could also be fit by discrete tholeiitic and calc-alkaline trends comparable to the pigeonite and hypersthene rock series. One of the reasons for the limited usage of these series as a basis for classification has been the problem of identifying the groundmass pyroxene. Although orthopyroxene is not observed as a modal phase in the Nicola Group, it is considered significant that samples lying along the hypersthene series trend in Fig. 10 contain high normative amounts of this mineral.

Minor and Trace Element Chemistry

The Nicola volcanics show a depletion in Ti, Nb, Zr and P which is typically calc-alkaline. TiO_2 ranges from 0.6 to 1.85%, but rarely

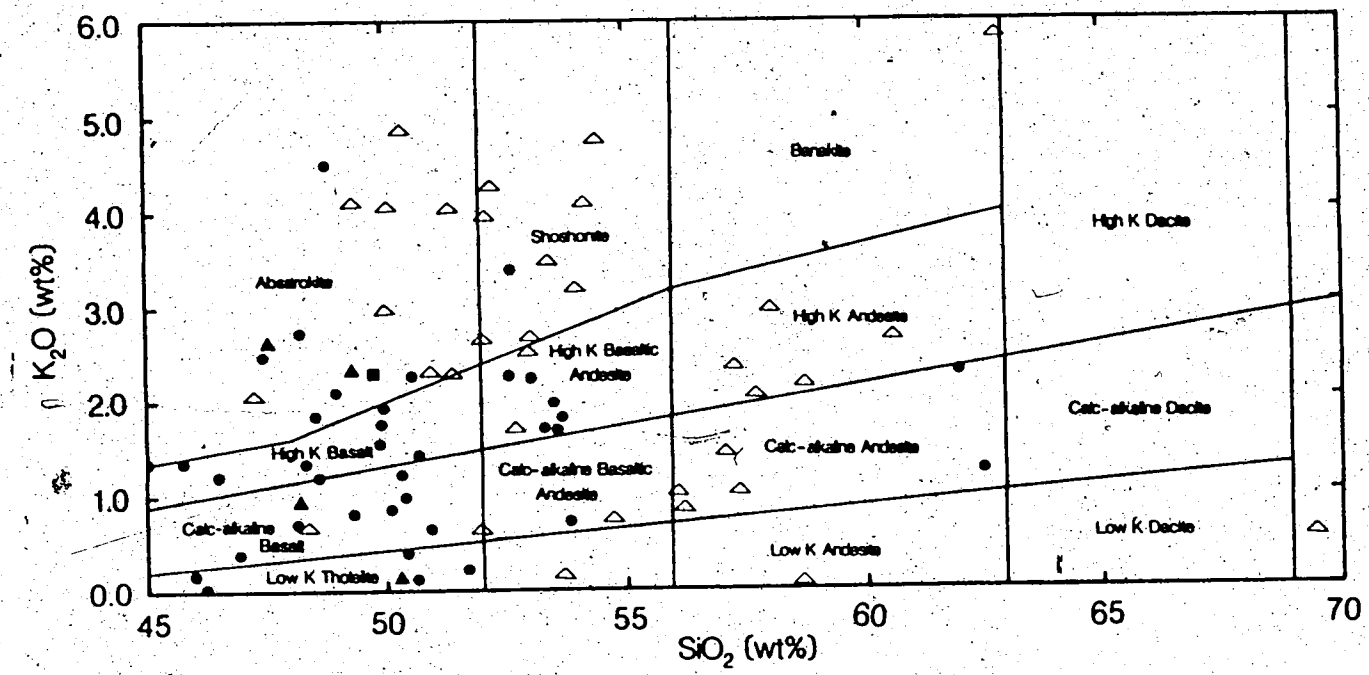

Fig. 8. K_2O versus silica classification diagram for the Nicola Group: • Nicola Group this study; △ Nicola Group analyses of Preto (1977) recalculated to 100% on a volatile-free basis; ▲ Copper Creek Formation; ■ Thompson assemblage.

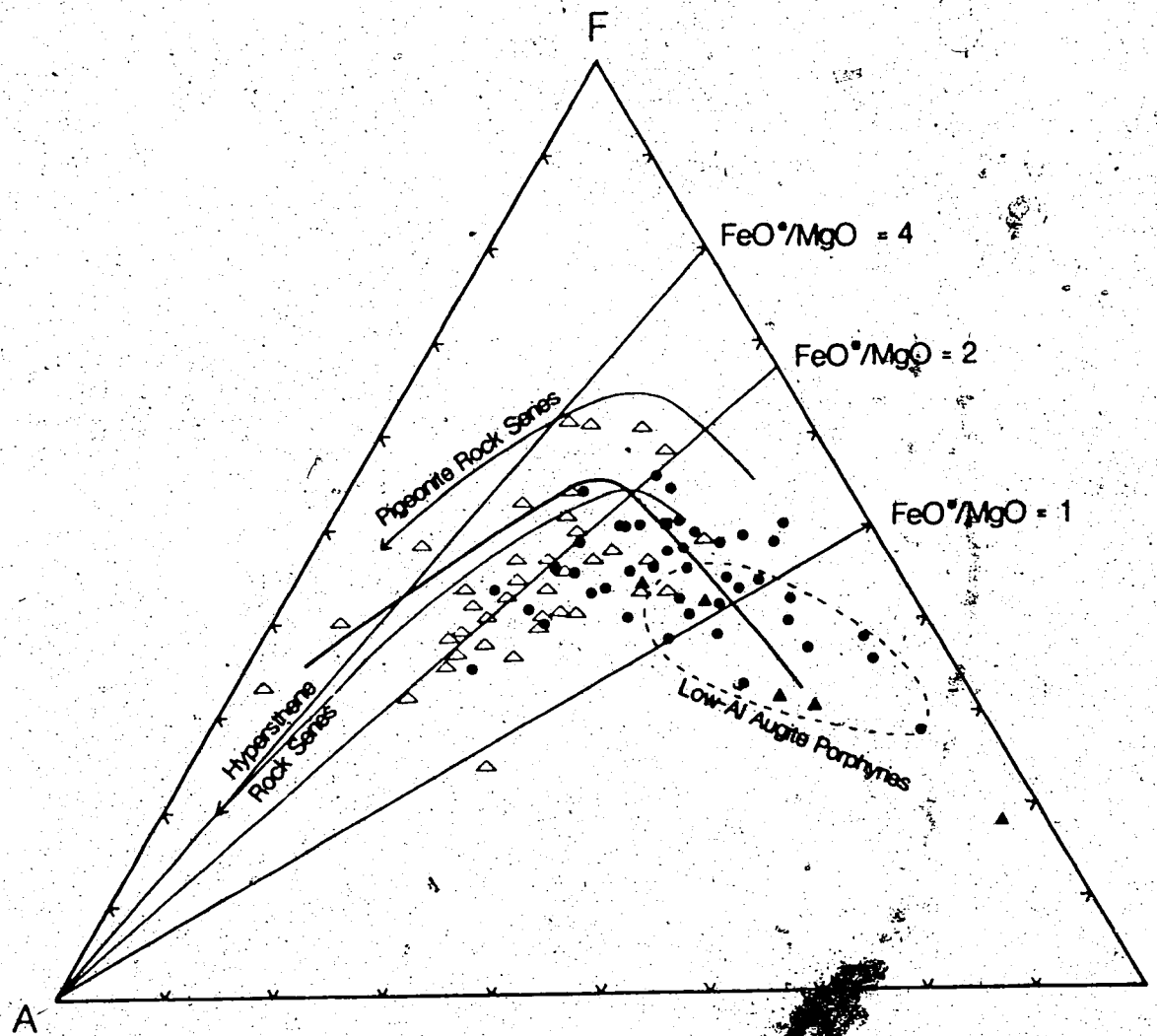

Fig. 9. AFM diagram for the Nicola Group. A=Na,0+K,0, F=FeO+0.8998Fe,0 MgO. Tholeiitic - calc-alkaline dividing line from Irvine and Baragar (1971). Trends for Pigeonite rock seri S), and Hypersthene rock series (HRS) are from Gill (1980). Symbols as for Fig. 8.

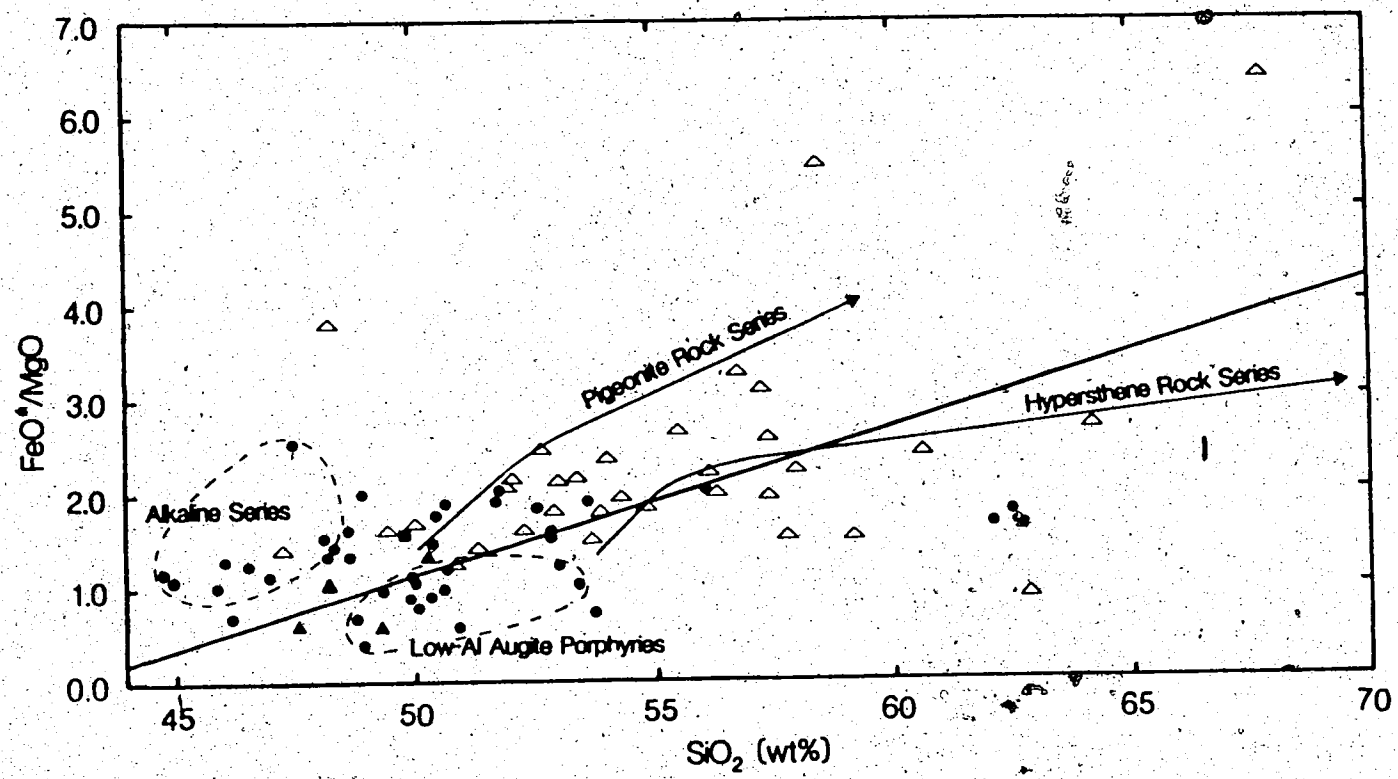

Fig. 10. Tholeiitic- calc-alkaline discrimination diagram for the Nicola Group. FeO* refers to total iron as FeO. Trends for Pigeonite rock series (PRS) and Hyperthene rock series (HRS) are from Gill (1980). Symbols as for Fig. 8.

exceeds 1%. Similarly, P_2O_5 ranges from 0.1 to 0.8%, with most samples falling in the range 0.2 to 0.4%. Nb averages 5 ppm, Zr 85 ppm. The immobile nature of these elements during low-grade metamorphism has led to their use in several classification schemes designed to deduce the original tectonic environment of altered basaltic rocks (Pearce and Cann 1973, Floyd and Winchester 1975). The use of discrimination diagrams which include a mobile element such as K or P allows further recognition of certain mineralogical trends on alteration (Smith and Smith 1976).

The Ti/100-Zr-3Y discrimination diagram of Pearce and Cann (1973) (Fig. 11) is considered to be the most reliable for altered rocks. On this diagram the Nicola volcanics fall entirely within the calc-alkaline and calc-alkaline- low K tholeiite fields. The four samples that lie outside the low K tholeiite in Fig. 11 are heavily calcitised or have undergone epidotisation. Constant Ti/Zr ratios of 75 combined with variable Sr content (70 to 1450 ppm) results in a scatter toward the Sr/2 apex on the Ti/100-Zr-Sr/2 diagram (Fig. 12). However, overlap into the same fields as for Fig. 11 is seen, and the individual distribution of points in both diagrams is similar. Scatter is also observed on the TiO_2-K_2O-P_2O_5 discrimination diagram (Fig. 13) of Pearce et al. (1975), reflecting the highly variable K content of the volcanics. TiO_2/P_2O_5 ratios decrease from 4 to 3 with increasing K content. Similar scatter has been equated with several forms of mineralogical alteration for the Australian Cliefden volcanics (Smith and Smith 1976): replacement of feldspar by epidote or pumpellyite was associated with low K content, whereas albitisation was associated with high K content. However, the K content of the Nicola Group cannot be linked to any particular mineralogy, reflecting either multiple phases of alteration, or a wider

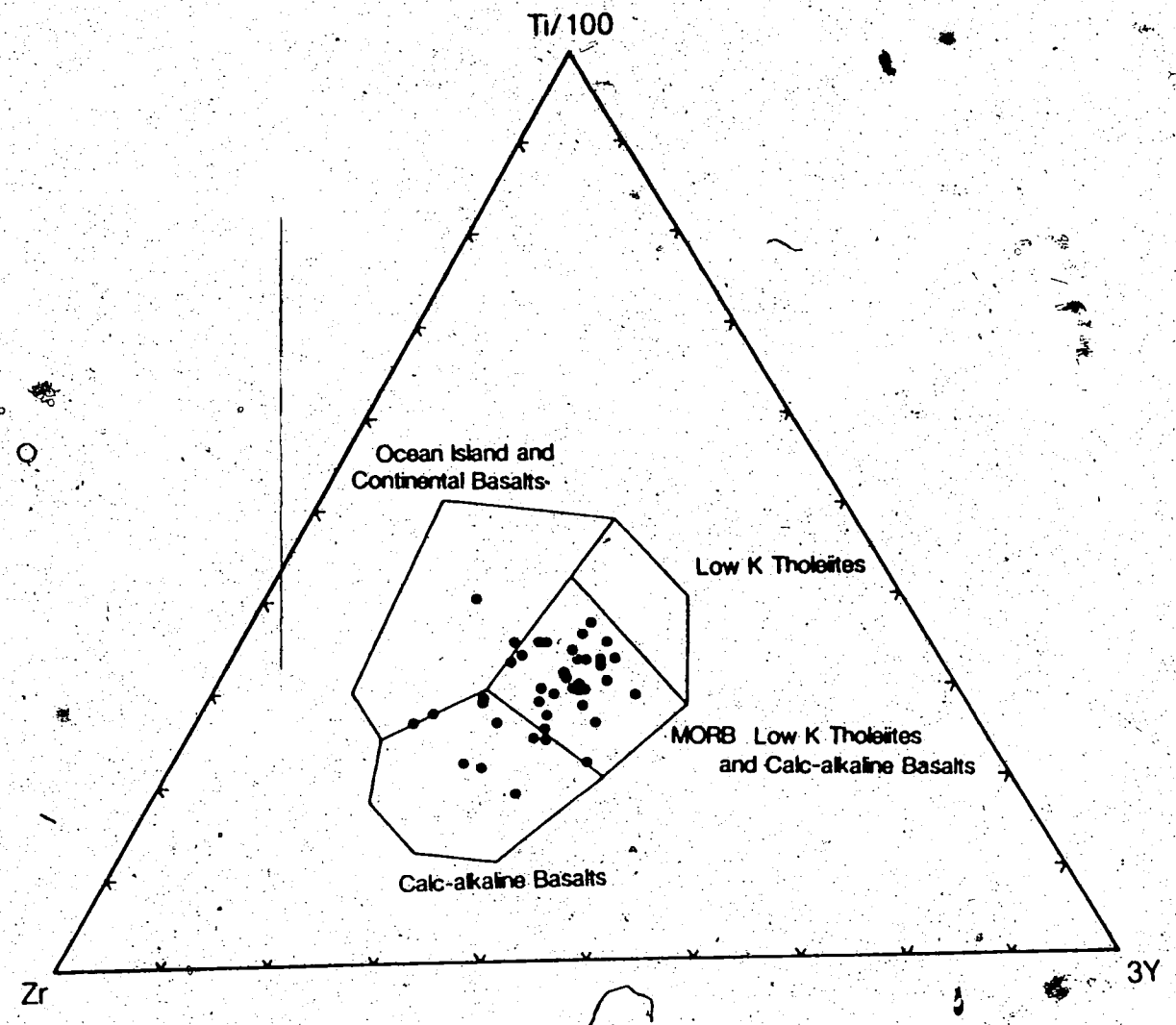

Fig. 11. Ti-Zr-Y discrimination diagram for the Nicola Group.

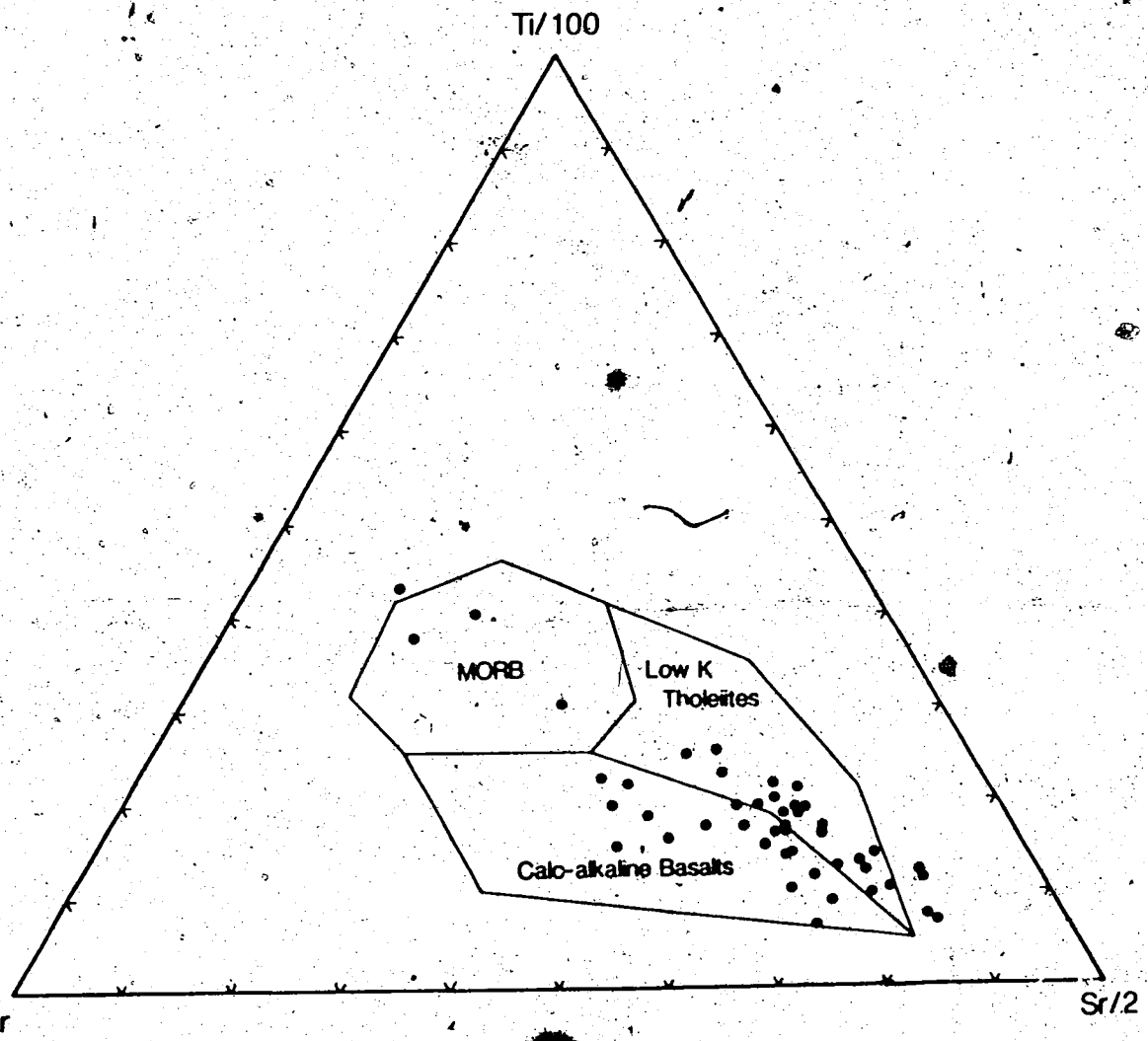

Fig. 12. Alteration effects shown by the Nicola Group of [redacted] Ti-Zr-Sr discrimination diagram of Pearce and Cann (1973). Epidotised and albitised basalts plot toward the Sr/2 apex, whereas pumpellyite- or prehnite-bearing basalts plot toward the Ti-Zr boundary.

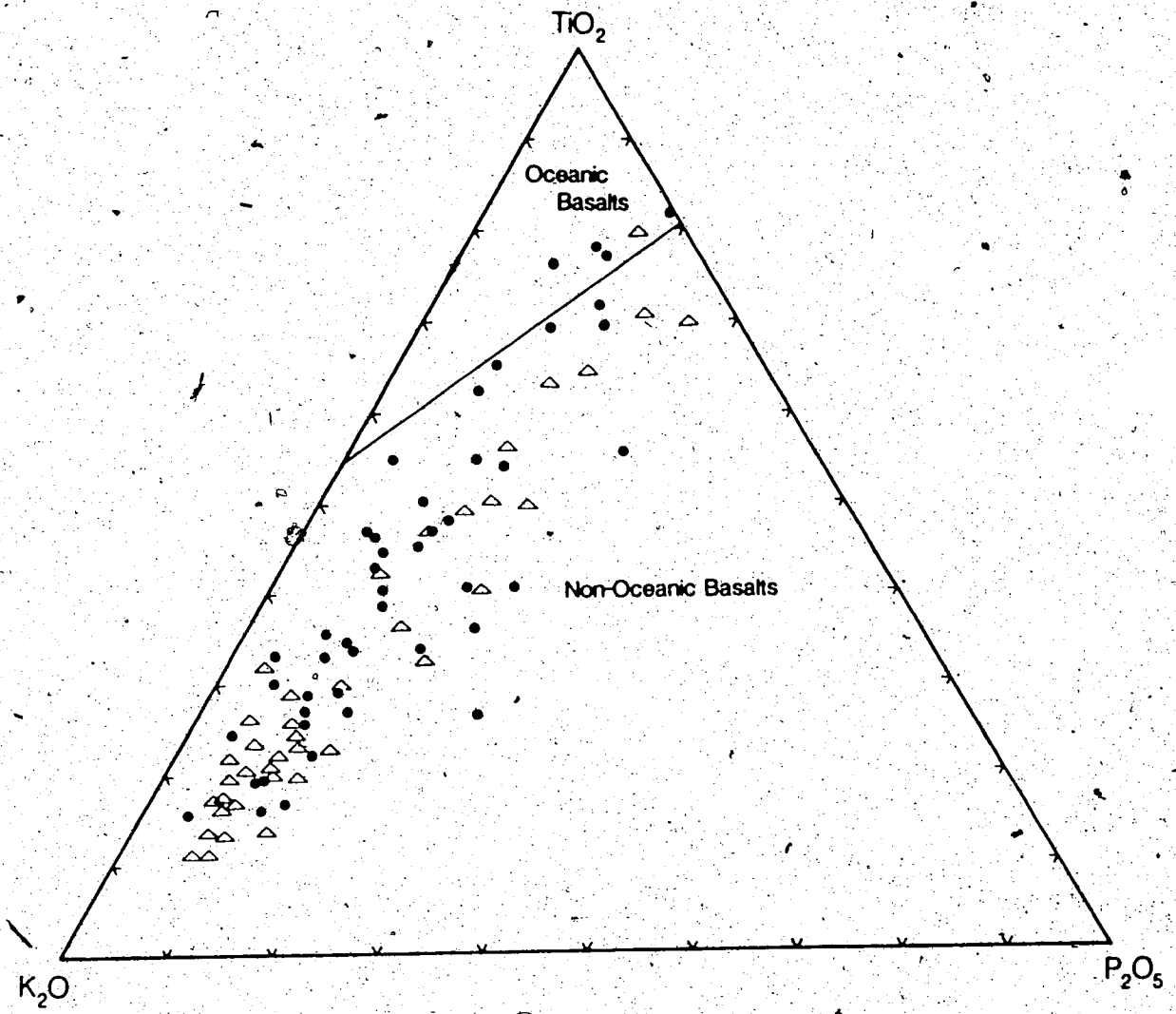

Fig. 13. TiO_2-K_2O-P_2O_5 discrimination diagram for the Nicola Group.

original compositional range.

Copper Creek and Thompson Volcanics

Major and trace element data for the Copper Creek Formation and Thompson assemblage (Table. 4b) confirm the chemical affinity of these volcanics to the Nicola Group. The four basalts from the Copper Creek Formation, in particular, have high MgO (>7.5%), low TiO_2 (<1.1%), low P_2O_5 (<0.37%) and variable alkali content. On Figs. 10 and 11 the Copper Creek basalts lie within the calc-alkaline field, reflecting their less altered nature. The picrite 1-22 from the Copper Creek Formation (Table 4b) has 35.6% MgO and 4.0% CaO, similar to enriched mantle estimates (Palme and Nickel 1985). The Al_2O_3 content (3.2%) of sample 1-22 is similar to that of spinel lherzolites (Maaloe and Aoki 1977). The most distinctive features of this rock, however, are the enrichments in minor and incompatible elements (1.88% K_2O, 250 ppm Ba, 30 ppm Rb).

Nd-Sr Isotopic Composition

The Nd and Sr isotopic compositions of eleven Nicola Group samples are presented in Table 5 .. High $^{87}Sr/^{86}Sr$ ratios resulting in scatter on a Rb-Sr isochron plot were previously ascribed to exchange of Sr with associated sedimentary material during low grade metamorphism (Preto et al. 1979). No age can be gained from the Sm-Nd system due to the small range in both Sm/Nd and $^{143}Nd/^{144}Nd$. Consequently, the Nd-Sr data have been corrected to an age of 220 Ma. $^{143}Nd/^{144}Nd$ shows a small range of only 3 ϵNd units from +4.9 to +7.8 . In contrast, $^{87}Sr/^{86}Sr$ ratios range from 0.7025 to 0.7042 . On a Nd-Sr isotopic plot (Fig. 14) the data lie close to the mantle array, overlapping the fields for the Marianas

Table 5.

Nd and Sr isotopic composition of the Nicola Group and Copper Creek Formation.

	Rb/Sr	$^{87}Sr/^{86}Sr$ m	$^{87}Sr/^{86}Sr$ c	Sm (ppm)	Nd (ppm)	Sm/Nd	$^{143}Nd/^{144}Nd$ m	$^{143}Nd/^{144}Nd$ c	εNd
Nicola Group									
2-78A	0.062	0.70476±2	0.70420	3.58	16.5	0.216	0.512858±38	0.512673	+6.3
2-85	0.065	0.70431±3	0.70372	3.05	10.5	0.290	0.512950±16	0.512703	+6.8
2-87C	0.010	0.70395±2	0.70387	3.28	11.5	0.285	0.512967±21	0.512723	+7.2
2-87E	0.099	0.70504±3	0.70411	2.40	7.04	0.341	0.512901± 9	0.512610	+5.0
2-92A	0.067	0.70429±2	0.70368	2.53	9.61	0.264	0.512918±12	0.512693	+6.6
2-92C	0.019	0.70389±2	0.70372	2.58	10.2	0.253	0.512961±11	0.512745	+7.7
2-96B	0.350	0.70571±2	0.70254	3.84	12.9	0.298	0.512858±14	0.512603	+4.9
2-97A	0.096	0.70401±3	0.70314	2.01	7.27	0.277	0.512934±33	0.512698	+6.7
2-97B	0.023	0.70571±2	0.70354	2.51	8.53	0.294	0.513002±23	0.512751	+7.8
2-97G	0.040	0.70356±3	0.70320	3.55	12.2	0.291	0.512939±27	0.512691	+6.6
2-98C	0.110	0.70474±2	0.70424	3.70	12.7	0.291	0.512938±21	0.512692	+6.6
2-98B	0.076	0.70439±3	0.70404	3.66	12.5	0.292	0.512945±16	0.512696	+6.7
2-208	0.142	0.70522±4	0.70394						
Copper Creek Formation									
2-91A	0.046	0.70403±3	0.70363	3.70	14.4	0.257	0.512837±16	0.512627	+5.1
2-91B	0.068	0.70404±3	0.70346	2.79	8.95	0.312	0.512983±13	0.512729	+7.1
2-91C	0.041	0.70393±3	0.70357				0.513005±17		
2-91D	0.003	0.70365±2	0.70363				0.512946±21		
1-22	0.130	0.70436±6	0.70324	0.60	2.10	0.285	0.512882±27	0.512649	+5.5

( )m measured isotopic ratio.

( )c Nicola Group isotopic ratios corrected to an age of 220 Ma, Copper Creek Group data to an age of 210 Ma.

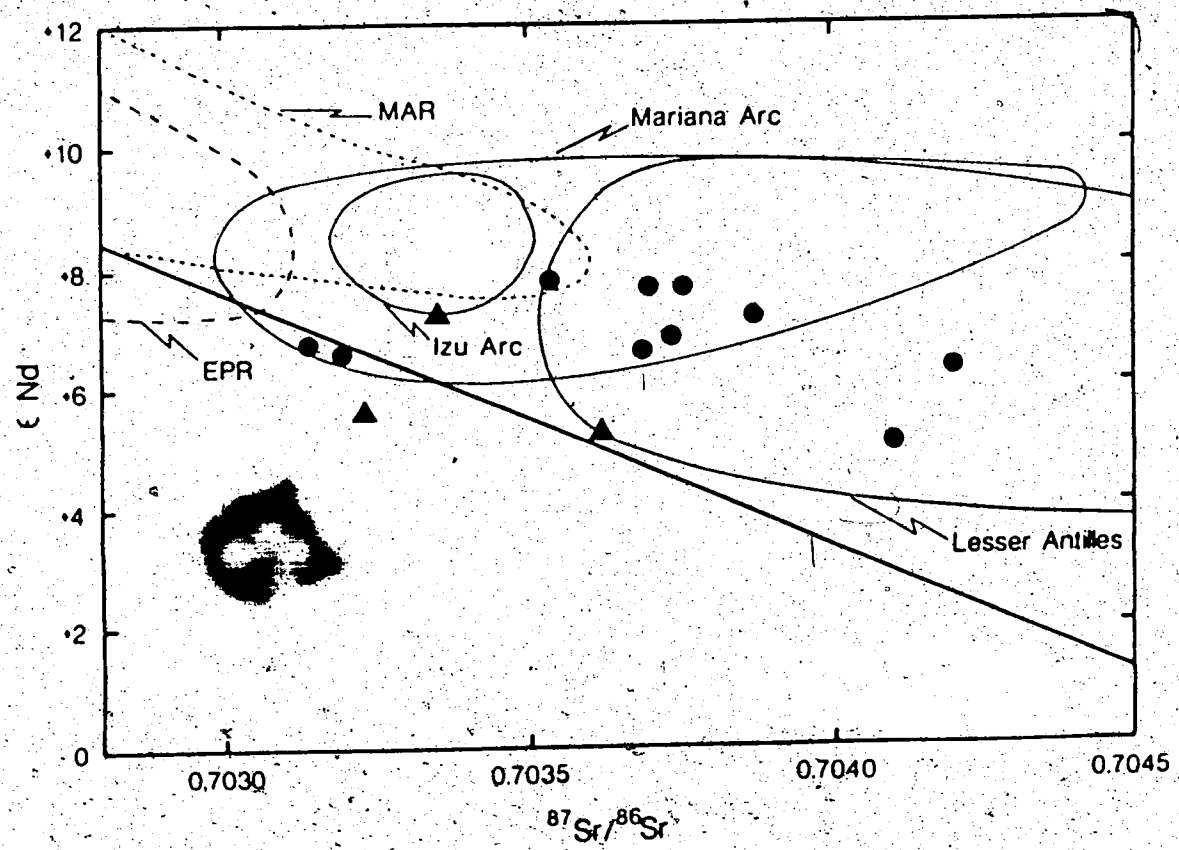

Fig. 14. Nd-Sr isotopic diagram for the Nicoya Group. Symbols as for Fig. 8. Also shown are fields for the Mariana arc (DePaolo and Wasserburg 1977, White and Patchett 1984); Izu arc (Nohda and Wasserburg 1981); Lesser Antilles (Hawkesworth and Powell 1979, Hawkesworth et al. 1979, White and Patchett 1984); East Pacific Rise (EPR) (Zindler et al. 1982); Mid-Atlantic Ridge (MAR) (O'Nions et al 1977, White and Hofmann 1982).

(White and Patchett 1984, Nodha and Wasserburg 1981, DePaolo and Wasserburg 1977, Meijer 1976) and Izu arcs (White and Patchett 1984). The more altered, calcitised samples have higher $^{87}Sr/^{86}Sr$ ratios, and overlap the field for the Lesser Antilles (White and Patchett 1984, Hawkesworth and Powell 1979, Hawkesworth et al. 1979). The trend toward elevated $^{87}Sr/^{86}Sr$ is considered a post-magmatic effect resulting from low grade metamorphism rather than from increasingly seawater altered material being added to the mantle wedge below the arc. Anomalously low $^{87}Sr/^{86}Sr$ ratios, such as for sample 2-96B, have also been found in the Mariana arc (Meijer 1976). However, 2-96B has particularly high Rb/Sr unlike other Rb-rich Nicola basalts such as 2-20B, and it is considered that the low $^{87}Sr/^{86}Sr$ ratio results from post magmatic introduction of Rb into the rock.

Isotopic data for the Copper Creek Formation have been corrected to a slightly younger age of 210 Ma (Table 5). The samples show a comparable range of ϵNd (+5.1 to +7.1) and Sm/Nd (0.26 to 0.31) to the Nicola Group. Less alteration is indicated by the tighter grouping of $^{87}Sr/^{86}Sr$ (0.7032 to 0.7037), and results in the Copper Creek samples lying within the Nd-Sr mantle array in Fig. 14.

Crystal Fractionation

In spite of the altered nature of the Nicola Group the range of Al_2O_3 (6.5 to 18.5%) and MgO (5 to 20%) in the basaltic samples can be related directly to the predominant phenocryst phase. The highly porphyritic nature of many samples suggests that crystal fractionation was significant in controlling the composition of the Nicola Group. Basalts of the augite cycle of Schau (1968, 1970), termed low-Al augite

porphyries (LAAP), have very low Al_2O_3 (6.5 to 11%) and high MgO (11 to 15.5%). Conversely, the basalts containing predominantly plagioclase phenocrysts have high Al_2O_3, CaO and Na_2O contents. On a graph of Al_2O_3 versus MgO (Fig. 15a) the LAAP define a trend extending to lower Al_2O_3 and higher MgO than for other calc-alkaline suites, which can be explained by the incorporation of cumulus augite or olivine. Nicola basalts with less than 10% MgO and greater than 13% Al_2O_3 define a scatter on the same diagram, indicating variable augite-olivine fractionation combined with plagioclase accumulation.

Augite fractionation is also suggested by the positive correlation of CaO and MgO (Fig. 15b). The scatter on the diagram is interpreted as varying amounts of augite-olivine accumulation, the LAAP plotting to higher MgO but showing only a slight enrichment in CaO. More clearly defined trends on Figs. 15a and 15b, are shown by the Copper Creek basalts, although their isotopic compositions indicate that these basalts cannot represent the differentiation products of single magma pulse. MgO decreases from 15 to 7.5% with only a moderate increase in Al_2O_3 indicative of olivine fractionation. CaO shows only a slight increase over the same range of MgO, consistent with this interpretation.

Classification of the Nicola Group

The low Ti, P, Zr and Nb contents of the Nicola volcanics and their position on the trace element discrimination diagrams (in particular on the Ti/100-Zr-3Y plot, Fig. 11) suggest that the lavas belong to an arc rather than an alkaline rift assemblage. More detailed characterisation of the arc requires the resolution as to whether the

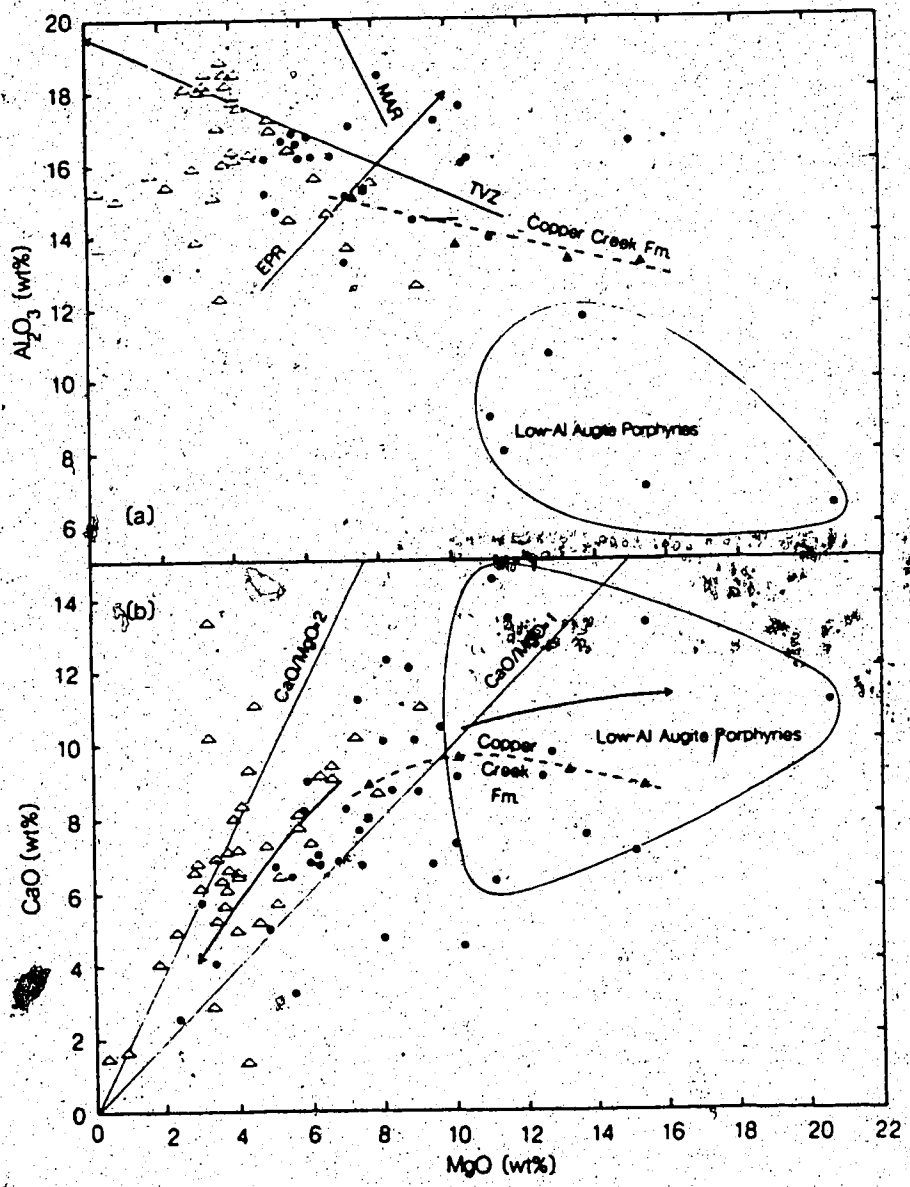

Fig. 15. Variation of (a) Al_2O_3 with MgO (b) CaO with MgO in the Nicola Group. Also shown in (a) are fractionation trends for the East Pacific Rise (EPR), Mid Atlantic Ridge (MAR), and Taupo Volcanic Zone (TVZ), representing fast-, medium-, and slow- spreading rifts, respectively (Flower 1980). The trend for the Copper Creek basalts is indicated by a broken line in both (a) and (b). Solid lines in (b) illustrate augite and/or olivine fractionation and accumulation trends inferred from the chemistry of the Nicola Group. Symbols as for Fig. 8.

alkali contents are a primary feature (Preto 1977, 1979) or result from alteration (Schau 1968).

Augite or olivine fractionation would increase the alkali contents of the lavas but it is unlikely that this mechanism alone could account for the high K_2O contents. To account for Na_2O/K_2O ratios of less than 2 in the LAAP requires the incorporation of augite crystals into a highly evolved melt. Such a process should also increase the concentrations of incompatible elements such as Ba, Zr and Nb, for which there is no evidence.

Rifting associated with oblique subduction has also been proposed to impart an alkaline character on the volcanics (Souther 1977). The modern analogue to such a tectonic environment would be the Taupo volcanic zone (TVZ) of New Zealand. However, the Nicola volcanics show little similarity to the TVZ lavas, which include a large proportion of intermediate and acidic rocks. In contrast, only 7.5% of the samples in Table 4a, and 20% of those of Preto (1977) have silica contents greater than 56%. Most significantly, in spite of the contention that the Taupo rift environment has led to K enrichment of the associated volcanics (Hodder 1984), the TVZ lavas are typically calc-alkaline (Cole 1979) and have considerably lower K_2O contents than the Nicola Group.

Low grade alteration of the Nicola Group is suggested by the trend in $^{87}Sr/^{86}Sr$ away from the mantle array in Fig.14 . The greater susceptability of the basaltic rocks to such alteration would account for the alkali content decreasing with increasing silica much less rapidly than the alkaline-subalkaline boundary. The less altered nature of the Copper Creek Formation indicates that the alteration took place shortly after the extrusion of the lavas, or that the alteration varied

with locality. Regional variation is supported by differences in the alkali contents of the Takla and Stuhini Groups (Souther 1977): the Takla volcanics are predominantly subalkaline, whereas the Stuhini are alkaline. Such alteration invalidates the contention of Preto (1977, 1979) that the occurrence of analcite in the Nicola Group indicates an alkaline association: pseudomorphing of sodic feldspars by analcite is common in prehnite-pumpellyite facies metamorphism (Deer et al. 1966).

Consequently, it is probable that an interpretation of the trends in Figs. 9 and 10 as alkaline is oversimplified. The progression toward alkali enrichment in Fig. 9 is particularly misleading in consideration of the paucity of intermediate and acidic volcanics. The FeO^*/MgO versus silica diagram (Fig. 10) has, therefore, been used as a basis for the division of the Nicola Group into three series: calc-alkaline, tholeiitic, and alkaline:

(1) Calc-alkaline: This series includes the low-Al augite porphyries and is is characterised by low FeO^*/MgO (Fig. 10), and low iron enrichment (Fig. 9), although at high MgO contents the samples may plot in the tholeiitic field. TiO_2 contents are less than 1%. Nb averages 4 to 5 ppm, Zr 70 ppm.

(2) Tholeiitic: This series is characterised by high FeO^*/MgO (Fig. 10) and iron enrichment (Fig. 9). Na_2O/K_2O ratios exceed 9 depending on the degree of albitisation. TiO_2 ranges from 0.95 to 1.35%, P_2O_5 from 0.1 to 0.3%. Ba, Sr and Rb contents are all low.

(3) Alkaline: An alkaline series is recognised from low silica and high minor and trace element contents (TiO_2 >1.4%, P_2O_5 >0.3%, Nb >6 ppm, Zr >110 ppm) similar to the ranges reported for other alkaline suites accompanying calc-alkaline volcanism (Arculus 1976). Two samples are

tentatively assigned to an absarokite-shoshonite series. Both have low Al_2O_3 (12 to 15%), moderate MgO (6 to 8%), high alkali contents, and Na_2O/K_2O ratios less than 1 . On the AFM plot (Fig. 9) no iron enrichment is observed. In minor element content TiO_2 averages 0.75%, P_2O_5 0.4% . Ba, Sr, Rb are greater than 1000, 600, and 50 ppm, respectively.

Amalgamation and Accretion of Terrane I to North America

Interpretation of the Slide Mountain terrane (SM) as a back-arc basin assemblage raises the question of the identity of the related arc. Conventional tectonic interpretations (Dickinson 1976, Monger and Price 1979) suggest that the Atlantic-type continental margin which had prevailed since the late Proterozoic developed into a Japanese-type margin during the early Devonian with the formation of a back-arc basin within the marginal shale facies of the miogeocline. A provenance for the basin sediments from North America is precluded by the occurrence of widespread contemporaneous carbonates along the continental margin (Monger et al. 1972) and thus requires an arc source to the west.

Early to mid-Devonian strata on the Harper Ranch subterrane to the west of the SM terrane have not been preserved. Late Devonian to early Permian strata of this subterrane are predominantly carbonates (Fig. 16a) (Monger 1982) making it an unlikely candidate for the arc. Of interest are the possible positions of the Bakerville (BV), Kootenay (KO) and Monashee (MO) terranes which now lie between the SM terrane and North America (Fig. 1). The conventional model requires both the removal of the proposed arc and the insertion of the BV, MO and KO terranes which would have to take place by transcurrent movement prior to the

amalgamation of Terrane I.

Both the BV and KO terranes contain mid-Palaeozoic plutons indicative of arc activity on these terranes (Monger et al. 1972, Dickinson 1976). Age estimates for the intrusions range from early Ordovician to early Mississippian, although a late Devonian age is favoured (Monger and Berg 1984). Given the uncertainty in age of the plutons and of the SM terrane, it is proposed that the SM back-arc ridge was related to arc activity on the BV and KO terranes. From the spatial relationship of the latter terranes, a westward-dipping subduction zone is required under the western margin of the BV, KO and MO terranes during the mid- to late Palaeozoic (Fig. 16b). The lack of volcaniclastic material within the carbonates of the continental margin is consistent with such an interpretation and requires that the arc developed remote from North America. The model is similar to that suggested for the relationship of the Lewis River and Anvil volcanics in the Yukon (Tempelman-Kluit 1979). Following cessation of volcanic activity on the BV, KO and SM terranes around 240 Ma, it is suggested that the western part of the SM terrane was subducted under the Quesnel terrane to form the Nicola arc (Fig. 16b). The Harper Ranch subterrane would then represent a fore-arc assemblage. Subduction continued until approximately 205 Ma when this second subduction zone became imbricated by the collision of Terrane I, the BV, KO and MO terranes and North America (Fig. 16b).

The spatial variation of the Nicola Group described by Preto (1977) would be expected from an east-dipping subduction zone but interpretation of the alkali contents of the Nicola Group as resulting from low-grade alteration negates this theory. The Cache Creek terrane

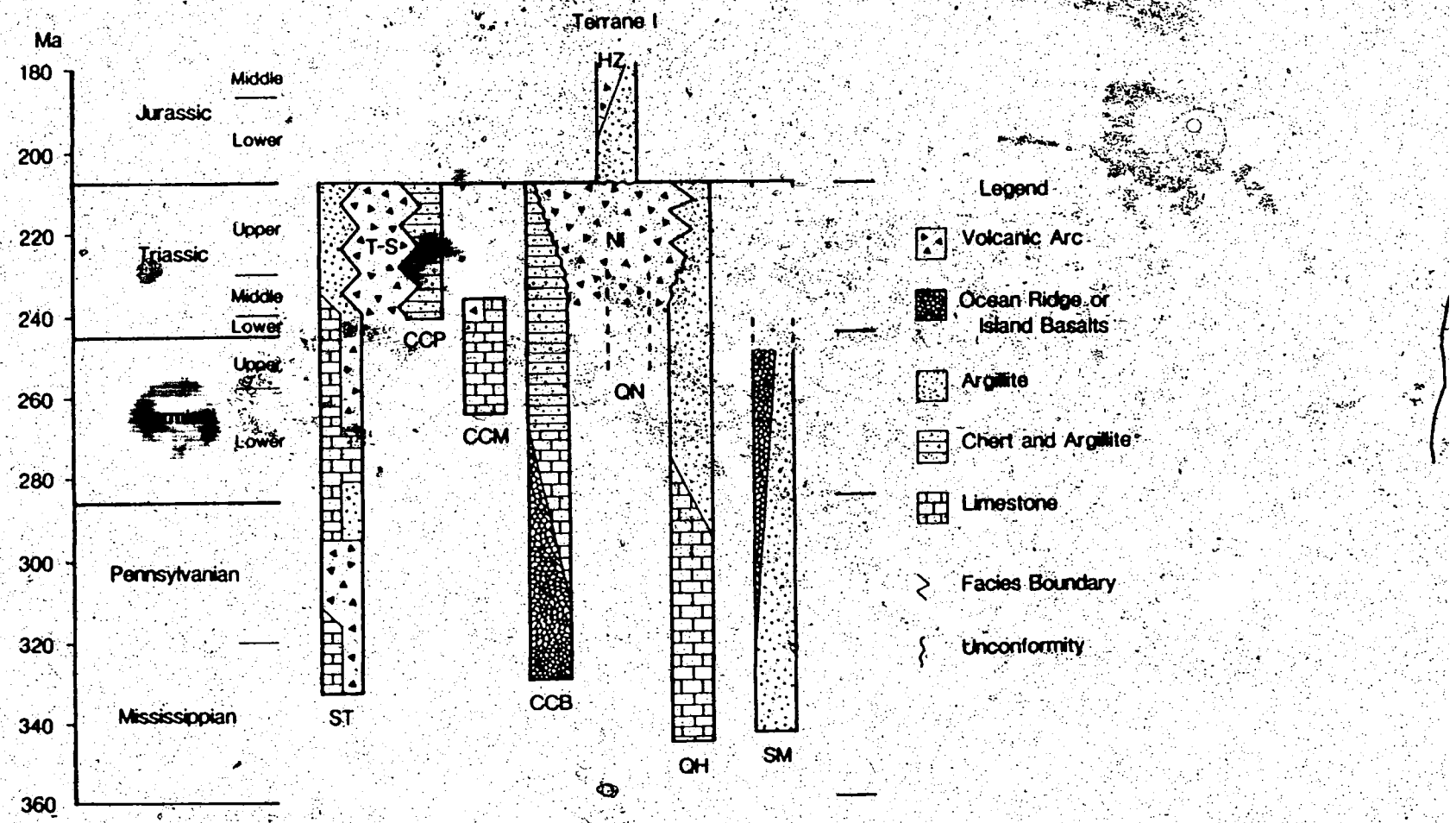

Fig. 16.(a) Schematic cross section through Terrane I showing stratigraphy and time of amalgamation of the component terranes. Abbreviations: ST- Stikine terrane; CCP- Cache Creek, Pavilion subterrane; CCM- Cache Creek, Marble Range subterrane; CCB- Cache Creek, Bonaparte subterrane; QN- Quesnel terrane; QH- Harper Ranch subterrane of Quesnel terrane; SM- Slide Mountain terrane; Arc assemblages; HZ- Hazelton; NI- Nicola; T-S Takla- Stuhini (northern British Columbia only). (after Monger 1977, Travers 1978, Monger 1981, Shannon 1981, Monger 1982, Saleeby 1983, Monger and Berg 1984).

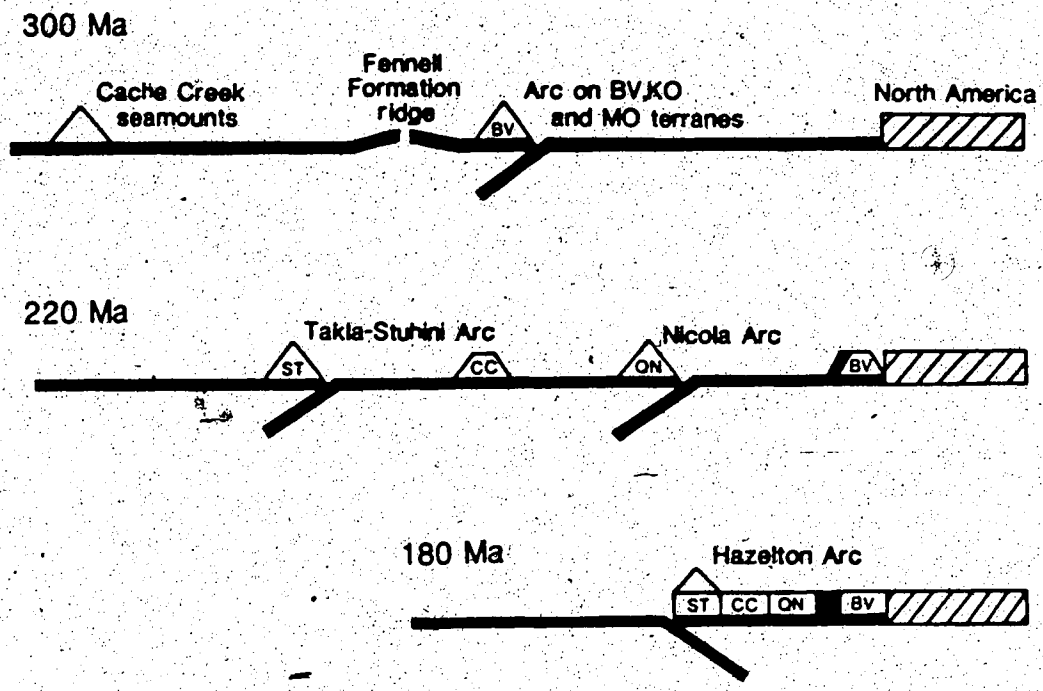

Fig. 16. (b) Schematic model for the formation of Terrane I. At 300 Ma volcanic arcs on the Bakerville (BV), Kootenay (KO) and Monashee (MO) terranes are separated from North America by an ocean basin of unknown extent. related back-arc activity forming the Slide Mountain terrane (SM) (illustrated by the Fennell Formation) requires a westward dipping subduction zone under these arcs. Ocean island basalts of the Cache Creek terrane are formed contemporaneously with the Fennell Formation. Back-arc activity ceases around 250 Ma with the accretion of the BV, KO and MO terranes to North America. Closure of the back-arc basin takes place by subduction under the eastern margin of the Quesnel (QN) terrane with the formation of the Nicola arc. Topographic irregularities on the back-arc ridge results in localised obduction of the SM terrane onto the BV, KO and MO terranes. Volcanic activity on the CC terrane also ceases around 250 Ma, and is followed by subsidence and the formation of reef limestones around the islands. A subduction zone of westward polarity under the Stikine terrane (ST) forms the Takla-Stuhini arc contemporaneously with the Nicola arc. The Takla-Stuhini subduction zone consumes the ocean basin separating the QN, CC and ST terranes, thus amalgamating the components of Terrane I. By 180 Ma Terrane I has been accreted to the BV, KO and MO terranes. Subduction under the western margin of Terrane I is initiated, forming the Hazelton arc.

has been interpreted as a subduction complex related to the Nicola arc (Travers 1978) but the oblique orientation of the Cache Creek subterranes to the arc axis is problematic. Interpretation of the Cache Creek melange as a result of the collision of ocean island material with the Quesnel terrane allows a westward-dipping subduction zone beneath the Nicola arc, but also requires the distance between the Quesnel and Stikine terranes to have been taken up by westward subduction beneath the Stikine terrane.

Accretion of terrane material to North America by the closure of a basin by subduction to the west or southwest has also been invoked by Chamberlain and Lambert (1985) who propose that the BV, KO and MO terranes (collectively termed Terrane III) along with Terranes I and II amalgamated to form the microcontinent Cordilleria, which was then accreted to North America in the late Cretaceous. The presence of mid-Cretaceous arc volcanics of the Spences Bridge Group (Chapter 5) along the western margin of Terrane I is in conflict with the persistence of a westward-dipping subduction zone so late in the Mesozoic. The westward-dipping subduction zone was probably imbricated during the early Jurassic, which is the generally accepted time of accretion of Terrane I to North America (Monger et al. 1982). Batholiths of mid-Jurassic to Cretaceous age within Terrane III represent the final stages of arc activity related to the closure of the basin between Terrane III and North America.

IV. Post-Jurassic Tectonics of Terrane I

Introduction

The post-accretion history of Terrane I has been dominated by interaction with the Pacific plates; therefore, it is pertinent to present a synthesis of the relative plate motions of the Pacific region from the mid-Jurassic to the present (Fig. 17). The positions for North America are those calculated by Coney (1978) using a hotspot reference frame, with adjustments for the rotation of the continent after Irving (1979). The diagrams display the relative positions of Terranes I and II and address the problem as to whether the interaction of the oceanic plates with North America is likely to have involved subduction or strike-slip motion. The representation of subduction zones is largely schematic, except where noted, and does not represent any specific arc.

154 Ma Late Jurassic

At this time the triple-junction between the Pacific, Farallon, and Phoenix plates is estimated at 10°S, 130°W with the Pacific-Phoenix, and Farallon-Phoenix ridges trending southwest and southeast, respectively (Henderson et al. 1984). The Farallon-Pacific ridge is orientated north or northeast and may have been offset by several major transform faults (Henderson et al. 1984). Palaeomagnetic data suggests a position of 23°N for Terrane I (Monger and Irving 1982), and either 20°N or 20°S for Terrane II and southern Alaska (Stone et al. 1982). The southerly latitude for Terrane II and southern Alaska is preferred by most authors because only a straightforward northeast movement is then required to bring these Terranes to their present position. However,

unless the Terranes are located between 40° and 90°W the southerly position is untenable because spreading at the Farallon-Phoenix ridge would drive them further south.

120 Ma Early Cretaceous

During the early Cretaceous the Pacific-Phoenix-Farallon triple-junction lay at a latitude of 20°S, between 80°and 100°W longitude (Coney 1978, Larson and Pitman 1972). The orientation of the Farallon-Phoenix and Pacific-Phoenix ridges at this time is uncertain, although an easterly trend for the Farallon-Phoenix ridge (Irving 1979, Larson and Chase 1972, Larson and Pitmann 1972) is consistent with the late Jurassic plate orientation. A northeast orientation of the Farallon-Phoenix ridge (Stone et al. 1982) intersects the western margin of Terrane I from approximately 130 to 120 Ma. The ridge would then be orientated almost perpendicular to the continental margin; therefore, the resultant interaction would probably be strike-slip motion in the vicinity of the Terrane. By this time there also existed, or had developed on the Pacific-Phoenix ridge, a second triple-junction resulting in the formation of the Bering plate (also termed Izanagi plate) (Engebretson et al. 1984).

83 to 82 Ma Mid-Cretaceous

A major reorganisation of the oceanic plates occurred in the mid-Cretaceous in response to the subduction of the Bering-Pacific and Bearing-Farallon ridge along the Siberian-Alaskan continental margin (Rea and Dixon 1983). This resulted in the formation of the Kula plate from the northern half of the Farallon plate by the generation of a

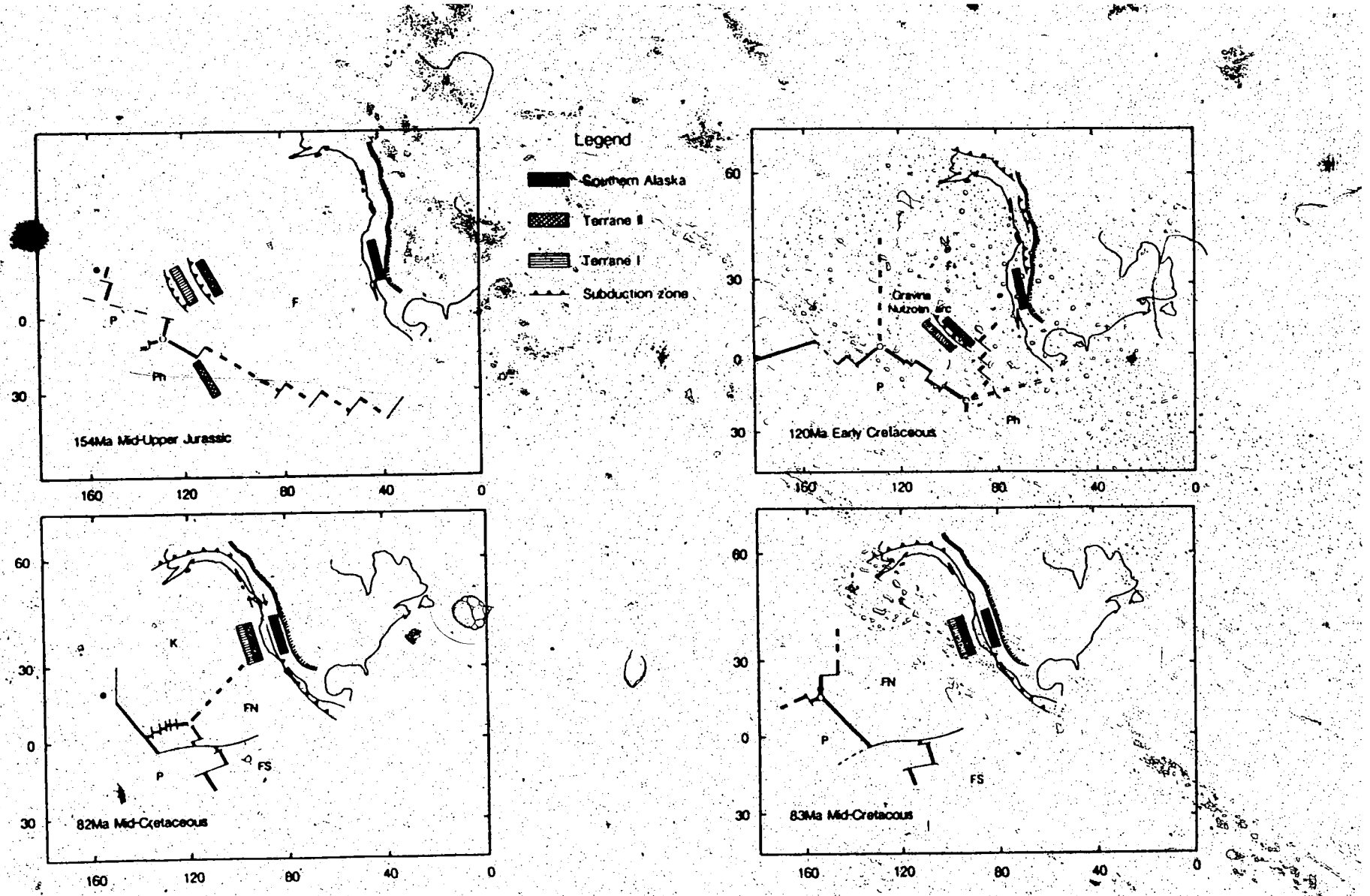

Fig. 17. Interaction of North America and the Pacific plates from the late Jurassic to the mid-Miocene. Also shown are the positions of Terranes I, II and southern Alaska, and the present location of the Hawaiian hot spot (•).

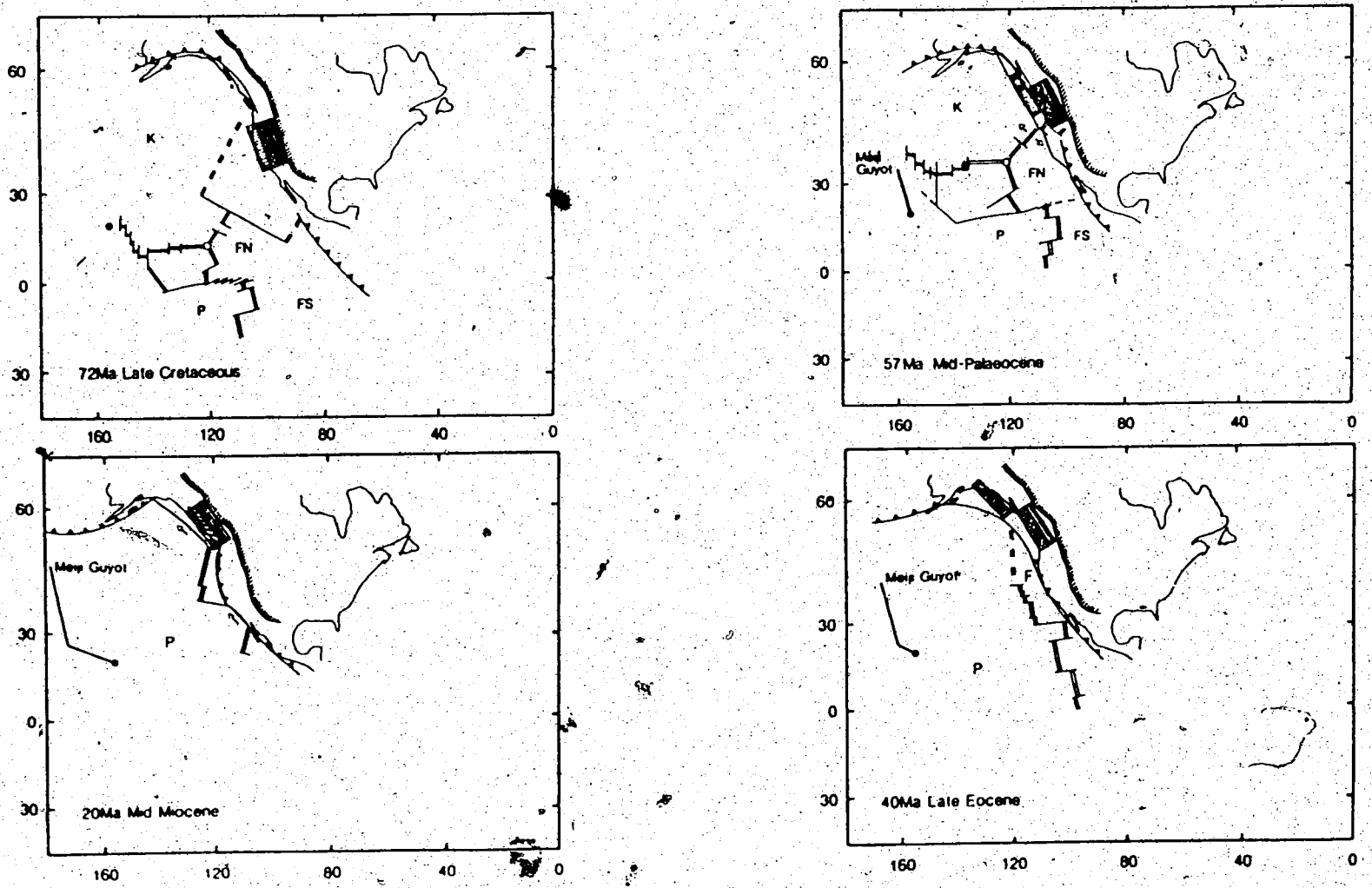
72Ma Late Cretaceous
57Ma Mid-Palaeocene
20Ma Mid Miocene
40Ma Late Eocene
Meiji Guyot
K
FN
FS
P
60
30
0
160
120
80
40

Fig. 17. contd.

northeast trending ridge (Woods and Davies 1982), and the separation of the remainder of the Farallon plate into Farallon North and Farallon South plates by transform faulting.

72 Ma Late Cretaceous

By the late Cretaceous southern Alaska and Terrane II had collided with the western margin of Terrane I forming the Coast Plutonic Complex (Monger and Irving 1980). Palaeomagnetic data gives an average position of 45°N for these Terranes at this time (Stone et al. 1982, Symons and Litalien 1984, Symons 1983, 1985). The location of the Kula-Farallon North ridge at this time is unknown; two extreme options (after Page and Engebretson (1984)) are illustrated . The northerly option, however, might interfere with the motion of southern Alaska. A ridge intersection with North America at 40°N , just south of the Terranes is more likely to have produced the observed northward translation.

Cenozoic to Recent

In the early Tertiary southern Alaska began to move northwards past Terrane II to its present position, possibly facilitated by transform faulting on the east-northeast trending Kula-Farallon North ridge (Wells et al. 1984). Accompanying strike-slip movement took place within Terranes I and II, as much as half the northward translation of these Terranes taking place in the early Tertiary (Symons 1985). The movement was accompanied by up to 45° clockwise rotation until the Terranes reached their present postion during the late Oligocene.

Magnetic anomalies in the northeast Pacific indicate a major reorganisation of the oceanic plates in the mid-Tertiary due to

cessation of activity on the Kula-Pacific ridge, caused by its collision with the Alaska-Aleutian arc. Timing of this event has been estimated between 56 (Byrne 1979) and 25 Ma (Jackson et al. 1972). The estimate of 43 Ma (Engebretson and Cox 1984) is preferred because it coincides with ages determined for the kink in the Hawaiian-Emperor island chain of 43.1 Ma (Dalyrimple and Clague 1976) and 37.8 Ma (McDougall 1979). As a result the Kula-Farallon ridge reorientated to a north-south axis, continuing the trend of the Farallon-Pacific ridge (Byrne 1979). The reconstruction is complicated by uncertainties in the position of southern Alaska during the mid-Tertiary.

Estimates for the timing of the intersection of the Farallon-Pacific ridge and North America vary from 55 Ma (Fox 1983) to as recent as 29 Ma (Atwater 1973). By 20 Ma much of the Farallon-Pacific ridge in the vicinity of southern California had been overidden by the continent with the development of the San Andreas fault system (Atwater 1970). In addition, the Farallon-North American plate convergence rate decreased significantly from 40 to 20 Ma, probably due to the resistance of increasingly young oceanic lithosphere to subduction as the proximity of the Farallon-Pacific ridge to the continent increased. The overall result of these events was a change from a predominantly right-lateral, strike-slip regime to an extensional environment within Terrane I during the mid-Tertiary. This in turn, affected the style of volcanism: calc-alkaline volcanism continued in response to the subduction of the Juan de Fuca and Pacific plates but back-arc extension can be considered responsible for the 17 to 6 Ma Columbia River basalts, and the 12 to 2 Ma Chilcotin basalts. In California, inland from the San Andreas fault system, extension unrelated to subduction resulted in the formation of

the Basin and Range Province from 15 Ma to the present.

V. Spences Bridge Group

Introduction

Volcanics of the Spences Bridge Group represent an arc built on the western margin of North America during the mid-Cretaceous. In southern British Columbia the Spences Bridge Group occur on the Quesnel, Cache Creek, Methow-Tyaughton and Stikine terranes (Fig. 1). To the north, rocks equivalent to the Spences Bridge Group occur on the western margin of the Stikine terrane as far as the Yukon-British Columbia border (Tipper et al. 1981). The exposures contain 50% clastic sediments and 50% calc-alkaline lavas (Thorkelson 1985), and are of tectonic significance because the Cretaceous is the accepted time of accretion of Terrane II to the western margin of Terrane I (Monger 1982).

The stratigraphy of the Spences Bridge Group has recently been revised (Thorkelson and Rouse, in prep.). A lower sequence, comparable to the Spences Bridge Group of Duffel and McTaggart (1952), Monger (1981, 1982), Monger and McMillan (1984), Thorkelson (1985) and Kingsvale Group of Preto et al. (1979), unconformably overlies late Triassic volcanics of the Nicola Group. The thickness of this unit exceeds 2400 m (Thorkelson 1985) and consists of ignimbrite flows, tuffs and agglomerates, with intercalated flows of basalt, andesite and rhyolite. An upper 600 m-thick unit, corresponding to the Upper Kingsvale Group of Duffell and McTaggart (1952), Kingsvale Group of Monger (1981, 1982), Monger and McMillan (1984), and amygdaloidal andesite unit of Thorkelson (1985), has been named the Spius Formation (Thorkelson and Rouse, in prep.). In contrast to the lower part of the Spences Bridge Group, the Spius Formation consists mainly of andesite

flows and contains only minor pyroclastic and sedimentary material.

Sampling was undertaken before this revision with the result that all but one of the samples collected belong to the lower part of the sequence.

Major Element Chemistry

Major and trace element data for 34 Spences Bridge Group volcanics are presented in Table 6. Silica contents range from 48 to 70%. The samples follow a calc-alkaline trend on an AFM diagram (Fig. 18) and on a FeO^*/MgO versus silica diagram (Fig. 19). Sample 2-101B lies in the tholeiitic field on these diagrams probably due to alteration. FeO^*/MgO ranges from 0.9 to 2.4, with an average of 1.5 . Six samples, 2-101F, 2-101I, 2-71C, 2-107, 2-71B, and 2-71G have FeO^*/MgO less than 1.1, and Mg-numbers greater than 67 (assuming $Fe_2O_3/FeO = 0.3$). All six have low silica (less than 55%) and high MgO (6 to 10%), and may represent primary melts from the mantle wedge. The remainder have lower MgO with Mg-numbers ranging from 49 to 67 .

On a K_2O versus SiO_2 diagram (Fig. 20) low, medium, and high K suites are recognised. Na_2O/K_2O ratios range from over 5 in the low K suites to less than 2 in the high K suites. K_2O exceeds Na_2O, and is unrelated to SiO_2 in the small number of samples from the high K suite. Thorkelson (1985) describes only low and medium K suites from exposures to the southeast of the study area which may suggest some regional variation.

TiO_2 and P_2O_5 contents are typically calc-alkaline, averaging 1.1% and 0.3% respectively.

Table 6.

Major and trace element chemistry of the Spences Bridge Group

	2-101I	2-101H	2-101F	2-71C	2-102A	2-69C	2-71F	2-107	2-71G
SiO_2	49.25	62.28	48.68	52.36	53.02	53.53	54.15	54.29	56.34
Al_2O_3	16.91	14.57	15.64	15.30	16.07	15.59	16.73	16.12	17.33
Fe_2O_3	9.99	7.39	11.22	9.63	10.02	10.41	8.79	8.70	7.40
MgO	9.89	3.71	9.18	9.13	6.34	4.77	5.57	8.94	6.65
CaO	9.94	5.16	9.36	8.32	9.04	7.13	8.49	6.35	6.32
Na_2O	2.51	4.64	3.47	2.60	3.12	3.84	3.48	2.90	3.28
K_2O	0.11	0.59	0.63	0.60	0.66	2.50	1.16	1.25	1.36
TiO_2	1.03	1.16	1.30	1.25	1.19	1.62	1.14	0.95	0.85
P_2O_5	0.20	0.36	0.31	0.43	0.36	0.43	0.32	0.31	0.32
S	0.01	0.01	0.02	0.20	0.01	0.01	0.01	0.03	0.01
MnO	0.15	0.13	0.19	0.18	0.16	0.17	0.17	0.16	0.13
Ba	144	176	289	346	581	1233	426	543	491
Nb	4	12	6	13	9	12	9	7	9
Zr	78	206	91	204	144	241	176	132	162
Y	20	27	15	24	24	32	26	24	21
Sr	616	418	580	760	756	794	691	690	754
Rb	6	14	16	10	11	37	15	19	20
Zn	89	75	88	73	82	85	74	82	64
Cu	101	59	69	56	54	97	76	56	61
Ni	22	9	79	87	13	11	145	77	28
mg	72	56	68	71	62	54	62	72	70

	2-102D	2-69A	2-70	2-69B	2-102E	2-102F	1-10	-102C	2-101G
SiO_2	58.07	59.79	60.25	60.52	67.19	69.66	50.	1.24	53.70
Al_2O_3	15.69	16.64	15.07	16.21	18.22	16.57	14.7	.72	18.45
Fe_2O_3	8.64	7.49	8.58	7.71	2.96	2.11	9.53	.21	8.84
MgO	4.64	4.19	4.01	3.03	0.58	1.32	6.21	.7	5.24
CaO	6.27	5.63	3.58	4.47	4.09	3.29	11.22		7.69
Na_2O	3.59	3.46	4.08	5.06	3.99	4.13	4.49		2.92
K_2O	0.94	1.40	2.01	1.63	2.04	2.38	1.60		2.05
TiO_2	1.45	0.97	1.61	1.04	0.45	0.36	1.32		0.83
P_2O_5	0.51	0.20	0.60	0.24	0.21	0.12	0.22	0.29	0.13
S	0.01	0.02	0.05	0.01	0.00	0.01	0.02	0.02	0.02
MnO	0.17	0.14	0.16	0.08	0.06	0.05	0.20	0.18	0.12
Ba	685	747	701	792	627	800	1135	1376	472
Nb	10	10	12	9	7	8	7	8	6
Zr	218	190	235	178	152	154	97	145	89
Y	36	23	35	22	19	12	17	23	17
Sr	413	811	534	845	286	374	875	595	610
Rb	16	21	40	33	37	47	27	44	45
Zn	107	73	94	64	53	40	65	87	70
Cu	30	73	55	68	9	9	49	62	43
Ni	4	23	1	22	9	4	90	43	16
mg	58	59	54	50	33	61	62	65	60

Table 6 contd.

	2-102B	2-101B	2-102H	2-102G	2-71A	2-71B	2-104A	2-104B	2-101C
SiO_2	57.26	57.90	60.60	63.30	68.56	54.59	54.08	57.63	55.22
Al_2O_3	15.45	22.44	16.39	19.38	15.61	16.72	17.91	17.06	15.34
Fe_2O_3	9.22	9.81	6.78	2.22	3.26	8.49	8.78	7.73	10.13
MgO	4.47	0.72	2.52	1.75	2.00	7.16	6.15	4.98	4.87
CaO	4.83	1.39	5.67	5.89	1.65	6.34	7.13	6.71	7.52
Na_2O	4.16	2.59	3.13	4.10	4.96	3.44	2.01	3.08	2.82
K_2O	2.52	2.82	3.27	2.77	3.12	1.87	2.61	1.48	2.08
TiO_2	1.40	1.79	1.13	0.39	0.55	0.97	1.00	0.97	1.44
P_2O_5	0.51	0.40	0.35	0.12	0.20	0.24	.18	0.20	0.43
S	0.00	0.01	0.01	0.01	0.01	0.02	0.01	0.02	0.02
MnO	0.18	0.14	0.13	0.07	0.08	0.15	0.15	0.15	0.14
Ba	1238	642	788	770	726	521	450	503	529
Nb	11	13	13	8	13	8	5	7	11
Zr	217	242	270	165	305	149	129	149	229
Y	35	38	34	14	31	20	27	24	30
Sr	379	443	405	406	453	823	493	671	642
Rb	35	58	65	54	65	31	43	20	34
Zn	102	91	84	33	56	67	88	82	86
Cu	51	61	30	4	22	78	63	32	85
Ni	4	19	7	4	7	34	14	7	18
mg	55		49	67	61	68	64	62	55

	2-71D	2-71E	2-103E	2-103B	2-105	2-106	2-107*
SiO_2	56.50	56.77	60.96	62.64	74.85	59.16	54.29
Al_2O_3	16.96	16.26	13.93	13.75	14.31	16.75	16.12
Fe_2O_3	8.46	9.25	8.43	7.33	2.29	6.86	8.70
MgO	3.76	4.95	5.08	3.02	0.27	4.08	8.94
CaO	7.08	6.23	5.07	5.86	1.29	6.76	6.35
Na_2O	3.60	3.33	4.13	4.67	5.46	3.68	2.90
K_2O	1.70	1.42	0.80	0.86	1.07	1.30	1.25
TiO_2	1.31	1.31	1.17	1.31	0.27	0.95	0.95
P_2O_5	0.34	0.31	0.27	0.45	0.10	0.35	0.31
S	0.06	0.01	0.00	0.01	0.01	0.01	0.03
MnO	0.22	0.21	0.16	0.19	0.07	0.11	0.16
Ba	660	728	37	313	415	597	543
Nb	10	10	8	8	11	15	7
Zr	231	221	159	185	202	198	132
Y	29	28	28	35	30	24	24
Sr	709	780	402	336	60	591	690
Rb	25	24	21	15	24	24	19
Zn	84	78	93	90	36	71	82
Cu	76	75	15	43	15	32	56
Ni	14	19	19			44	77
mg	53	58	61	51	23	60	72

* Spius Formation

Major elements recalculated to 100% on a volatile-free basis.
Trace elements in ppm.
mg calculated assuming $Fe_2O_3/FeO=0.3$

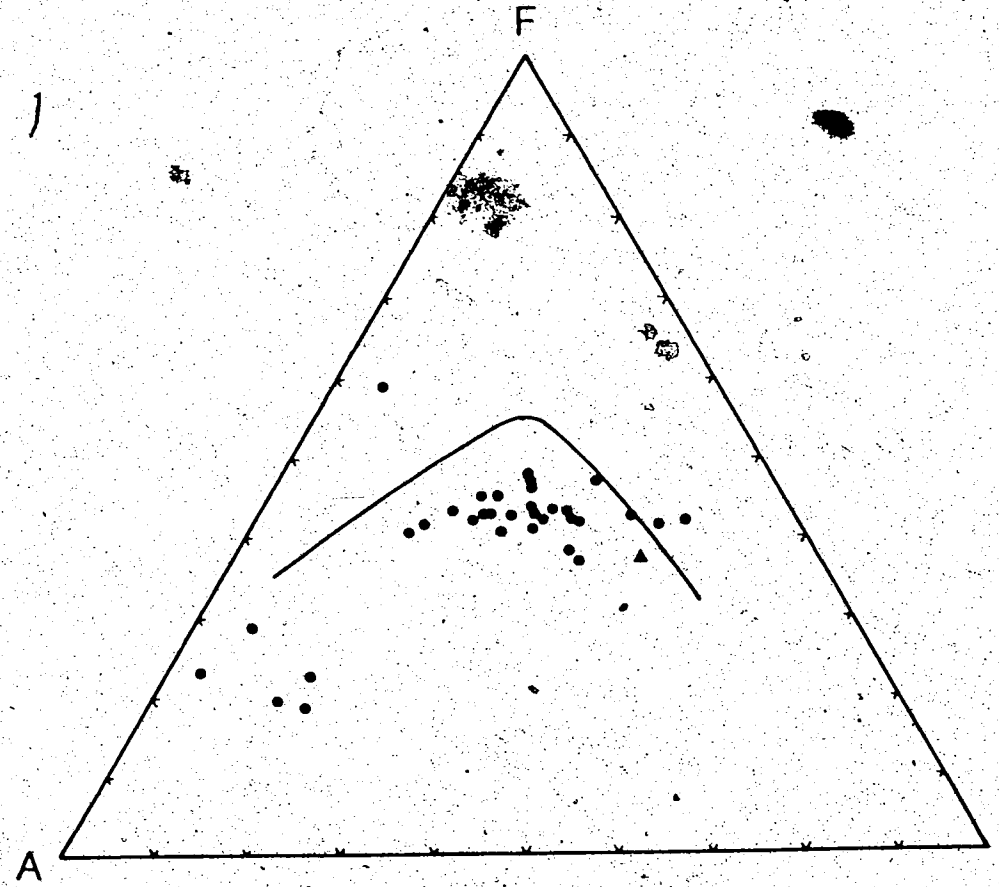

Fig. 18 AFM diagram for the Spences Bridge Group. A=Na,O+K,O, F=FeO+O 8998Fe,O,, M=MgO. • lower part of Spences Bridge Group ; ▲ Spius Formation. Tholeiitic- calc-alkaline boundary from Irvine and Barager (1971).

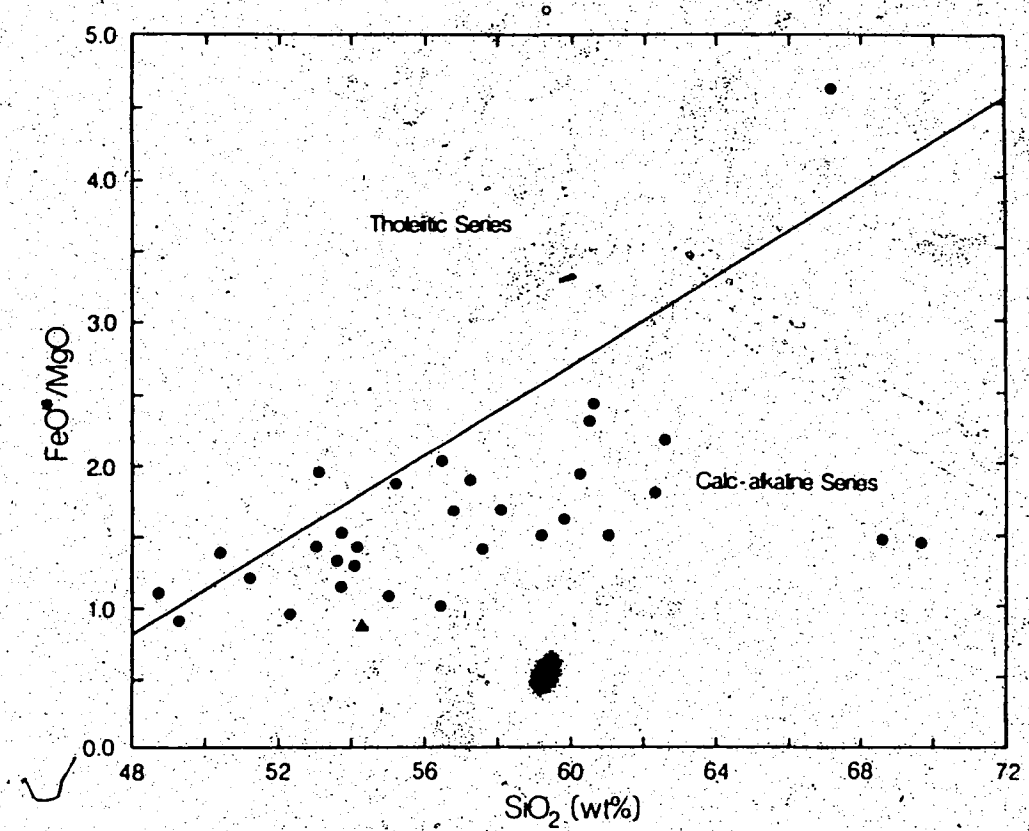

Fig. 19 Tholeiitic- calc-alkaline discrimination diagram for the Spences Bridge Group. FeO* refers to total iron as FeO. Symbols as for Fig. 18.

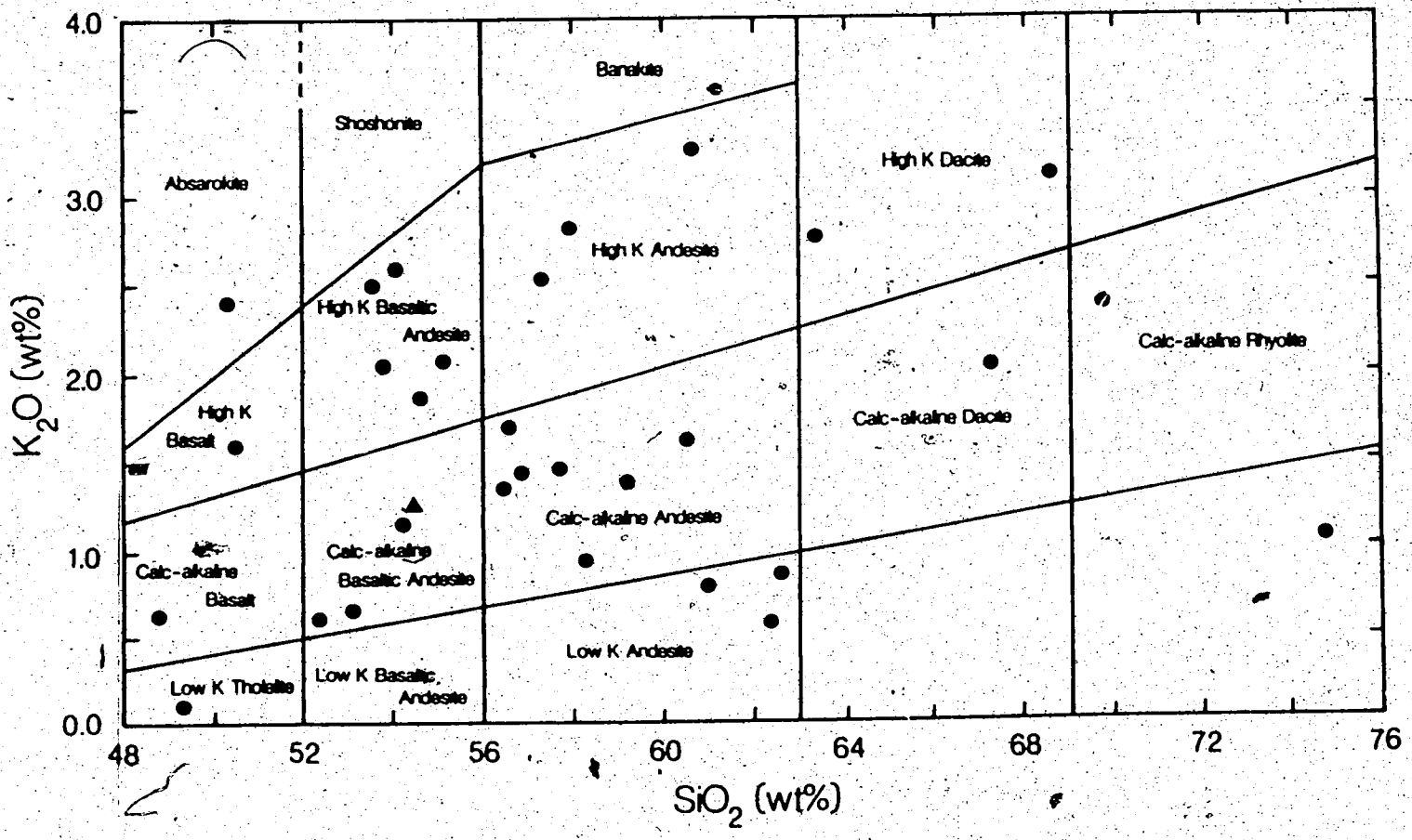

Fig. 20. K_2O versus silica classification diagram for the Spences Bridge Group. Symbols as for Fig. 18

Trace Element Chemistry

The variation in Rb, Sr, Ba, Y, Nb, Zr, and Ni with silica content are shown in Fig. 21 . The abundances of Rb and Ba show the same division into high, medium and low series as for K content. Thus the high K samples have 27 to 65 ppm Rb and 700 to 400 ppm Ba. In the low K samples, Rb contents increase from less than 10 ppm in the basalts to 25 ppm at high silica contents. Similarly, Ba increases from 150 to 450 ppm. Concentrations of Rb and Ba in the medium K suite are intermediate. Strontium, in contrast, is unrelated to K content, but shows a decrease from 900 to 300 ppm with increasing silica. Ni decreases from 90 ppm in the basalts to concentrations of less than 10 ppm. Ni contents are generally less than 30 ppm, and attest to the evolved nature of many of these rocks. Concentrations of Zr and Nb are high for calc-alkaline rocks, reaching concentrations of 270 ppm and 15 ppm respectively, between 54 and 56% silica (Fig. 21).

Nd-Sr Isotopic Composition

Nd and Sr isotopic data for 18 Spences Bridge Group samples are presented in Table 7. Fourteen samples (excluding 2-105) define a Rb-Sr isochron of 115±35 Ma with initial ratio 0.70334±8 (Fig. 22), in good agreement with the 112±5 Ma Rb-Sr isochron of Preto et al. (1979). The $^{87}Sr/^{86}Sr$ ratios measured by Preto et al. (1979) are significantly higher, resulting in a higher initial ratio of 0.70379±4 . The Spius Formation sample analysed here falls close to the 112 Ma isochron, whereas the two samples considered discordant by Preto et al. (1979) fall close to the 115 Ma isochron. The range in $^{87}Sr/^{86}Sr$ requires that either the Spences Bridge Group are isotopically heterogenous on a

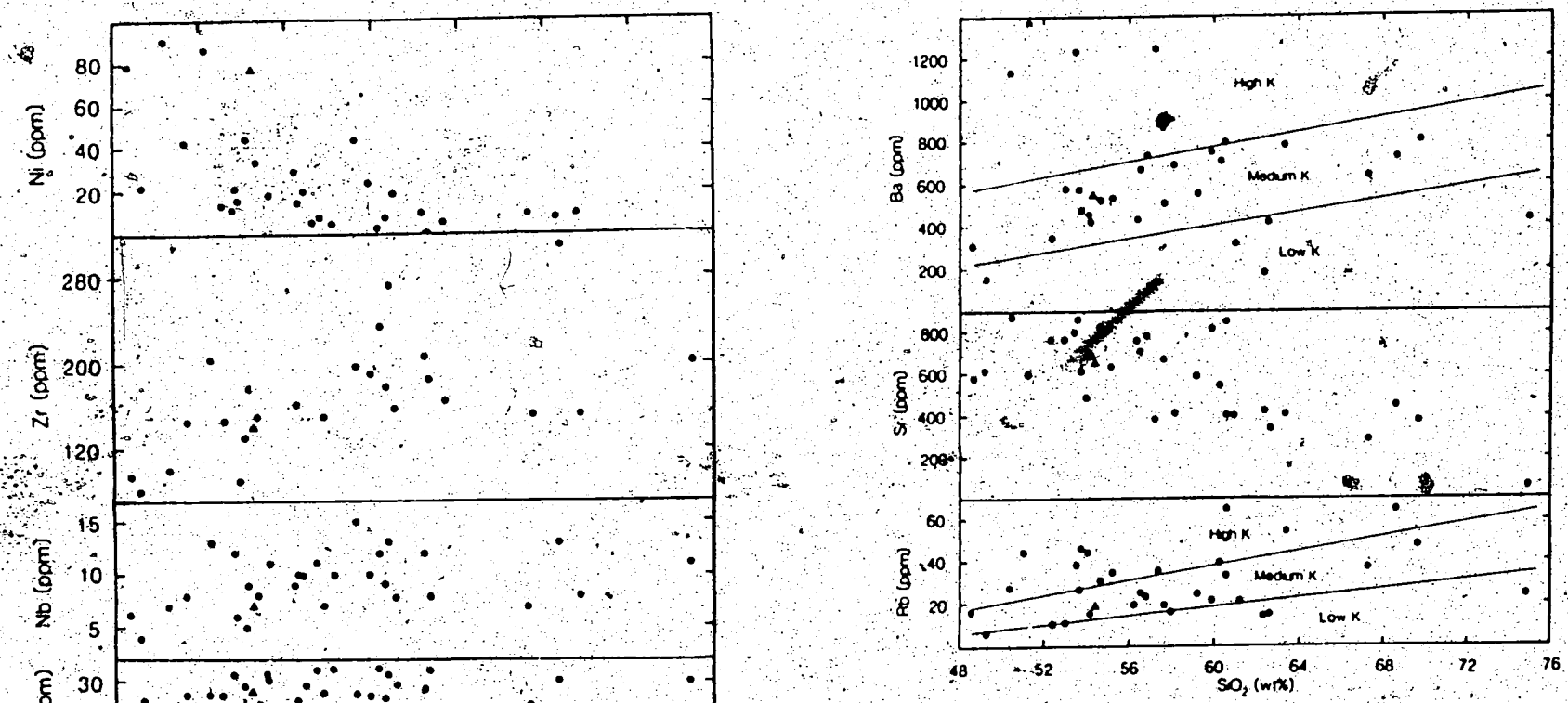

Fig. 21. Trace element variation with silica in the Spences Bridge Group. Symbols as for Fig. 18.

Table 7.

Nd and Sr isotopic composition of the Spences Bridge Group.

	Rb/Sr	$^{87}Sr/^{86}Sr$ m	$^{87}Sr/^{86}Sr$ c	Sm (ppm)	Nd (ppm)	Sm/Nd	$^{143}Nd/^{144}Nd$ m	$^{143}Nd/^{144}Nd$ c	εNd
Lower Series									
2-104B	0.029	0.70341±3	0.70328	4.23	18.0	0.236	0.512955±18	0.512852	+7.0
2-101B	0.121	0.70382±2	0.70322	7.08	31.3	0.226	0.512997±23	0.512899	+7.9
2-101C	0.053	0.70357±2	0.70333	6.02	26.5	0.227	0.512863±26	0.512764	+5.3
2-102F	0.126	0.70403±3	0.70345	2.25	12.3	0.182	0.512871±15	0.512792	+5.8
2-102D	0.039	0.70342±3	0.70324	6.71	29.5	0.228	0.512910±21	0.512813	+6.3
2-102E	0.129	0.70413±2	0.70354				0.512772±34		
2-102C	0.074	0.70383±4	0.70349				0.512938±12		
2-71A	0.143	0.70394±2	0.70328				0.512930±11		
2-101E	0.031	0.70360±3	0.70346				0.512925±21		
2-70	0.075	0.70358±3	0.70324				0.512908±11		
2-71D	0.035	0.70330±4	0.70314				0.512935±14		
2-101J	0.018	0.70343±2	0.70334				0.512895±16		
2-106	0.040	0.70371±2	0.70352	3.10	17.7	0.213	0.512847± 6	0.512754	+5.1
2-105	0.401	0.70556±2	0.70372				0.512914±20		
Spius Formation									
2-107	0.027	0.70373±2	0.70360	3.96	17.6	0.225	0.512878±17	0.512693	+5.6

( )m measured isotopic ratio

( )c isotopic ratio corrected to an age of 112 Ma.

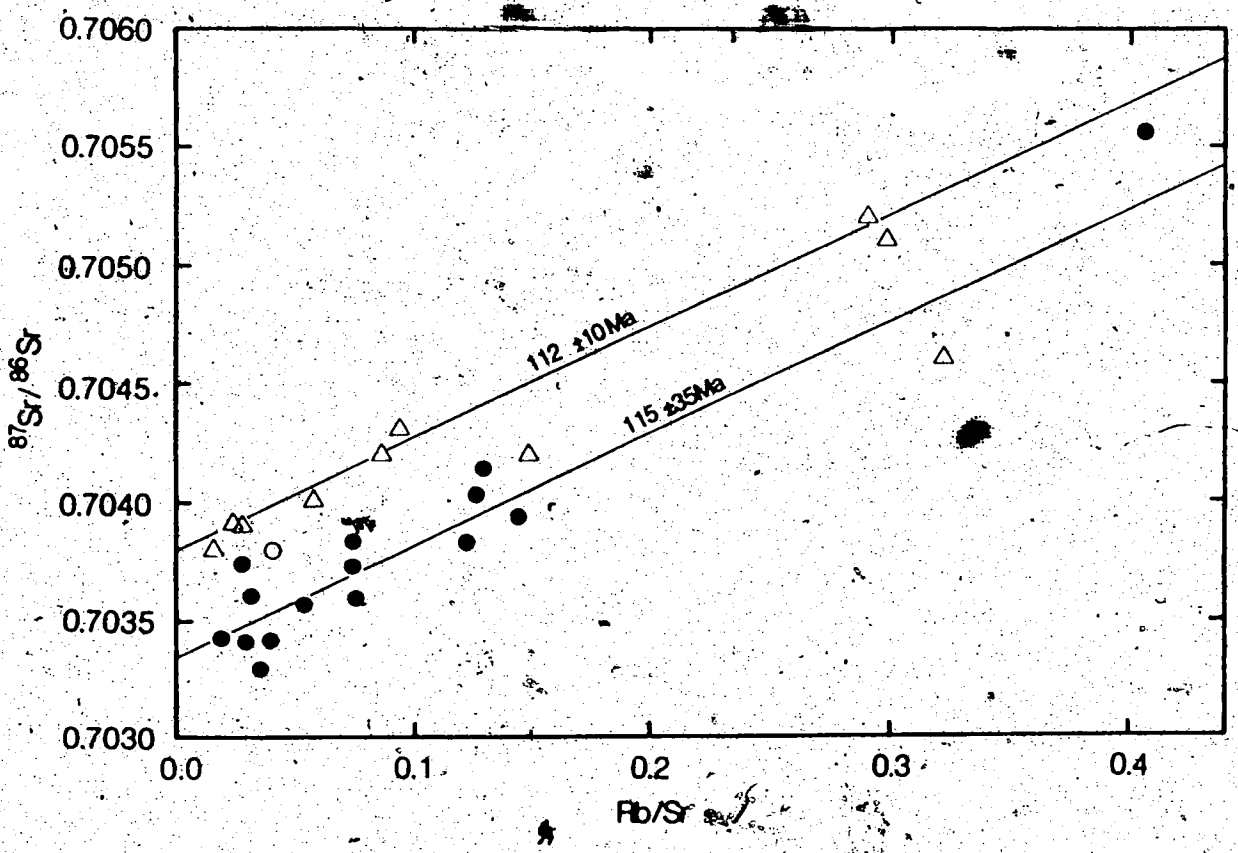

Fig. 22. Rb/Sr isochron diagram for the Spences Bridge Group: • lower part of Spences Bridge Group, this study; △ data of Preto et al. (1979); Spius Formation.

regional scale, or that the scatter results from post-magmatic alteration, in which case the data should be interpreted as a single group.

K-Ar ages of 94.4±3.4 Ma for the lower part of the Group, 91.7±3.3 Ma for the Spius Formation (Thorkelson 1985), and 91.6±3 Ma on an unspecified part of the Group (Church et al. 1979), are significantly lower than the Rb-Sr ages. The latter are considered more reliable despite the larger associated errors. The Nd and Sr data in Table 7 have, therefore, been corrected to an age of 112 Ma. The samples have ϵNd values from +5.5 to +8 and $^{87}Sr/^{86}Sr$ ratios from 0.7031 to 0.7036 , similar to the Nicola Group. On a Nd-Sr isotopic diagram (Fig. 23) the Spences Bridge Group overlap the fields of the Mariana (White and Patchett 1984, DePaolo and Wasserburg 1977) and Izu arcs (Nodha and Wasserburg 1981).

Crustal Contamination

The Spences Bridge Group contain abundant plagioclase, clinopyroxene and more rarely, orthopyroxene phenocrysts indicative of fractional crystallisation in shallow crustal magma chambers. At the time of extrusion of the Spences Bridge Group, the underlying Nicola Group volcanics have ϵNd between +4.5 and +7.5 . This range is directly comparable to that shown by the Spences Bridge Group but significant contamination is considered unlikely as no trend toward the elevated $^{87}Sr/^{86}Sr$ compositions which characterise the Nicola Group is observed. Furthermore, the Spences Bridge Group samples with highest silica contents also have the highest ϵNd values, above the range for the Nicola Group. Contamination by a high $^{143}Nd/^{144}Nd$ crustal component,

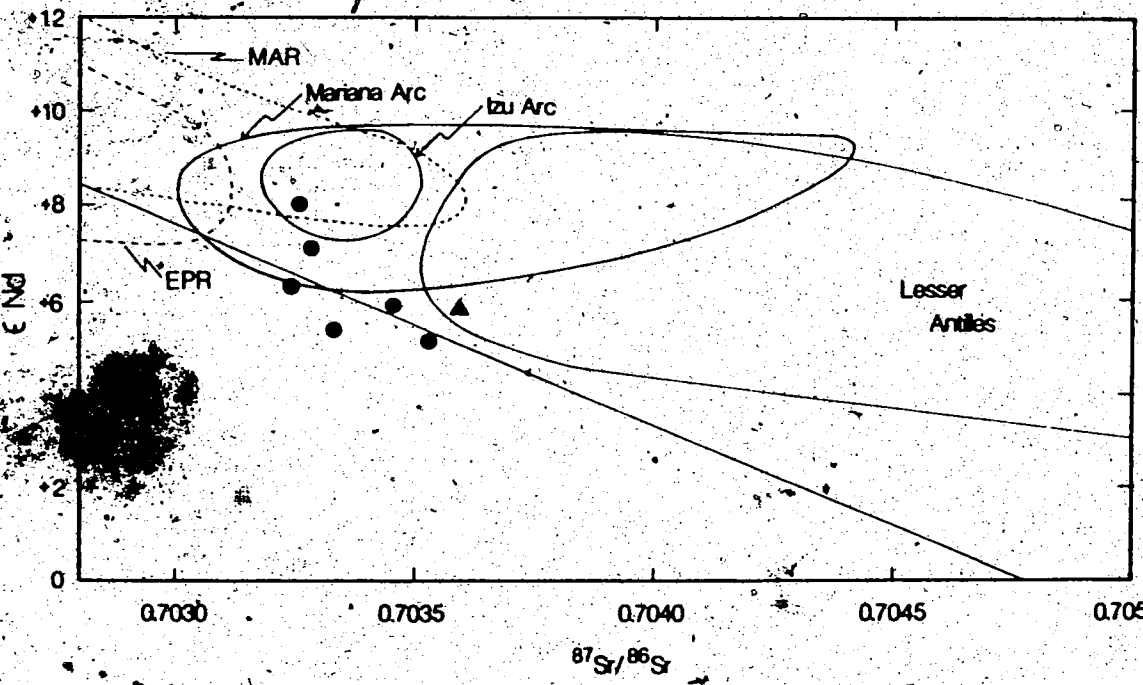

Fig. 23. Nd-Sr isotopic diagram for the Spences Bridge Group. Symbols as for Fig. 18. Other data sources given in legend to Fig. 14.

possibly the original oceanic crust on which the Nicola arc was built, could account for the ϵ_{Nd} values, but should also impart a trend toward high $^{87}Sr/^{86}Sr$ ratios if the oceanic crust had suffered seawater alteration. The range of isotopic compositions shown by the Spences Bridge Group, therefore, is considered to result primarily from source region heterogeneity.

Tectonic Setting

The age and location of the Spences Bridge Group requires the presence of an eastward-dipping subduction zone beneath the western margin of Terrane I during the mid-Cretaceous. The presence of such an arc conflicts with tectonic models (Chamberlain and Lambert 1985) which require a westward-dipping subduction zone beneath the eastern margin of Terrane I at this time.

The departure from the mantle trend shown by arc volcanics is attributed to the incorporation of a subducted slab-sediment component into the source region of the volcanics (Hawkesworth 1982, White and Patchett 1984). The isotopic signature of an island arc is thus largely a function of the nature and quantity of sediment subducted. The Sunda, Banda and Lesser Antilles arcs which have the highest $^{87}Sr/^{86}Sr$ and lowest $^{143}Nd/^{144}Nd$ ratios, have thick sequences of terrigenous sediment in front of the arc (White and Patchett 1984). The proximity of the isotopic compositions of the Spences Bridge Group to the mantle array suggests a low input of subducted sediment into the trench. This in turn could be used to support an argument that at the time of formation of the arc, Terrane II was not situated close to North America. Accretion of Terrane II to the western margin of Terrane I may be recorded by the

K-Ar data.

VI. Kamloops Group

Introduction

Early to mid-Eocene calc-alkaline volcanics of the Kamloops Group form part of a belt of early Tertiary volcanic activity which extended from Wyoming to the Yukon-British Columbia border (Ewing 1981a). The Kamloops Group is widespread throughout Terrane I (Fig. 24) and comprises a 1 to 3 km thick sequence predominantly of basalts and andesites. More silicic differentiates are limited to rare late-stage rhyolite plugs. K-Ar work (Ewing 1981a, and references therin) has delineated the main phase of volcanic activity to between 52 and 48 Ma, with sporadic eruptions continuing until 42 Ma.

During the time of eruption of the Kamloops Group, the tectonic regime was still dominated by right-lateral strike-slip motion. Terrane I underwent some 7° of northward translation and 15° of clockwise rotation during the Eocene and Oligocene (Symons 1985). This tectonic regime accounts for the distribution of the volcanics in a series of small fault-bounded basins linked by a more extensive fault system on which displacements of as much as 12 km have been suggested (Ewing 1981a). Within the basins, the more basaltic rocks were erupted from fissures or low shield volcanoes, whilst the andesites formed large cone complexes (ibid.).

Mineralogy

The mineralogy of the Kamloops Group comprises phenocrysts of augite, pigeonite and labradorite in a groundmass of andesine laths with interstitial pyroxenes and glass. Euhedral olivine phenocrysts, often

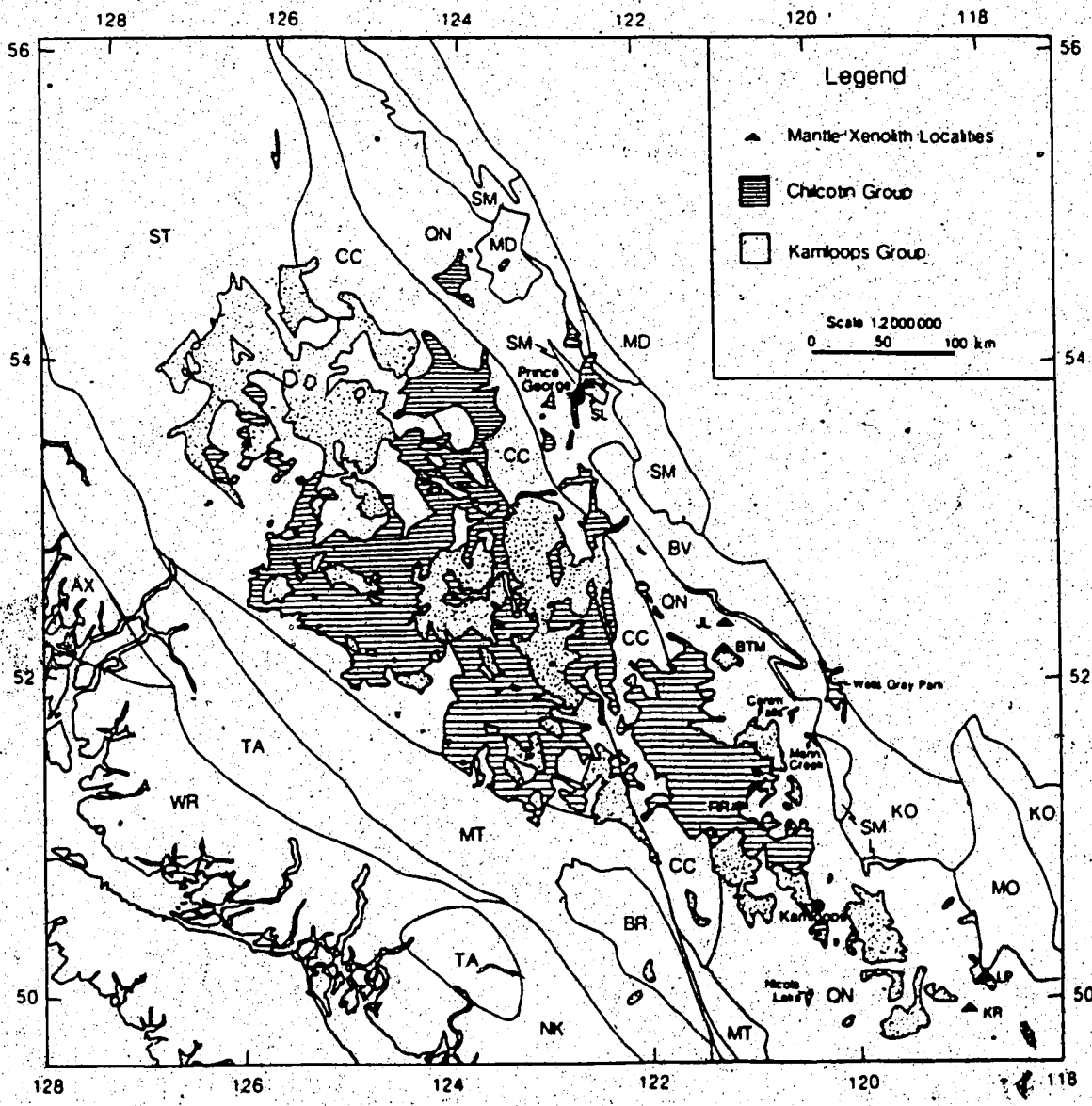

Fig. 24. Distribution of Kamloops Group and Chilcotin Group rocks in southern British Columbia. Terrane designation as for Fig 1. Also shown are the positions of the Summit Lake (SL), Jacques Lake (JL), Big Timothy Mountain (BTM), Lightning Peak (LP) and Kettle River (KR) xenolith localities (after Tipper et al. 1981, Monger and Berg 1984).

with glomeroporphyritic texture similar to the pyroxenes, are common in the more basic samples. Euhedral magnetite and, more rarely, hornblende or biotite, may also occur.

Major Element Chemistry

The major and trace element chemistry of the Kamloops Group has been described in detail by Ewing (1981b). However, the analyses of 52 Kamloops Group volcanics presented in Table 8. show some important differences in the relative abundances of rock types. The silica contents of the samples in this study range from 51 to 74%, although most are andesites with between 55 and 63% SiO_2. The samples of Ewing (1981b) cover a wider silica range (49 to 77%) but are mostly basalts and basaltic andesites. Discrepancies between the alkali contents presented here and those of Ewing (1981b) are evident on the K_2O versus SiO_2 classification diagram (Fig. 25). Only four samples, 1-20A, 2-27A, 2-27B and 2-54A lie in the absarokite-shoshonite-banakite field in Fig. 25 , compared to one third of the analyses of Ewing (1981b). These differences are considered to reflect sampling bias rather than analytical error or any regional variation. The results suggest that the intermediate rocks are at least as abundant as those of basic composition.

The calc-alkaline nature of the volcanics is readily apparent from the minimal iron enrichment on both AFM (Fig. 26) and FeO^*/MgO versus silica (Fig. 27) diagrams. Five samples, 1-14A, 1-14B, 1-19D, 1-19L and 2-54A, have FeO^*/MgO less than 1.1 and Mg-numbers greater than 67 (assuming $Fe_2O_3/FeO = 0.3$). All five have SiO_2 less than 56%, MgO greater than 6.5%, and may represent primary mantle-derived melts. TiO_2 contents

Table 8.

Major and trace element chemistry of the Kamloops Group.

	1-14A	1-14B	1-15A	1-16	1-19G	1-19J	1-11	1-13	1-15C
SiO_2	54.89	55.56	59.45	61.03	65.90	68.10	55.48	55.98	59.36
Al_2O_3	12.66	12.93	14.43	15.10	15.76	13.69	15.31	16.36	15.23
Fe_2O_3	8.92	8.70	7.81	6.87	4.02	3.77	7.97	9.03	7.54
MgO	9.17	8.27	3.64	2.93	1.56	2.62	6.12	3.81	3.68
CaO	7.78	7.66	6.84	5.22	3.06	3.14	8.90	7.16	5.44
Na_2O	2.98	3.10	3.44	4.29	4.77	3.99	1.91	3.81	4.17
K_2O	1.70	1.91	2.53	3.00	3.82	3.61	2.63	2.17	2.90
TiO_2	1.21	1.18	1.20	0.97	0.72	0.70	1.09	1.15	1.08
P_2O_5	0.49	0.53	0.48	0.46	0.30	0.29	0.41	0.34	0.48
S	0.07	0.04	0.03	0.02	0.03	0.05	0.01	0.02	0.02
MnO	0.13	0.12	0.16	0.11	0.07	0.04	0.15	0.16	0.09
Ba	1128	1167	1418	1373	2238	2033	1802	1428	1310
Nb	14	14	16	13	15	14	12	8	17
Zr	137	131	196	200	241	209	169	136	200
Y	21	20	22	20	19	16	23	24	22
Sr	885	866	875	754	869	873	880	683	848
Rb	30	27	52	75	98	71	39	54	70
Zn	83	79	84	77	66	66	91	84	81
Cu	50	48	38	32	35	26	52	48	48
Ni	175	147	59	42	39	41	36	35	64
mg	72	71	54	52	50	64	66	52	55

	1-21B	1-20A	1-19A	1-19B	1-19C	1-19D	1-17	1-18A	1-19L
SiO_2	57.55	61.65	55.26	54.73	54.79	56.81	59.04	73.32	55.61
Al_2O_3	15.79	12.38	15.15	15.09	14.78	13.66	15.40	14.68	13.54
Fe_2O_3	8.70	9.19	8.54	8.84	8.69	8.27	8.41	1.80	8.40
MgO	3.21	6.09	5.56	6.38	6.37	6.54	3.01	0.66	6.80
CaO	5.73	11.84	7.14	6.82	7.15	7.26	6.29	1.15	7.74
Na_2O	3.83	2.20	3.47	3.42	3.38	3.40	3.68	2.98	3.66
K_2O	3.05	3.24	2.90	2.79	2.89	2.36	2.36	4.98	2.29
TiO_2	1.41	1.18	1.26	1.24	1.23	1.16	1.14	0.29	1.17
P_2O_5	0.52	0.46	0.55	0.50	0.55	0.40	0.52	0.09	0.43
S	0.07	0.07	0.04	0.04	0.04	0.04	0.00	0.02	0.03
MnO	0.14	0.30	0.12	0.15	0.13	0.09	0.15	0.03	0.13
Ba	1490	1960	1331	1308	1318	1614	1036	1555	1498
Nb	13	9	11	11	12	11	11	12	10
Zr	157	117	128	126	130	155	190	189	143
Y	21	22	25	23	27	21	22	14	20
Sr	983	944	814	813	844	1207	676	222	1236
Rb	48	64	73	76	79	34	56	147	34
Zn	111	67	70	71	74	80	78	49	82
Cu	45	47	45	46	38	48	57	13	39
Ni	65	93	57	55	48	153	31	49	121
mg	48	63	62	65	65	67	48	48	67

Table 8. contd.

	2-25	2-26A	2-26B	2-26C	2-27A	2-27B	2-28	2-49A	2-49B
SiO_2	56.87	55.31	54.75	55.03	59.52	59.00	65.98	63.37	63.12
Al_2O_3	14.24	17.49	17.29	17.52	16.82	17.44	17.18	14.91	14.93
Fe_2O_3	8.78	8.50	7.86	8.46	6.35	5.96	3.71	6.77	6.35
MgO	6.61	4.61	4.52	4.56	2.44	2.55	1.54	2.03	2.71
CaO	5.76	5.80	8.25	7.10	4.59	4.27	3.43	4.79	5.17
Na_2O	3.34	3.85	3.34	3.40	4.46	4.22	3.33	3.71	2.90
K_2O	2.34	2.28	1.91	1.84	3.94	4.70	3.93	2.80	3.42
TiO_2	1.32	1.41	1.31	1.33	1.15	1.12	0.54	1.06	0.93
P_2O_5	0.56	0.62	0.58	0.58	0.63	0.60	0.29	0.40	0.36
S	0.03	0.02	0.02	0.03	0.01	0.05	0.01	0.00	0.01
MnO	0.15	0.10	0.16	0.15	0.08	0.11	0.06	0.07	0.09
Ba	961	1172	841	628	2250	2511	1896	1204	1233
Nb	16	20	18	19	25	28	15	16	13
Zr	200	254	227	231	363	414	287	256	250
Y	23	21	20	21	21	28	19	19	17
Sr	694	656	556	543	1162	1098	834	674	714
Rb	74	61	51	53	133	151	147	71	93
Zn	89	95	87	98	72	80	72	81	87
Cu	57	65	41	38	5			49	58
Ni	56	38	25	31	9	5	3	26	47
mg	66	58	59	58	49	52	51	48	52

	2-49C	2-49D	2-50A	2-50B	2-50C	2-50D	2-52	2-53	2-54A
SiO_2	65.25	63.35	61.42	61.76	60.85	61.88	62.04	61.13	51.76
Al_2O_3	14.09	15.11	15.04	15.29	15.42	15.38	14.71	15.15	16.31
Fe_2O_3	6.73	6.39	7.27	7.14	7.30	6.96	6.59	6.68	9.29
MgO	1.75	2.36	3.73	2.67	3.79	2.43	3.22	3.28	7.44
CaO	4.24	5.15	5.49	5.36	5.55	5.37	5.50	5.70	6.19
Na_2O	3.75	3.31	2.90	3.09	3.26	3.26	3.81	3.85	3.22
K_2O	2.75	2.89	2.48	3.08	2.13	3.12	2.46	2.45	3.72
TiO_2	1.02	0.95	1.13	1.11	1.11	1.08	1.02	1.05	0.91
P_2O_5	0.38	0.38	0.41	0.40	0.44	0.40	0.54	0.63	0.91
S	0.01	0.01	0.03	0.01	0.03	0.01	0.01	0.01	0.01
MnO	0.04	0.09	0.10	0.10	0.11	0.10	0.08	0.08	0.24
Ba	1179	1311	1100	1096	1146	1106	1133	1201	836
Nb	15	14	14	14	14	15	15	15	8
Zr	252	253	257	254	256	256	240	242	132
Y	18	17	19	20	20	20	19	20	27
Sr	643	739	657	656	668	659	784	836	808
Rb	86	68	74	93	63	88	76	75	50
Zn	85	83	87	89	93	88	95	90	84
Cu	48	54	41	40	45	44	17	30	33
Ni	18	42	23	27	23	30	29	37	7
mg	40	48	57	49	57	47	58	56	67

Table 8. cont'd.

	2-54B	2-54C	2-55	2-62	2-63	2-67	2-72A	2-72B	2-72C
SiO_2	60.39	60.52	62.13	70.25	70.29	70.48	59.89	60.33	59.06
Al_2O_3	15.17	15.25	15.17	16.42	16.40	15.98	15.49	15.16	15.83
Fe_2O_3	7.00	7.46	6.13	1.85	1.96	2.23	6.30	6.33	6.75
MgO	3.89	2.96	3.18	0.88	1.00	0.62	5.32	5.52	4.28
CaO	5.93	5.78	5.33	2.63	2.38	3.72	6.13	5.79	6.84
Na_2O	3.57	3.90	3.95	4.49	4.46	3.51	3.61	3.63	3.83
K_2O	2.29	2.31	2.56	2.93	3.01	2.63	1.92	1.94	1.92
TiO_2	1.06	1.14	0.95	0.32	0.33	0.57	0.88	0.86	0.95
P_2O_5	0.61	0.60	0.54	0.15	0.13	0.24	0.40	0.36	0.38
S	0.00	0.01	0.01	0.05	0.02	0.01	0.01	0.02	0.03
MnO	0.08	0.08	0.07	0.03	0.03	0.01	0.05	0.05	0.12
Ba	1049	1048	1147	1171	1158	1296	1022	995	1054
Nb	14	15	13	7	7	8	8	9	9
Zr	226	229	232	149	152	171	192	195	204
Y	21	20	18	4	5	15	15	13	14
Sr	781	791	783	624	596	1169	900	809	842
Rb	67	72	68	64	66	57	42	41	29
Zn	104	87	80	48	49	50	83	88	85
Cu	44	43	38	40	16	42	48	46	56
Ni	39	38	34	1	4	8	97	58	75
mg	59	50	57	55	56	41	68	69	62

	2-73	2-74A	2-74B	2-74C	2-75	2-76
SiO_2	66.59	63.09	62.03	66.03	57.30	56.88
Al_2O_3	13.19	16.93	16.75	15.60	14.12	15.54
Fe_2O_3	7.88	5.08	5.56	4.21	7.37	7.84
MgO	0.96	2.05	2.17	2.23	5.33	4.86
CaO	3.45	4.34	4.72	3.46	8.53	6.86
Na_2O	3.17	4.04	4.19	3.90	3.38	3.88
K_2O	2.89	3.38	3.43	3.61	1.99	2.00
TiO_2	1.14	0.59	0.64	0.51	1.22	1.35
P_2O_5	0.69	0.39	0.39	0.34	0.56	0.61
S	0.01	0.01	0.02	0.01	0.18	0.17
MnO	0.04	0.09	0.10	0.09	0.18	0.17
Ba	1640	2458	2512	2004	975	1036
Nb	19	12	12	11	12	14
Zr	279	226	227	216	204	227
Y	19	25	24	22	21	22
Sr	1005	1440	1499	1040	904	928
Rb	61	88	90	95	43	47
Zn	88	81	87	68	81	105
Cu	35		12	12	39	49
Ni	25	1	3	1	55	54
mg	24	51	50	57	65	61

Major elements recalculated to 100% on a volatile-free basis.
Trace element abundances in ppm.
mg calculated assuming $Fe_2O_3/FeO=0.3$

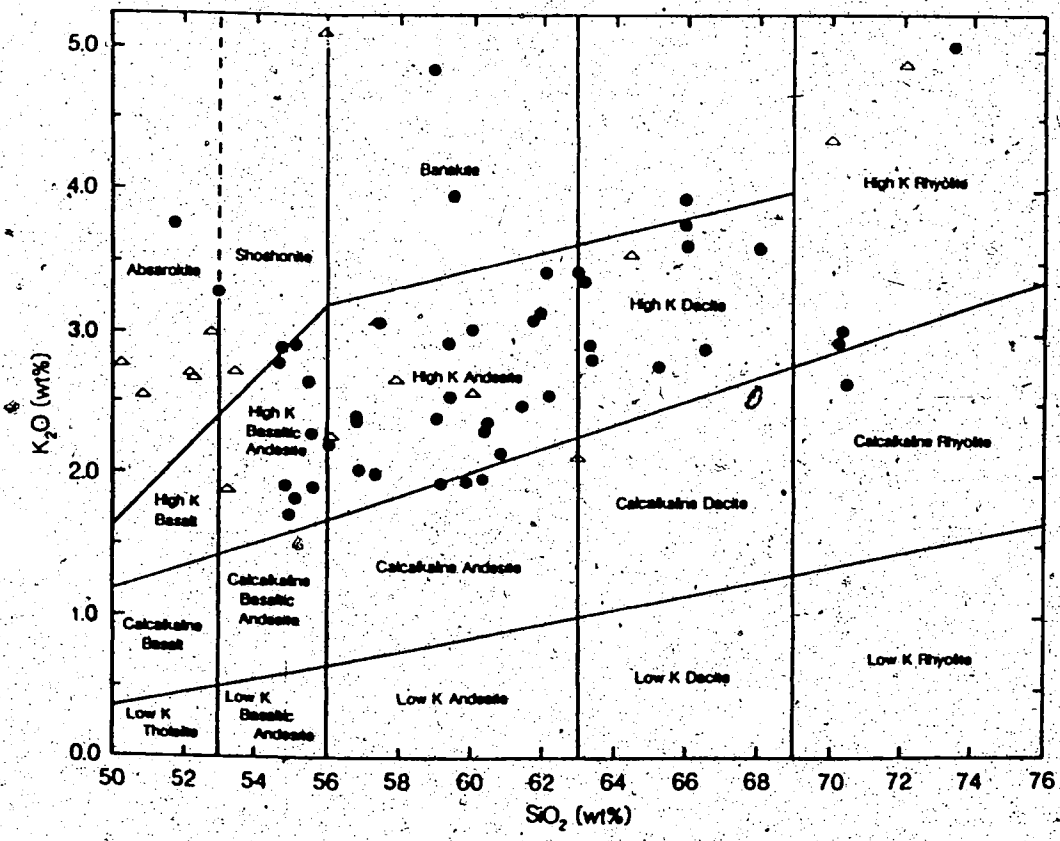

Fig. 25. K_2O versus silica classification diagram for the Kamloops Group. Data sources: •this study; △ Ewing (1981b).

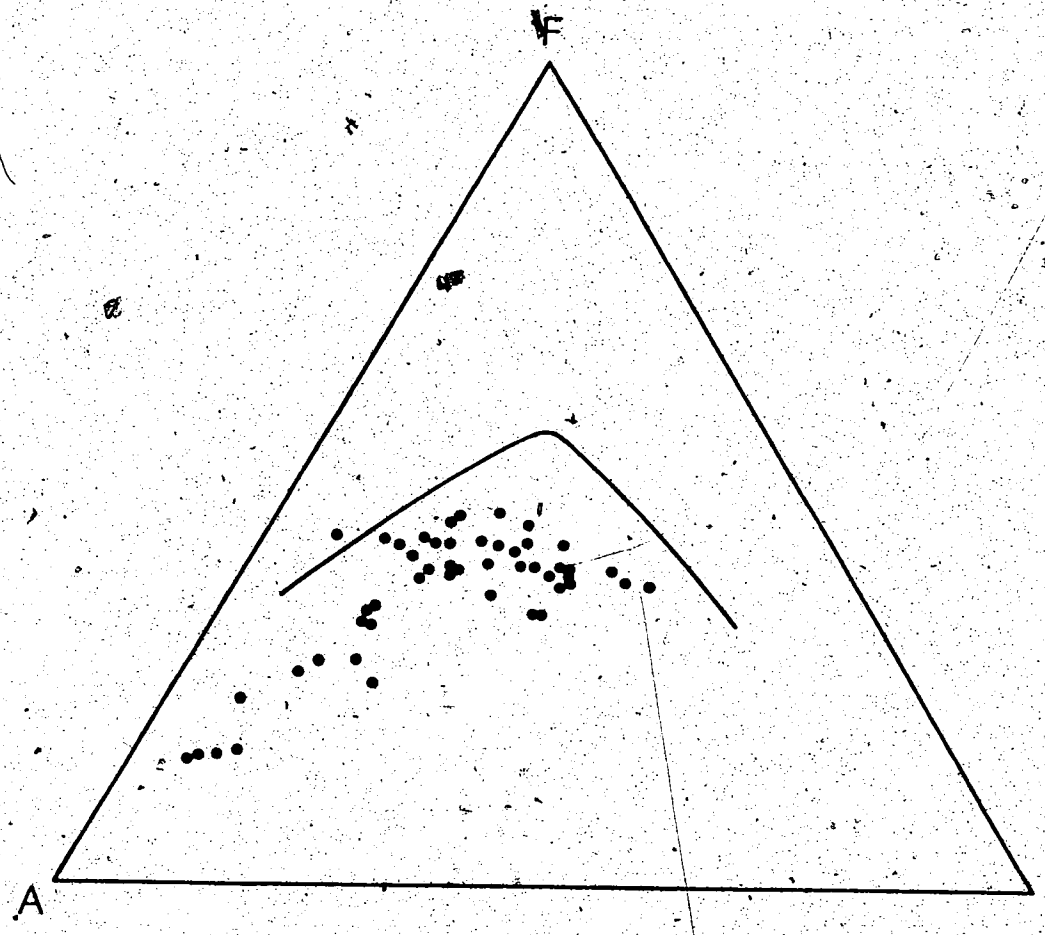

Fig. 26. AFM diagram for the Kamloops Group. A=Na,O+K,O, F=FeO+0.8998Fe,O,, M=MgO. Tholeiitic/ calc-alkaline boundary from Irvine and Baragar (1971).

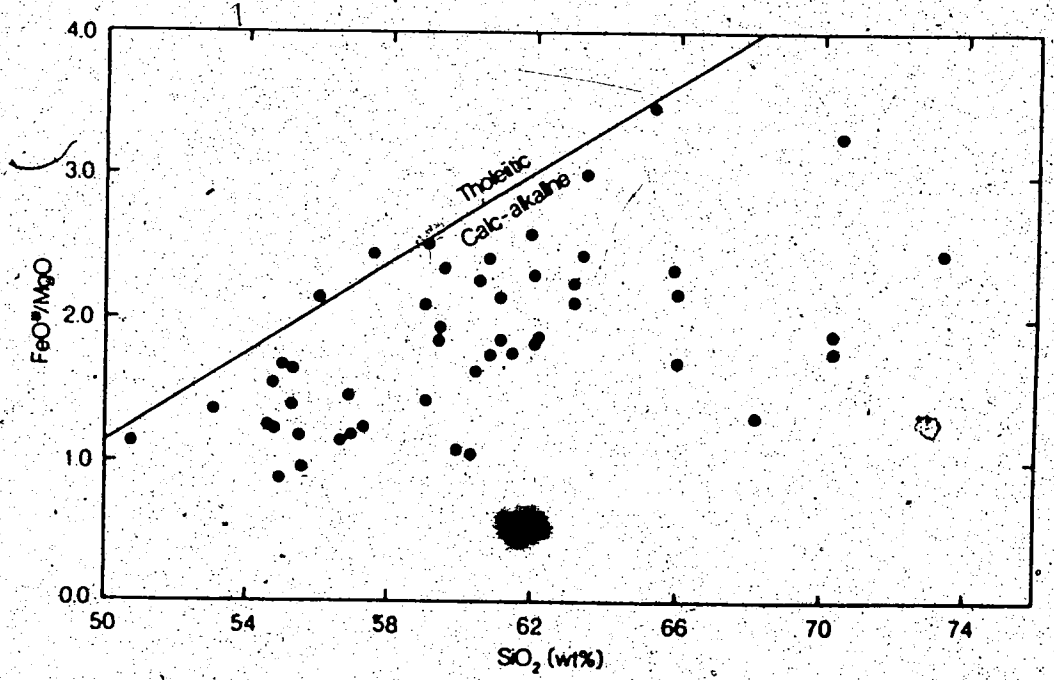

Fig. 27. Tholeiitic- calc-alkaline discrimination diagram for the Kamloops Group. FeO* refers to total iron as FeO.

of the Kamloops Group (less than 1.0%) are typically calc-alkaline, whereas the P_2O_5 contents, which reach 0.9%, are unusually high.

Trace Element Chemistry

The Kamloops Group are characterised by very high Ba and Sr contents. In the basalts and basaltic andesites Ba may reach 1500 ppm, Sr 1250 ppm. Concentrations of Zr (130 to 400 ppm) and Nb (8 to 28 ppm) are high for calc-alkaline rocks. Rb ranges from 30 to 150 ppm, showing a close covariance with the K content. Ni contents reach 175 ppm in the basalts with Mg-numbers greater than 67, but are generally less than 40 ppm, indicating an evolved origin for most of the samples.

Nd-Sr Isotopic Composition

Nd and Sr isotopic compositions of the Kamloops Group are presented in Table 9. The data have been corrected for an age of 50 Ma. Where not measured, Sm/Nd was estimated by comparison with similar samples. This approximation increases the errors by less than 0.2 ϵ Nd units because of the restricted Sm/Nd range (0.15 to 0.21) and young age of the Kamloops Group. Only 2-74C and 2-27A (both belonging to the shoshonite suite), and rhyolite 1-18B, have Sm/Nd less than 0.17 ; therefore, a more realistic increase would be less than 0.05 ϵNd units.

On a Nd-Sr isotopic diagram (Fig. 28) all samples lie within the mantle array, the more depleted samples overlapping the more enriched basalts of the Chilcotin Group. The Kamloops Group fall almost entirely between the fields for the Grande Ronde, Wanapum and Imnaha basalts of the Columbia River Province. The slightly positive ϵNd values and low $^{87}Sr/^{86}Sr$ ratios, are inconsistent with the high Nd/Sm and Rb/Sr ratios

Table 9.

Nd and Sr isotopic composition of the Kamloops Group

	Rb/Sr	$^{87}Sr/^{86}Sr$ m	$^{87}Sr/^{86}Sr$ c	Sm (ppm)	Nd (ppm)	Sm/Nd	$^{143}Nd/^{144}Nd$ m	$^{143}Nd/^{144}Nd$ c	εNd
1-17	0.083	0.70406±1	0.70389	5.67	29.3	0.195	0.512806±16	0.512768	+3.8
1-18B	0.662	0.70588±2	0.70452	2.93	19.0	0.154	0.512742±16	0.512742	+2.7
1-14A	0.034	0.70431±2	0.70424	5.92	31.5	0.188	0.512737±17	0.512700	+2.5
1-19B	0.093	0.70453±2	0.70434	5.25	25.5	0.206	0.512762±25	0.512722	+2.9
2-63	0.111	0.70404±2	0.70381	3.02	17.2	0.175	0.512829±17	0.512795	+4.4
2-50D	0.133	0.70421±3	0.70394	5.89	31.1	0.188	0.512819±22	0.512782	+4.1
2-74C	0.091	0.70498±2	0.70479	6.59	40.5	0.163	0.512646±15	0.512614	+0.8
2-27A	0.114	0.70545±2	0.70522	7.53	50.2	0.152	0.512502±14	0.512472	-1.9
1-11	0.044	0.70488±2	0.70478			0.20	0.512610±28	0.512571	0.0
1-20A	0.068	0.70434±3	0.70420			0.20	0.512736±32	0.512697	+2.4
1-21B	0.049	0.70417±3	0.70407			0.19	0.512887±20	0.512850	+5.4
1-19C	0.094	0.70432±2	0.70413			0.20	0.512770±28	0.512731	+3.1
1-19J	0.081	0.70428±2	0.70412			0.17	0.512730±15	0.512697	+2.4
1-19A	0.090	0.70445±2	0.70426			0.20	0.512743±17	0.512704	+2.6
1-15C	0.075	0.70442±2	0.70426			0.19	0.512682±14	0.512645	+1.4
2-73	0.061	0.70415±3	0.70403			0.17	0.512848±22	0.512815	+4.7
2-52	0.097	0.70426±3	0.70406			0.17	0.512884±27	0.512 [illegible]	+5.4

( )c isotopic ratio corrected to an age of 50 Ma

( )m measured isotopic ratio.

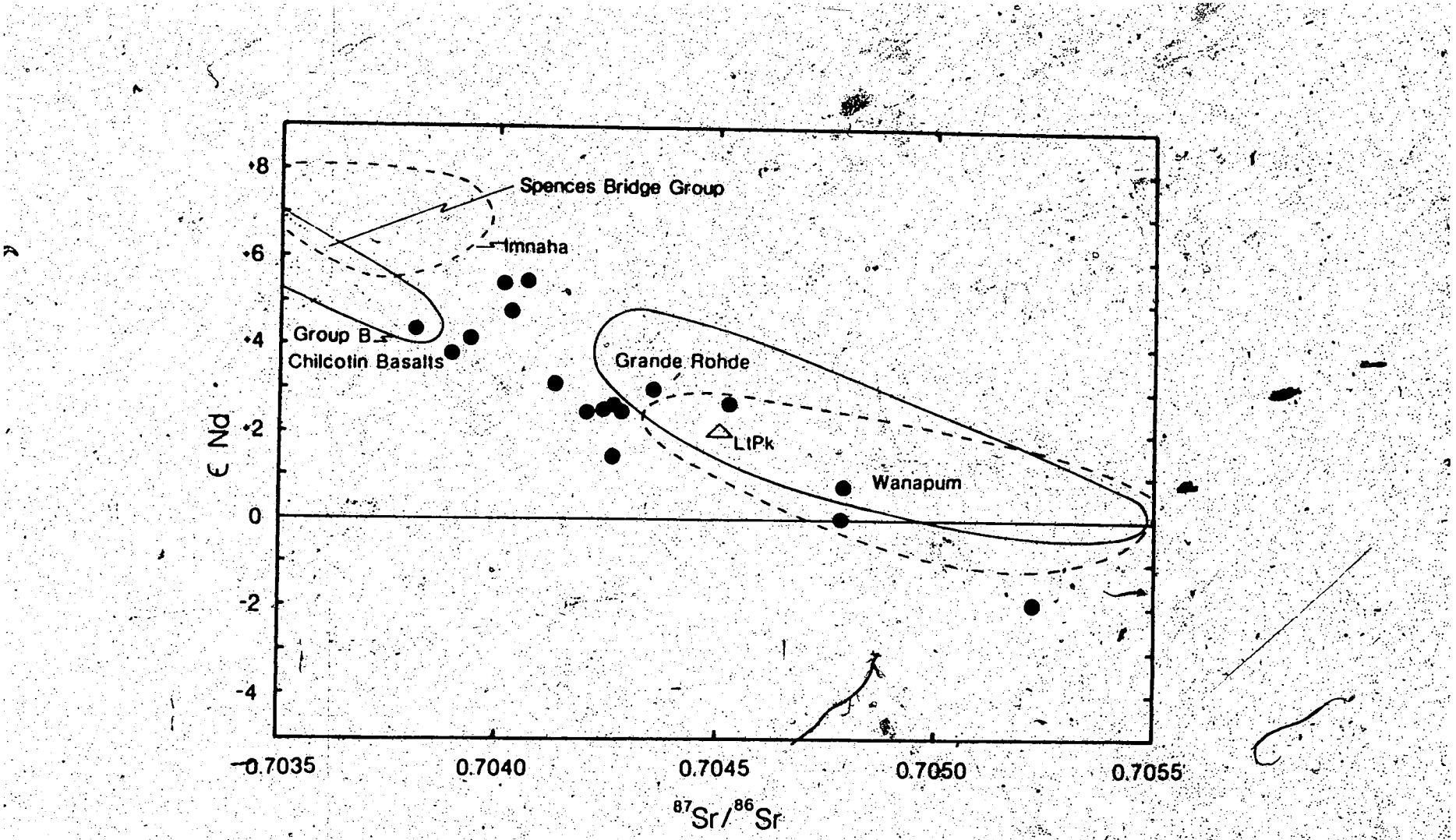

Fig. 28. Nd-Sr isotopic diagram for the Kamloops Group. Other data sources: Lesser Antilles (Hawkesworth and Powell 1979, Hawkesworth et al. 1979, White and Patchett 1984), Columbia River basalts (Carlson et al. 1981, Carlson 1984).

(0.04 to 0.11) and indicate long term low Nd/Sm and Rb/Sr in the source region.

Crustal Contamination

Ewing (1981b) suggested that an eastward increase in $^{87}Sr/^{86}Sr$ of the Kamloops Group resulted from contamination by underlying Precambrian continental crust, the extent of which was delineated by a line running approximately north-south along 120°W through Kamloops. Exposures to the east of this line were demonstrated to have $^{87}Sr/^{86}Sr$ ratios of 0.7068 to 0.7078 compared to ratios of 0.7038 to 0.7042 for those to the west. An objection to this interpretation is that geophysical evidence (e.g. Gough 1986) shows the Precambrian crust to terminate at the Rocky Mountain Trench or, in southern British Columbia, within the Kootenay Arc, well to the east of the Kamloops Group. Unfortunately, no exposures to the east of this inferred line were collected as sampling was focused on obtaining a cross-section of Terrane I along a line southwest-northeast, perpendicular to the strike of the volcanics. No evidence for any regional variation in $^{143}Nd/^{144}Nd$ or $^{87}Sr/^{86}Sr$ was noted in this study. Samples 2-27A and 1-11 are from the northeast corner of the study area and should represent the most distant activity from the arc front. Both have high $^{87}Sr/^{86}Sr$ and low $^{143}Nd/^{144}Nd$ ratios, but similar enrichment was also noted in samples from the southwest. The model of Ewing (1981b) is further challenged by many of the samples here having $^{87}Sr/^{86}Sr$ ratios within the range 0.7042 to 0.7058 suggested to divide the exposures.

Crustal contamination may be estimated from plots of $^{87}Sr/^{86}Sr$ or $^{143}Nd/^{144}Nd$ versus SiO_2 (Fig. 29). The diagram shows a scatter which

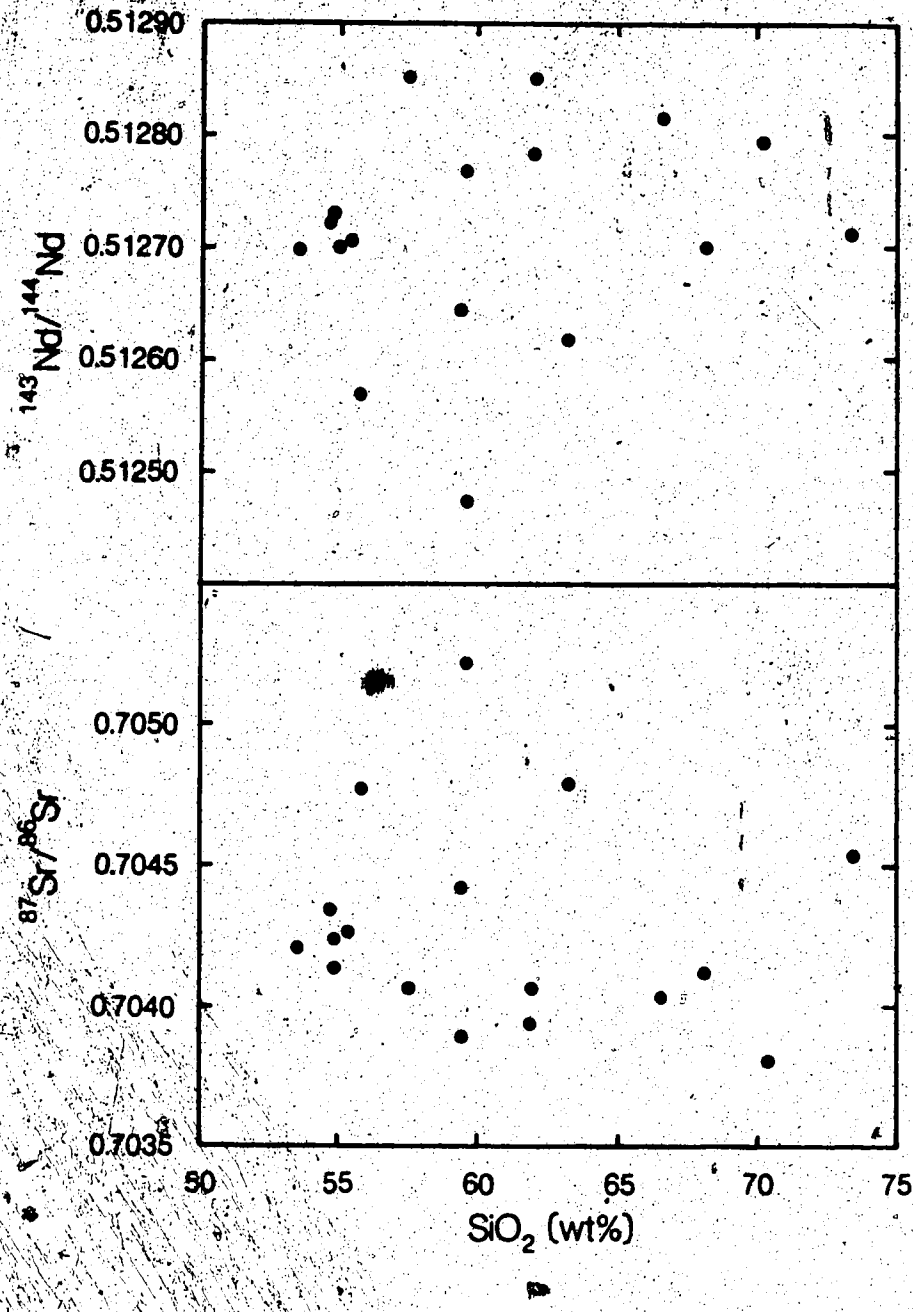

Fig. 29. Assessment of crustal contamination in the Kamloops Group: (a) $^{87}Sr/^{86}Sr$ versus SiO_2; (b) $^{143}Nd/^{144}Nd$ versus SiO_2 .

indicates lower $^{87}Sr/^{86}Sr$ and higher $^{143}Nd/^{144}Nd$ ratios with increasing SiO_2. This is exactly the opposite expected for contamination with old crustal material and suggests either original mantle heterogeneity, or contamination by oceanic crust which forms a basement to the underlying terranes. Mantle heterogeneity is favoured as the most primary lavas have isotopic compositions approaching the median for the group, which would require two distinct types of contamination to account for the higher and lower isotopic ratios of the other samples. In addition, no regular increase in $^{143}Nd/^{144}Nd$ or decrease in $^{87}Sr/^{86}Sr$ with increasing silica is noted where successive flows (1-19A,L series), presumably from the same vent, have been analysed.

Crystal Fractionation

The Kamloops Group volcanics were considered the result of a two stage fractionation process by Ewing (1981b). For samples with greater than 65% SiO_2, low pressure differentiation in shallow crustal magma chambers was invoked to explain the reduction of plagioclase and absence of pyroxene. The paucity of rhyolites suggests that this process was only of local importance. However, Rb/Sr ratios higher than those of the more primary lavas (which have Rb/Sr ratios from 0.028 to 0.032), indicate some degree of plagioclase fractionation for most samples. Differentiation trends between 50 and 65% SiO_2 were modelled by amphibole fractionation as indicated by the decrease in K/Rb (Fig. 30) and increase in FeO^*/MgO (Fig. 27) with increasing silica. Amphibole is rarely observed in the Kamloops Group, although it may have dehydrated during magma ascent. Clots of plagioclase, pyroxene and magnetite, observed in thin section, may represent relics of this process (Stewart

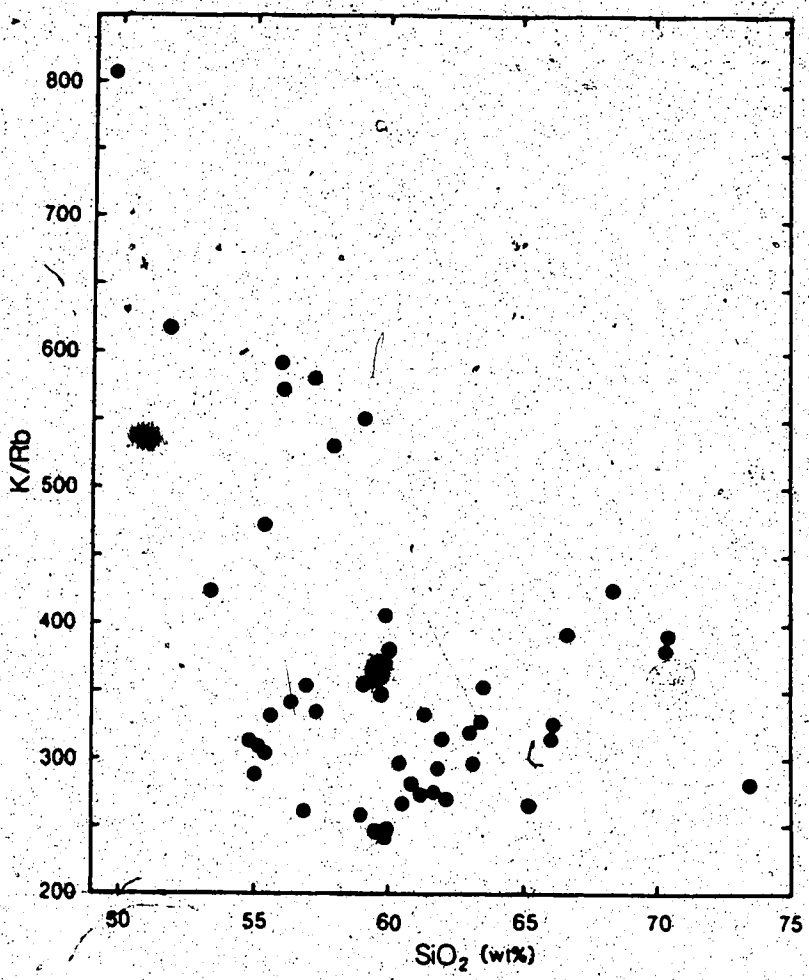

Fig. 30. K/Rb variation with [illegible] the Kamloops Group.

1975). Recharging and mixing of magmas is indicated by the variation of Ni at low MgO contents.

Petrogenesis

High Y contents indicate that garnet was not a residual phase in the source region of the Kamloops Group (Ewing 1981b). The depth to the base of the crust (30 to 35 km) precludes the existence of a plagioclase lherzolite stability field; therefore, the Kamloops Group are concluded to have originated within the spinel lherzolite facies. The source region must have been unusually rich in P, Zr and Nb to account for the high concentrations of these elements in the lavas. The calc-alkaline nature of the volcanics requires a hydrous melt. In Fig. 29 the amphibole-bearing spinel lherzolite LtPk (described in detail in Chapter 8) has similar $^{143}Nd/^{144}Nd$ and $^{87}Sr/^{86}Sr$ ratios to the Kamloops Group and is suggested as possible source material.

Tectonic Setting

The origin and tectonic setting of the Kamloops Group is important to the understanding of early Tertiary tectonics in British Columbia because the volcanics mark the last activity before the late Eocene plate reorganisation. The principal difficulty explaining the calc-alkaline nature of the Kamloops Group is the distance inland of the exposures, some 400 km from the nearest possible trench for a subduction-related origin. Subduction beneath Terrane II from the late Cretaceous to early Tertiary is indicated by the plutons of this age in the Coast Plutonic Complex (Souther 1977). However, it is not known whether the time of emplacement of the plutons overlaps that of the

extrusion of the Kamloops Group. If the Coast Plutonic Complex is interpreted as a metamorphic welt resulting from the collision of Terrane II with Terrane I (Monger et al. 1982) the existence of a subduction zone is not essential..

Plate reconstructions are inconsistent with a subduction zone off the west coast during the early Tertiary. The proximity of the Kula-Farallon ridge and its orientation perpendicular to the margin of Terrane II (Fig. 17) suggests that the motion between North America and the Kula and Farallon plates should have been strike-slip in nature. Further problems arise with the position of southern Alaska. In the model of Wells et al. (1984) (from which Fig. 17 is largely drawn) southern Alaska is placed off the western margin of Terrane II. Allowing for uncertainties in the position and orientation of the Kula-Farallon ridge, this would result in an even greater trench-arc distance.

From K_2O contents at 60% silica, Ewing (1980b) postulated an origin for the Kamloops Group above a northeast dipping subducted slab underlying Terrane I at a depth of 200 to 300 km. This depth is considerably greater than the 100 to 150 km suggested for most arcs (Gill 1980) and suggests that the K^{40} depth relationship is inaccurate. Any subducted slab during the early Tertiary should have been been at shallow depth, undeplating the continent, as the proximity of the Kula-Farallon and Farallon-Pacific ridge systems would have resulted in the slab being relatively young and buoyant.

The presence of a relict imbricate subduction zone beneath Terrane I after the accretion of Terrane II has been postulated by Goodwin (1978). Although it is unlikely that such a slab could have survived from its origin at 80 Ma, it would have served to enrich the

subcontinental mantle with the formation of minerals such as amphibole. Partial melting 30 Ma later in response to a different tectonic regime may have resulted in the generation of the Kamloops Group.

VII. Chilcotin Group Basalts

Introduction

The Chilcotin basalts form a 50000 km² plateau of late Miocene to Pliocene age in Central British Columbia (Fig. 24) (Bevier 1983b). A back-arc setting has been suggested for the basalts (ibid.) because of the presence of coeval calc-alkaline volcanics of the Pemberton belt, 150 km to the west. The stratigraphy of the plateau is poorly known but K-Ar dating (ibid.) has recognised two eruptive phases between 10 and 6 and between 3 and 2 Ma. The Chilcotin Group is thus contemporaneous with the Saddle Mountains basalts of the Columbia River Province 400 km to the south, but differ significantly in eruptive style. The Chilcotin basalts are of the basaltic plains type (Greeley 1982), with localised flows being erupted from low shield volcanoes (Bevier 1983b) often marked by late-stage gabbro or dolerite plugs (Farquharson 1973). The thickness of the plateau varies between 5 and 140 m (Bevier 1983a). Outside the main plateau, at localities such as Mann Creek and Canim Falls (Fig. 24), isolated activity continued until as recently as 0.5 Ma (C. Hickson, pers. comm.).

The plateau is cut in the north by alkaline basalts of the Anahim Belt (Bevier et al. 1979). The belt decreases in age from Miocene in the west to Recent in the east, and has been interpreted as lithospheric fracturing above the northern end of the subducted Juan de Fuca Plate, or to represent the trace of a mantle hot spot beneath British Columbia (Bevier et al 1979). The youngest centres in the belt occur in the Wells Gray Park area to the east of the Chilcotin plateau. Older basalts at this locality, the 0.56 to 0.15 Ma valley-filling assemblage of Hickson

and Souther (1984), are geochemically similar to the Chilcotin Group and have been included in this study.

Major and Trace Element Chemistry

The Chilcotin basalts were classified as transitional (Bevier 1983a) because both petrographically and on an AFM diagram (Fig. 31) they resemble alkali basalts yet fall in both the alkaline and subalkaline fields on a silica versus alkalis diagram (Fig. 32). The basalts analysed in this study were both nepheline- and hypersthene-normative, although quartz normative basalts have also been reported (Bevier 1983a). Silica contents range from 47 to 53% (Table 10). Silicic differentiates are unknown. Al_2O_3 ranges from 13 to 18 % and CaO from 6 to 11%. MgO is more variable (5 to 14%) and is inversely correlated with CaO (Fig. 33). Mg-numbers range from 46 to 67, but for most samples are between 60 and 65. Alkali contents are generally high, Na_2O and K_2O ranging from 2 to 5% and from 0.5 to 1.7% respectively, with Na_2O/K_2O ratios of 3.5 to 4.5 . TiO_2 reaches a maximum of 3% but is usually between 1.5 and 2%. P_2O_5 correlates positively with TiO_2 and reaches concentrations of up to 0.6%.

All samples show depletion in Rb (9 to 25 ppm), Ba (140 to 400 ppm) and Y (18 to 25 ppm). The overall low Rb contents are in contrast to a marked enrichment in Sr in several samples (Fig. 34). Nb contents range fro 15 to 30 ppm, and for many samples are only slightly higher than in the Kamloops Group. Zr contents of 120 to 230 ppm are lower than in the Kamloops Group.

REE data are presented in Table 11 and as chondrite normalised plots in Fig. 35. All samples show slight to moderate LREE enrichment

Table 10.

Major and trace element chemistry of the Chilcotin Group.

Group A	Alkali basalts and dolerites								
	2-99C	2-99D	RR	2-99A	2-99B	2-66B	2-66C	2-66D	2-30B
SiO_2	52.08	52.29	50.16	49.41	56.59	57.48	48.26	44.89	44.58
Al_2O_3	16.76	17.78	15.09	8.39	15.15	15.87	13.32	12.21	15.15
Fe_2O_3	9.00	8.46	11.63	9.62	9.14	8.23	11.21	11.53	14.65
MgO	4.09	3.62	7.17	14.30	5.48	5.44	10.44	12.75	6.79
CaO	9.28	8.95	7.49	15.82	8.01	6.62	8.59	11.19	9.55
Na_2O	4.54	4.74	4.63	0.79	2.96	3.48	2.91	1.79	2.35
K_2O	1.63	1.69	0.98	0.56	0.81	1.22	1.97	1.57	2.67
TiO_2	1.92	1.74	2.12	0.79	1.21	1.08	2.42	2.49	3.69
P_2O_5	0.58	0.61	0.55	0.11	0.43	0.39	0.67	1.33	0.42
S	0.00	0.00	0.01	0.00	0.03	0.01	0.05	0.08	0.02
MnO	0.13	0.12	0.17	0.20	0.18	0.17	0.16	0.17	0.17
Ba	331	320	478	140	196	499	683	592	197
Nb	32	32	33	2	7	13	38	69	55
Zr	142	146	229	30	84	164	179	281	208
Y	19	18	25	16	37	23	25	30	29
Sr	822	825	713	180	381	684	508	757	374
Rb	16	15	15	17	26	16	33	28	59
Zn	67	66	78	50	62	65	85	81	96
Cu	60	68	71	37	52	40	68	37	71
Ni	104	102	152	103	14		158	163	64

Group B								
	2-11	2-11A	2-11B	1-12	2-14A	2-14C	2-14D	2-24A
SiO_2	48.54	49.26	48.95	47.92	48.21	47.87	48.07	49.19
Al_2O_3	15.25	16.97	17.04	13.58	14.48	14.67	14.59	16.70
Fe_2O_3	12.24	11.31	11.09	14.62	13.00	12.89	13.02	11.31
MgO	6.54	5.23	5.05	7.20	8.58	8.54	8.53	4.86
CaO	9.30	10.39	10.93	8.96	9.14	9.39	9.03	9.72
Na_2O	3.64	3.81	3.72	2.97	3.39	3.44	3.62	4.25
K_2O	1.53	0.81	0.89	0.88	0.89	0.85	0.86	1.28
TiO_2	2.13	1.69	1.81	3.01	1.79	1.81	1.75	2.05
P_2O_5	0.59	0.35	0.35	0.57	0.32	0.33	0.34	0.47
S	0.06	0.00	0.00	0.02	0.00	0.00	0.00	0.00
MnO	0.18	0.17	0.17	0.20	0.19	0.19	0.18	0.15
Ba	282	291	284	199	314	309	319	405
Nb	30	20	18	30	18	22	18	31
Zr	150	129	125	208	125	128	124	180
Y	24	22	22	29	23	22	23	23
Sr	568	460	476	443	401	437	402	546
Rb	23	21	18	20	22	23	23	20
Zn	81	78	76	106	98	90	92	72
Cu	53	37	18	27	50	48	33	48
Ni	88	49	48	50	171	168	159	105

Table 10. contd.

	2-24B	2-24C	2-24D	2-29	2-41A	2-43B	2-44B	2-81
SiO_2	47.70	49.32	47.68	49.00	50.18	49.04	49.49	48.91
Al_2O_3	15.32	15.85	15.25	13.81	15.21	14.43	14.69	15.61
Fe_2O_3	12.81	12.04	12.79	13.69	13.54	13.19	12.28	12.25
MgO	6.98	6.26	7.93	8.58	4.75	6.69	7.28	6.89
CaO	9.85	9.01	9.30	8.60	9.98	9.62	9.41	9.27
Na_2O	3.63	3.98	3.64	3.15	2.47	3.72	3.63	3.84
K_2O	1.09	1.08	0.98	0.69	1.54	0.83	0.79	0.90
TiO_2	2.05	1.91	1.87	1.94	1.88	1.94	1.90	1.78
P_2O_5	0.37	0.40	0.38	0.37	0.28	0.35	0.37	0.35
S	0.00	0.00	0.00	0.00	0.01	0.01	0.01	0.03
MnO	0.19	0.16	0.18	0.18	0.13	0.17	0.15	0.17
Ba	335	367	343	209	222	276	233	464
Nb	24	27	24	15	18	27	26	24
Zr	143	159	138	113	31	145	158	161
Y	24	21	21	24	22	21	23	24
Sr	459	495	459	372	1061	418	445	451
Rb	26	15	22	20	13	10	9	14
Zn	86	89	85	107	95	102	92	81
Cu	44	43	44	65	36	40	50	75
Ni	155	133	173	143	102	190	169	130

Group C

	2-36	2-37A	2-37B	2-38	2-40	2-41B	2-42	2-43A	2-44A
SiO_2	47.66	48.10	47.70	50.49	49.86	48.56	49.60	49.07	50.16
Al_2O_3	13.37	15.55	15.31	12.82	14.81	13.45	12.86	12.70	15.09
Fe_2O_3	13.44	12.55	12.80	13.17	13.09	13.10	13.18	13.38	11.63
MgO	12.75	7.09	7.24	11.30	7.81	10.36	12.28	13.25	7.17
CaO	8.76	9.34	9.74	7.24	8.38	9.29	7.16	6.43	7.49
Na_2O	1.95	4.31	4.03	2.43	3.33	2.67	2.09	1.75	4.63
K_2O	0.31	0.73	0.76	0.63	0.66	0.52	0.57	1.18	0.98
TiO_2	1.36	1.68	1.83	1.44	1.53	1.55	1.80	1.67	2.12
P_2O_5	0.21	0.46	0.39	0.30	0.33	0.28	0.28	0.37	0.55
S	0.01	0.02	0.00	0.01	0.01	0.01	0.01	0.02	0.01
MnO	0.19	0.17	0.18	0.17	0.17	0.19	0.16	0.17	0.17
Ba	139	286	277	205	195	180	233	256	478
Nb	9	22	21	15	14	13	16	25	33
Zr	84	119	120	108	114	94	127	133	229
Y	21	22	23	19	23	23	20	19	21
Sr	246	465	458	312	339	458	293	602	899
Rb	12	19	20	9	9	16	8	21	15
Zn	89	104	109	102	98	102	97	97	78
Cu	24	39	40	53	100	109	35	52	71
Ni	49	142	147	153	135	131	184	257	152

Major elements recalculated to 100% on a volatile-free basis.
Trace elements in ppm.

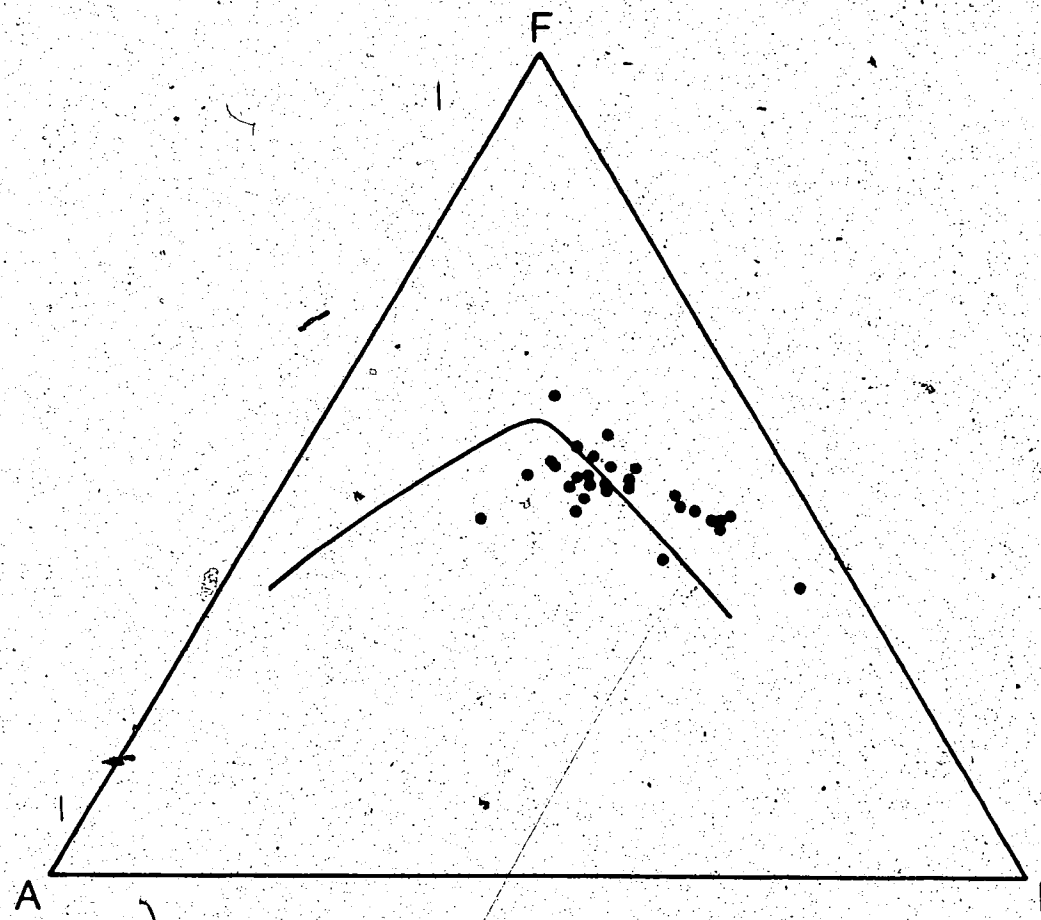

Fig. 31. AFM diagram for the Chilcotin Group. A=Na$_2$O+K$_2$O, F=FeO+0.8998Fe$_2$O$_3$, M=MgO. Tholeiitic- calc-alkaline boundary from Irvine and Baragar (1971).

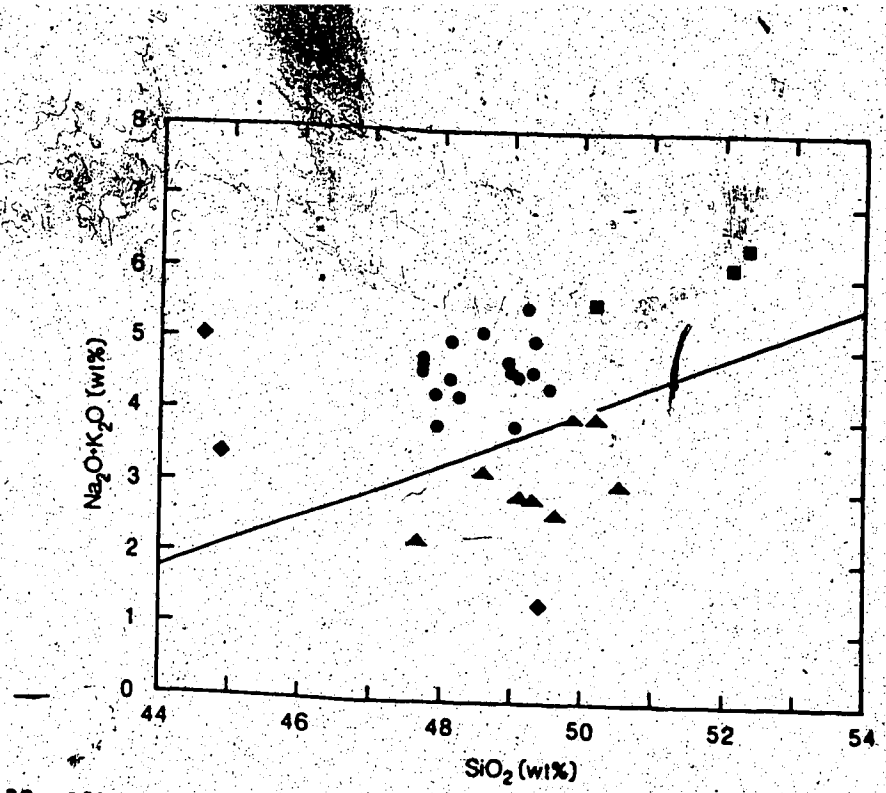

Fig. 32. Alkalis versus silica diagram for the Chilcotin Group; ■ group A; ● group B; ▲ group C; ◆ alkaline basalts. Alkaline-subalkaline dividing line from Irvine and Barager (1971).

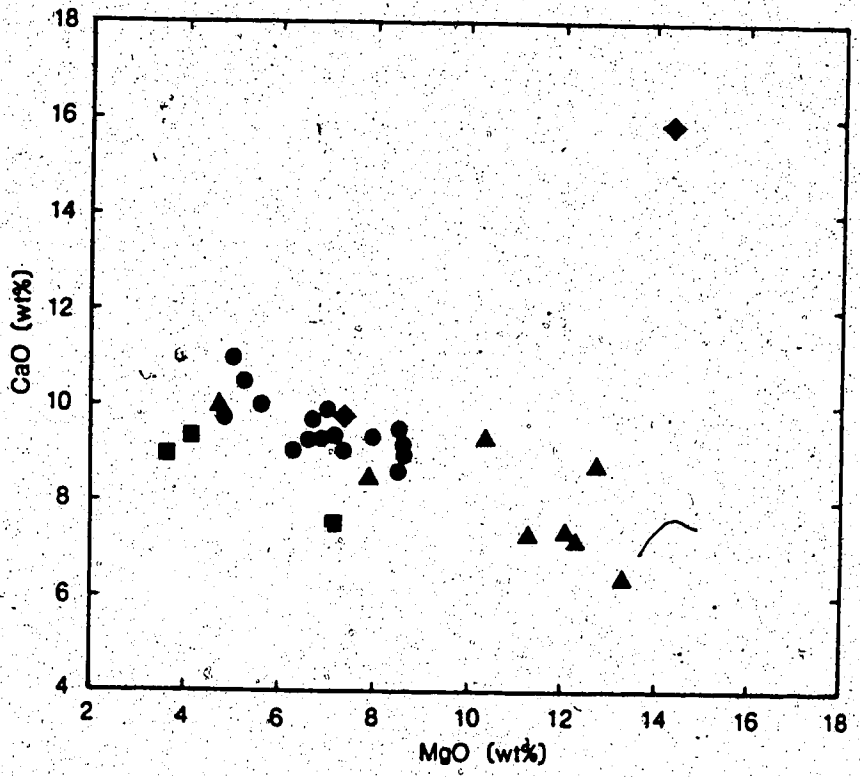

Fig. 33. CaO versus MgO diagram for the Chilcotin Group. Symbols as for Fig. 32.

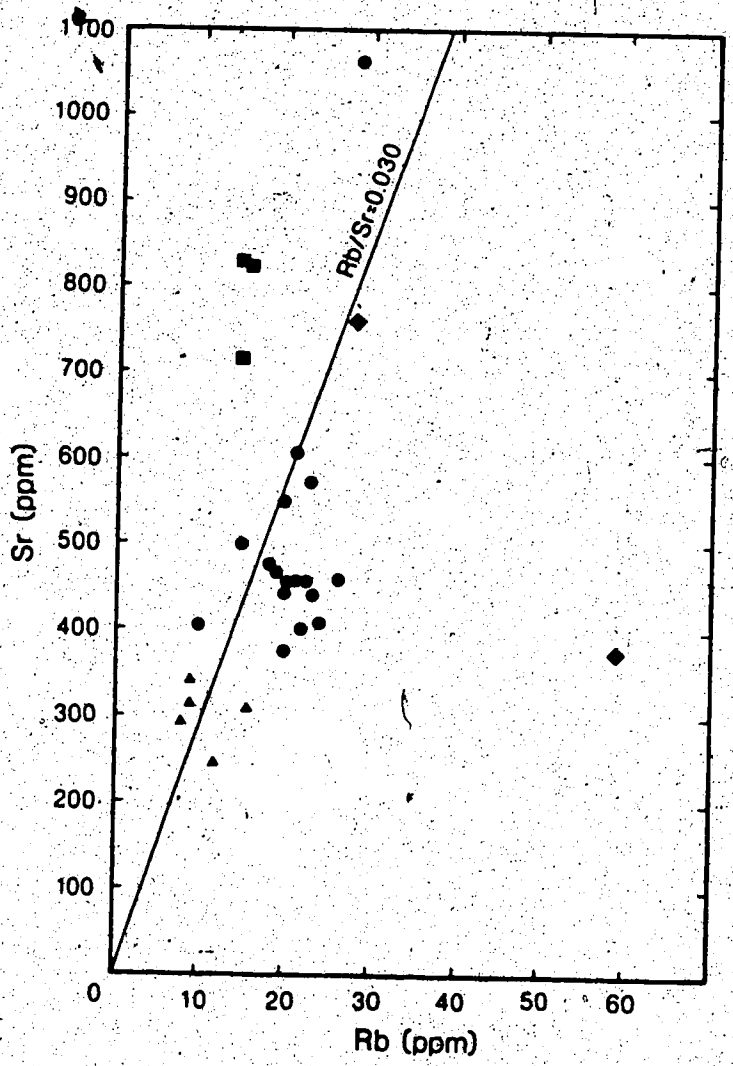

Fig. 34. Rb versus Sr diagram for the Chilcotin Group. Symbols as for Fig. 32.

Table 11.

REE element concentrations (in ppm) for the Chilcotin Group.

	Group A		Group B				Group C				Other basalts		
	RR	2-99D	2-11A	2-24C	2-29	2-41A	2-36	2-37B	2-41B	2-43A	2-30B	2-99A	2-99B
La	21.4	21.2	15.4	18.4	12.1	10.5	7.11	17.8	9.72	14.4	33.3	3.56	12.2
Ce		45.4			27.1	22.5	16.1		22.6			9.20	30.3
Pr	6.92	5.50		5.62	4.24			5.57	3.01		9.19	1.28	
Nd	27.7	22.8	19.0	22.0	24.7		11.2	19.6	13.3		43.0	6.49	19.2
Sm	6.18	4.95	4.49	4.99	4.75	3.87	3.03	4.80	3.60	4.20	7.81	2.03	5.08
Eu	2.11	1.88	1.63	1.77	1.75	1.34	1.31	1.90	1.37	1.50	2.54	0.75	1.34
Gd	5.66	4.09	3.85	4.97	5.00				4.15	3.72	5.85		5.42
Tb		0.61			0.77	0.74	0.71			0.60		0.39	0.89
Dy	4.74	3.41	4.00	4.87	4.23			5.54	3.61	3.71	5.51	2.63	5.15
Ho	0.99	0.61	0.84	0.97	0.83			1.18	0.68	0.75		0.56	1.06
Er	2.51	1.46		2.56	2.08							1.60	
Yb	2.41	0.95	2.17	2.09	1.78	1.37	1.78	3.22	1.93	1.77	2.69	1.50	2.44
Lu	0.24	0.12	0.22	0.20	0.22	0.20	0.27	0.48	0.23	0.22	0.17	0.22	0.29
Eu/Eu*	+1.19	+1.38	+1.27	+1.18	+1.26	+1.13	+1.21	+1.26	+1.17	+1.24	+1.29	+1.13	+1.2
(La/Yb)n	5.9	14.9	4.7	5.9	4.5	5.1	2.7	3.7	3.4	5.4	8.3	1.6	3.3

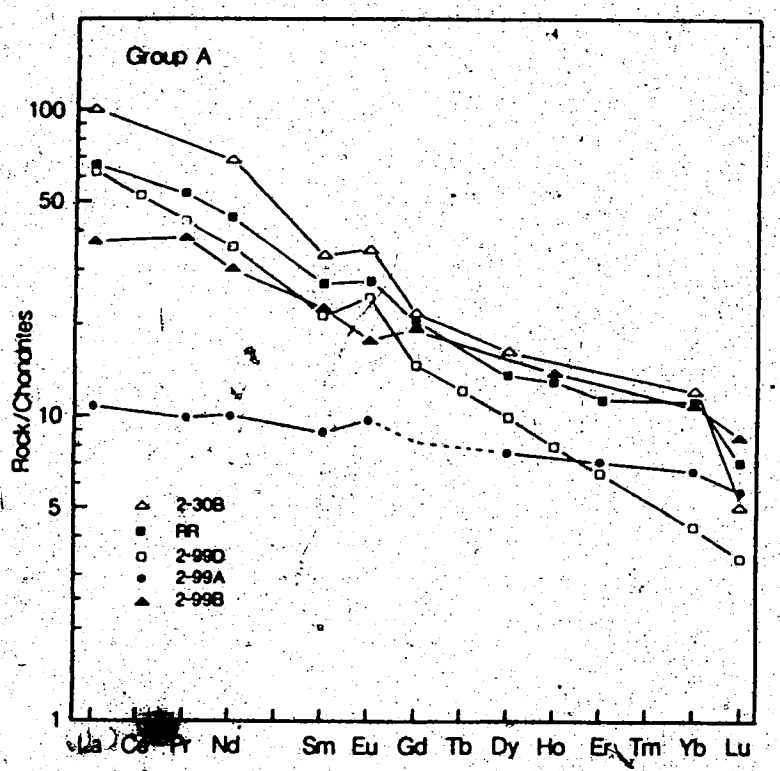

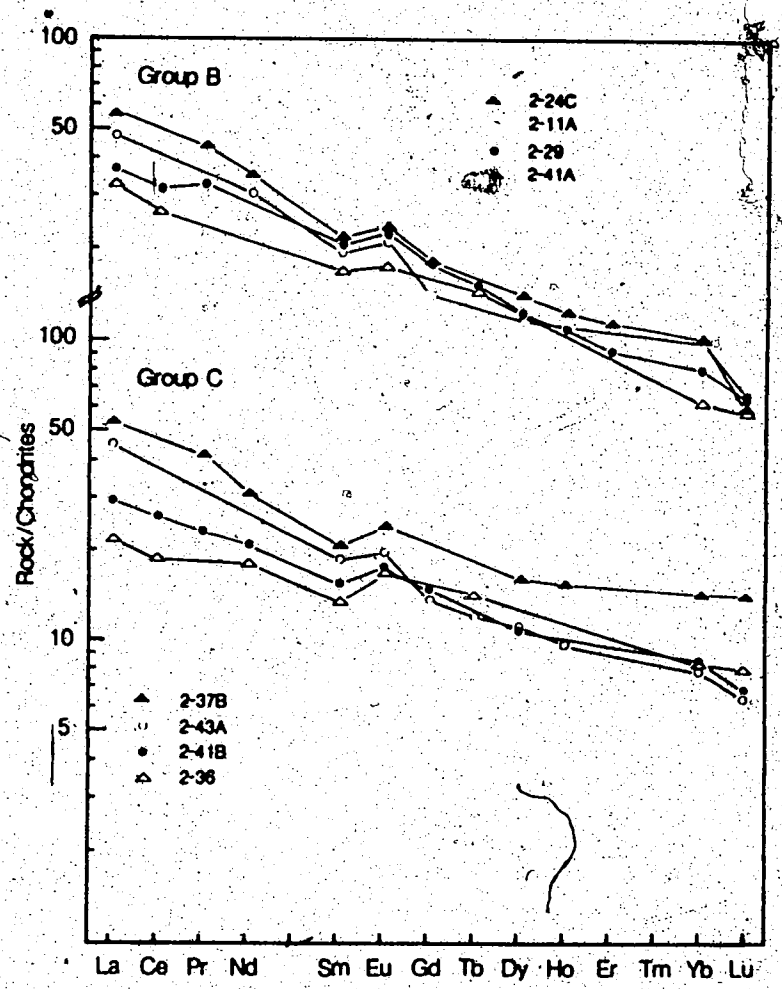

Fig. 35. Chondrite normalised REE plots for the Chilcotin basalts.

with (La/Yb)n ratios ranging from 3 to 15, and small positive Eu anomalies of Eu/Eu^{*} +1.1 to +1.3 .

Nd-Sr Isotopic Composition

Nd-Sr isotopic compositions for the Chilcotin basalts are presented in Table 12. The basalts have moderately depleted $^{143}Nd/^{144}Nd$ ratios of 0.51310 to 0.51284 and $^{87}Sr/^{86}Sr$ ratios of 0.7028 to 0.7039 (Fig. 36). The Chilcotin Group overlap the fields for the Kamloops Group, East Pacific Rise and associated seamounts (Zindler et al. 1984), Hawaii (Chen and Frey 1983, Stille et al. 1983) and the more depleted basalts of the Columbia River (Carlson et al. 1981, Carlson 1984) and Basin and Range Provinces (Hart 1985). In contrast, the compositions of the alkali basalts 2-30B ($^{143}Nd/^{144}Nd$ =0.51270, $^{87}Sr/^{86}Sr$ =0.7047) and 2-66D ($^{143}Nd/^{144}Nd$ =0.51274, $^{87}Sr/^{86}Sr$ =0.7039), which have been tentatively included in the Chilcotin Group, are closer to the bulk Earth value.

Sm/Nd ratios range from 0.33 to 0.22 , the lowest ratios being found in the most isotopically depleted basalts. The Sm/Nd ratios thus contrast the positive ϵNd values which imply a time integrated LREE depletion in the source region. Rb/Sr ratios range from 0.018 to 0.055, both higher and lower than the bulk Earth value of 0.030 . On a Rb/Sr versus $^{87}Sr/^{86}Sr$ plot the basalts show a scatter on and to the right of the geochron, showing no evidence for a mantle isochron.

Discussion

The Chilcotin basalts which have the most depleted isotopic compositions ($^{143}Nd/^{144}Nd$ ratios of 0.51307 to 0.51302 and $^{87}Sr/^{86}Sr$

Table 12.

Nd and Sr isotopic compositions of Chilcotin basalts.

	Rb/Sr	$^{87}Sr/^{86}Sr$	Sm/Nd	$^{143}Nd/^{144}Nd$	εNd
Group A					
2-99C	0.019	0.70279±3		0.513075± 9	+8.5
2-99D	0.018	0.70281±2	0.217	0.513074±13	+8.5
Group B					
2-1	0.024	0.70385±3		0.512846±13	+4.1
1-5A	0.035	0.70375±3		0.512894±21	+5.0
1-9D	0.040	0.70296±3		0.513000±16	+7.1
2-11A	0.046	0.70344±3	0.236	0.512938±15	+5.9
2-14A	0.055	0.70372±4		0.512901±20	+5.2
2-14C	0.053	0.70376±2		0.512916±16	+5.4
2-24C	0.030	0.70353±2	0.227		
2-29	0.054	0.70346±2	0.193	0.512950±33	+6.1
1-12	0.045	0.70285±3		0.513006±25	+7.2
2-41A	0.012	0.70367±1		0.512913± 7	+5.4
Group C					
2-36	0.049	0.70321±4	0.270	0.513007±12	+7.2
2-37A	0.041	0.70280±2		0.512998± 6	+7.0
				0.513003± 7	+7.1
2-37B	0.044	0.70302±2	0.245	0.512975±25	+6.6
2-40	0.026	0.70315±2		0.512965±19	+6.4
2-41B	0.052	0.70329±3	0.270	0.512904±14	+5.2
2-42	0.027	0.70318±3		0.513020±16	+7.5
2-43A	0.035	0.70308±3		0.512986±16	+6.8
Alkali and other basalts					
2-30B	0.158	0.70467±2	0.182	0.512704±17	+1.3
2-99A	0.094	0.70415±3	0.312	0.512858± 9	+4.3
2-99B	0.068	0.70426±3	0.265	0.512915±15	+5.4
2-66B	0.023	0.70371±1		0.512852±17	+4.2
2-66D	0.037	0.70394±3	0.190	0.512739±19	+2.0

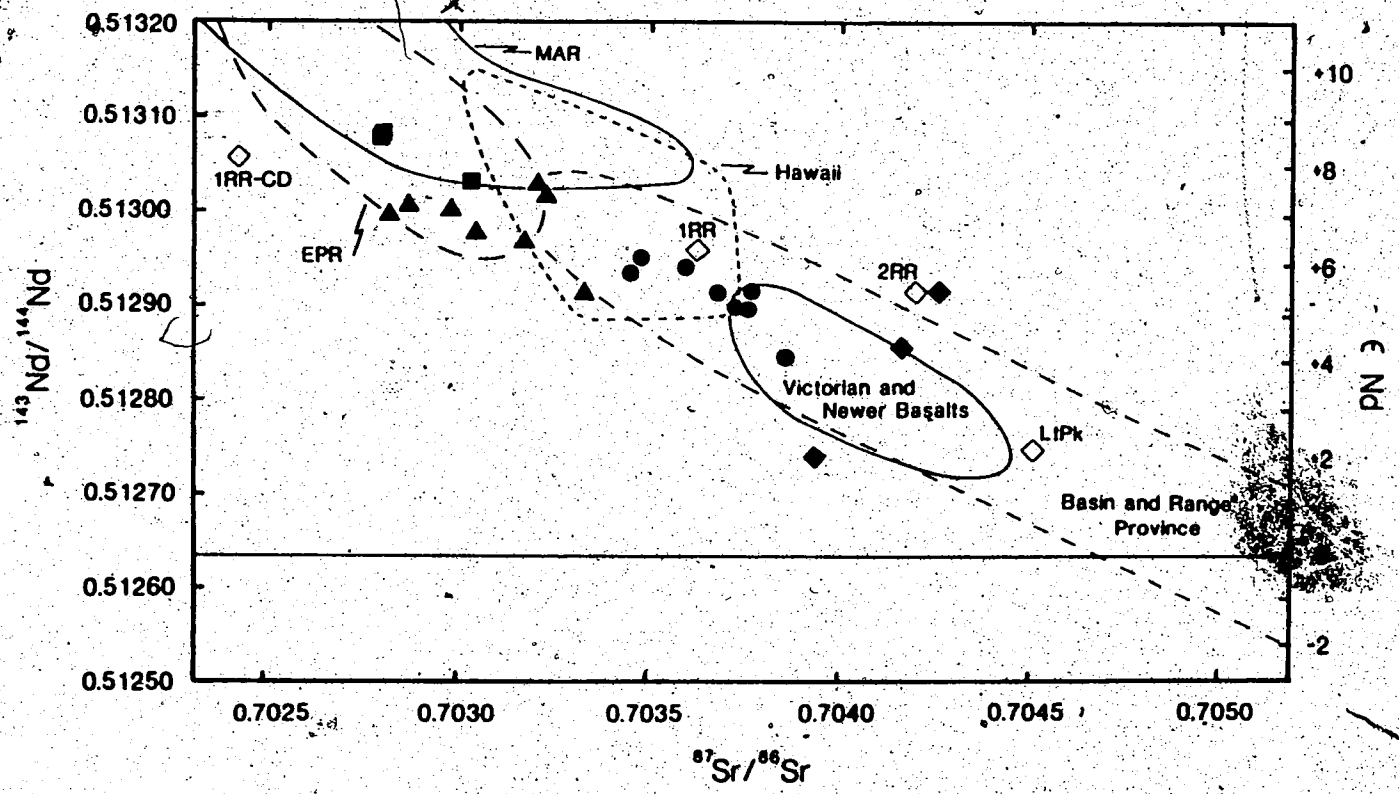

Fig. 26. Nd-Sr isotopic diagram for the Chilcotin Group: • group A; • group B; ▲ group C; ● alkali basalts 2-308 and 2-66D; ○ Rayfield River spinel lherzolite nodules (see Chapter 8). Also shown are fields for the Mid-Atlantic Ridge (MAR) (O'Nions et al. 1977, White and Hofmann 1982), East Pacific Rise (EPR) (Zindler et al. 1984), Hawaii (O'Nions et al. 1977, Chen and Frey 1983, Stille et al. 1983), Victorian and Newer basalts of southern Australia (McDonough et al. 1985), and the Basin and Range Province (Hart 1985).

ratios of 0.7028 to 0.7030), 2-99C, 2-99D and RR, show the greatest enrichment in minor and trace elements, whereas the basalts that show the most tholeiitic affinity have isotopic compositions ($^{143}Nd/^{144}Nd$ ratios of 0.51302 to 0.51297 and $^{87}Sr/^{86}Sr$ ratios of 0.7029 to 0.7033) in the middle of the range. Consequently, as a basis on which to discuss the petrogenesis of the basalts, the samples have been divided into three groups:

(1) Group A (Alkaline). This group is represented by the hawaiites 2-99C, 2-99D from Nicola Lake, and RR from the southern end of the main plateau. All samples are nepheline-normative. The group is characterised by high SiO_2 (50 to 52%), Al_2O_3 (16 to 18%), Na_2O (4.5 to 5%), TiO_2 (2%) and P_2O_5 (0.6%), and certain trace element enrichments, notably in Sr, Zr, Nb and to a lesser extent Ba. Low Y abundances for a given silica content complement (La/Yb)n ratios of 6 to 15. Group A has the most depleted isotopic compositions: $^{143}Nd/^{144}Nd$ >0.51300 and $^{87}Sr/^{86}Sr$ <0.7030 .

(2) Group B (Transitional). This group has lower SiO_2 (47 to 50%) and slightly lower Al_2O_3 (14.5 to 17%), Na_2O (3 to 4%), TiO_2 (1.5 to 2%) and P_2O_5 (0.3 to 0.35%) compared to group A. The samples may be nepheline- or hypersthene-normative. The trace element chemistry is characterised by moderate to high Ba (300 to 400 ppm), Sr (>400 ppm), Rb (>15 ppm), and (La/Yb)n ratios of 4.7 to 6.0 . Group B has the most enriched isotopic compositions: $^{143}Nd/^{144}Nd$ ratios of 0.51295 to 0.51284 and $^{87}Sr/^{86}Sr$ ratios of 0.7034 to 0.7041 .

(3) Group C (Tholeiitic). This group is characterised by low SiO_2 (47 to 50%), Al_2O_3 (13.5 to 15%), Na_2O(<3%), TiO_2 (<2%) and P_2O_5 (<0.35%); but has high MgO (>9%). Low alkali content places the basalts in the

subalkaline field (Fig. 32). The samples are hypersthene- or quartz-normative and are restricted to the main plateau. Low trace element concentrations, notably of Ba (<250 ppm), Sr (<400 ppm) and Nb (<16 ppm), complement low $(La/Yb)_n$ ratios of 2.7 to 5.4 . Y contents of 21 to 23 ppm are similar to those of group B. Isotopic compositions ($^{143}Nd/^{144}Nd$ ratios of 0.51300 to 0.51290 and $^{87}Sr/^{86}Sr$ ratios of 0.7028 to 0.7034) are intermediate between groups A and B.

It is stressed that the division is primarily to provide a working basis on which to model the the isotopic, major and trace element trends. All three groups show similar major and trace element features which differ primarily in magnitude (Fig. 37).

Crystal Fractionation and Magma Mixing

The inverse correlation of MgO with CaO, similar to the Greenland Province basalts (Basaltic Volcanism Study Project 1981), is an unusual feature for continental basalts and is accentuated by the division into groups A, B and C (Fig. 33). The wide range in MgO content is ascribed to olivine fractionation as this mineral is the principal phenocryst phase. The variation in CaO requires either some degree of plagioclase fractionation or source region heterogeneity. On a Rb-Sr plot (Fig. 34) groups A and B form a diverging trend away from the low Rb, low Sr group C basalts. No trend toward Rb enrichment due to plagioclase fractionation is seen in any group.

The importance of magnetite fractionation is illustrated by a plot of TiO_2 versus Nb (Fig. 38). At TiO_2 concentrations of up to 1.5%, the samples lie on a line of TiO_2/Nb = [illegible] resulting from the crystallisation of the assemblage olivine, clinopyroxene and plagioclase (Pearce and

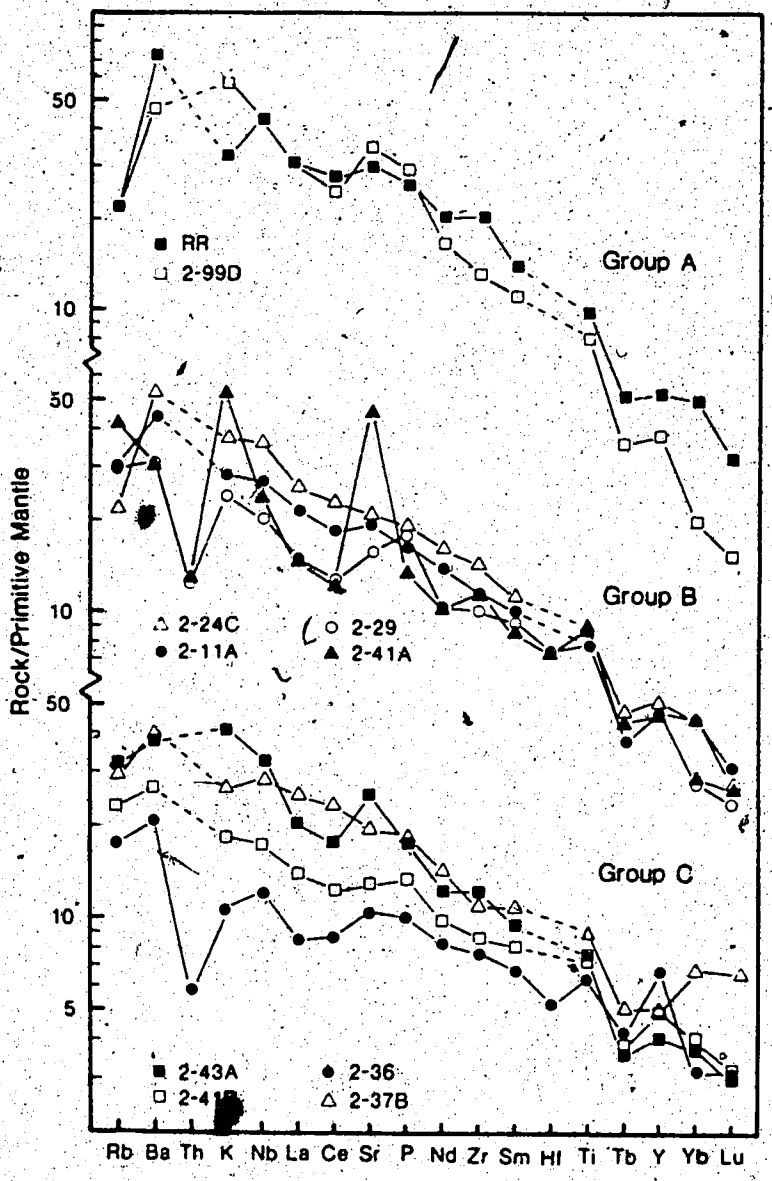

Fig. 37. Trace element abundances of group A, B and C Chilcotin basalts normalised to the primitive mantle values of McDonough et al. (1985). The elements are arranged in order of increasing compatability from left to right. All three groups show similar patterns which differ only in the degree of incompatible element enrichment.

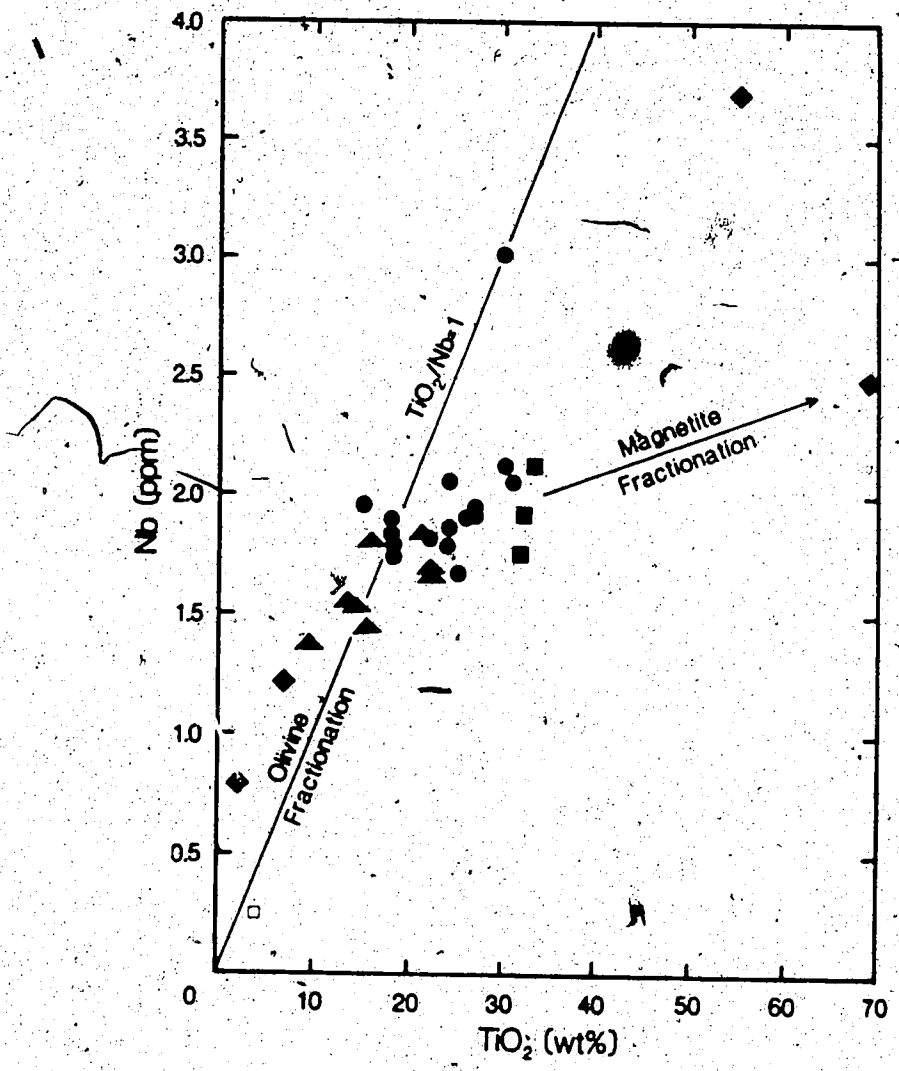

Fig. 38. TiO_2 versus Nb diagram for the Chilcotin basalts. The line $TiO_2/Nb = 1$ corresponds to the crystallisation of olivine, clinopyroxene and plagioclase. The deviation from this line above 1.5% TiO_2 results from the fractionation of magnetite. TiO_2/Nb ratios greater than 1 arise from the contribution of amphibole or phlogopite to the melt. Symbols as for Fig. 32 .

Norry 1979). Sample 2-99A has TiO_2/Nb =2 , which may indicate the contribution of amphibole to the melt. Magnetite fractionation is indicated by the deviation of the majority of the samples (mostly belonging to groups A and B) from the TiO_2/Nb =1 line at TiO_2 contents greater than 1.5%.

Evidence for magma mixing is illustrated by a plot of MgO versus Ni (Fig. 39). The MgO-Ni data define a pattern which is interpreted as the result of repeated olivine fractionation and recharge in a deep seated magma chamber. Group C have higher Ni and MgO contents (Fig. 39), suggesting derivation from a more primary melt.

Crustal Contamination

Trends toward enriched isotopic compositions have often been interpreted as contamination by older, more radiogenic crustal material (Carlson et al. 1981, Mahoney et al. 1982, Menzies et al. 1984, Downes 1984). Alternatively it has been argued that the observed chemical and isotopic variations result from mantle heterogeneities or are imparted upon mixing of mantle components (DePaolo 1983, McDonough et al. 1985).

In view of the restricted silica range shown by the Chilcotin basalts, contamination effects should be better observed when the isotopic composition is plotted against MgO content (Fig. 40) as this may be considered an inverse measure of differentiation. Group B, which from their localised occurrence away from the main plateau, would be the most succeptible to crustal contamination, define a cloud clearly separated from groups A and C which can only be attributed to original magmatic heterogeneity. Groups A and C show a rough positive correlation, opposite to the trend expected from crustal contamination.

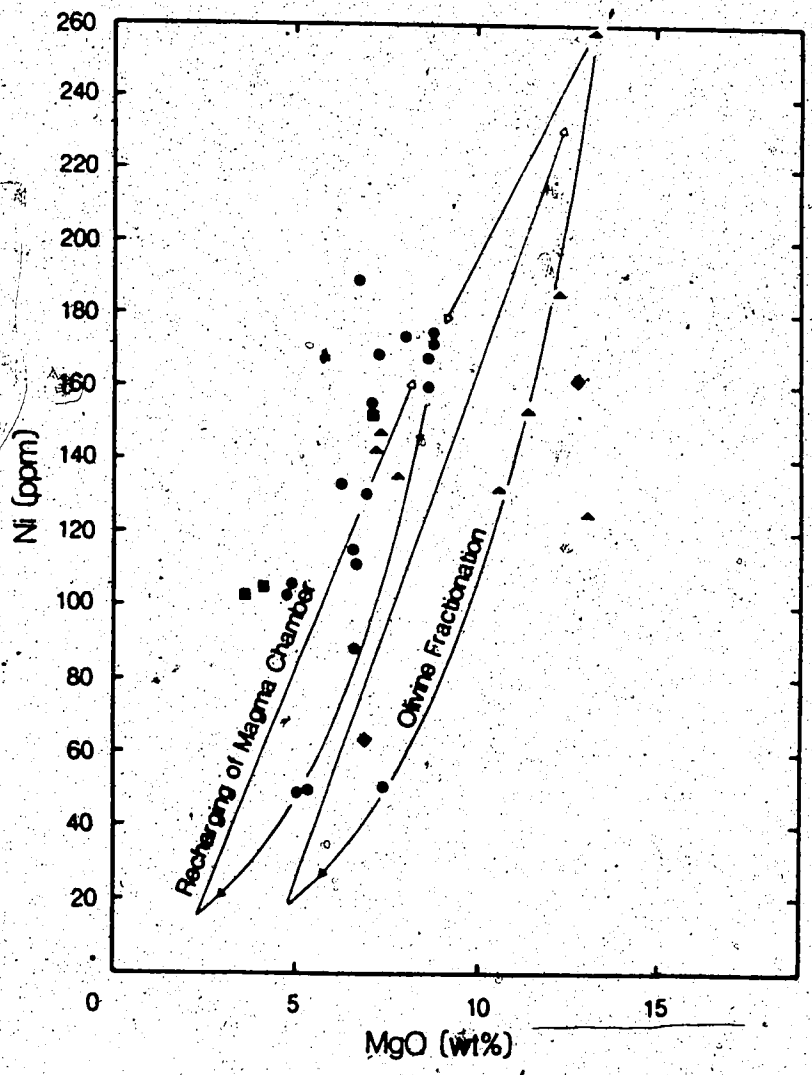

Fig. 39. MgO versus Ni diagram for the Chilcotin Group. The positive correlation of MgO and Ni results from olivine fractionation. The scatter on this diagram may be accounted for by repeated olivine fractionation and magma recharge in a deep-seated magma chamber. Symbols as for Fig. 32.

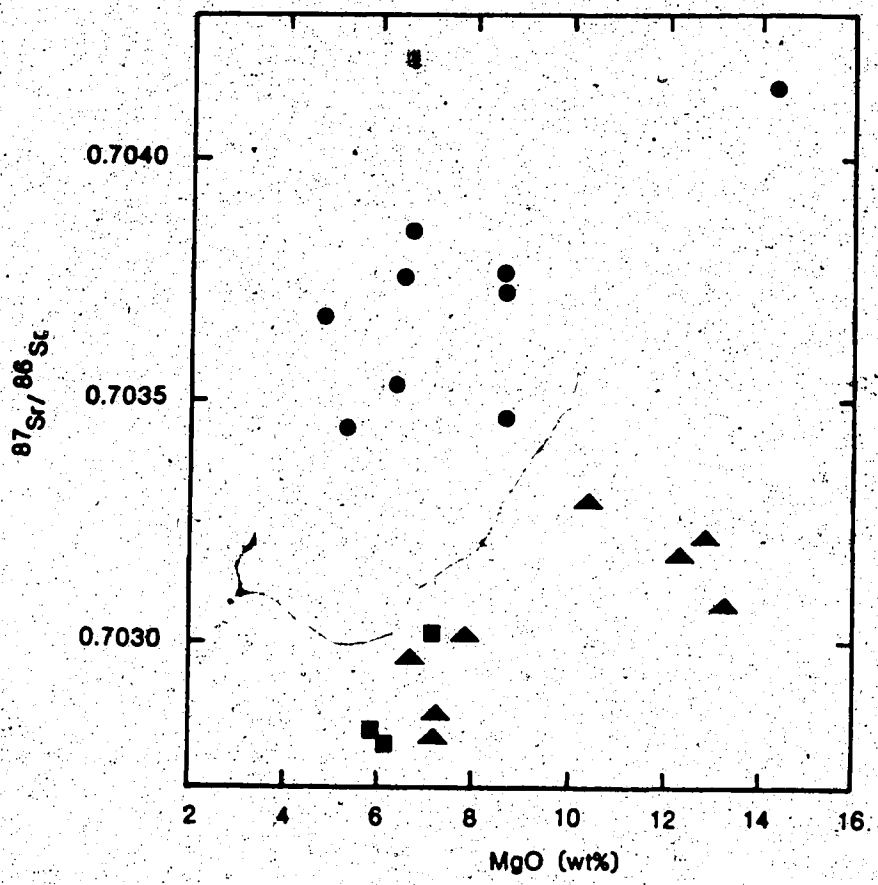

Fig. 40. Assessment of crustal contamination in the Chilcotin Group: $^{87}Sr/^{86}Sr$ versus MgO. Symbols as for Fig. 36.

Table 13.

Nd-Sr isotopic data for crustal xenoliths found in basalt RR.

Sample	Rb ppm	Sr ppm	Rb/Sr	$^{87}Sr/^{86}Sr$	$^{143}Nd/^{144}Nd$	ε Nd
RR-P1				0.70384±2		
RR-2PA	34.9	1636	0.021	0.70351±2	0.512991±19	+6.9

Gabbroic xenoliths comprising 5% of the rock were found with spinel lherzolite nodules in the hawaiite RR. The xenoliths are mostly 1 cm in diameter but occasionally reach 5 cm. Internal fractures indicate an accidental origin. Isotopic compositions measured on two such xenoliths are presented in Table 13. Assimilation of 1% gabbroic xenoliths (1640 ppm Sr, $^{87}Sr/^{86}Sr$ =0.7035) and 20% spinel lherzolite (31.5 ppm Sr, $^{87}Sr/^{86}Sr$ =0.7045) would only increase the $^{87}Sr/^{86}Sr$ ratio of a basalt (500 ppm Sr, $^{87}Sr/^{86}Sr$ =0.7028) by one part in 10^3. In consideration of the rapid ascent rates required for survival of the lherzolite nodules (of the order of hours to days) it is concluded that the crustal residence time of RR was too short to allow significant contamination. The xenolith RR2-PA and hawaiite RR have a similar, characteristically low Rb/Sr ratio of 0.019; therefore, it is probable that the xenoliths represent vent-filling material from a previous magmatic episode. This Rb/Sr ratio is characteristic of the dolerite plugs associated with the Chilcotin Group (Farquharson 1973), whereas the Chilcotin basalts generally have Rb/Sr ratios of 0.03 to 0.05.

Isotopic and Trace Element Correlations

The positive correlation of the REE and P_2O_5 in basic magmas has been suggested to indicate apatite control on REE abundances in the mantle during magma genesis (Beswick and Carmichael 1978, Metcalfe and Smith 1986). McDonough et al. (1985) demonstrated that the P_2O_5/Nd ratio for continental basalts and ocean island basalts averages 170±30 , comparable to the primitive mantle estimates of Sun (1982) of P_2O_5/Nd =150 . The P_2O_5/Nd ratio for nine Chilcotin basalts (Fig. 41) is 202, similar to the ratios of the Tasmanian basalts and the Australian Newer

basalts (McDonough et al. 1985). Two samples, the hawaiite 2-99D and the alkali basalt 2-30B lie significantly off the P_2O_5-Nd correlation line. A similar feature is illustrated by the P_2O_5-Sm relationship (Fig. 41) where a second line of lower gradient may be drawn through samples 2-99A, 1-5A, and 2-30B. From the slope of the regression lines in Fig. 41 an average Sm/Nd ratio of 0.195 is calculated for the whole group. A feature of both Nd- and Sm- P_2O_5 diagrams is that the linear regression line does not pass through the origin but at zero phosphorous content indicates Nd and Sm contents of 0.47 and 0.99 ppm respectively. Given the uncertainty in the P_2O_5 concentrations it is debatable whether these intercepts are significant. Frey et al. (1980) have argued that both P and the REE behave as incompatible elements on melting and are partitioned strongly into the melt. By this argument, the line should pass through the origin , but this would only appear to be valid if all the REE reside in a phosphate phase. If clinopyroxene or garnet also contributed to the melt and were residual in the source region then there should be no such requirement.

The data in Fig. 41 could also be fitted by curves, and hence be interpreted as a mixing relationship between high P_2O_5, REE-rich and zero P_2O_5, REE-poor components. Samples with low REE and low P_2O_5 contents, which might result from high degrees of partial melting, show greater REE concentrations than expected from a linear REE-P_2O_5 relationship due to increasing contributions from phases such as clinopyroxene. A plot of Sm/Nd versus P_2O_5 (Fig. 41) shows that at low P contents the Sm/Nd ratio is greater than 0.27 , but decreases to 0.22 at 0.6% P_2O_5 . Again the data are considered indicative of mixing between high Sm/Nd, low P_2O_5, REE-poor and low Sm/Nd, high P_2O_5, REE-rich

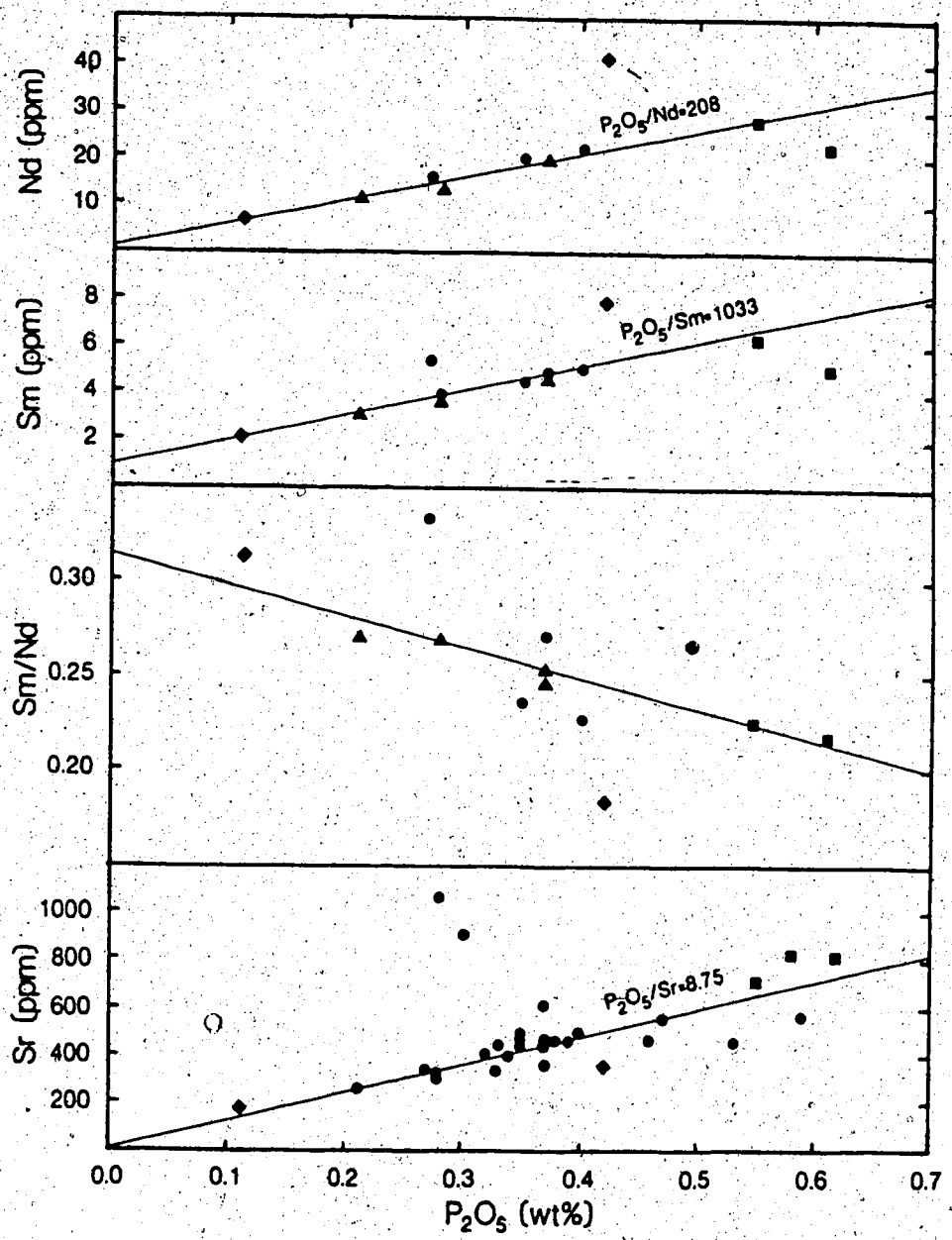

Fig. 41. Variation of Nd, Sm, Sm/Nd and Sr with P_2O_5 in the Chilcotin Group. Symbols as for Fig. 32 except for Sr versus P_2O_5 where groups B and C have not been divided.

components.

If the control on the REE content by P has been a long term effect in the mantle, correlation between $^{143}Nd/^{144}Nd$ (Fig. 42), and hence also $^{87}Sr/^{86}Sr$ (Fig. 42), and the P_2O_5 content of the basalt should be expected. On both graphs a diverging trend with the group A samples as the common endmember occurs. The trends are strengthened when the data of Bevier (1983a) is included. $^{87}Sr/^{86}Sr$ data for the dolerite plugs (Farquharson 1973) fall within the fields for groups B and C (Fig. 43), but also include samples with higher $^{87}Sr/^{86}Sr$ with respect to P_2O_5 than group B. The identification of a third trend encompassing the dolerites, alkali basalt 2-30B and diorite 2-99B is not considered valid because of the widely differing rock types. Combined P_2O_5-isotopic data for other suites of continental basalts are lacking. The individual groups of the Columbia River Province (McDougall 1976, Carlson et al. 1981), and Basin and Range Province (Hart 1985) show a strong negative correlation, almost independent of P_2O_5 content (Fig. 43). Tholeiites from Mull (Beckinsale 1978) and Hawaii (Roden et al. 1984) also show large variations in $^{87}Sr/^{86}Sr$ for little change in P_2O_5. Conversely, alkali basalts from the Cantal region (Chauval and Jahn 1984, Downes 1984), Australia (McDonough et al. 1985) and Mull (Beckinsale et al. 1978) show a large range of P_2O_5 with little variation in $^{87}Sr/^{86}Sr$. The position of several alkalic differentiates and silicic volcanics are also shown in Fig. 43. Although these invariably lie toward higher $^{87}Sr/^{86}Sr$ and lower P_2O_5, forming an inverse correlation that reflects crustal contamination, this possibility is rejected for the Chilcotin Group because of the restricted silica range.

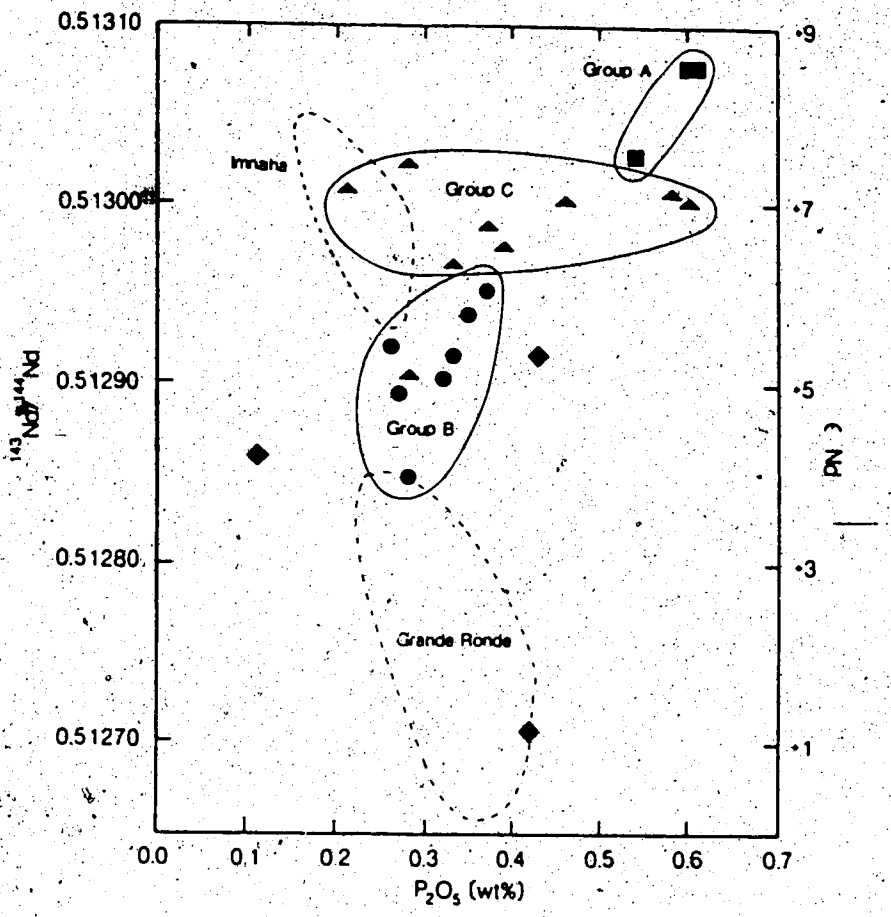

Fig. 42. $^{143}Nd/^{144}Nd$ versus P_2O_5 diagram for the Chilcotin Group. Data for the Columbia River basalts from Carlson et al. (1981). Symbols as for Fig. 36.

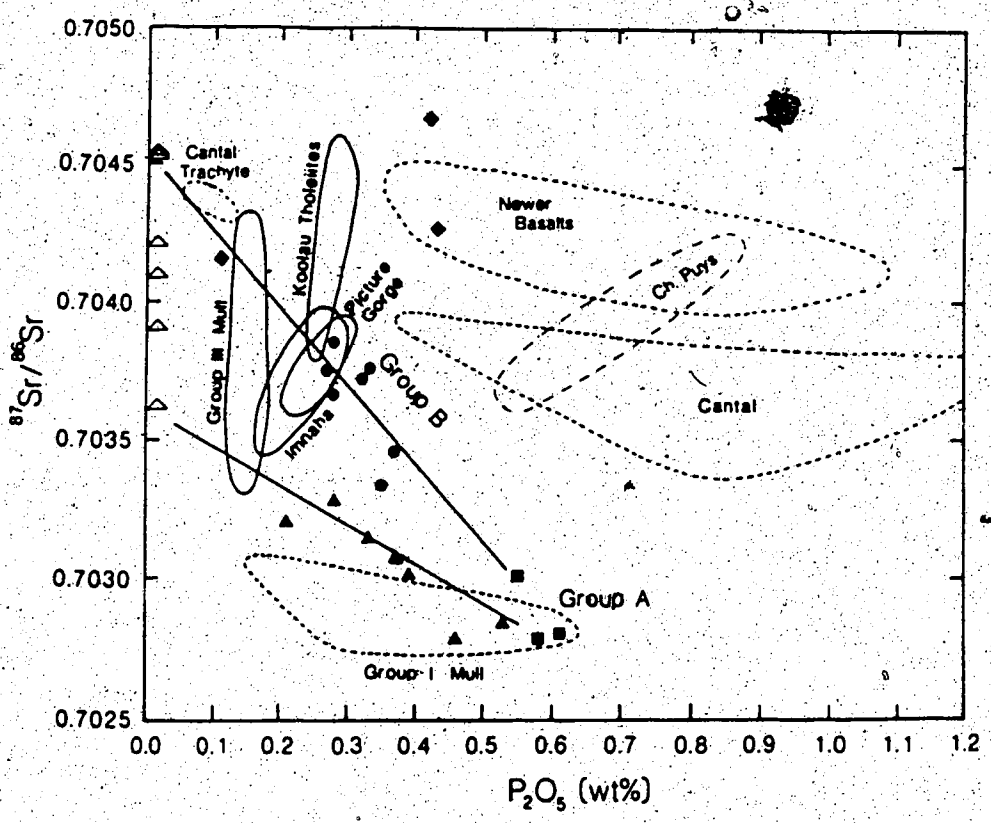

Fig. 43. $^{87}Sr/^{86}Sr$ versus P_2O_5 diagram for the Chilcotin Group. Symbols as for Fig. 36. Also shown are the fields for basalts from the Basin and Range Province (Hart 1985), Cantal Region (Chauval and Jahn 1984; Downes 1984), Columbia River basalts (Carlson et al. 1981), Hawaii (Roden et al. 1984), Mull (Beckinsale et al. 1978), and southeastern Australia (McDonough et al. 1985). Isotopic compositions of spinel lherzolite xenoliths (⏢) from Rayfield River and Lightning Peak for an assumed P_2O_5 content of 0.1%.

Binary Mixing Model for the Chilcotin Basalts

The positive correlation of Nd-Sr isotopic compositions shown by basaltic rocks can be considered to result from the binary mixing of two isotopically distinct mantle reservoirs (DePaolo 1979). Of these, the depleted mantle reservoir (DM), with high $^{143}Nd/^{144}Nd$ and low $^{87}Sr/^{86}Sr$, is considered to be homogeneous and to have resulted from an ancient depletion event. The other reservoir, considered to be enriched mantle (EM), is less homogeneous and has low $^{143}Nd/^{144}Nd$ and high $^{87}Sr/^{86}Sr$. The heterogeneity of the EM generates a range of mixing hyperbolae about a binary mixing curve even for only two end members (Anderson 1982). However, the Nd-Sr isotopic array can also be generated from an infinite number of reservoirs lying along the mantle trend, all of which were derived by fractionation of a homogeneous initial reservoir at some time in the past (DePaolo 1979). Magmas derived from such a series of reservoirs should show a positive correlation between $^{143}Nd/^{144}Nd$ and Sm/Nd and between $^{87}Sr/^{86}Sr$ and Rb/Sr. More frequently basaltic suites show time-integrated depleted isotopic signatures inconsistent with the observed high Rb/Sr and Nd/Sm ratios, or large-ion lithophile element (LIL) enrichment. Such basalts are unlikely to have been produced from an infinite series of mantle reservoirs unless all reservoirs behaved coherently. The concept of mantle metasomatism has often been invoked in such circumstances to produce the high Rb/Sr and Nd/Sm ratios and the corresponding LIL enrichment observed in alkaline melts (e.g. Menzies and Murthy 1980b).

High Rb/Sr and Nd/Sm ratios, and LIL enrichment in isotopically depleted basalts may also be produced by very small degrees of partial melting of a DM source. Several models (Chen and Frey 1983, 1985,

Anderson 1985) have shown the ability of melts so produced to account for the Nd-Sr isotopic array by binary mixing with an EM reservoir, whilst at the same time accounting for the geochemical features of the resulting rocks. In these models the La/Ce ratio is used as a measure of the LIL enrichment as neither of these elements is likely to be affected by crystal fractionation, whilst $^{87}Sr/^{86}Sr$ is used to as a measure of the time-integrated LIL enrichment.

On a binary plot of these ratios, the mixing curves are controlled by the choice of parameters for the mantle components. The chemical and isotopic composition of the DM component may be specified fairly rigorously and the La/Ce ratios calculated for varying degrees of partial melting. In both the models of Chen and Frey (1983) (C-F model) and Anderson (1985) (A-model) this component was considered to be oceanic mantle garnet lherzolite consisting of 60% olivine , 25% orthopyroxene, 10% clinopyroxene and 5% garnet, with 0.31 ppm La, 0.95 ppm Ce, and 13.2 ppm Sr. $^{87}Sr/^{86}Sr$ was assumed to be 0.7023 . The C-F and A-models differ in the choice of EM component: in the C-F model this component is specified only as having 0.71 ppm La, 1.90 ppm Ce and 23.7 ppm Sr with $^{87}Sr/^{86}Sr$ =0.7047 , thus representing a composition close to the bulk Earth. In the A-model the EM component is isotopically more enriched having $^{87}Sr/^{86}Sr$ =0.7202, and La/Ce =0.5 . These differences result in a considerable shift in the mixing lines but do not affect the overall conclusions from the models.

La/Ce and $^{87}Sr/^{86}Sr$ data for the Chilcotin basalts have been plotted on both the C-F and A-model mixing curves in Fig. 44. Where not measured directly, Ce abundances have been inferred from the chondrite normalised plots in Fig. 35. No attempt to change the parameters used in

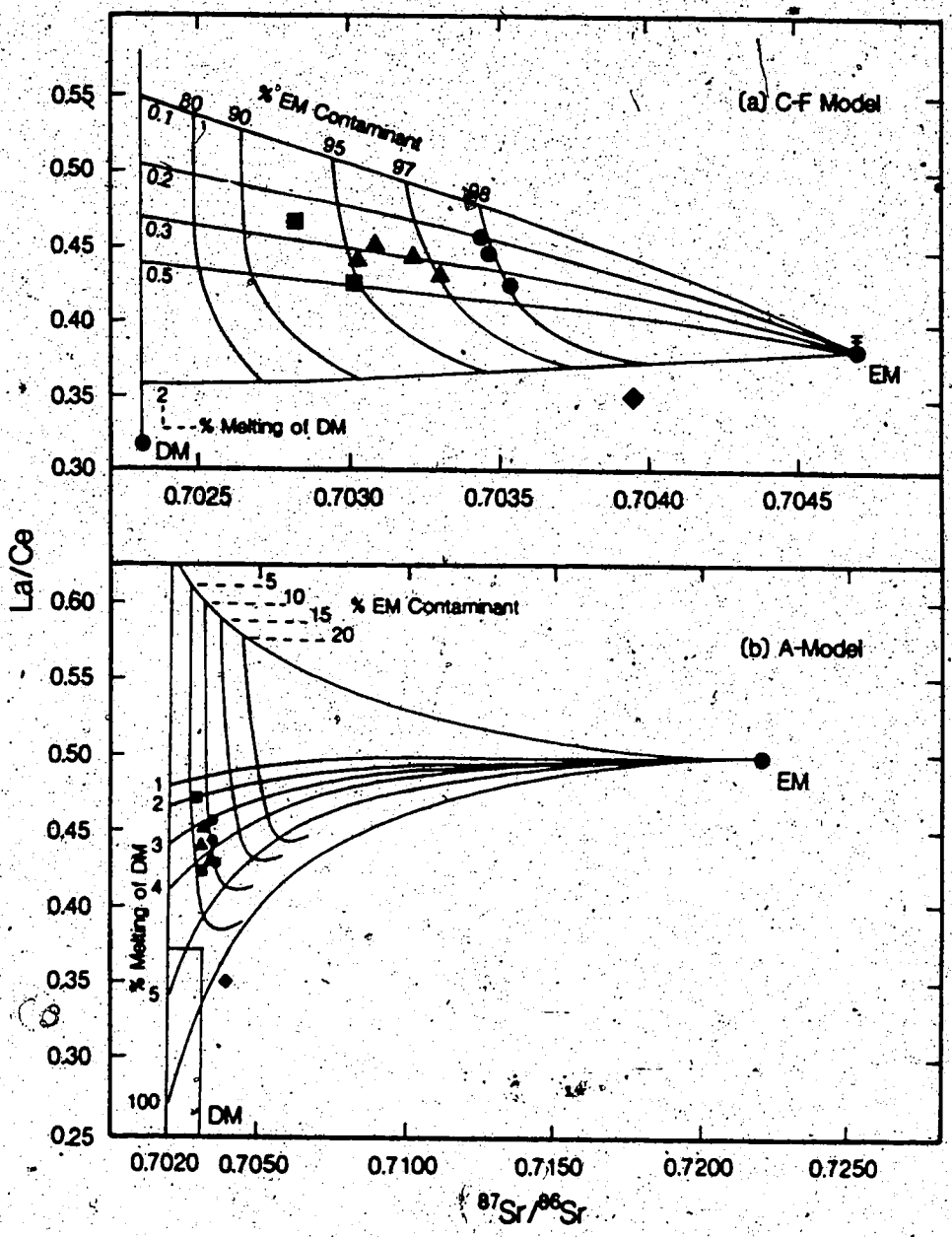

Fig. 44. Chilcotin basalts plotted on the La/Ce versus $^{87}Sr/^{86}Sr$ binary mixing models of (a) Chen and Frey (1983) (C-F model); (b) Anderson (1985). Characteristics of the depleted mantle (DM) and enriched mantle (EM) components are discussed in the text. Near-horizontal lines in both models indicate the degree of partial melting of the DM component required to produce the observed La/Ce ratio. Near-vertical lines indicate the degree of contamination of the melt with the EM component. Vertical bar on EM in (a) indicates the La/Ce ratio of the melt derived from this component for 0 to 10% partial melting. Symbols as for Fig. 36.

either model has been made.

Apart from the samples 2-99A, 2-99B, 2-30B and 2-66D, which have questionable affiliation to the Chilcotin Group, the basalts show a restricted La/Ce range from 0.42 to 0.47 , this variation being similar for groups A, B and C. In the C-F model the La/Ce ratio can be satisfied by 0.3% melting of the DM whereas in the A-model this figure is somewhat higher at 2 to 4%. The three groups, A, B and C, require increasing amounts of contamination from the EM component in both models: detailed predictions are given in Table 14. Of the alkali basalts, 2-30B has higher $^{87}Sr/^{86}Sr$ than the EM component in the C-F model and cannot, therefore, be accounted for by the model. The high La/Ce ratio of 2-30B would require a very small degree of partial melting if the $^{87}Sr/^{86}Sr$ of the EM component was increased. Conversely, 2-66D, which has a low La/Ce ratio, cannot be accounted for by the A-model. It is possible that this feature arises from a low La/Ce ratio in the source region due to the presence of amphibole which is not taken into account in the mixing models.

It should be noted that the amount of EM contaminant is not synonymous with the degree of partial melting of the EM component. As discussed by Chen and Frey (1983), the La/Ce ratio of the melt derived from the EM component will be relatively insensitive to the degree of partial melting. Approximately 12 to 16% melting of this component was suggested for the generation of the Hawaiian basalts. The most significant feature of the models is the low degree of partial melting of the DM component, because this must account for the high Rb/Sr and Nd/Sm ratios, and the LIL enrichment of the isotopically depleted melts.

Table 14.

Percent melting of depleted mantle (DM) component and percent enriched mantle (EM) contaminant required in the melt-contamination models of Chen and Frey (1983) (C-F Model), and of Anderson (1985) (A-Model) to produce the La/Ce and $^{87}Sr/^{86}Sr$ ratios of the Chilcotin basalts. NA indicates sample cannot be accounted for by the model.

	C-F Model		A-Model	
Group/Sample	%DM melting	%EM contaminant	%DM melting	%EM contaminant
A	0.25-0.5	93-95	2-4	7
B	0.2-0.4	98	2.5-4	10-12
C	0.25-0.4	95-97	3-4	7-10
2-30B	NA	NA	5	15
2-66D	3	95	NA	NA
2-99A	1	99	50	6

A feature of the Hawaiian basalts in the C-Y model is that their La/Ce range requires variation in the degree of melting of the DM component. This contradicts the results of Richter and Mackenzie (1985) who contend that the output of melt from the DM component should only decrease slightly with time. This is not a problem for the genesis of the Chilcotin Group which have constant La/Ce and, if the degree of melting of the DM is fixed at either 0.3% (C-F model), or 3.5% (A-model) (Table 14), the sequence of eruption should be controlled by the amount of EM contamination. The output of the EM component should decay faster than that of the DM component because of its higher initial fluid fraction (Richter and Mackenzie 1985). Consequently, the Chilcotin basalts should become progressively more enriched in the DM component over time, regardless of the model or parameters used for the components. This is consistent with the observed eruption sequence; group B which require the greatest imput from the EM component occur on the periphery of the main plateau and probably constitute the first stages of activity at a given locality.

VIII. Spinel lherzolites as Direct Evidence of the Mantle Beneath BC

Introduction

Mantle xenoliths occur frequently in late Tertiary to Recent alkali basalts throughout central British Columbia (Littlejohn and Greenwood 1974, Fiesinger and Nicholls 1977). Although fifteen localities have been studied, most of the work has focussed on the petrography and mineral chemistry of the xenoliths (Fujii and Scarfe 1982, Ross 1983, Brearley et al. 1984). The principal localities in southern British Columbia are shown in Fig. 24.

The majority of the xenoliths are Type I Cr-diopside bearing spinel lherzolites. Websterite, harzburgite, and dunite are less common within this suite. Type II black-clinopyroxene-bearing xenoliths, mostly wehrlites or clinopyroxenites, also occur at most localities, but are far less abundant than the Type I xenoliths (Fujii and Scarfe 1982, Brearley et al. 1984). The clinopyroxene in the Type II xenoliths has been identified as an Al-Ti-rich, Cr-poor chrome diopside rather than the aluminous augite which characterises Type II xenoliths sensu stricto (Ross 1983). Composite Type I/II xenoliths, banded on a millimetre scale have also been reported (Brearley et al. 1984). Amphibole-bearing lherzolites are extremely rare, and have been reported only from Lightning Peak in southern British Columbia (Brearley and Scarfe 1984), and from one locality in northern British Columbia (Higgins and Allen 1985).

The Type I xenoliths have been divided into 'depleted' and 'undepleted' categories on the basis of the Ti/Cr ratio in their diopsides (Ross 1983). These categories may also be recognised from the

appearence of the xenoliths, the 'undepleted' group being homogeneous, containing mostly spinel lherzolites. The 'depleted' lherzolites are inhomogeneous, and include harzburgites and dunites which contain thin (1 to 2 cm) bands of websterite or spinel lherzolite (ibid.). The use of the the term 'undepleted' is misleading as the xenoliths were shown to have undegone some enrichment from their phase chemistry (ibid.). The term 'less-depleted' will be used in preference in this work.

Sampling

Xenoliths from three localities, Summit Lake, Lightning Peak, and Rayfield River, were selected for whole rock major and trace element analysis, and Nd-Sr isotopic analysis. All three localities, as for most others in central British Columbia, lie within the Quesnel terrane (Fig. 24).

Xenoliths from Summit Lake have been previously described by Ross (1983) and Brearley et al. (1984). Of twelve xenoliths selected for study, nine are Type I spinel lherzolites; the other three are Type II wehrlites. The host basalt has been included in the Miocene Endako Group (Souther 1977), but may be significantly younger, if not post-glacial in age (Brearley et al. 1984). Alternatively, Ross (1983) proposes an age of 26 Ma for this basalt.

The host basalt at Rayfield River (sample RR) is classified as group A hawaiite of the Chilcotin basalts. The evolved composition of RR is unusual in that the other nodule-bearing xenoliths from British Columbia are of alkali basalt to nephelinite composition (Littlejohn and Greenwood 1974, Fiesinger and Nicholls 1977, Fujii and Scarfe 1982, Higgins and Allen 1985). Ultramafic xenoliths comprise 20% of the flow

and are considerably more rounded and smaller than at other localities such as Summit Lake or Lightning Peak. Maximum sizes of up to 10 cm were recorded for the xenoliths, although most are less than 5 cm in diameter. Three xenoliths (1RR, 2RR and RR218) and one Type I cumulate xenolith (RR61) which were considered representative of the population Rayfield River, were selected for isotopic and trace element analysis. Only RR61 was large enough for whole-rock XRF analysis. 2RR and RR218 are classified as homogeneous Type I spinel lherzolites. 1RR is an inhomogeneous Type I harzburgite containing a 1 cm websterite vein. 1RR-CD, a large (3 mm) chrome diopside crystal from this vein was also analysed. The overall small size of the xenoliths precluded crushing by swing-mill, and thus the grain size could not be homogenised after disaggregetion. This heterogeneity is reflected in the range of isotopic compositions on separate aliquots (designated A, B, etc.) of the sample powders.

Only one xenolith, the amphibole-bearing Type I spinel lherzolite described by Brearley and Scarfe (1984) (labelled LtPk), was analysed from the Lightning Peak locality. The 2.5 Ma age of the host basalt at Lightning Peak (ibid.) overlaps the last phase of activity of the Chilcotin basalts.

Major Element Chemistry

In major element chemistry (Table 15a) the xenoliths are divided into two groups corresponding to the Type I and II classification. The Type II xenoliths exhibit a similar but slightly higher MgO range of 40.5 to 42.5% compared to the Type I xenoliths which have 39 to 42% MgO. MgO contents for both groups are greater than the enriched mantle

Table 15.

(a) Major and trace element chemistry of spinel lherzolites from Summit Lake and Lightning Peak.

	SL141	S1170A	SL201	SL390	LtPK	S1174	SL120	SL153	SL200
SiO_2	41.03	43.30	43.82	43.99	44.19	46.03	41.91	40.09	40.43
Al_2O_3	1.10	2.77	3.47	2.36	3.69	3.27	2.22	2.39	2.24
FeO	14.25	8.88	8.79	8.34	8.67	9.59	10.13	10.74	11.41
MgO	41.73	41.31	39.98	41.91	39.04	37.17	40.69	42.59	41.27
CaO	0.89	2.86	2.84	2.50	3.27	2.88	4.08	3.31	3.77
Na_2O	0.06	0.00	0.15	0.06	0.20	0.15	0.00	0.00	0.00
K_2O	0.00	0.00	0.00	0.00	0.00	0.00	0.00	0.00	0.00
TiO_2	0.02	0.07	0.10	0.06	0.12	0.10	0.14	0.12	0.13
P_2O_5	0.00	0.00	0.00	0.00	0.01	0.00	0.01	0.01	0.01
S	0.01	0.01	0.01	0.01	0.01	0.00	0.01	0.02	0.01
NiO	0.18	0.26	0.24	0.28	0.24	0.21	0.27	0.25	0.22
Cr_2O_3	0.36	0.38	0.44	0.37	0.41	0.16	0.17	0.16	0.18
MnO	0.24	0.14	0.14	0.13	0.14	0.16	0.17	0.16	0.18
Ba	25	21	30	11	14	40	27	17	26
Nb	2	3	3	3	3	4	4	3	5
Zr	9	10	10	10	13	13	17	14	15
Y	2	4	4	4	5	5	5	4	5
Sr	9.37	7.56	8	5	10.5	16	22	14	18.8
Zn	70	51	59	55	50	55	53	66	58
Cu	6	32	28	31	29	36	29	24	13
mg	84	89	89	90	89	87	88	88	87

(b) Major and trace element composition of the Summit Lake host basalt SL121/2, Rayfield River host basalt RR; and cumulate xenolith RR61.

	SL121/2	RR	RR61
SiO_2	46.21	50.16	49.11
Al_2O_3	16.99	15.09	7.87
Fe_2O_3	10.01	11.63	9.81
MgO	7.89	7.17	16.35
CaO	10.01	7.49	15.52
Na_2O	3.45	4.63	0.87
K_2O	2.93	0.98	0.00
TiO_2	1.73	2.12	0.25
P_2O_5	0.60	0.55	0.03
S	0.01	0.01	0.01
MnO	0.16	0.17	0.18
Ba	1753	478	55
Nb	78	33	4
Zr	190	229	19
Y	24	25	11
Sr	719	713	36
Rb	86	15	
Zn	55	71	38
Cu	57	71	81
Ni	141	152	344

Major elements recalculated to 100% on a volatile-free basis.
Trace elements in ppm.

estimate of 35.5% MgO (Palme and Nickel 1985), but overlap the primitive mantle estimate of 41% MgO of Maaloe and Aoki (1977). SL174, which has 37% MgO, is not included in the discussion because of the visibly altered nature of this xenolith. It has been included in the data set for illustration of the trends of lherzolites on weathering.

Despite the restricted MgO ranges, both groups show good correlation of major elements with this oxide (Fig. 45) which is a ubiquitous feature of spinel lherzolites worldwide (Maaloe and Aoki 1977). The Type I xenoliths have 2.5 to 3.3% CaO similar to pyrolite (3.1% CaO). The Type II xenoliths have 3.3 to 4% CaO, approaching the enriched mantle estimate of 4.4% (Palme and Nickel 1985). FeO (10 to 11%) and MnO (0.16 to 0.18%) are both high in the Type II xenoliths compared to the lower and more restricted ranges in the Type I xenoliths (8.3 to 9% and 0.14 to 0.15%, respectively). The enrichment in Ca, Fe and Mn shown by the Type II xenoliths reflects their clinopyroxene composition. Conversely, the Type I xenoliths have high Cr_2O_3 contents of 0.37 to 0.44%, compared to 0.3 to 0.37% in the Type II xenoliths. The high Cr_2O_3 content of LtPk (0.41%) is consistent with the Cr-rich nature of other xenoliths from the Lightning Peak locality (Ross 1983). Both Type I and II xenoliths show similar variations in Al_2O_3 (2.2 to 3.7%) and NiO (0.22 to 0.28%). Silica contents of the Type I xenoliths (43 to 44.5%) are far higher than those of the Type II xenoliths (40 to 42%).

SL141 is an unusually iron-rich Type I lherzolite. FeO and MnO contents of 14.25% and 0.24% respectively, are far higher than in the other Summit Lake xenoliths whilst Al_2O_3 (1.1%) and CaO (0.99%) are much lower. The xenolith is depleted in TiO_2 and NiO, although Cr_2O_3 falls within the range of the other xenoliths and the silica content is

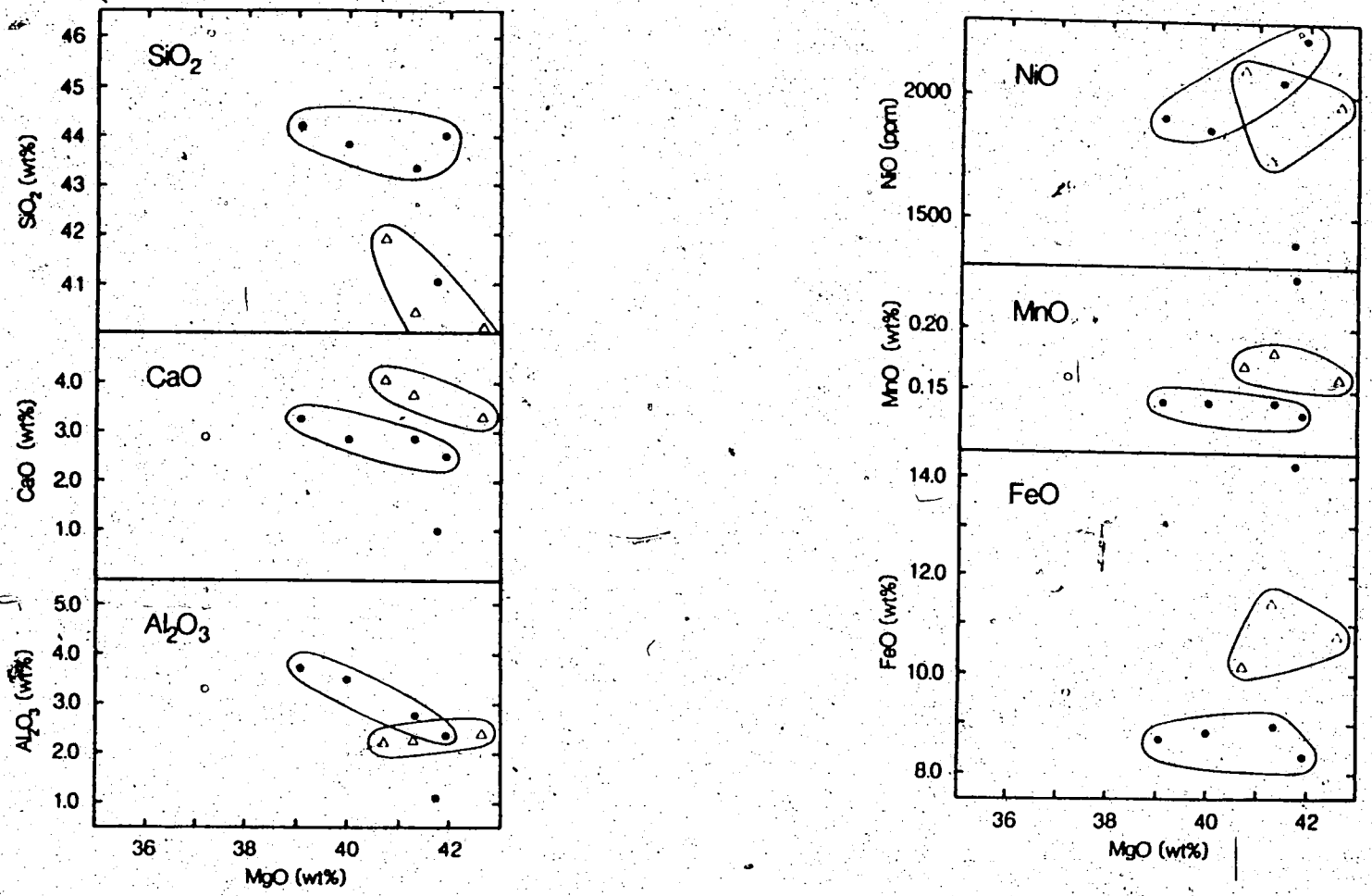

Fig. 45. Major element variation with MgO in spinel lherzolites from Lightning Peak and Summit Lake. • Type I xenoliths; △ Type II xenoliths, ○ SL174 . SL141 is the Type I xenolith plotting outside the field for these xenoliths.

similar to the Type II xenoliths. The chemical trends shown by SL141 are similar to those of the iron-rich Spring Mount lherzolite from southern Australia (Wilkinson and Binns 1977). Both nodules are distinct from other iron-rich lherzolites from Kilbourne Hole (Basaltic Volcanism Study Project 1981) and from central France (Hutchison et al. 1975) which have less than 12% FeO and resemble Type II xenoliths in bulk composition.

Trace Element Content

Trace elment contents for the Summit Lake xenoliths and LtPk normalised to the primitive mantle abundances of McDonough et al. are presented in Fig. 46. Rb, Sm and Nd were not determined on all samples; therefore, it was not possible to arrange the elements in order of increasing compatability on the diagram. Sr, Ba, Nb, Zr and Y as determined by XRF (Table 15a) are considered accurate to ±20% at the low concentrations in question. Rb, Sr, Sm and Nd were determined by mass spectrometry isotope dilution on selected samples. Both Type I and II xenoliths show similar trends: Zr and Y contents show a limited range close to the primitive mantle abundances of 11.1 and 4.69 pm, respectively. Ba (10 to 30 ppm) and Nb (3 to 5 ppm) are enriched as much as six times the primitive mantle value. Both Sr and Ti are depleted from 0.8 to 0.3 times primitive mantle abundances, except in SL120 where the Sr content (22 ppm) approaches the primitive mantle value. Rb is extremely depleted in all Type I and II xenoliths except SL141. The absolute concentrations of Rb (0.02 to 0.3 ppm) and Sr (5 to 22 ppm) fall within the range of 'depleted but fertile mantle', and are in contrast to the Ba contents (11 to 30 ppm) which are more characteristic

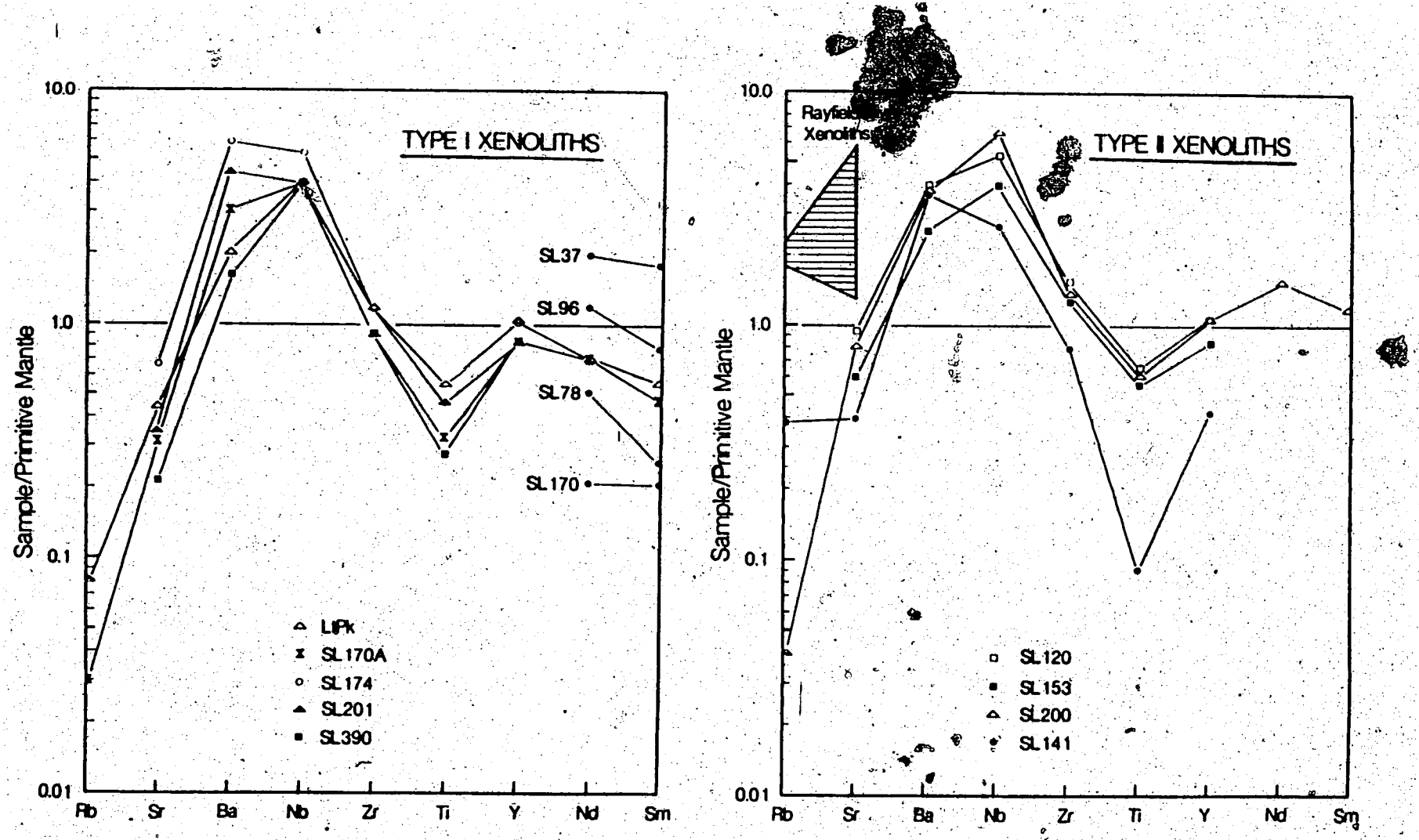

Fig. 46. Trace element abundances of spinel lherzolites from Lightning Peak, Rayfield River and Summit Lake normalised to the primitive mantle values of McDonough et al. (1985); (a) Type I xenoliths from Summit Lake and LtPk; (b) Type I xenoliths from Rayfield River and Type II xenoliths from Summit Lake.

of metasomatised mantle (Roden and Murthy 1985).

The high Zr and Sr contents of the Type II xenoliths are evident on plots of MgO versus Sr and MgO versus Zr (Fig. 47). The similarity in Ba contents in the two groups gives a characteristic Sr/Ba ratio of 0.3 for the Type I xenoliths and 0.76 for Type II. Nd and Sm data show that the nodules are enriched or depleted in LREE relative to the primitive mantle abundances, but all have Sm/Nd less than chondritic. Of the chalcophile trace elements, Zn is expected to substitute for Fe^{2+}, and shows a positive correlation with FeO content. Zn abundances of 50 to 59 ppm in the Type I xenoliths and 53 to 66 ppm in Type II, are similar to the primitive mantle estimates of Jagoutz et al. (1979) and Sun (1982). Cu behaves as an incompatible element with respect to the lherzolite mineralogy, and shows only a rough correlation with FeO. Cu contents range from 13 to 24 ppm in the Type II xenoliths and from 28 to 32 ppm in the Type I xenoliths. The latter range includes the upper mantle estimate of 30 ppm (Sun 1982). SL141 has 70 ppm Zn and 6 ppm Cu, and represents an extreme example of the fractionation of chalcophile elements in a silicate mineralogy.

REE were determined by the method of Duke and Smith (1986) on the Type I spinel lherzolite RR218 and LtPk. The data are presented in Table 16 and as chondrite normalised plots in Fig. 48. RR218 has very low REE concentrations, from 0.07 to 0.2 times chondritic, and shows a V-shaped pattern with a Eu/Eu^* value of +2.06 . LtPk also displays a V-shaped pattern but has REE abundances closer to chondritic values and a smaller Eu anomaly of Eu/Eu^* +1.32 . The La depletion relative to Ce is caused by the presence of amphibole.

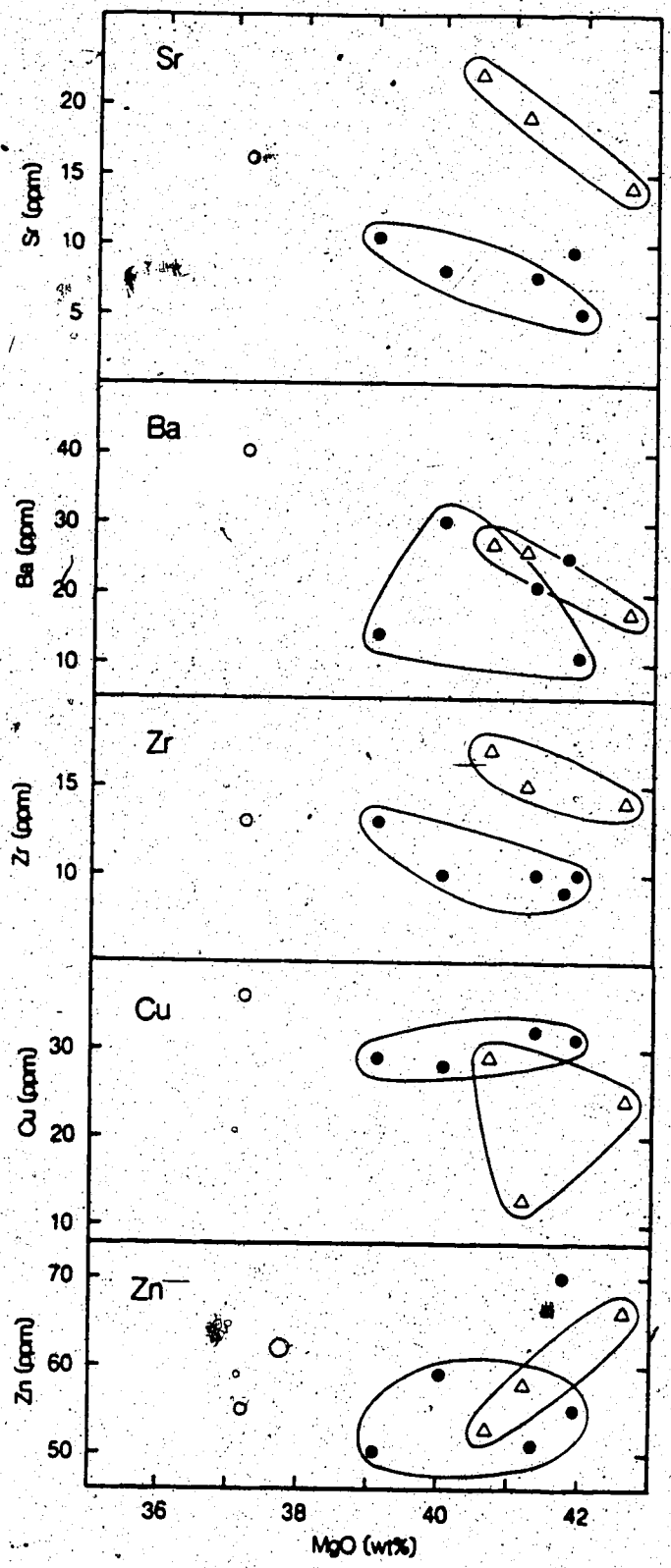

Fig. 47. Trace element variation with MgO in spinel lherzolites from Lightning Peak and Summit Lake spinel. Symbols as for Fig. 45.

Table 16.

REE abundances for xenoliths LtPk (in ppm) and RR218 (in ppb).

	La	Ce	Nd	Sm	Eu	Gd	Tb	Dy	Ho	Er	Yb	Lu
LtPk	0.37	1.37	1.05	0.25	0.10	0.20	0.07	0.55	0.14	0.47	0.52	0.064
RR218	63.2	145		18.0	13.5		4.75	37.3	10.3		45.0	7.64

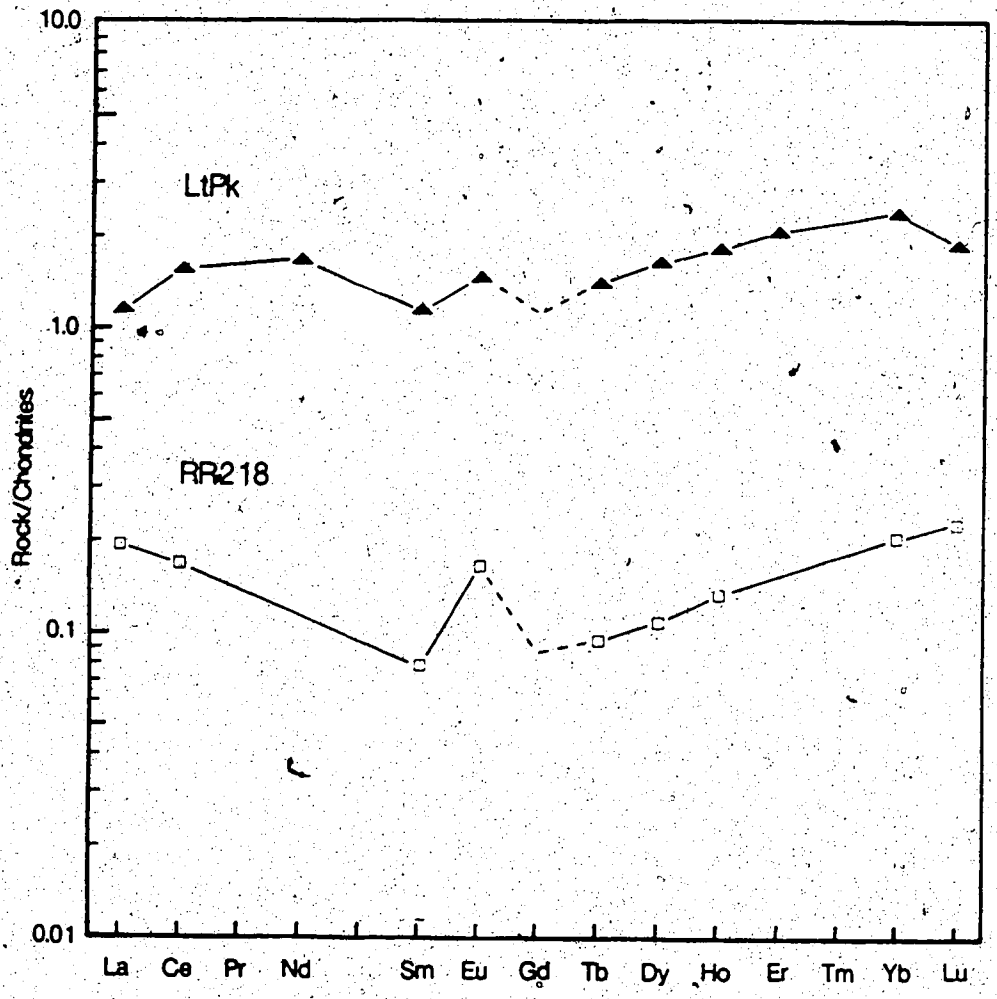

Fig. 48. Chondrite normalised rare earth element patterns of spinel lherzolites LtPk and RR218

Host Basalts

The major element chemistry and petrography of the Summit Lake and Lightning Peak host basalts have been discussed by Brearley et al. (1984) and Brearley and Scarfe (1984). The Summit Lake host basalt, SL121/2, has been re-analysed by XRF (Table 15b) to determine the trace element chemistry. The basalt was classified as a basanitoid or potassic series alkali basalt by Brearley et al. (1984). The principal major element feature of SL121/2 is the high K_2O content of 2.9% giving a K_2O/Na_2O ratio of 0.85 , and is accompanied by a high Rb content of 55 ppm. Sl121/2 is also enriched in Ba (1750 ppm) and Nb (78 ppm) but not particularly so in Zr (190 ppm). The Y content of 24 ppm is comparable to the group B and C Chilcotin basalts. The Ba/Y ratio of 72 , is far removed from the included xenoliths which have Ba/Y ratios of less than 7.5 . This suggests that the basalt was generated by a small degree of partial melting of an amphibole or phlogopite bearing spinel lherzolite source. SL121/2 (duplicate sample SL128/9) has a slightly enriched isotopic composition of $^{143}Nd/^{144}Nd$ =0.51261 and $^{87}Sr/^{86}Sr$ =0.70574 (Table 17). Unlike many other alkali basalts, the isotopic ratios are not contradicted by the observed Sm/Nd or Rb/Sr ratios of 0.176 and 0.120, respectively. A model age of 500 Ma is calculated from both Rb-Sr and Sm-Nd systems for derivation of SL121/2 from a MORB-source reservoir with present day ϵNd +8 .

A large plagioclase megacryst (MCSL71B), greater than 5 cm in diameter, was found to have a similar, but significantly higher $^{87}Sr/^{86}Sr$ ratio of 0.70594 compared to SL121/2. The megacryst cannot, therefore, have been in equilibrium with the basalt. A mantle origin for the megacryst is unlikely because the crust under Summit Lake is 35 km

Table 17.

Nd and Sr isotopic compositions of spinel lherzolites, related [redacted] and host basalts.

Sample		Rb (ppm)	Sr (ppm)	Rb/Sr	$^{87}Sr/^{86}Sr$	Sm (ppm)	Nd (ppm)	Sm/Nd	$^{143}Nd/^{144}Nd$	εNd
Summit Lake										
SL121/2	Basanitoid	86	719	0.120	0.70574±3	6.47	36.2	0.176	0.512612±19	-0.5
SL128/9					0.70573±2				0.512612±30	-0.5
MCSL71B	Megacryst				0.70594±2					
SL37	Type I	0.045	10.6	0.0042	0.70509±5	0.814	2.69	0.303	0.512802±32	+3.2
SL78	"	0.085			0.71191±4	0.114	0.701	0.163	0.511594±35	-20.4
SL96	"	0.279	10.7	0.0260	0.70618±4	0.352	1.60	0.220	0.512039±43	-11.6
SL141	"	0.262	9.37	0.0280	0.71017±2				0.512410±38	-4.4
SL170	"		6.34		0.70419±4	0.094	0.288	0.242	0.512778±50	+2.8
SL170A	"	0.019	7.56	0.0025	0.70602±8	0.214	0.965	0.222		
SL200	Type II	0.025	18.8	0.0013	0.70587±8	0.524	2.11	0.249	0.512988±65	+6.9
Lightning Peak										
LtPk	Type I	0.052	10.2	0.0051	0.70453±15	0.253	0.965	0.262	0.512747±24	+2.1
Rayfield River										
RR	Hawaiite	15	713	0.0210	0.70301±2	6.18	27.7	0.223	0.513025±10	+7.6
1RR	Type I	1.26	89.8	0.0140	0.70362±2	0.145	0.527	0.276	0.512961±34	+6.3
1RR-B	"	1.35	97.9	0.0138	0.70373±2					
2RR	"	3.20	114	0.0280	0.70421±2	0.155	1.07	0.145	0.512916±46	+5.4
2RR-B	"			0.0392	0.70389±3					
RR218A	"	1.47	31.5	0.0467	0.70455±1	0.180	0.710	0.253		
RR218B	"	1.55	141	0.0110	0.70391±3					
RR218C	"	1.47	30.3	0.0484	0.70409±3					
1RR-CD1	Chrome Diopside	0.273	59.6	0.0046	0.70242±8				0.513055±55	+8.2
RR61	Type I cumulate				0.70358±4				0.512944±33	+6.0

thick, precluding the existence of a plagioclase lherzolite stability field in the mantle. It is possibile that the megacryst originated from a previous magmatic episode which ponded at the base of the crust. Such underplating is an important feature of the model for continental basaltic volcanism of Cox (1980). The isotopic composition of the megacryst implies a more isotopically enriched source for the preceding melt.

Isotopic Composition of the Mantle Xenoliths

The Summit Lake xenolithe and LtPk show considerable variation in $^{143}Nd/^{144}Nd$ (0.51160 to 0.51300) and in $^{87}Sr/^{86}Sr$ (0.7040 to 0.7102) (Table 17) compared to spinel lherzolites elsewhere (Menzies and Murthy 1980, Zashu et al. 1980, Roden et al. 1984, Menzies et al. 1985, Sun 1985). Three Type I xenoliths, SL37, S170 and LtPk, show a restricted range of $^{143}Nd/^{144}Nd$ (0.51275 to 0.51280) and $^{87}Sr/^{86}Sr$ (0.7042 to 0.7051), similar to the lherzolites from Rayfield River, and lie within the field for continental and ocean island basalts (Fig. 49). Other Type I xenoliths from Summit Lake have $^{143}Nd/^{144}Nd$ ratios of 0.51159 to 0.51241 and $^{87}Sr/^{86}Sr$ ratios of 0.7062 to 0.7102, similar to the compositions of kimberlites and related rocks (McCulloch et al. 1983). The Type II xenolith SL200 has significantly higher $^{143}Nd/^{144}Nd$ (0.51299) but similar $^{87}Sr/^{86}Sr$ (0.7059) to the Type I samples. All xenoliths have low Rb/Sr (0.001 to [illegible]) and Sm/Nd ratios (0.16 to 0.30). On a Rb-Sr isochron plot the Summit Lake xenoliths scatter to the right of the geochron and cannot be interpreted as showing any age relationship. Three xenoliths, SL37, SL78, and SL96, lie on a Sm-Nd isochron of 2221±130 Ma (Fig. 50).

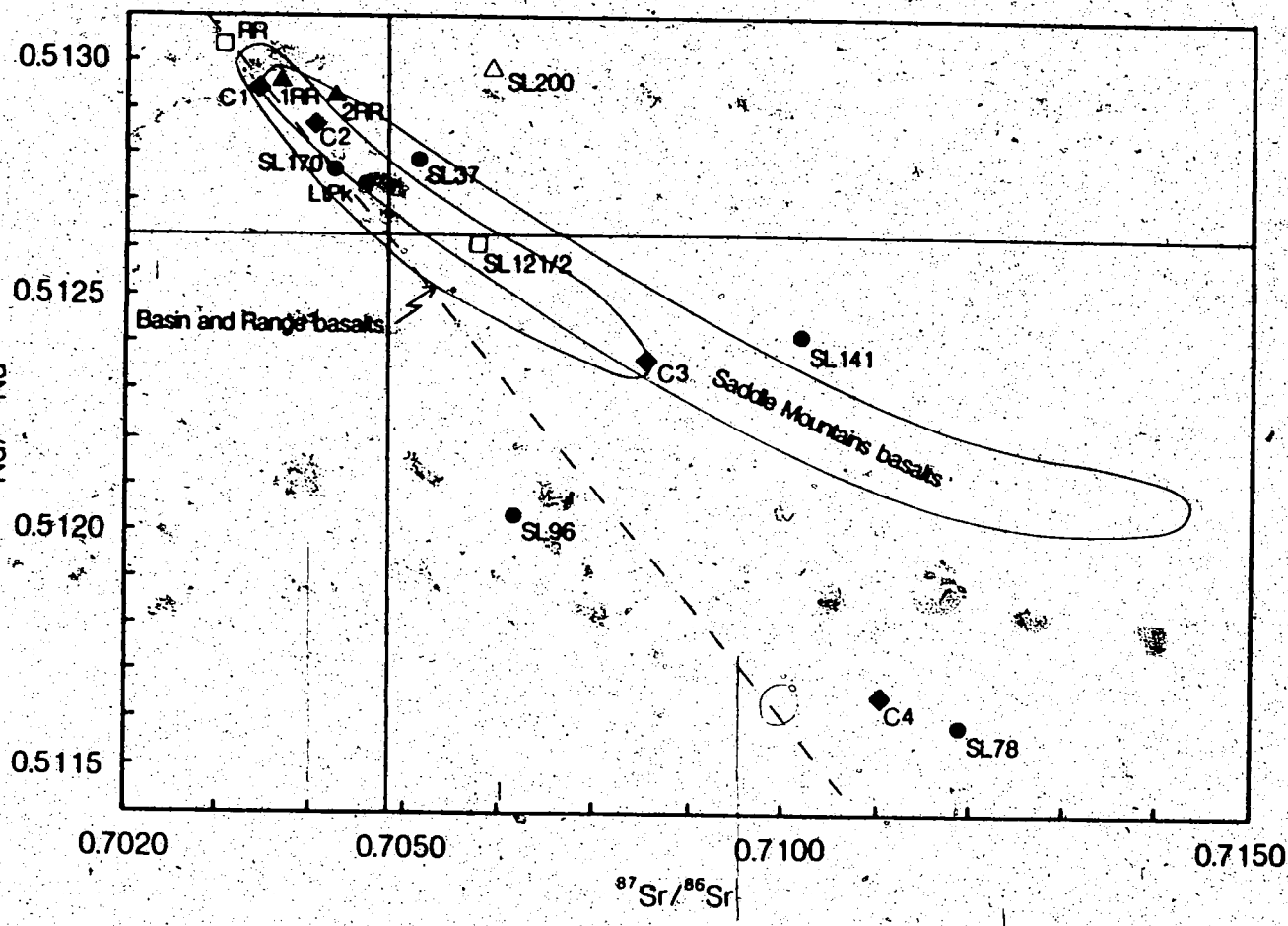

Fig. 49. Nd-Sr isotopic diagram for spinel lherzolites from Lightning Peak, Rayfield River and Summit Lake. • Type I xenoliths; △ Type II xenoliths; ▲ Rayfield River xenoliths; □ host basalts. Fields for the Saddle Mountain basalts from Carlson (1984), and for the Basin and Range Province from Hart (1985). Also shown are the mantle components C1 to C4 invoked in the genesis of the Columbia River basalts (Carlson 1984).

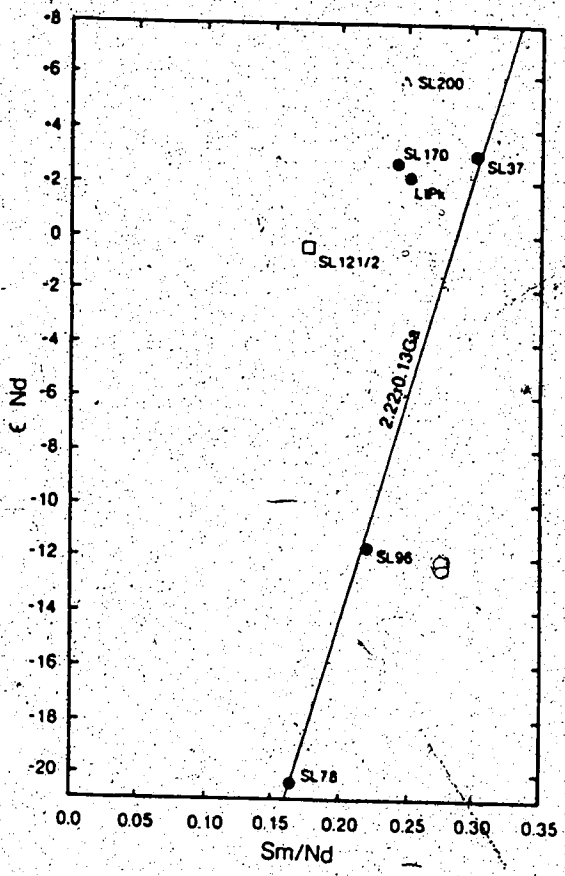

Fig. 50. Sm-Nd isochron plot for spinel lherzolites from Summit Lake.

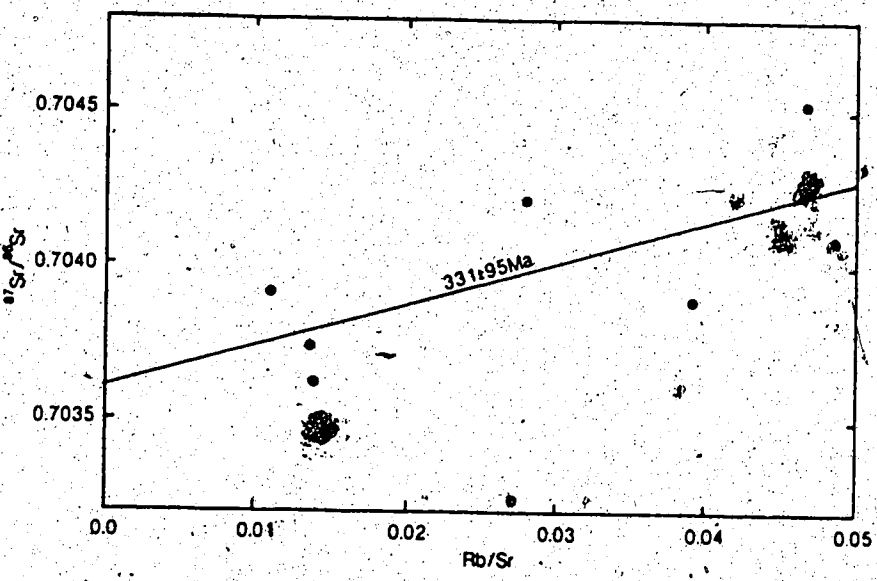

Fig. 51. Rb-Sr isochron plot for spinel lherzolites from Rayfield River.

The Nd and Sr isotopic compositions of the Rayfield River xenoliths ($^{87}Sr/^{86}Sr$ ratios of 0.7036 to 0.7045 and $^{143}Nd/^{144}Nd$ ratios of 0.51291 to 0.51296) are significantly more enriched than the host basalt RR which has $^{87}Sr/^{86}Sr$ =0.7032 , $^{143}Nd/^{144}Nd$ =0.51302. A whole rock isochron of age 331±95 Ma, initial ratio 0.70361 , is defined by the Rb-Sr isotopic data for the Rayfield River xenoliths (Fig. 51). The xenoliths overlap the isotopic compositions of the group B Chilcotin basalts (Fig. 36), but at a given $^{87}Sr/^{86}Sr$ ratio, have slightly higher $^{143}Nd/^{144}Nd$. The diopside lRR-CD has very depleted isotopic ratios ($^{87}Sr/^{86}Sr$ =0.70242 , $^{143}Nd/^{144}Nd$ =0.51307) compared to the host basalt.

Origin of the Major and Trace Element Trends

The enrichment in MgO and corresponding depletion in other major elements, relative to primitive mantle abundances, shown by spinel lherzolites worldwide results from partial melt extraction (Basaltic Volcanism Study Project 1981). Spinel lherzolites, therefore, are interpreted as the residua from the comparatively small degrees of melt extraction incurred incurred by alkali basalt genesis. More depleted xenoliths, such as harzburgites, are interpreted as residua from larger degrees of melt extraction during tholeiite genesis (Menzies 1983). Frey and Green (1974) labelled the residual component (A), whilst a second component (B) was proposed to account for the enrichment in P, K, Ti, LREE, Th and U shown by some lherzolites over their counterparts with similar major element chemistry and mineralogy. This resulted in the suffix A or B being added to the Type I mineralogical classification scheme. As component (B) resides in clinopyroxene, this resulted in the distinction that Type IA xenoliths have clinopyroxenes with LREE

depleted profiles whilst Type IB xenoliths contain clinopyroxenes with LREE enrichment. Both Types IA and IB are further subdivided into metasomatised and unmetasomatised varieties, the former being recognised by the presence of hydrous phases such as amphibole (Menzies 1983).

Clinopyroxenes from Type IA xenoliths give Sm-Nd model ages of 1 to 4 Ga (Menzies et al. 1985), interpreted as evidence for widespread partial melting in the mantle during this time interval. Type IB clinopyroxenes give younger model ages of 0.3 to 0.9 Ga and have isotopic ratios that do not represent a time-integrated response to the observed Sm/Nd ratio. The model ages, high Nd/Sm and LREE enrichment of the xenoliths analysed here suggests affiliation to Type IB. Diopsides from Type IB lherzolites show positive Eu anomalies (Menzies et al. 1985) but these are invariably of lower magnitude than observed in RR218. The Eu anomaly of RR218 is more characteristic of mantle mica (Irving and Frey 1984, Menzies et al. 1985) or plagioclase (Irving and Frey 1984). The REE pattern of RR218 is similar to that of the harzburgite Kal67 of Kurat et al. (1980), a leached fraction of which was highly enriched in Ba, K, La, Sm and Eu and, to a lesser extent in Fe, Mn, Co, Na, Yb and Lu, all of which must have resided in an intergranular phase. The Rb, Sr and Eu enrichment shown by RR218 suggests the residence of these incompatible elements in a similar grain bounday phase.

LtPk is slightly less depleted than the Type I xenoliths from Summit Lake but its similarity in major and trace element chemistry indicates that the metasomatisation has not significantly altered the composition of the material. The Ba content of LtPk is abnormally low compared to the other spinel lherzolites, with the exception of the

refractory SL390. On a plot of MgO versus Ba (Fig. 47) LtPk lies on a line from the Type I xenoliths toward the bulk Earth composition. This suggests that a slightly different enrichment mechanism affected the xenolith, or that large scale trace element heterogeneity is present in the mantle beneath British Columbia.

The higher Ca, Fe, Mn, Zr and Sr contents of the Type II xenoliths are consistent with the suggestion that the clinopyroxenes in such xenoliths are precipitates from an alkalic liquid at high pressure (Irving 1980). The low Rb and similar Ba contents, compared to the Type I xenoliths, result from the incompatibility of these elements in the clinopyroxene structure. Type II xenoliths have moderately depleted $^{143}Nd/^{144}Nd$, characteristic of the parent alkalic liquid (Menzies 1983). Whilst the $^{143}Nd/^{144}Nd$ ratio of SL200 is consistent with such an origin, the elevated $^{87}Sr/^{86}Sr$ requires a complex multi-stage history.

Relationship of Xenoliths to Mantle Components

The isotopic composition of the ultramafic nodules provides direct evidence for the existence of both isotopically depleted and enriched mantle beneath western North America. Recent studies on the Columbia River basalts (Carlson 1984) and Basin and Range Province (Hart 1985) have required the involvement of such mantle material as mixing components in the genesis of the basalts from these regions. The similarity of the isotopic characteristics, particularly of the Summit Lake xenoliths, to the mantle components C1 to C4 proposed for the Columbia River basalts (Carlson 1984) is marked:

Component C1 represents depleted mantle and has $\epsilon Nd > +6.5$, $^{87}Sr/^{86}Sr < 0.7035$, similar to the lherzolite lRR.

Component C2 has ϵNd of +4.5 and $^{87}Sr/^{86}Sr$ =0.7040 , similar to 2RR, SL200, SL170, S137 and LtPk.

Component C3, important in the genesis of the Saddle Mountains basalt, has $^{143}Nd/^{144}Nd$ similar to SL141 but has lower $^{87}Sr/^{86}Sr$. Iron-rich lherzolites such as SL141 have been proposed as the source material for anorogenic andesites such as the Columbia River basalts (Wilkinson and Binns 1977).

Component C4 represents old silicic continental crust and has ϵNd values from -20 to -30 and $^{87}Sr/^{86}Sr$ ratios from 0.7100 to 0.7150 . The isotopic composition of SL78 demonstrates that this component may reside in the mantle, obviating the requirement for crustal contamination, estimated at as much as 30% for the more isotopically enriched members of the Columbia River basalts.

Evolution of the Mantle Beneath British Columbia

Sm-Nd model ages have been calculated for the xenoliths from Fig. 52 . The depleted mantle growth curve (DMS) corresponding to a present day ϵNd of +12 intersects the xenolith evolution lines between 0.3 and 1.8 Ga. Ocean ridge basalts commonly have ϵNd as low as +8 (Jacobsen and Wasserburg 1979, McCulloch et al. 1980); therefore, a curve corresponding to the evolution of such a reservoir (LDMS) has also been drawn to represent a lower ϵNd limit for the depleted mantle. The xenolith evolution lines intersect the LDMS curve between 0.1 and 1.6 Ga, similar to the age range of spinel lherzolites from other localities in British Columbia (Sun 1985). The evolution lines of SL37, SL78, and SL96 intersect around 2.2 Ga on Fig. 52 as would be expected from the Sm-Nd isochron plot. The initial ratio of ϵNd +7 is far higher than the

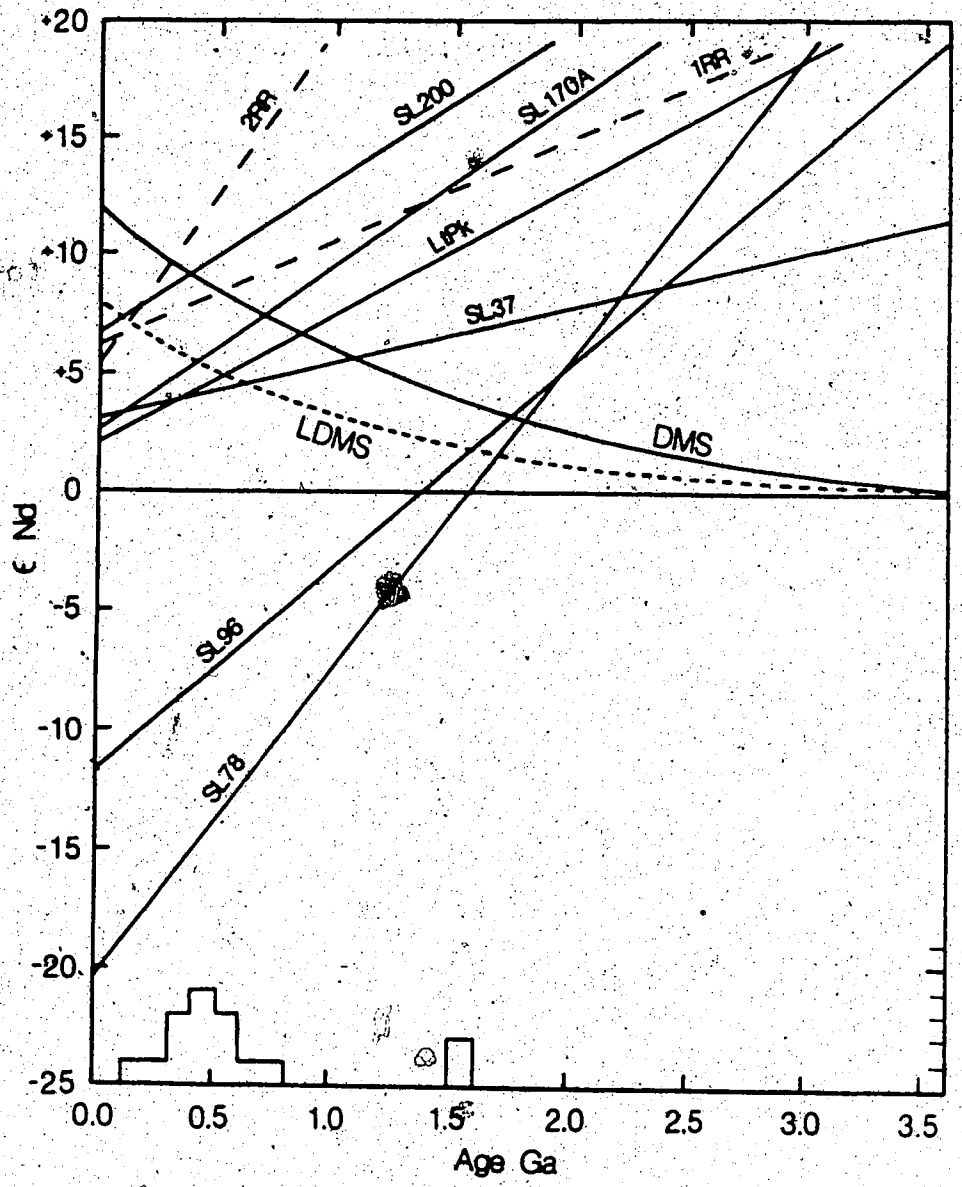

Fig. 52. εNd versus Time diagram illustrating the model ages for spinel lherzolites from Lightning Peak, Rayfield River and Summit Lake. The depleted mantle schematic (DMS) curve represents the evolution of a depleted mantle reservoir to a present day εNd of +12, and corresponds to the average of the most depleted rocks of differing ages that have been analysed by the Sm-Nd method (DePaolo and Wasserburg 1976, Jacobsen and Wasserburg 1979). The lower depleted mantle schematic (LDMS) curve represents the corresponding evolution of a less-depleted resevoir to present day εNd of +8 . Also shown is a histogram (scale on right y-axis) of Rb-Sr ages for fifteen spinel lherzolites from nearby localities in British Columbia (Sun 1985) (The 331Ma age for the Rayfield River xenoliths has also been included).

ϵNd of +2 for the DMS curve at this time. However, the DMS curve does not place a strict upper limit on the maximum ϵNd of the mantle because the curve represents an average of the most depleted rocks of differing age that have been analysed (Jacobsen and Wasserburg 1979, DePaolo and Wasserburg 1976). Mantle with ϵNd of +7 could have been generated from a reservoir with MORB-like Sm/Nd by 2.2 Ga, but only if the original depletion event took place prior to 4.2 Ga. Most Archaean mantle-derived rocks have isotopic compositions close to the bulk Earth values (Patchett 1983), although there is a growing amount of data (Zindler 1982, Ashwal et al. 1985 and references therein) to suggest that by 2.5 to 2.7 Ga certain regions, notably the Superior Province, were underlain by depleted mantle with ϵNd as high as +5 .

The Rayfield River xenoliths 1RR and 2RR intersect LDMS at approx. 100 Ma, much more recently than the 331 Ma age indicated for these xenoliths by the Rb-Sr system. The average of the two model ages for derivation of these xenoliths from the DMS would correspond more closely to the Rb-Sr age.

In contrast to the Sm-Nd systematics, the Rb/Sr ratios are generally an order of magnitude lower than chondritic and are inconsistent with the high $^{87}Sr/^{86}Sr$ ratios. This causes the ϵSr of the xenoliths to decrease toward the present because the higher Rb/Sr of the bulk Earth causes the chondritic $^{87}Sr/^{86}Sr$ to increase much more rapidly (Fig. 53). The exception is RR218 which has higher Rb/Sr, similar to the majority of nodules from Jacques Lake, Big Timothy Mountain, Kettle River and Lassie Lake (Sun 1985), and could have been derived from a depleted mantle reservoir in a single stage. Three possibilities to account for the high $^{87}Sr/^{86}Sr$ and low Rb/Sr ratios of the xenoliths are

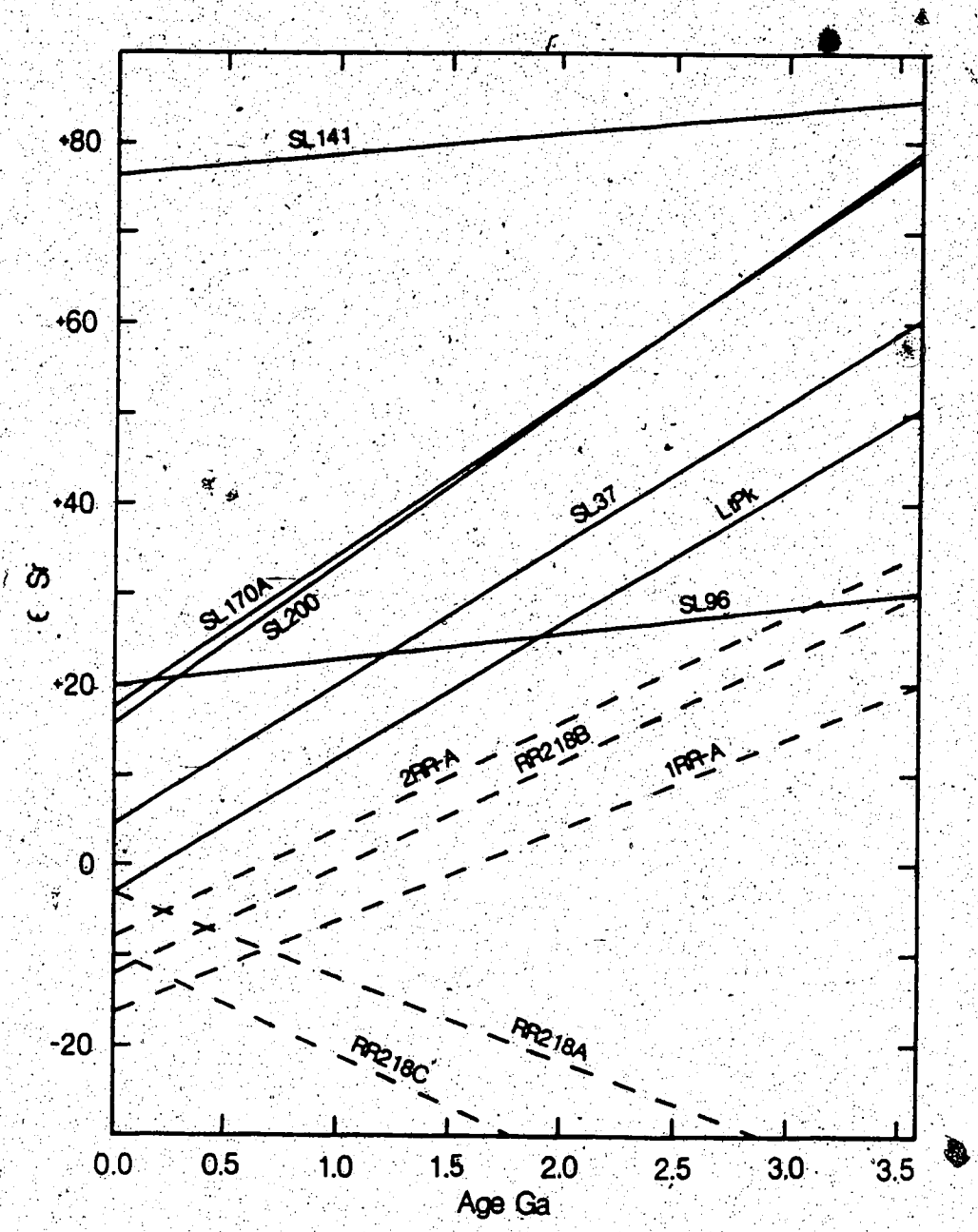

Fig. 53. εSr versus Time plot for spinel lherzolites from Lightning Peak, Rayfield River and Summit Lake.

considered:

(1) Low Rb/Sr and high $^{87}Sr/^{86}Sr$ ratios, similar to those of the Summit Lake nodules and LtPk, have been observed in spinel lherzolites from Itinome-gata, Japan (Zashu et al. 1980), implying a subduction-related origin. Brearley et al. (1984) suggested that the pargasite in LtPk was precipitated from an aqueous fluid, derived from an underlying subducted slab. The Nd-Sr isotopic evolution of the xenoliths is illustrated in Fig. 54. At the calculated Sm-Nd model ages all Summit Lake xenoliths and LtPk have ϵNd values of +2 to +7 and ϵSr values of +5 to +25 (corresponding to $^{87}Sr/^{86}Sr$ ratios of 0.7050 to 0.7065) and lie within the present day field for island arcs. Also shown in Fig. 54 is the field for modern oceanic sediments which have ϵNd values of -2 to -14 and ϵSr values of +60 to +350 (O'Nions et al. 1978, DePaolo and Wasserburg 1979, Piepgras et al. 1979, White et al. 1985). The young model ages (less than 0.5 Ga) of LtPk, SL37, and SL200 could mark the mixing of depleted mantle with such sediment. SL96 has a model age of 1.7 Ga, and is more difficult to model because its ϵNd of +2 and ϵSr of +25 at that time would require a relatively enriched sediment end member.

However, the model ages are for derivation from the LDMS curve which corresponds to the more enriched isotopic compositions of MORB. Few modern arcs (the Mariana and Izu arcs would be exceptions) have such depleted isotopic ratios. If the observed isotopic signatures of the xenoliths result from the equilibration of a slab-sediment-derived component with depleted mantle, this event could have occurred at any time along the evolution lines in Fig. 54. Such a model may account for the evolution paths, but it is difficult to explain how such an event

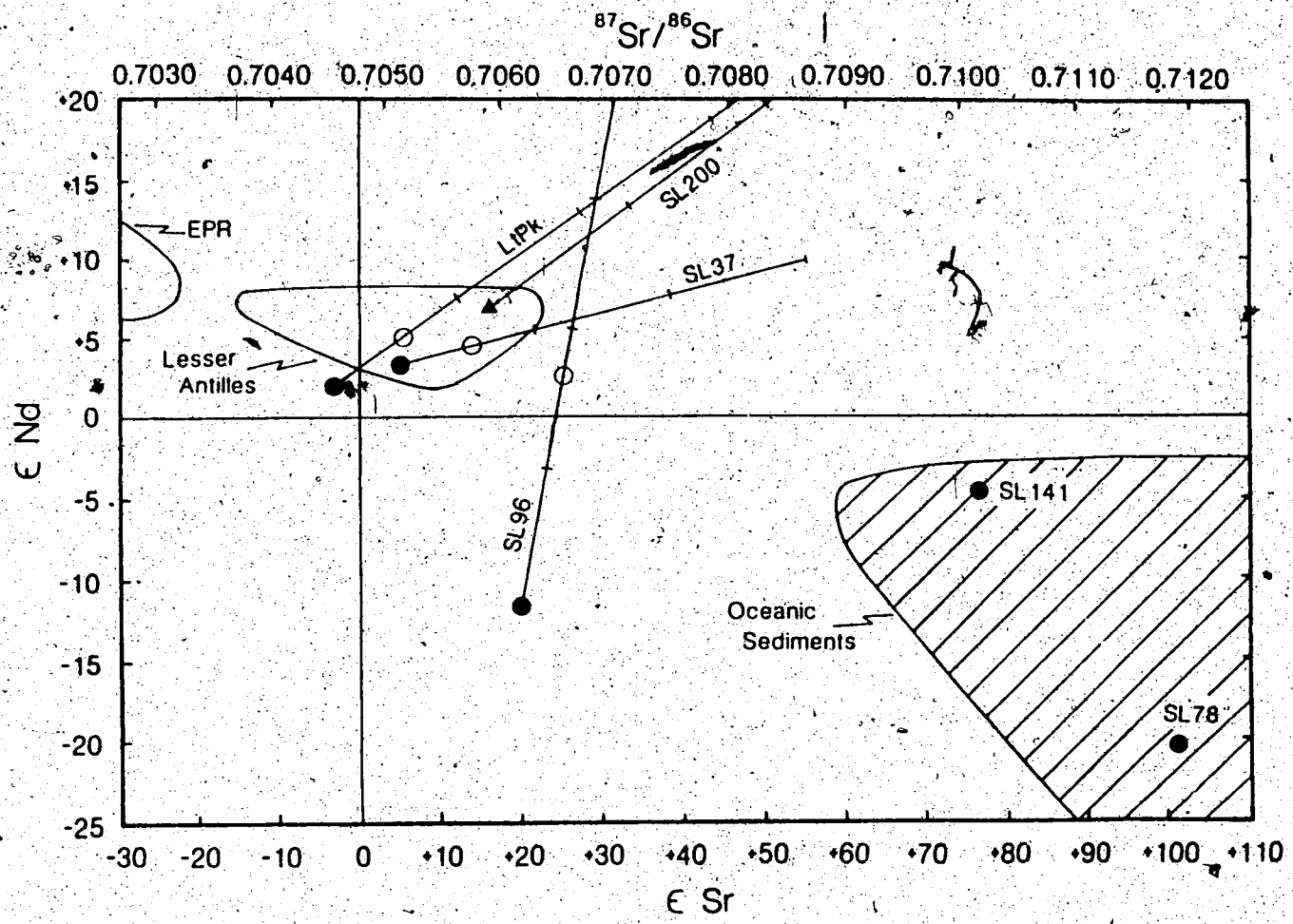

Fig. 54. εNd versus εSr diagram showing the evolution of the isotopic ratios of spinel lherzolites from Lightning Peak and Summit Lake. The low Rb/Sr and Sm/Nd ratios of the xenoliths results in both εNd and εSr decreasing toward the present as indicated by the evolution lines. Bars on these mark 1 Ga intervals from the present. • indicates the present εNd and εSr of the xenoliths, whilst ○ indicates εNd, εSr of the xenolith at the model age calculated in Fig. 52 (for derivation from a depleted resevoir corresponding to present day Nd of +8). Also shown are fields for the East Pacific Rise (EPR) (Zindler et al. 1984), oceanic sediments (O'Nions et al. 1978, DePaolo and Wasserburg 1979, Piepgras et al. 1979, White et al. 1985, and Lesser Antilles (Hawkesworth and Powell 1979, Hawkesworth et al. 1979, White and Patchett 1984).

would result in the low Rb/Sr ratios of the xenoliths, particularly when the concept of the incorporation of the sediment is to explain the LIL enrichment observed in arc lavas. Most oceanic sediments have Rb/Sr ratios from 0.25 to 1.0 (White et al. 1985). Only calcareous oozes would be likely to have similar Rb/Sr ratios to the xenoliths, and the subduction of such material alone is unlikely. A depletion event to produce the observed trace element ratios would be essential after equilibration of the mantle and sediment.

(2) A second explanation is that an ancient depletion event affected the mantle material leaving a harzburgite residue. Rb and Sr are both incompatible in olivine and enstatite; therefore, such a residue would have Rb/Sr greater than chondritic and would evolve to high $^{87}Sr/^{86}Sr$. The depletion event would also result in high Sm/Nd, producing an accompanying increase in $^{143}Nd/^{144}Nd$. A calculation shows that over 2 Ga harzburgite composed of 70% olivine with 0.1 ppm Rb, 1 ppm Sr, and 30% enstatite with 0.2 ppm Rb, 2 ppm Sr, could produce ϵSr +81 from a chondritic initial ratio.

The model is consistent with the suggestion (Brearley et al. 1984) that SL141 represents a cumulate texturally re-equilibrated within the upper mantle, but requires later enrichment of the harzburgite to produce the observed major and trace element variations, and an accompanying decrease in Rb/Sr . A depletion event to lower the Rb/Sr ratio, as proposed for model (1), is not feasible because the initial depletion event to produce the high Rb/Sr ratio would leave the material incapable of yielding a basaltic melt. The Rb/Sr ratio would have to be lowered by a metasomatic event. This would require that the metasomatic fluid be a basaltic melt, because equilibration with a hydrous

metasomatic fluid would result in too high a Rb/Sr ratio. The crucial requirement is that the metasomatising melt did not significantly lower the $^{87}Sr/^{86}Sr$ ratios of the depleted material.

(3) The ability of Rb-rich mantle minerals such as amphibole or phlogopite to produce abnormally high $^{87}Sr/^{86}Sr$ has been documented by Cohen et al. (1984). If an enrichment event resulted in the formation of amphibole or phlogopite, the evolution of the $^{87}Sr/^{86}Sr$ ratios in the mantle material would then be dominated by the high Rb/Sr of these minerals. A later depletion event, presumably recorded by the Sm-Nd model ages, would be required to remove the amphibole or phlogopite hence lowering the Rb/Sr ratio but leaving high $^{87}Sr/^{86}Sr$, provided the event also caused isotopic re-equilibration. This model may be considered an extension of (1), although the enrichment mechanism need not be related to subduction.

The first model is considered the most feasible, although it is stressed that the three models are neither unique nor mutually exclusive, but represent the simplest possible sequence of events to produce the observed $^{87}Sr/^{86}Sr$ and Rb/Sr ratios.

IX. Relationship of Xenoliths to Miocene to Recent volcanism

Characteristics of the Mantle Beneath British Columbia

Geothermal gradients and depth-composition profiles for Summit Lake, Lightning Peak and six other xenolith localities in the Canadian Cordillera have been calculated by Ross (1983). It is probable that the two-pyroxene thermobarometer used by Ross (1983) resulted in high equilibration temperatures but this will not have affected the internal consistency of the depth-composition profiles. Simplified depth-composition profiles for Lightning Peak, and also for the Big Timothy Mountain and Jacques Lake localities which are between Summit Lake and Rayfield River (Fig. 24) are shown in Fig. 55. The profile for Summit Lake is essentially the same as that for Lightning Peak. The base of the crust at approximately 30 km depth beneath Terrane I (Stacey 1973, Cumming et al. 1979) precludes the existence of a plagioclase lherzolite stability field in the upper mantle. All profiles show metacumulate material overlying a layer of less-depleted lherzolite. The less-depleted lherzolite grades into depleted lherzolite at depths of around 45 km at Summit Lake and Lightning Peak, and around 40 km at Big Timothy Mountain and Jacques Lake. This transition also corresponds to the asthenosphere which lies at depths of 40 to 50 km (Wickens 1977). The profiles for Big Timothy Mountain and Jacques Lake also have a zone of cumulate material above the metacumulates, extending to a depth of 35 km. It is possible that enrichment in the less-depleted lherzolites is caused by fluids derived from this layer.

A high velocity layer (8.0 to 8.5km s^{-2}) at a depth of 60 km was reported to the east of the study area at 50°N (Mereu et al. 1977) and

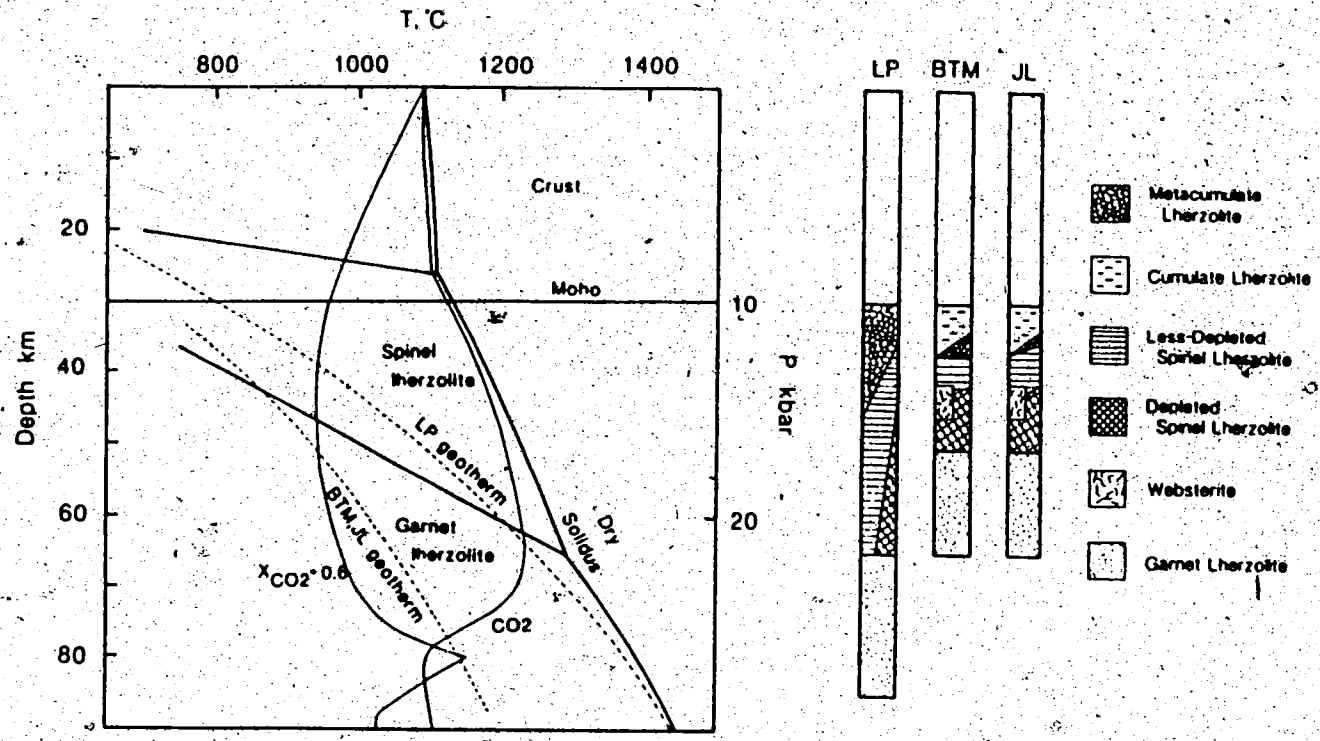

Fig. 55. Temperature-depth profile of the mantle beneath south-central British Columbia in relation to the lherzolite mineral facies and solidi. Geotherms for the Big Timothy Mountain (BTM) and Jacques Lake (JL) xenolith localities as calculated by two-pyroxene geothermobarometry (Ross 1983) are similar to the geotherm of Ranalli (1980) calculated from olivine microrheology. The elevated geotherm for the Lightning Peak locality (LP) (Ross 1983) is considered to represent a maximum thermal profile resulting from mantle upwelling. The depth of the base of the crust, ca. 30 km (Wickens 1977) precludes the existence of a plagioclase lherzolite stability field in the upper mantle. Peridotite-CO_2, $-H_2O$ solidii for fluid phase compositions XCO_2 =1.0 , and XCO_2 =0.6 (after Morse 1980) indicate a fluid composition XCO_2 =0.8 to produce a melt with a liquidus temperature of 1250° at the garnet lherzolite-spinel lherzolite phase boundary. Sections at right illustrate the compositional profile of the spinel lherzolite facies beneath the BTM, JL and LP xenolith localities (after Ross 1983).

probably extends beneath the Chilcotin basalt plateau. Although such velocities are too high to associate with any particular mantle phase, similar anomalous velocities in oceanic mantle have been considered to result from the appearence of garnet (Green and Liebermann 1976). Consequently, this feature is considered to mark the garnet lherzolite-spinel lherzolite phase boundary.

As the host basalts of the xenoliths have ages of less than 3 Ma the profiles and geothermal gradients were considered evidence for a late Tertiary mantle diapir under Terrane I (Ross 1983). From their steeper geothermal gradients the Summit Lake and Lightning Peak localities were interpreted as the core whilst the Big Timothy Mountain and Jacques Lake localities represented the flanks. Because Jacques Lake and Big Timothy Mountain are located between Summit Lake and Lightning Peak the model is not consistent with a single diapir. The spatial extent of the diapir corresponds to a layer of high electrical conductivity, the Canadian Cordilleran Regional conductor (CCR), resulting from partial melting caused by adiabatic upwelling in the mantle (Gough 1986). The top of the CCR at 15 to 30 km depth, lies within the the crust, where high conductivity was interpreted either as partial melting, or the percolation of hydrothermal fluids (ibid.). At 119.5°W, 49°S, to the southeast of the study area, the thickness of the CCR was estimated at 30 to 70 km, which results in its base lying between 45 and 100 km depth. Although the CCR may lie at different depths elsewhere, the essential feature is that the partial melt is present in both the spinel lherzolite and garnet lherzolite facies. The results of Ross (1983), taken as evidence for a series of diapirs, can be interpreted as fine structure on this large scale upflow.

The driving force for the upflow could be deep-seated mantle convection associated with the subducted Kula-Farallon ridge, and now largely decoupled from the Juan de Fuca ridge which represents the Kula-Farallon remnant. The alternative explanation, that the CCR is related to the ascent of melt above the subducted Juan de Fuca plate is untenable (Gough 1986), because the plate loses its identity before it reaches Terrane I (Riddihough 1979, Ellis et al. 1983). This of course, does not preclude the existence of a cooler, more extensive slab originating at a more distant ridge position, underlying Terrane I at some time in the past.

Evidence cited by Gough (1986) for a deep source of convection includes the existence of a low velocity layer at 250 km depth (as shown by tomographic profiles) extending from the Gulf of California to the Canadian Cordillera but not beneath the Juan de Fuca ridge. Whilst it is considered debatable whether tomographic profiles (e.g. Anderson and Dziewonski 1984) have the resolution to distinguish such features, a shift in the location of the mantle upflow associated with the ridge to predominantly beneath the continent, is attractive to account for the late Eocene transition from calc-alkaline (Kamloops Group) to alkaline volcanism (Chilcotin Group), and the change from right lateral strike-slip movement to an extensional regime characterised by normal faulting.

The ridge-upflow decoupling could feasibly result from the resistance of an increasingly hot and buoyant slab to subduction, causing a reduction in the spreading rate on the ridge as the proximity of the continent increased. Since the upflow feeding the ridge is driven by larger scale convective forces, there would be no requirement for the

upflow to remain with the ridge and, therefore, could have been overridden by the continent. The implication of the large lateral displacements from the base to the top of such convection, as shown by the tomographic maps, is that once overridden by the continent, the upflow would continue to pull oceanic mantle into the subcontinental environment.

Volatile Components

The relationship of the geotherms to the lherzolite phase diagram and peridotite-CO_2-H_2O solidi (Morse 1980) are shown in Fig. 55. The Lightning Peak geotherm intersects the dry garnet lherzolite solidus at 90 km depth but extraction of melt from this region would result in an unrealistically high liquidus temperature. Evidence for the participation of both CO_2 and H_2O in the genesis of the Chilcotin basalts comes from their distribution on the Chayes normative diagram (Fig. 56). Two trends, one toward the nepheline normative field, the other toward the quartz normative field, follow the paths suggested for the effect of these volatiles on the melting of peridotite (Mysen and Boettcher 1975). Group C are predominantly hypersthene- or quartz-normative; group B equally hyperthene- or nepheline-normative, and group A exclusively nepheline-normative. This distribution suggests that CO_2, H_2O or both may be present in the source region of groups B and C, but CO_2 is predominant in the source region of group A.

The Big Timothy Mountain-Jacques Lake geotherm intersects the XCO_2 =1 solidus at 70 to 80 km. The same geotherm also intersects the XCO_2 =0.6 solidus at a depth of 50 km, but melting in this region would result in a liquidus temperature of only 1050°C. Elevation of this

geotherm to close to the position of the LP geotherm would result in melting around the garnet lherzolite-spinel lherzolite phase boundary at a fluid composition of XCO_2 0.7 to 0.9 and would yield a suitable liquidus temperature of 1250 to 1275°C for a group A melt.

Nature of the EM and DM components

In the C-F mixing model the EM component was modelled as a plume rising from the lower mantle, which then caused partial melting in the DM wall rock. Conversely, in the A-model the EM component is considered to be the mantle through which melts produced from the DM component must rise. The spatial relationships of the components are thus interchangeable. For the Chilcotin basalts, the model of a rising plume would appear the more appropriate from the geophysical evidence. The trace element and isotope geochemistry of the group A Chilcotin basalts, in which the contribution of the DM component is most pronounced, indicate that the plume is oceanic mantle garnet lherzolite.

No garnet-bearing xenoliths occur in British Columbia; therefore, homogeneity of the DM component must be assumed. The DM component may also represent a metasomatic phase derived from garnet lherzolite, residing within the spinel lherzolite facies. A garnet-spinel websterite (Kal03) reported from Austria by Kurat et al. (1980), was considered to result from the recrystallisation of a tholeiitic melt derived from the garnet lherzolite facies, within the spinel lherzolite stability field. The feasibility of segregating melts formed by less than 1% partial melting has been questioned (Richter and MacKenzie 1985) and, for this reason, the A-model with its higher degrees of partial melting would appear the more attractive. By invoking a metasomatic component in the

genesis of the Chilcotin basalts the requirement for very small degrees of partial melting and for efficient mixing of the DM and EM components are removed because the metasomatised host material would simultaneously undergo partial melting.

The presence of the CCR in both the garnet lherzolite and spinel lherzolite facies implies that the EM component must be represented by the subcontinental spinel lherzolite. The diversity of spinel lherzolite xenoliths from British Columbia invites comment on their suitability to represent the EM, or alternatively the DM component. Both the C-F and A-models compensate for the lack of a metasomatic component by deriving the LIL enrichment of the melt from small degrees of partial melting. It is unlikely that the Summit Lake xenoliths, with their marked depletion in Rb and to a lesser extent in Sr, could produce a basaltic liquid. However, lherzolites such as found at Summit Lake may still represent a source component in basalt genesis because of the unlikelihood of more than one component in a multi-component mixing system to represent metasomatised material. This is indicated by the depletion of Rb relative to Sr in the trace element-primitive mantle-normalised plots for the Chilcotin Group (Fig. 37) or the Tertiary to Recent basalts of southern Australia (McDonough et al. 1985). Metasomatised lherzolite shows no such depletion (Roden and Murthy 1985) and basalts derived from such material should be enriched in Rb relative to Sr.

The Rayfield River xenoliths, in contrast, have Rb and Sr contents within the range of metasomatised mantle and have Nd-Sr isotopic compositions which parallel the trend of the Chilcotin basalts across the mantle array (Fig. 36). This relationship indicates the involvement of such xenoliths in the genesis of the Chilcotin Group, and suggests

the presence of at least two more components, corresponding to the websterite band in xenolith 1RR (as represented by the chrome-diopside 1RR-CD), and moderately depleted spinel lherzolite (such as xenoliths RR218 or 2RR). The very low $^{87}Sr/^{86}Sr$ (similar to chrome diopsides in xenoliths from several other localities in British Columbia (Sun 1985)) and high $^{143}Nd/^{144}Nd$ ratios of 1RR-CD invalidate the assumption that garnet lherzolite represents the only DM component. Sm/Nd was not measured on the websterite to determine its affinity to Type 1A or 1B, and consequently its La/Ce ratio and the resulting effect on the melting of the DM component in the mixing calculation cannot be assessed directly. Clinopyroxenes in Type 1B xenoliths have La/Ce ratios close to the chondritic value (Menzies et al. 1985); therefore, particularly in the C-F model, the addition of this component would not significantly alter the positions of the mixing lines.

Sr/Ba ratios for the xenoliths, Chilcotin basalts, and Kamloops Group basalts with mg greater than 60 are illustrated in Fig. 57. Low Sr/Ba ratios of approximately 0.3 , similar to the Type I xenoliths are present only in the Summit Lake host basalt (SL121/2 has Sr/Ba =0.4) and some Columbia River basalts. The Kamloops Group basalts have Sr/Ba =0.85 , similar to the Type II xenoliths.

The Chilcotin basalts have Sr/Ba ratios of 1.3 to 2.1 , with several samples, notably the group A hawaiites, having values approaching the primitive mantle estimate of 3.5 . As Ba is a more incompatible element in the lherzolite mineralogy than Sr, the Sr/Ba ratio might increase only with increasing degrees of partial melting. The Ba depletion of the Chilcotin basalts cannot, therefore, be reconciled with derivation of the basalts from Type I xenoliths as found

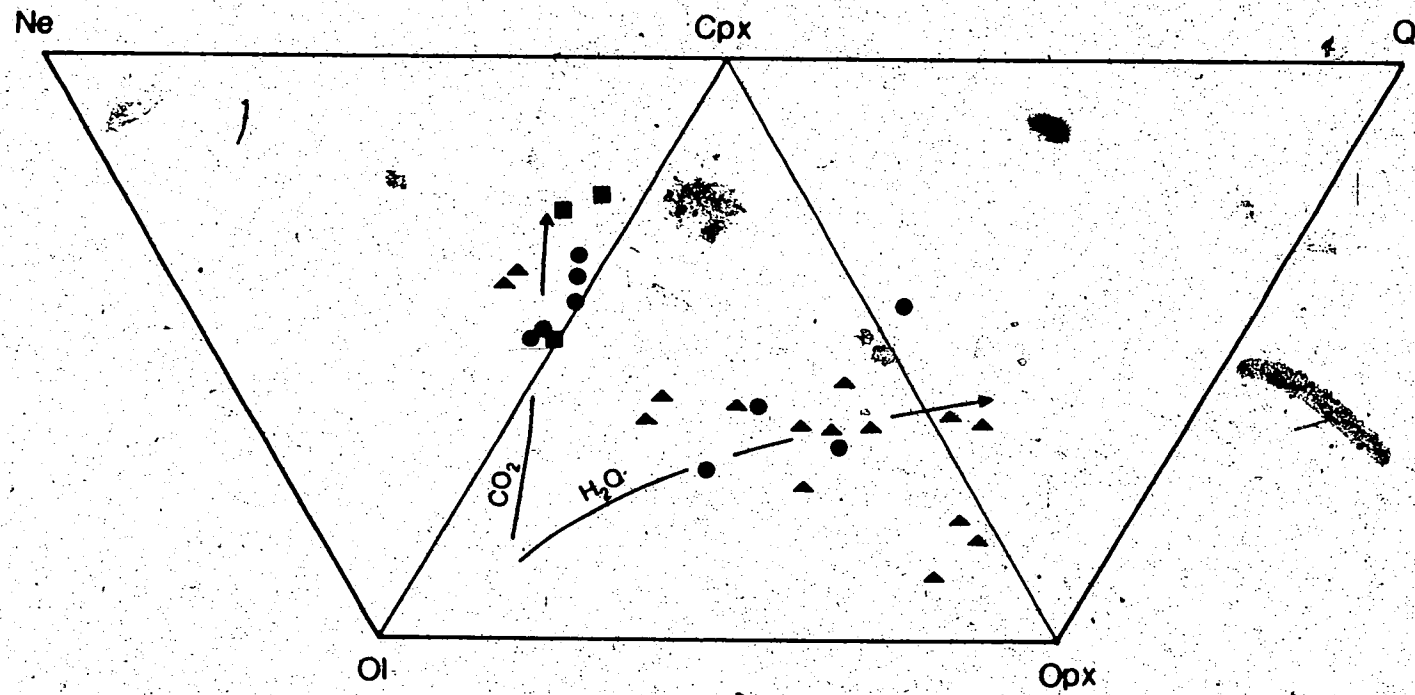

Fig. 56. Chayes normative diagram for the Chilcotin Group. Melting trends for predominantly CO_2-saturated and H_2O peridotite are from Mysen and Boettcher (1975).

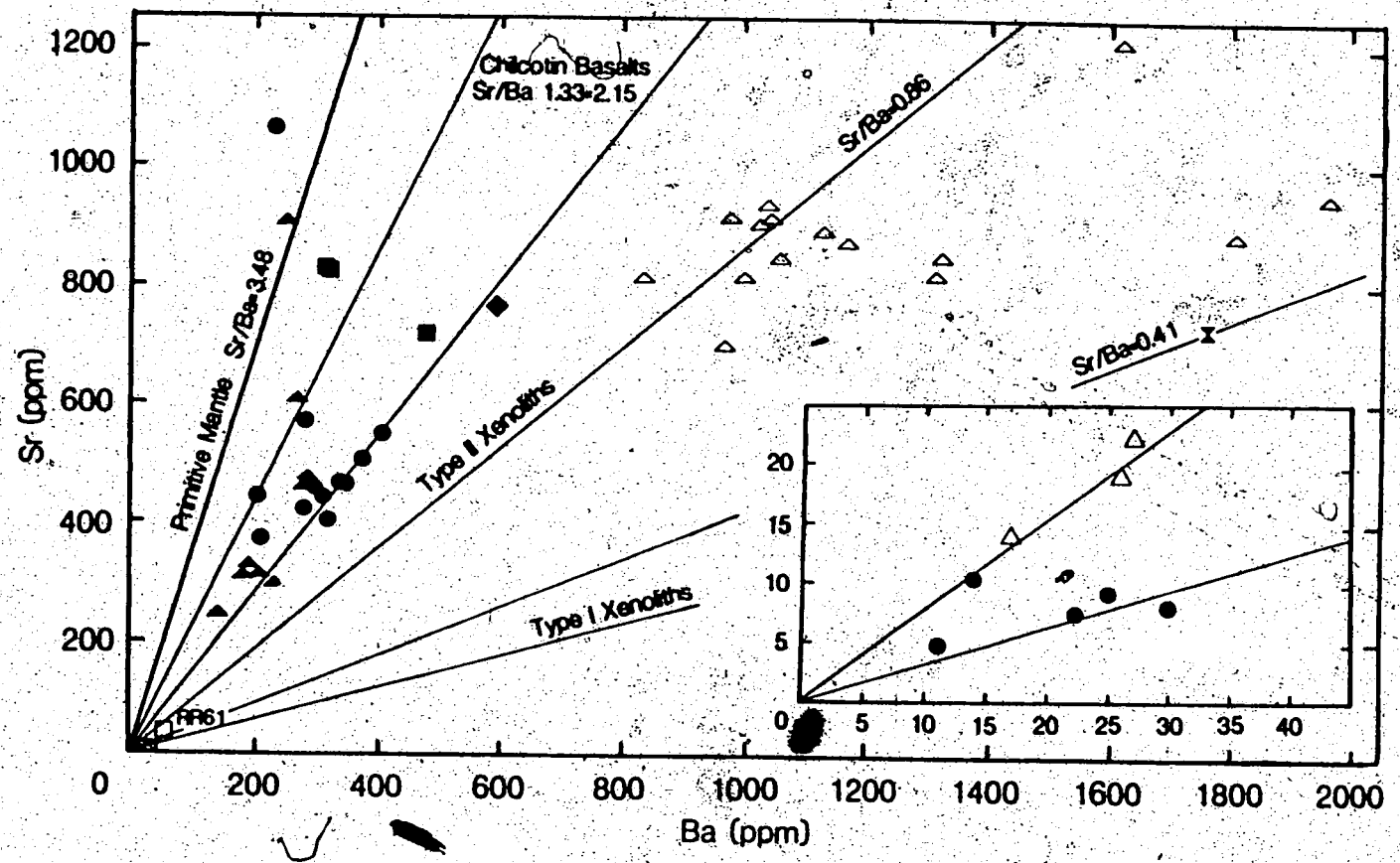

Fig. 57. Sr variation with Ba in the Chilcotin basalts (■ group A; ● group B; ▲ group C), the more primary (Mg-numbers >60) Kamloops Group basalts (△) and SL121/2 (⧗). Inset: enlargement of the region from 0 to 45 ppm Ba, 0 to 25 ppm Sr, showing the diverging trend caused by the higher Sr contents of the Type II (Δ) compared to the Type I (○) xenoliths. Primitive mantle Sr/Ba ratio from McDonough et al. (1985).

at Summit Lake. Lherzolite such as LtPk, which is relatively depleted in Ba similar to the Type II xenoliths, may be considered a suitable mixing component. The moderately depleted isotopic signature of LtPk suggests that the C-F mixing model is more appropriate to the Chilcotin basalts, but would require considerable revision to incorporate the lower La/Ce ratio of LtPk. The validity of the argument is reinforced by the fact that the group A hawaiites, which have Sr/Ba approaching the primitive mantle value, require the smallest amount of EM component in their genesis. The DM component must, therefore, have Sr/Ba close to the primitive mantle value. The positive Eu anomalies shown by the Chilcotin basalts may be explained by the incorporation of lherzolite such as LtPk and RR218 as mixing components. Leeman (1976) demonstrated that the small positive Eu anomalies shown by many suites of basalts could be generated by retention of clinopyroxene in the source region. Alternatively, the anomalies could be inherited directly from the source lherzolite.

Significance of the Isotopic Correlations with P_2O_5

Interpretation of the group A basalts as resulting from a small degree of partial melting of a depleted source, and the group B and C basalts as representing increasing amounts of contamination to the melt by enriched subcontinental mantle, allows a reappraisal of the trends shown on the $^{143}Nd/^{144}Nd$ versus P_2O_5 or $^{87}Sr/^{86}Sr$ versus P_2O_5 diagrams (Figs. 42 and 43). For the purposes of this discussion only the latter will be considered on account of the greater data spread shown on the diagram.

In addition to the three groups of basalts, also plotted on Fig. 43 are the isotopic compositions of the Rayfield River xenoliths and LtPk for an assumed P_2O_5 content of 0.01% for each xenolith. The xenoliths fall entirely within the fan described by the group C and B regression lines and, as in the C-F or A-models, can be interpreted as a contaminating component. The P_2O_5 content is proportional to the degree of partial melting of the mixing components. The position of the individual samples along the regression lines indicates the degree of mixing of the components. Compared to the La/Ce versus $^{87}Sr/^{86}Sr$ diagram the diverging trend of the group B and C basalts indicates the presence of the two EM components inferred from the Nd-Sr isotopic relationships. Melts contaminated by both of the EM components are rare.

With regard to the other suites plotted on Fig. 43 , the small range of $^{87}Sr/^{86}Sr$ and large variation in P_2O_5 shown by the alkali basalts is interpreted as the result of variable, but small, degrees of partial melting of a fairly homogeneous source. The low, constant P_2O_5 and variable $^{87}Sr/^{86}Sr$ of the tholeiites suggests large degrees of melting of a heterogenous source, or the contribution of several source components.

X. Conclusion

Formation of Terrane I

The isotopic systematics of the principal volcanic units of the Slide Mountain, Quesnel, and Cache Creek terranes have been studied in order to determine the character of crust added to the North America by accretion tectonics since the late Palaeozoic.

The Fennell Formation of the Slide Mountain terrane comprises a suite of Mississippian-Permian spilitised metabasalts. In spite of this alteration, the basalts resemble N-type MORB in their major and trace element chemistry. Isotopic compositions from ϵNd +7.6 to +9.6 are similar to modern ridge basalts. $^{87}Sr/^{86}Sr$ ranges from 0.7025 to 0.7042, the higher values being due to seawater alteration. No compositional or isotopic differences are noted between kaersutite and non-kaersutite-bearing samples. The presence of kaersutite and the resemblance of the basalts to N-type MORB suggests a back-arc origin.

Contemporaneous basalts in the Bonaparte subterrane of the Cache Creek terrane show similar alteration to the Fennell Formation, but resemble T- and P-type MORB in their major and trace element chemistry, and are classified as ocean island tholeiites. Isotopic compositions of ϵNd +4.5 to +6.0 indicate derivation from a Hawaiian-type mantle plume.

The late Triassic Nicola Group comprise the oldest volcanics in the Quesnel terrane. Their major element chemistry is characterised by a predominance of silica contents between 46 and 54%, coupled with high, variable alkali contents resulting from prehnite-pumpellyite to greenschist facies metamorphism. Classification by conventional AFM and alkalis-silica diagrams is not possible. Calc-alkaline and tholeiitic

trends are identified on a FeO^*/MgO discrimination diagram. Low abundances of high field strength elements Ti, P, Nb and Zr indicate an arc origin. Isotopic compositions of the Nicola Group, ϵNd +5 to +8 and $^{87}Sr/^{86}Sr$ 0.7031 to 0.7042, are typical of oceanic arcs. The trend to elevated $^{87}Sr/^{86}Sr$ results from low grade metamorphism, rather than from incorporation of slab-sediment-derived material into the source region.

Young crust added to the continents by terrane accretion, therefore, includes a significant proportion of ocean floor and ocean island material in addition to arc assemblages. Much of this material has a depleted isotopic signature which has important implications for studies which invoking crustal material as a contaminant of mantle-derived rocks, or which concern the generation of granitic batholiths along continental margins.

Post-Accretional History of Terrane I

The Spences Bridge Group, a series of low, medium and high K calc-alkaline volcanics, represent an arc formed on the western margin of Terrane I during the mid-Cretaceous. A Rb-Sr isochron for the volcanics of 115±35 Ma is in good agreement with previous age estimates. The isotopic composition of the volcanics, ϵNd +5.5 to +8.0 and $^{87}Sr/^{86}Sr$ 0.7031 to 0.7042, shows no indication of assimilation of underlying Nicola Group strata, and their position close to the mantle array on a Nd-Sr isotopic diagram indicates that subducted sediment did not play a major part in the genesis of the volcanics. The arc constrains the time of accretion of Terrane II to Terrane I to be after 110 Ma.

The Kamloops Group comprises a suite of high K calc-alkaline volcanics which were erupted throughout Terrane I during the Eocene. The isotopic composition of the Kamloops Group, ϵNd +5.5 to -2 and $^{87}Sr/^{86}Sr$ 0.7038 to 0.7052, shows no evidence of crustal contamination or regional variation. Plate reconstructions for the mid-Tertiary result in an arc-trench distance of over 400 km; therefore, it is proposed that the Kamloops Group originated over a shallow subducted slab underplating Terranes I and II.

Late Tertiary volcanism is represented by the Miocene-Pliocene Chilcotin basalts in British Columbia, and the Columbia River basalt in Washington and Oregon. Both groups were erupted in similar tectonic environments but differ considerably in chemical and isotopic composition. The Chilcotin Group have moderately depleted isotopic compositions, $^{143}Nd/^{144}Nd$ 0.51310 to 0.51284 and $^{87}Sr/^{86}Sr$ 0.7028 to 0.7039. The most isotopically depleted Chilcotin basalts show the greatest minor and trace element enrichment, although this trend is not continued throughout the group. The most chemically depleted basalts have isotopic compositions within the middle of the range. The basalts are divided into three groups: A (alkaline), B (transitional), C (tholeiitic). Application of the binary mixing models of Chen and Frey (1983) and Anderson (1985) suggests that group A is produced by a small degree (less than 5%) of partial melting of a depleted mantle component, mixing with melt produced from an enriched mantle component. Groups C and B result from successively greater amounts of contamination by the enriched mantle component.

The depleted component must have $\epsilon Nd > +8$, $^{87}Sr/^{86}Sr < 0.7030$, and be garnet-bearing to account for the high (La/Yb)n ratios and low Y

abundances of group A. The candidate material is oceanic mantle garnet lherzolite, introduced into the subcontinental environment by the decoupling of deep-seated mantle upwelling from under the Juan de Fuca Ridge. Source region metasomatism is not an implicit feature of the mixing models because the LIL enrichment of the melts derived from the depleted source are accounted for by small degrees of partial melting. The representation of the depleted component by a metasomatic phase derived from such lherzolite resolves the problem of extracting small degrees of partial melt to mix with the enriched component because both metasomatic phase and host lherzolite would melt simultaneously.

The models do not explain the more enriched isotopic compositions of group B relative to group C. These are resolved on a P_2O_5 versus $^{143}Nd/^{144}Nd$, or P_2O_5 versus $^{87}Sr/^{86}Sr$ diagram, the interpretation of which is analagous to the La/Ce-$^{87}Sr/^{86}Sr$ diagram of the binary mixing models. On these diagrams the Chilcotin basalts form a diverging trend with the high P_2O_5 group A basalts as the common member. The clear isotopic separation of groups B and C, both of which have low P_2O_5 contents, requires the presence of two 'enriched' mantle components. These are identified as moderately depleted mantle with $\epsilon Nd = +5$ and $^{87}Sr/^{86}Sr = 0.7040$, in the genesis of group C, and mantle with approximately bulk Earth composition, $\epsilon Nd < +2$, $^{87}Sr/^{86}Sr > 0.7045$, in the genesis of group B. High Y contents and low (La/Yb)n ratios of groups B and C require both enriched mantle components to be spinel lherzolite rather than garnet lherzolite. The lack of overlap between groups B and C on the P_2O_5-isotopic diagrams suggests that either component may dominate the spinel lherzolite section. The presence of a fourth component, with high $^{143}Nd/^{144}Nd$ and low $^{87}Sr/^{86}Sr$ is required to

account for the transitional nature of several samples between groups A and C.

Spinel lherzolites from Rayfield River, Summit Lake and Lightning Peak localities provide late Cenozoic samples of the subcontinental mantle and record a complex series of depletion and enrichment events in their chemical and isotopic composition. Whole xenolith XRF results show all xenoliths to be depleted to varying extents relative to primitive mantle compositions. Type II xenoliths are enriched in Ca, Fe, Mn, Zr and Sr, but have similar Al, Ba and Ni, compared to their Type I counterparts.

Lightning Peak and Summit Lake xenoliths show a considerable range of isotopic compositions ($^{143}Nd/^{144}Nd$ ratios of 0.51160 to 0.51300 and $^{87}Sr/^{86}Sr$ ratios of 0.7040 to 0.7102), providing direct evidence for the existence of both enriched and depleted mantle beneath western North America. The xenoliths give Sm-Nd model ages of 0.1 to 0.7 and 1.5 to 1.6 Ga for derivation from a reservoir corresponding to present day ϵNd +8 . The model ages are comparable to the Rb-Sr mineral isochrons of Sun (1985) for xenoliths from nearby localities in British Columbia. The lack of ages between 0.7 and 1.5 Ga corresponds to the period during which the west coast of North America is considered to have been a passive continental margin.

The contradictory low Rb/Sr and high $^{87}Sr/^{86}Sr$ ratios of the xenoliths requires at least a two-stage evolution. The proposed model for the generation of these features is th[illegible]ted mantle material equilibrated with a metasomatic fluid de[illegible] from subducted oceanic crust and associated sediment. Either the metasomatic fluid had sufficiently high $^{87}Sr/^{86}Sr$ and low $^{143}Nd/^{144}Nd$ to alter the isotopic

composition of the xenoliths to close to their present values, or this growth occurred in a phase such as amphibole or phlogopite, produced as a consequence of the metasomatism. In either case, a depletion event is required to produce the low Rb/Sr ratio and LIL depletions observed in the xenoliths.

The Sm-Nd model ages cannot relate to any specific event, however, because at the time of the depletion event the ϵNd of the xenoliths may lie anywhere within the range of island arcs. The xenoliths bear considerable isotopic similarity to the mantle components C2 to C4 invoked in the genesis of the Columbia River basalts (Carlson 1984). The spatial variation of the xenolith localities indicates that throughout the mantle beneath western North America, varying proportions of the same mantle components have been produced.

The amphibole-bearing Type I spinel lherzolite LtPk has similar isotopic composition and incompatible element ratios to the enriched mantle component inferred in the genesis of the group B Chilcotin basalts, but would also be an appropriate source component for the Kamloops Group volcanics. The generation of these two groups of Tertiary volcanics may account for the rarity of amphibole-bearing spinel lherzolite xenoliths from central British Columbia. Xenoliths such as lRR from Rayfield River, which has ϵNd =+6 , $^{87}Sr/^{86}Sr$ =0.7036 , represent the 'enriched' mantle component in the generation of the group C Chilcotin basalts. A websterite band in lRR is a suitable candidate for the fourth, depleted, component which contributes to groups A and C.

None of the Summit Lake xenoliths is considered to be a suitable mixing component in the genesis of the Chilcotin Group because of the high Ba contents of the xenoliths, which should be imparted to the melt,

and because of the enriched isotopic compositions of the xenoliths. One extremely iron-rich xenolith (SL141) is similar in chemistry to the source material proposed for anorogenic andesites (Wilkinson and Binns 1977), and has isotopic composition similar to C3 of Carlson (1984). This material is particularly suited as a source material for the Columbia River basalts. The xenolith may represent a cumulate from an ocean ridge environment enriched by subduction processes after incorporation into the subcontinental mantle.

The differences between the Columbia River basalts and the Chilcotin Group could arise from an influence of such iron-rich material in the case of the former, whilst the latter are dominated by melt from the oceanic garnet lherzolite. Both basalt provinces together with the Kamloops Group, share similar source components within the subcontinental spinel lherzolite facies, the heterogeneity of which has been produced by subduction processes accompanying terrane accretion over the last 200 Ma.

XI. Bibliography

Aggarwal P. K., Fujii T. and Nesbitt B. E. (1984) Magmatic composition and tectonic setting of altered volcanic rocks of the Fennell Formation, British Columbia. Can. J. Earth Sci. 21, 743-752.

Allegre C. J., Ben Othman D., Polve M. and Richard P. (1979) The Nd-Sr isotopic correlation in mantle materials and geodynamic consequences. Phys. Earth Planet. Int. 19, 293-306.

Anderson D. L. (1985) Hotspot magmas can form by fractionation and contamination of mid-ocean ridge basalts. Nature 318, 145-149.

Anderson D. L. and Dziewonski A. M. (1984) Seismic Tomography. Sci. Am. 251-4, 60-68.

Anderson D. L. (1982) Isotopic evolution of the mantle: the role of magma mixing. Earth planet. Sci. Lett. 57, 1-12.

Arculus R. J. (1976) Geology and geochemistry of the alkali basalt-andesite association of Grenada, Lesser Antilles island arc. Bull. Geol. Soc. Am. 87, 612-624.

Ashwal L. D., Wooden J. L., Phinney W. C. and Morrison D. A. (1985) Sm-Nd and Rb-Sr isotope systematics of an Archaean anorthosite and related rocks from the Superior Province of the Canadian Shield. Earth Planet. Sci. Lett. 74, 338-346.

Atwater T. and Molnar P. (1973) Relative motion of the Pacific and North American plates deduced from sea floor spreading in the Atlantic, Indian and South Pacific Oceans. Proc. Conference on tectonic problems of the San Andreas fault system. Stanford University Press, 136-148.

Atwater T. (1970) Implications of plate tectonics for the Cenozoic tectonic evolution of western North America. Bull. Geol. Soc. Am. 81, 3513-3536.

Avraham Z. and Nur A. (1983) An introductory overview to the concept of displaced terranes. Can. J. Earth Sci. 20, 994-999.

Basaltic Volcanism Study Project (1981) Basaltic Volcanism on the Terrestrial Planets. Pergamon Press. 1286p.

Beckinsale R. D., Pankhurst R. J., Skelhorn R. R. and Walsh J. N. (1978) Geochemistry and petrogenesis of the early Tertiary lava pile on the Isle of Mull, Scotland. Contrib. Mineral. Petrol. 66, 415-427.

Beswick A. E. and Carmichael I. S. E. (1978) Constraints on mantle source compositions imposed by phosphorous and the rare-earth elements. Contrib. Mineral. Petrol. 67, 317-330.

Bevier M. L. (1983a) Implications of chemical and isotopic composition for petrogenesis of Chilcotin Group basalts, British Columbia. J. Petrol. 24, 207-226.

Bevier M. L. (1983b) Regional stratigraphy and age of Chilcotin Group basalts, south-central British Columbia. Can. J. Earth Sci. 20, 515-524.

Bevier M. L., Armstrong R. L. and Souther J. G. (1979) Miocene peralkaline volcanism in west-central British Columbia- its temporal and plate-tectonic setting. Geology 7, 389-392.

Brearley M. B. and Scarfe C. M. (1984) Amphibole in a spinel lherzolite xenolith: evidence for volatiles and partial melting in the upper mantle beneath southern British Columbia. Can. J. Earth Sci. 21, 1067-1072.

Brearley M. B., Scarfe C. M. and Fujii T. (1984) The petrology of ultramafic xenoliths from Summit Lake, near Prince George, British Columbia. Contrib. Mineral. Petrol. 88, 53-63.

Byrne T. (1979) Late Palaeocene demise of the Kula-Pacific spreading centre. Geology 7, 341-344.

Campbell R. B. and Tipper H. W. (1971) Geology of Bonaparte Lake map area, British Columbia. Geol. Surv. Canada Map 1278A (1:250 000 scale) and Memoir 363, 80p.

Carlson R. W. (1984) Isotopic constraints on Columbia River flood basalt genesis and the nature of the subcontinental mantle. Geochim. Cosmochim. Acta 48, 2357-2372.

Carlson R. W., Lugmair G. W. and Macdougall J. D. (1981) Columbia River volcanism: the question of mantle heterogeneity or crustal contamination. Geochim. Cosmochim. Acta 45 , 2483-2499.

Chamberlain V. E. and Lambert R. StJ. (1985) Cordilleria, a newly defined Canadian microcontinent. Nature 314, 707-713.

Chauval C. and Jahn B.-M. (1984) Nd-Sr isotope and REE geochemistry of alkali basalts from the Massif Central, France. Geochim. Cosmochim. Acta 48 , 93-110.

Chen C.-Y. and Frey F. A. (1985) Trace element and isotopic geochemistry of lavas from Haleakala volcano, E. Maui, Hawaii: implications for the origin of Hawaiian basalts. J. Geophys. Res. 90, 8743-8768.

Chen C.-Y. and Frey F.A. (1983) Origin of Hawaiian tholeiite and alkalic basalt. Nature 302, 785-789.

Church B. N., Matheson A. and Hora Z. D. (1979) Combustion metamorphism in the Hat Creek area, British Columbia. Can. J. Earth Sci. 16, 1882-1887.

Cockfield W. E. (1947) Map 886A (1:253 440 scale) Nicola Lake. Canada Dept. Mines and Resources Publ.

Cohen R. S., O'Nions R. K. and Dawson J. B. (1984) Isotope geochemistry of xenoliths from East Africa: implications for development of mantle reservoirs and their interaction. Earth Planet. Sci. Lett. 68, 209-220.

Cohen R. S. and O'Nions (1982) The lead, neodymium and strontium isotopic structure of ocean ridge basalts. J. Petrol. 23, 299-324.

Cole J. W. (1979) Structure, petrology, and genesis of Cenozoic volcanism, Taupo Volcanic Zone, New Zealand- a review. N. Z. J. Geol. Geophys. 22, 631-657.

Coney P. J., Jones D. L. and Monger J. W. H. (1980) Cordilleran suspect terranes. Nature 288, 329-333.

Coney P. J. (1978) Mesozoic-Cenozoic Cordilleran plate tectonics. Geol. Soc. Am. Mem. 152, 33-50.

Cox K. G. (1980) A model for flood basalt vulcanism. J. Petrol. 21, 629-650.

Cumming W. B., Clowes R. M. and Ellis R. M. (1979) Crustal structure from a seismic refraction profile across southern British Columbia. Can. J. Earth Sci. 16, 1024-1040.

Dalrymple G. B. and Clague D. A. (1976) Age of the Hawaiian-Emperor bend. Earth Planet. Sci. Lett. 31, 313-329.

Deer W. A., Howie R. A. and Zussman J. (1966) An Introduction to the Rock-Forming minerals. Longman. 528p.

DePaolo D. J. (1983) Comment on "Columbia River volcanism: the question of mantle heterogeneity or crustal contamination" by R. W. Carlson, G. W. Lugmair and J. D. Macdougall. Geochim. Cosmochim. Acta 47, 841-844.

DePaolo D. J. (1981) Nd Isotopic studies: some new perspectives on Earth structure and evolution. EOS 62, 137-140.

DePaolo D. J. (1979) Implications of correlated Nd and Sr isotopic variations for the chemical evolution of the crust and mantle. Earth Planet. Sci. Lett. 43, 201-211.

DePaolo D. J. and Wasserburg G. J. (1979) Petrogenetic mixing models and Nd-Sr isotopic patterns. Geochim. Cosmochim. Acta 43, 615-627.

DePaolo D. J. and Wasserburg G. J. (1977) The sources of island arcs as indicated by Nd and Sr isotopic studies. Geophys. Res. Lett. 4, 465-468.

Dick H. J. B. (1982) The petrology of two back-arc-basins of the northern Phillipine Sea. Am. J. Sci. 282, 644-700.

Dosso L. and Murthy V. R. (1980) A Nd isotopic study of the Kerguelen islands: inferences on enriched oceanic mantle sources. Earth Planet. Sci. Lett. 48, 268-276.

Duffell S. and McTaggart K. C. (1952) Ashcroft map-area, British Columbia. Geol. Surv. Canada. Mem. 262, 122pp.

Duke M. J. M. and Smith A. D. (in press) Rare Earth Element Determination in Silicate Rocks using Neutron Activation Analysis and Mass Spectrometry. J. Radioanal. Nucl. Chem.

Ellis R. M., Spence G. D., Clowes R. M., Waldron D. A., Jones I. F., Green A. G., Forsyth D. A., Mair J. A., Berry M. J., Mereu R. F., Kanasewich E. R., Cumming G. L., Hajnal Z., Hyndman R. D., McMechan G. A. and Loncarevic B. D. (1983) The Vancouver Island seismic project: a CO-CRUST onshore-offshore study of a convergent margin. Can. J. Earth Sci. 20, 719-741.

Engebretson D. C., Cox A. and Gordon R. G. (1984) Relative motions between oceanic plates of the Pacific basin. J. Geophys. Res. 89, 10291-10310.

Ewart A. (1982) The mineralogy and petrology of Tertiary-Recent orogenic volcanic rocks: with special reference to the andesite-basaltic compositional range. In: Orogenic Andesites and Related Rocks (ed. R. S: Thorpe), pp 25-98. Wiley Interscience.

Ewing T. E. (1981a) Regional stratigraphy and structural setting of the Kamloops Group, south-central British Columbia. Can. J. Earth Sci. 18, 1464-1477.

Ewing T. E. (1981b) Petrology and geochemistry of the Kamloops Group volcanics, British Columbia. Can. J. Earth Sci. 18, 1478-1491.

Farquharson R. B. (1973) The petrology of late Tertiary dolerite plugs in the south Cariboo region, British Columbia. Can. J. Earth Sci. 10, 205-225.

Fiesinger D. W. and Nicholls J. (1977) Petrography and petrology of Quaternary volcanic rocks, Quesnel Lake region, east-central British Columbia. Geol. Assoc. Can. Special Paper 16, 25-38.

Flower M. J. F. (1980) Accumulation of calcic plagioclase in ocean-ridge tholeiite: an indication of spreading rate? Nature 287, 530-532.

Fox K. F., Jr. (1983) Melanges and their tectonic bearing on late Mesozoic and Tertiary subduction and interplate translation at the west edge of the North American plate. U.S. Geol. Surv. Prof. Paper 1198, 40p.

Frey F. A. (1984) Rare earth element abundances in upper mantle rocks. In: Geochemistry of the REE Elements. (ed. P. Henderson), pp 153-203. Elsevier.

Frey F. A., Roden M. F. and Zindler A. (1980) Constraints on mantle

source compositions imposed by phosphorous and the rare earth elements. Contrib. Mineral. Petrol. 75, 165-173.

Frey F. A., Green D. H. and Roy S. D. (1978) Integrated models of basalt petrogenesis: a study of quartz tholeiites to olivine melilitites from south eastern Australia utilising geochemical and experimental petrological data. J. Petrol. 19, 463-513.

Frey F. A. and Green D. H. (1974) The mineralogy, geochemistry and origin of lherzolite inclusions in Victorian basanites. Geochim. Cosmochim. Acta 38, 1023-1059.

Fujii T. and Scarfe C. M. (1982) Petrology of ultramafic nodules from West Kettle River, near Kelowna, southern British Columbia. Contrib. Mineral. Petrol. 80, 297-306.

Gill J. B. (1980) Orogenic Andesites and Plate Tectonics. Springer Verlag. 390p.

Gough D. I. (1986) Mantle upflow tectonics in the Canadian Cordillera. J. Geophys. Res. 91, 1909-1920.

Greeley R. (1982) The Snake River Plain, Idaho: representative of a new category of volcanism. J. Geophys. Res. 87, 2705-2712.

Green D. H. and Liebermann R. C. (1976) Phase equilibria and elastic properties of a pyrolite model for the oceanic upper mantle. Tectonophysics 32, 61-92.

Grette J. F. (1979) Cache Creek and Nicola Groups near Ashcroft, British Columbia. MSc. thesis, University of British Columbia.

Hall-Beyer B. M. (1976) Geochemistry of some ocean-floor basalts of central British Columbia. MSc. thesis, University of Alberta.

Hart W. K. (1985) Chemical and isotopic evidence for mixing between depleted and enriched mantle, northwestern USA. Geochim. Cosmochim. Acta 49, 131-144.

Hawkesworth C. J. (1982) Isotope characteristics of magmas erupted along destructive plate margins. In Orogenic Andesites and Related Rocks (ed. R. S. Thorpe), p[illegible] Wiley Interscience.

Hawkesworth C. J. [redacted]ell M. (1980) Magma genesis in the Lesser Antilles [redacted]arc. Earth Planet. Sci. Lett. 51, 297-308.

Hawkesworth C. J., O'Nions R. K. and Arculus R. J. (1979) Nd and Sr isotope geochemistry of island arc volcanics, Grenada, Lesser Antilles. Earth Planet. Sci. Lett. 45, 237-248.

Hawkesworth C. J., O'Nions R. K., Pankhurst R. J., Hamilton P. J. and Evensen N. M. (1977) A geochemical study of island-arc and back-arc tholeiites from the Scotia sea. Earth Planet. Sci. Lett. 36, 253-262.

Hellman P. L. and Henderson P. (1977) Are rare earth elements mobile during spilitisation? Nature 267, 38-40.

Henderson L. J., Gordon R. G. and Engebretson D. C. (1984) Mesozoic aseismic ridges on the Farallon plate and southward migration of shallow subduction during the Laramide orogeny. Tectonics 3, 121-132.

Hickson C. J. and Souther J. G. (1984) Late Cenozoic volcanic rocks of the Clearwater-Wells Gray area, British Columbia. Can. J. Earth Sci. 21, 267-277.

Higgins M. D. and Allen J. M. (1985) A new locality for primary xenolith-bearing nephelinites in northwestern British Columbia. Can. J. Earth Sci. 22, 1556-1559.

Hodder A. P. W. (1984) Late Cenozoic rift development and intra-plate volcanism in northern New Zealand inferred from geochemical discrimination diagrams. Tectonophysics 101, 293-318.

Hofmann A. W. and White W. M. (1983) Ba, Rb and Cs in the Earth's mantle. Z. Naturforsch. 38, 256-266.

Humphris S. E., Thompson G., Schilling J. G. and Kingsley R. H. (1985) Petrological and geochemical variations along the Mid-Atlantic Ridge between 46°S and 32°S: Influence of the Tristan da Cunha mantle plume. Geochim. Cosmochim. Acta 49, 1445-1464.

Hutchison R., Chambers A. L., Paul D. K. and Harris P.G. (1975) Chemical variation among French ultramafic xenoliths- evidence for a heterogenous upper mantle. Mineral. Mag. 40, 153-170.

Irvine T. N. and Barager W. R. A. (1971) A guide to the chemical classification of the common volcanic rocks. Can. J. Earth Sci. 8, 523-548.

Irving A. J. and Frey F. A. (1984) Trace element abundances in megacrysts and their host basalts: constraints on partition coefficients and megacryst genesis. Geochim. Cosmochim. Acta 48, 1201-1221.

Irving A. J. (1980) Petrology and geochemistry of composite ultramafic xenoliths in alkalic basalts and implications for magmatic processes within the mantle. Am. J. Sci. 280A, 389-426.

Irving E. (1981) Phanerozoic continental drift. Earth Planet. Sci. Lett. 24, 197-204.

Irving E. (1979) Palaeopoles and palaeolatitudes of North America and speculations about displaced terranes. Can. J. Earth Sci. 16, 699-694.

Jackson E. V., Silver E. A. and Dalrymple G. B. (1972) Hawaiian-Emperor chain and its relation to Cenozoic circumpacific tectonics. Bull. Geol. Soc. Am. 83, 601-618.

Jacobsen S. B. and Wasserburg G. J. (1979) Nd and Sr isotopic study of the Bay of Islands ophiolite complex and evolution of mid-ocean ridge basalts. J. Geophys. Res. 84, 7429-7445.

Jagoutz E., Palme H., Baddenhausen H., Blum K., Cendales M., Dreibus G., Spettel B., Lorenz V. and Wanke H. (1979) The abundances of major, minor and trace elements in the Earth's mantle as derived from primitive ultramafic nodules. Proc. Lunar. Sci. Conf. 10th, 2031-2050.

Jones D. L., Cox A., Coney P. and Beck M. (1982) The growth of western North America. Sci. Am. 245-5, 70-128.

Kurat G., Palme H., Spettel B., Baddenhausen H., Hofmeister H., Palme C. and Wanke H. (1980) Geochemistry of ultramafic xenoliths from Kapfenstein, Austria: evidence for a variety of upper mantle processes. Geochim. Cosmochim. Acta 44, 45-60.

Larson R. L. and Chase C. G. (1972) Late Mesozoic evolution of the western Pacific ocean. Bull. Geol. Soc. Am. 83, 3627-3644.

Larson R. L. and Pitman W. C. (1972) World-wide correlation of Mesozoic magnetic anomalies, and its implications. Bull. Geol. Soc. Am. 83, 3645-3662.

Leeman W. P. (1976) Petrogenesis of McKinney (Snake River) olivine tholeiite in light of rare-earth element and Cr/Ni distribution. Bull. Geol. Soc. Am. 87, 1582-1586.

LeRoex A. P., Dick H. J. B., Erlank M., Reid A. M., Frey F. A. and Hart S. R. (1983) Geochemistry, mineralogy and petrogenesis of lavas erupted along the southwest Indian ridge between the Bouvet Triple Junction and 11 degrees east. J. Petrol. 24, 267-318.

Littlejohn A. H. and Greenwood H. J. (1974) Lherzolite nodules in basalts from British Columbia, Canada. Can. J. Earth Sci. 11, 1288-1308.

Ludden J. N. and Thompson G. (1979) An evaluation of the behaviour of the rare earth elements during the weathering of sea-floor basalt. Earth Planet. Sci. Lett. 43, 85-92.

Maaloe S. and Aoki K.-I. (1977) The major element composition of the upper mantle estimated from the composition of lherzolites. Contrib. Mineral. Petrol. 63, 161-173.

Mahoney J., Macdougall J. D., Lugmair G. W., Murali A. V., Sankar Das M. and Gopalan K. (1982) Origin of the Deccan Traps flows at Mahabaleshwar inferred from Nd and Sr isotopic and chemical evidence. Earth Planet. Sci. Lett. 60, 47-60.

McCulloch M. T., Jaques A. L., Nelson D. R. and Lewis J. D. (1983) Nd and Sr isotopes in kimberlites and lamproites from western Australia: an enriched mantle origin. Nature 302, 400-403.

McCulloch M. T., Gregory R. T., Wasserburg G. J. and Taylor H. P., Jr. (1981) Sm-Nd, Rb-Sr, and $^{18}O/^{16}O$ isotopic systematics in an oceanic crustal section: evidence from the Samail Ophiolite. J. Geophys. Res. 86, 2721-2735.

McCulloch M. T. and Wasserburg G. J. (1978) Sm-Nd and Rb-Sr chronology of continental crust formation. Science 200, 1003-1011.

McDonough W. F., McCulloch M. T. and Sun S.-S. (1985) Isotopic and geochemical systematics in Tertiary-Recent basalts from

southeastern Australia and implications for the evolution of the sub-continental lithosphere. Geochim. Cosmochim. Acta 49, 2051-2068.

McDougall I. (1979) Age of shield-building volcanism of Kauai and linear migration of volcanism in the Hawaiian Island chain. Earth Planet. Sci. Lett. 46, 31-42.

McDougall I. (1976) Geochemistry and origin of basalt of the Columbia River Group, Oregon and Washington. Bull. Geol. Soc. Am. 87, 777-792.

Meijer A. (1976) Pb and Sr isotopic data bearing on the origin of volcanic rocks from the Mariana island-arc system. Bull. Geol. Soc. Am. 87, 1358-1369.

Menzies M., Kempton P. and Dungan M. (1985) Interaction of continental lithosphere and asthenospheric melts below the Geronimo volcanic field, Arizona, USA. J. Petrol. 26, 663-693.

Menzies M. A., Leeman W. P. and Hawkesworth C. J. (1984) Geochemical and isotopic evidence for the origin of continental flood basalts with particular reference to the Snake River Plain, Idaho, USA. Philos. Trans. R. Soc. Lond. Ser. A. 310, 643-660.

Menzies M. (1983) Mantle ultramafic xenoliths in alkaline magmas: evidence for mantle heterogeneity modified by magmatic activity. In: Continental Basalts and Mantle Xenoliths (eds. C. J. Hawkesworth and M. J. Norry), pp 111-138; Shiva.

Menzies M. and Murthy V. R, (1980a) Nd and Sr isotope geochemistry of hydrous mantle nodules and their host alkali baalts: implications for local heterogeneities in metasomatically veined mantle. Earth Planet Sci. Lett. 46, 323-334.

Menzies M. and Murthy V. R. (1980b) Mantle metasomatisation as a precursor to the genesis of alkaline magmas- isotopic evidence. Am. J. Sci. 280-A, 622-638.

Mereu R. F., Majumdar S. C. and White R. E. (1977) The structure of the crust and upper mantle under the highest ranges of the Canadian Rockies from a seismic refraction survey. Can. J. Earth Sci. 14, 196-208.

Metcalfe P. and Smith A. D. (1986) Apatite control on Sm and Nd in Quaternary basalts of Well's Gray Park, British Columbia. GAC-MAC Progr. Abstr. 11, I01.

Monger J. W. H. and Berg H. C. (1984) Lithotectonic terrane map of western Canada and southwestern Alaska. In: Lithotectonic Terrane Map of the North American Cordillera. (eds. N. J. Silberling and D. L. Jones), U. S. Geol. Surv. Open File Rep. 84-523, B1-B31.

Monger J. W. H. and McMillan W. J. (1984) Bedrock geology of Ashcroft (92I) map area. Geol. Surv. Canada, Open File 980.

Monger J. W. H. (1982) Geology of Ashcroft map area, southwestern British Columbia. Current Research, Part A, Geol. Surv. Canada Paper 82-1A, 293-297.

Monger J. W. H., Price R. A. and Tempelman-Kluit D. J. (1982) Tectonic accretion and the origin of the two major metamorphic and plutonic welts in the Canadian Cordillera. Geology 10, 70-75.

Monger J. W. H. (1981) Geology of parts of western Ashcroft map area, southwestern British Columbia. Current Research, Part A, Geol. Surv. Canada Paper 81-1A, 185-189.

Monger J. W. H. and Irving E. (1980) Northward displacement of north-central British Columbia. Nature 285, 289-293.

Monger J. W. H. and Price R. A. (1979) Geodynamic evolution of the Canadian Cordillera- progress and problems. Can. J. Earth Sci. 16, 770-791.

Monger J. W. H. (1977) Upper Palaeozoic rocks of the western Canadian Cordillera and their bearing on Cordilleran evolution. Can. J. Earth Sci. 14, 1832-1859.

Monger J. W. H., Souther J. G. and Gabrielse H. (1972) Evolution of the Canadian Cordillera: a plate tectonic model. Am. J. Sci. 272, 577-602.

Moorbath S. (1978) Age and isotopic evidence for the evolution of continental crust. Philos. Trans. R. Soc. London. Ser. A. 288, 401-413.

Morse S. A. (1980) Basalts and Phase Diagrams. Springer Verlag. 493p.

Mysen B. O. and Boettcher A. L. (1975) Melting of a hydrous mantle: II. geochemistry of crystals and liquids formed by anatexis of mantle peridotite at high pressures and high temperatures as a function of controlled activities of water, hydrogen, and carbon dioxide. J. Petrol. 16, 549-593.

Nodha S. and Wasserburg G. J. (1981) Nd and Sr isotopic study of volcanic rocks from Japan. Earth Planet. Sci. Lett. 52, 264-276.

O'Nions R. K., Carter S. R., Cohen R. S., Evensen N. M. and Hamilton P. J. (1978) Pb, Nd and Sr isotopes in oceanic ferromanganese deposits and ocean floor basalts. Nature 273, 435-438.

O'Nions R. K., Hamilton P. J and Evensen N. M. (1977) Variations in $^{143}Nd/^{144}Nd$ and $^{87}Sr/^{86}Sr$ ratios in oceanic basalts. Earth Planet. Sci. Lett. 34, 13-22.

Page B. M. and Engebretson D. C. (1984) Correlation between the geological record and computed plate motions for central California. Tectonics 3, 133-155.

Palme H. and Nickel K. G. (1985) Ca/Al ratio and composition of the Earth's upper mantle. Geochim. Cosmochim. Acta 49, 2123-2132.

Patchett P. J., White W. M., Feldman H., Kielinczuk S. and Hofmann A. W. (1984) Hafnium/rare earth element fractionation in the sedimentary system and crustal recycling into the Earth's mantle. Earth Planet. Sci. Lett. 69, 365-378.

Patchett P. J., Kouvo O., Hedge C. E. and Tatsumoto M. (1981) Evolution of continental crust and mantle heterogeneity: evidence from Hf isotopes. Contrib. Mineral. Petrol. 78, 279-297.

Pearce J. A. and Norry M. J. (1979) Petrogenetic implications of Ti, Zr, Y and Nb variations in volcanic rocks. Contrib. Mineral. Petrol. 69, 33-47.

Pearce J. A. and Cann J. R. (1973) Tectonic setting of basic volcanic rocks determined using trace element analysis. Earth Planet. Sci. Lett. 19, 290-300.

Pearce T. H., Gorman B. E. and Birkett T. C. (1975) The TiO_2-K_2O-P_2O_5 diagram: a method of discrimination between oceanic and non-oceanic basalts. Earth Planet. Sci. Lett. 24, 419-426.

Perfit M. R., Gust D. A., Bence A. E., Arculus R. J. and Taylor S. R. (1980) Chemical characteristics of island arc basalts: implications for mantle sources. Chem. Geol. 30, 227-256.

Peto P. and Armstrong R. L. (1976) Strontium isotopic study of the composite batholith between Princeton and Okanagan Lake. Can. J. Earth Sci. 13, 1577-1583.

Piepgras D. J., Wasserburg G. J. and Dasch E. J. (1979) The isotopic composition of Nd in different ocean masses. Earth Planet. Sci. Lett. 45, 223-236.

Preto V. A. (1979) Geology of the Nicola Group between Merritt and Princeton. British Columbia Ministry of Energy Mines and Petroleum Resources Bull. 69, 90p.

Preto V. A., Osatenko M. J., McMillan W. J. and Armstrong R. L. (1979) Isotopic dates and strontium isotopic ratios for plutonic and volcanic rocks in the Quesnel Trough and Nicola Belt, southcentral British Columbia. Can. J. Earth Sci. 16, 1658-1672.

Preto V. A. (1977) The Nicola Group: Mesozoic volcanism related to rifting in southern British Columbia. Geol. Assoc. Canada Special Paper 16, 39-57.

Ranalli G. (1980) Rheological properties of the upper mantle in Canada from olivine microrheology. Can. J. Earth Sci. 17, 1499-1505.

Rees C. J., Irving E. and Brown R. L. (1985) Secondary magnetism of Triassic-Jurassic pyroclastic rocks of the Quesnel terrane, Quesnel Lake, B.C. Geophys. Res. Lett. 12, 498-501.

Richter F. M. and McKenzie D. (1981) Dynamical models for melt segregation from a deformable matrix. J. Geol. 92, 729-740.

Riddihough R. P. (1979) Gravity and structure of an active margin-British Columbia and Washington. Can. J. Earth Sci. 16, 350-363.

Roden M. F. and Murthy V. R. (1985) Mantle metasomatisation. Ann. Rev.

Earth Planet. Sci. 13, 269-296.

Roden M. F., Frey F. A. and Clague D. A. (1984) Geochemistry of tholeiitic and alkalic lavas from the Koolau Range, Oahu, Hawaii: implications for Hawaiian volcanism. Earth Planet Sci. Lett. 69, 141-158.

Roden M. F., Frey F. A. and Francis D. M. (1984) An example of consequent mantle metasomatisation in peridotite inclusions from Nunivak Island, Alaska. J. Petrol. 25, 546-577.

Ross J. V. (1983) The nature and rheology of the Cordilleran upper mantle of British Columbia: inferences from peridotite xenoliths. Tectonophysics 100, 321-357.

Saleeby J. B. (1983) Accretionary tectonics of the North American Cordillera. Ann. Rev. Earth. Planet. Sci. 15, 45-73.

Schau M. P. (1970) Stratigraphy and structure of the type area of the Upper Triassic Nicola Group in British Columbia. Geol. Assoc. Canada Special Paper 6, 123-135.

Schau M. P. (1968) Geology of the Upper Triassic Nicola Group in south central British Columbia. Ph.D. thesis, University of British Columbia.

Shannon K. R. (1981) The Cache Creek Group and contiguous rocks near Cache Creek, British Columbia. Current Research, Geol. Surv. Canada Paper 81-1A, 217-221.

Smith R. E. and Smith S. E. (1976) Comments on the use of Ti, Zr, Y, Sr, K, P and Nb in classification of basaltic magmas. Earth Planet. Sci. Lett. 32, 114-120.

Souther J. G. (1977) Volcanism and tectonic environments in the Canadian Cordillera- a second look. Geol. Assoc. Canada Special Paper 16, 3-24.

Stacey R. A.(1973) Gravity anomalies, crustal structure, and plate tectonics in the Canadian Cordillera. Can. J. Earth Sci. 10, 615-628.

Stewart D. C. (1975) Crystal clots in calc-alkaline andesites as

breakdown products of high-Al amphiboles. Contrib. Mineral. Petrol. 53, 195-204.

Stille P., Unruh D. M. and Tatsumoto M. (1983) Pb, Sr, Nd and Hf isotopic evidence of multiple sources for Oahu, Hawaii basalts. Nature 304, 25-29.

Stone D. B., Panuska B. C. and Packer D. R. (1982) Palaeolatitudes versus time for southern Alaska. J. Geophys. Res. 87, 3697-3707.

Sun M. (1985) Sr isotopic study of ultramafic nodules from Neogene alkaline lavas of British Columbia, Canada, and Josephine Peridotite, southwestern Oregon, USA. MSc. thesis, University of British Columbia.

Sun S.-S. (1982) Chemical composition and origin of the Earth's primitive mantle. Geochim. Cosmochim. Acta 46, 179-192.

Symons D. T. A. (1985) Palaeomagnetism of the Triassic Nicola volcanics and geotectonics of the Quesnellia subterrane of Terrane I, British Columbia. J. Geodynamics 2, 229-244.

Symons D. T. A. and Litalien C. R. (1984) Paleomagnetism of the Lower Jurassic Copper Mountain intrusions and the geotectonics of Terrane I, British Columbia. Geophys. Res. Lett. 11, 685-688.

Symons D. T. A. (1983) New paleomagnetic data for the Triassic Guichon batholith of south-central British Columbia and their bearing on Terrane I tectonics. Can. J. Earth Sci. 20, 1340-1344.

Tempelman-Kluit D. J. (1979) Transported cataclastic ophiolite and granodiorite in Yukon: evidence of arc-continent collision. Geol. Surv. Canada Paper 79-14, 27pp.

Tempelman-Kluit D. J., Gordey S. P. and Read B. C. (1976) Stratigraphic and structural studies in the Pelly Mountains, Yukon Territory. Geol. Surv. Canada Paper 76-1A, 97-106.

Thorkelson D. J. (1985) Geology of the mid-Cretaceous volcanic units near Kingsvale, southwestern British Columbia. Current Research, Geol. Surv. Canada Paper 85-1B, 333-339.

Thorkelson D. J. and Rouse G. E. (in prep.) Revised stratigraphic

nomenclature and age determinations for mid-Cretaceous volcanic rocks, in southwestern British Columbia.

Tipper H. W., Woodsworth G. J. and Gabrielse H. (1981) Tectonic assemblage map of the Canadian Cordillera and adjacent parts of the United States of America. Map 1505A, Geol. Surv. Canada Dept. Energy Mines and Resources.

Travers W. B. (1978) Overturned Nicola and Ashcroft strata and their relation to the Cache Creek Group, southwestern Intermontane belt, British Columbia. Can. J. Earth Sci. 15, 99-116.

Wallace W. K. and Engebretson D. C. (1984) Relationship between plate motions and late Cretaceous to Paleogene magmatism in southwestern Alaska. Tectonics 3, 295-315.

Wells R. E., Engebretson D. C., Snavely P. D., Jr. and Cox R. S. (1984) Cenozoic plate motions and the volcanotectonic evolution of western Oregon and Washington. Tectonics 3, 275-294.

White W. M. and Patchett J. (1984) Hf-Nd-Sr isotopes and incompatible element abundances in island arcs: implications for magma origins and crust-mantle evolution. Earth Planet. Sci. Lett. 67, 167-185.

White W. M., Dupre B. and Vidal P. (1985) Isotope and trace element geochemistry of sediments from the Barbados Ridge-Demerara Plain region, Atlantic ocean. Geochim. Cosmochim. Acta 49, 1875-1886.

Wickens A. J. (1977) The upper mantle of southern British Columbia. Can. J. Earth Sci. 14, 1100-1115.

Woods M. T. and Davies G. F. (19[illegible]te Cretaceous generation of the Kula plate. Earth Planet. [illegible]tt. 58, 161-166.

Zashu S., Kaneoka I. and Aoki K. I. (1980) Sr isotope study of mafic and ultramafic inclusions from Itinome-gata, Japan. Geochemical Journal. 14, 123-128.

Zindler A., Staudigel H. and Batiza R. (1984) Isotope and trace element geochemistry of young Pacific seamounts: implications for the scale of upper mantle heterogeneity. Earth Planet. Sci. Lett. 70, 175-195.

Zindler A. (1982) Nd and Sr isotopic studies of komatiites and related rocks. In: Komatiites (eds. N. T. Arndt and E. Nisbet), pp 399-420. Allen and Unwin.

Zonenshain L. P., Kuzmin M. I. and Kononov M. V. (1985) Absolute reconstructions of the Palaeozoic oceans. Earth Planet. Sci. Lett. 74, 103-116.

XII. Appendix I: Sample Localities

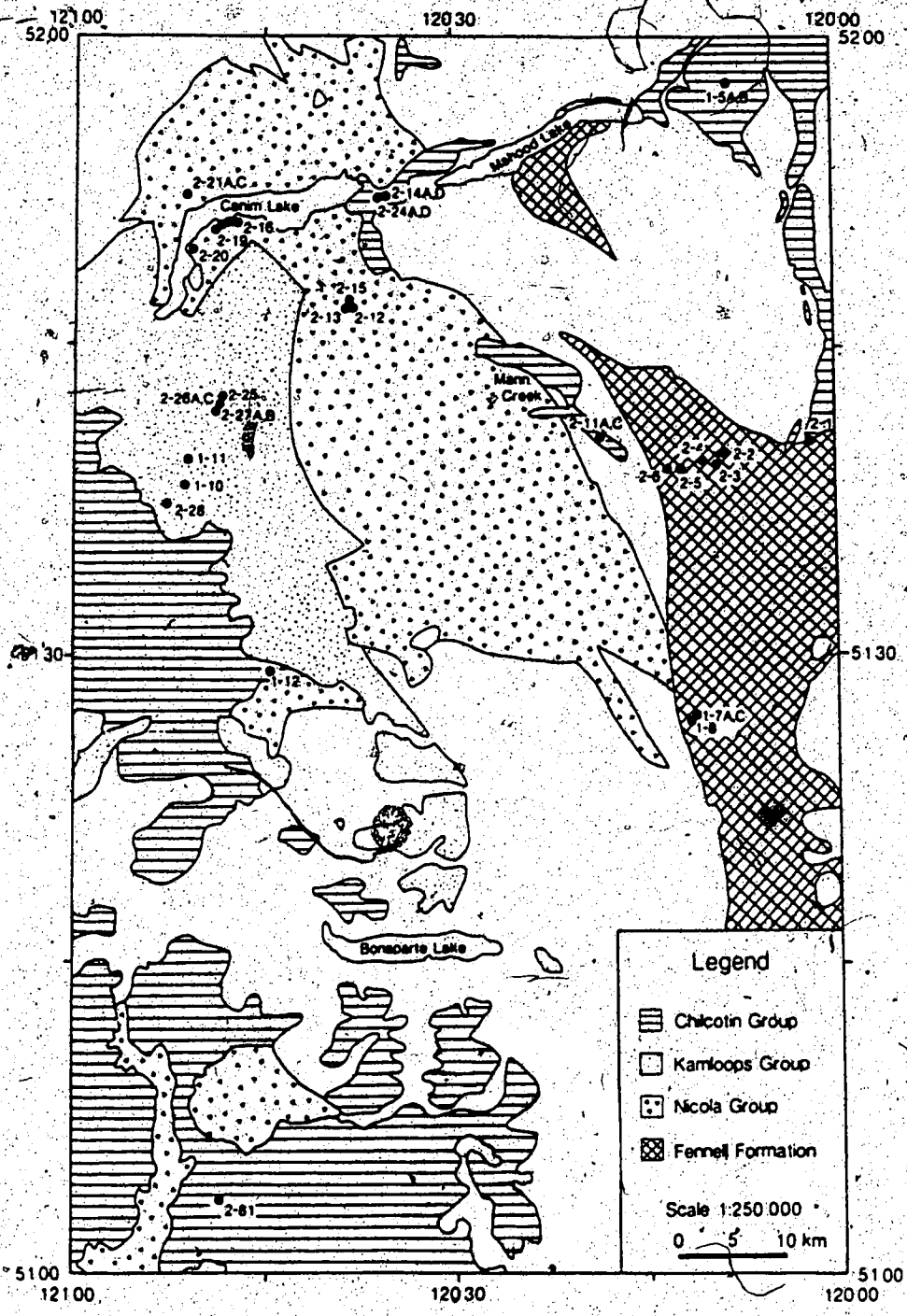

Fig. 58. Geological map showing sample localities in the Bonaparte Lake region of south-central British Columbia (after Campbell and Tipper, 1971). • Sample locality.

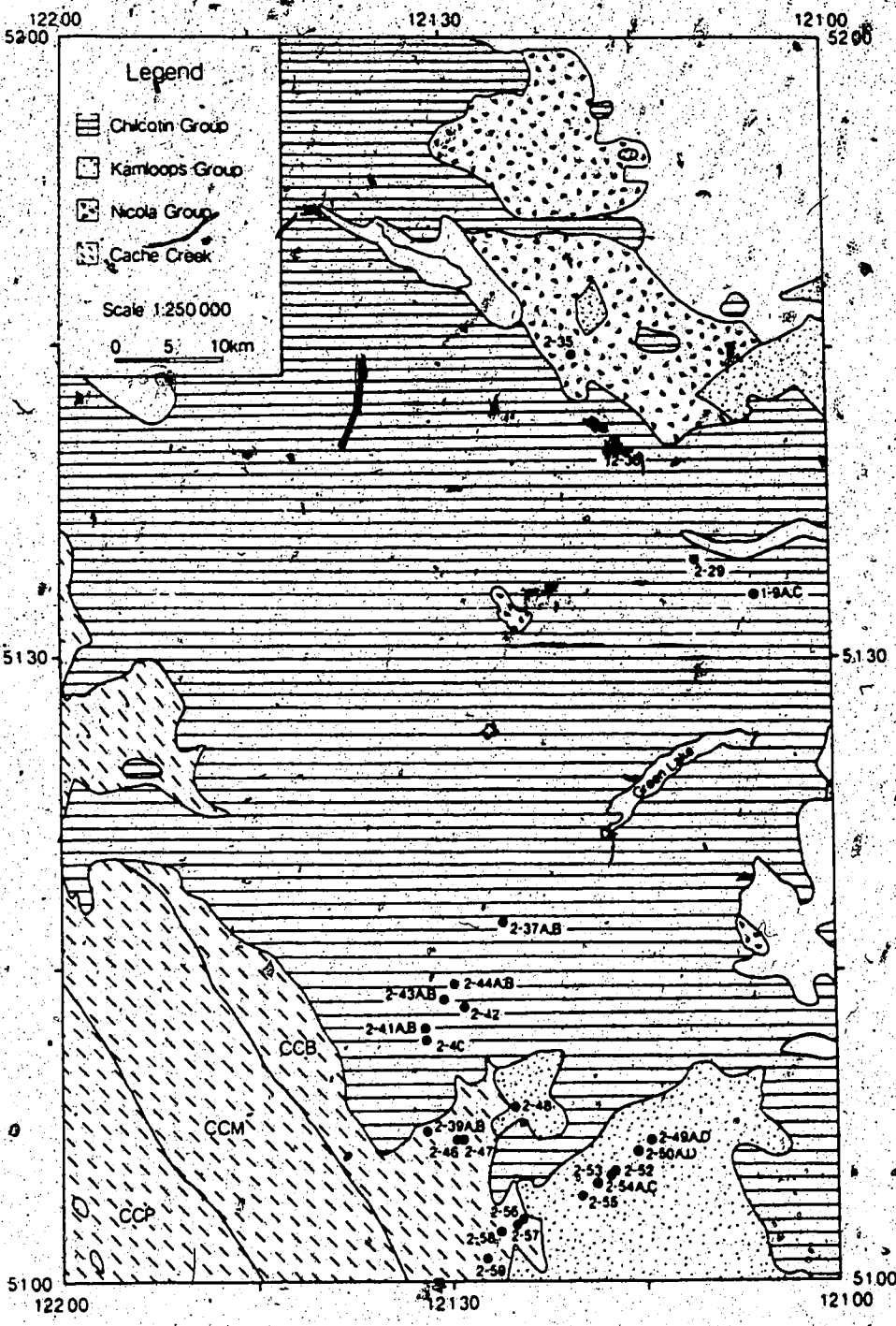

Fig. 59. Geological map showing sample localities in the 100 Mile House region of south-central British Columbia (after Campbell and Tipper 1971). Division of Cache Creek Group into Pavillion (CCP), Marble Range (CCM), and Bonaparte (CCB) subterranes after Monger and Berg (1984). ● Sample locality; ▲ Rayfield River xenolith locality.

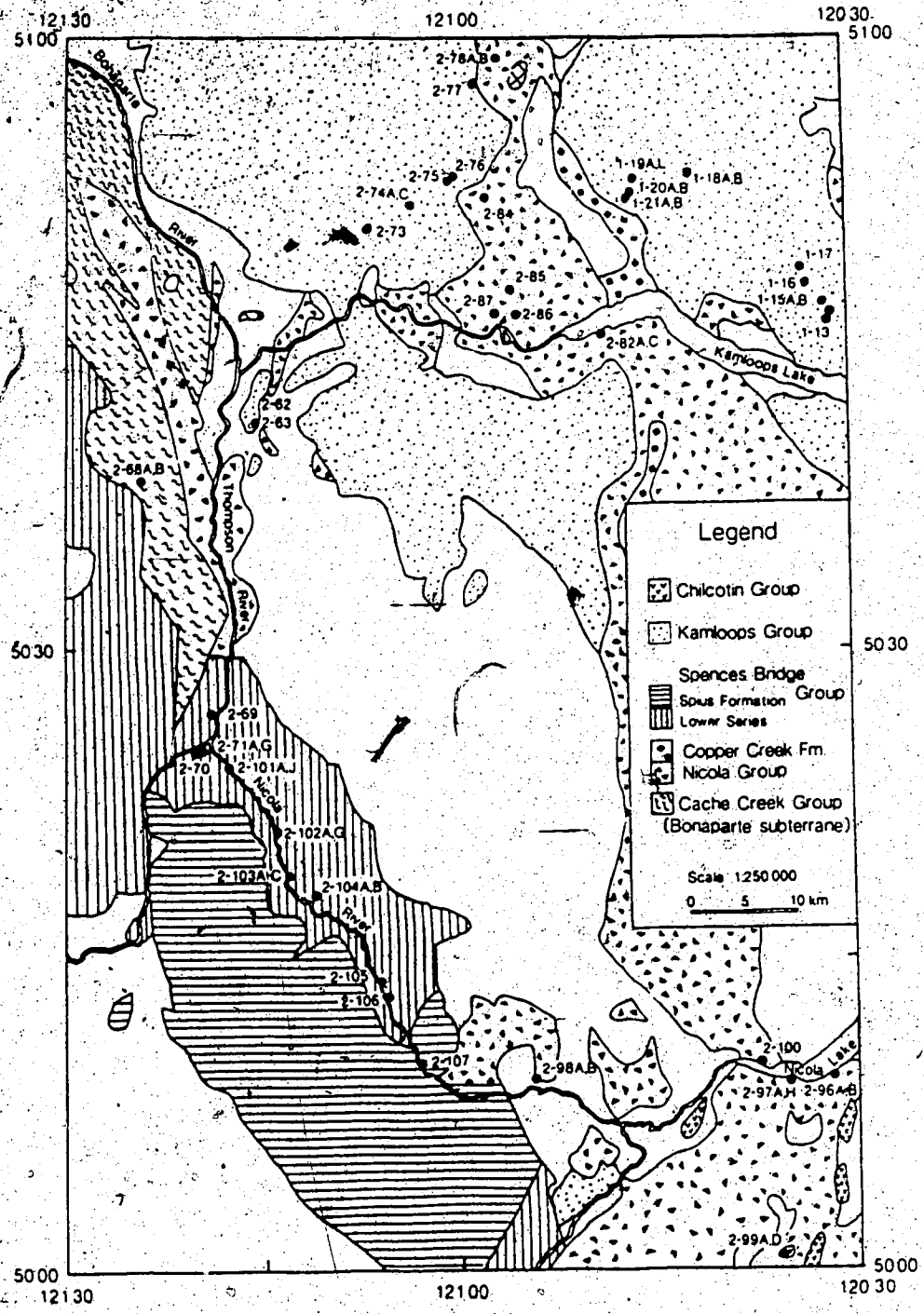

Fig. 60. Geological map showing sample localities in the Ashcroft-Nicola Lake region of south-central British Columbia (after Cockfield 1947, Duffell and McTaggart 1952, Monger 1981, Shannon 1981, Monger 1982, Monger and McMillan 1984). • Sample locality.

XIII. Appendix II: Procedures for Nd and Sr Isotopic Analysis

Chemical Procedures

A sample size of 0.3 to 0.5 g, corresponding to at least 3 ug Nd and 50 ug Sr, was suitable for most samples. Low Nd and Sr contents of the spinel lherzolites dictated the use of 3 to 10 g sample sizes. For mass spectrometry isotope dilution analyses, aliquots of mixed ^{145}Nd-^{149}Sm or ^{87}Rb-^{84}Sr spike solutions were added prior to initial decomposition.

Samples were decomposed overnight by refluxing with a 3:1 mixture of 25M HF:16M HNO_3 in screw capped teflon vessels. The samples were centrifuged to separate the Rb-bearing supernatant and Sr-, REE-containing fluoride residue.

For Rb analysis the supernatant was evaporated to dryness, treated twice with 16M HNO_3 and baked. Rb and other alkalis were leached from the residue in x2 distilled H_2O for loading onto the mass spectrometer filament.

The Sr, REE- containing residue was treated twice with 2 ml 16M HNO_3, evaporated to dryness and baked to remove HF. The nitrate residue was dissolved in 10 ml 2.3M HCl before precipitation of the hydroxides with concentrated ammonia. Care was taken at this stage not to increase the pH sufficiently as to cause the precipitation of $Mg(OH)_2$. After centrifuging, the supernatant was discarded and the hydroxide precipitate dissolved in 5 drops of 25M HF. The cloudy white suspension obtained was evaporated to incipient dryness to remove ammonia, then treated with a further 5 drops of 25M HF, 1 ml 6M HCl, and made up to 10 ml with x2 distilled H_2O before refluxing for 1hr to dissolve as much

iron as possible.

After centrifuging, the fluoride residue was treated twice with 2 ml 16M HNO_3 and the sequence through to the hydroxide precipitation stage repeated until the precipitate was small enough to dissolve in 2 ml 2.3M HCl. Incomplete dissolution at this stage was often noted, although the white gelatinous residue generally dissolved on standing for several days, or after the addition of further 2.3M HCl. The residue, although not specifically analysed, was considered to be a hydrated aluminium complex, and as such to contain little REE. Consequently, at this stage the precipitate was often discarded after centrifuging.

Ion-Exchange Procedures

A three column ion-exchange procedure was used for the purification of Sm and Nd. The coherence of Sr with the REE group through the chemical procedures allows the separation of this element at the first ion-exchange column stage. AG50W-X8, 100-200 mesh cation resin was used throughout the procedures:

Column 1

Iron, the REE and Sr were separated on a 24x0.6 cm column by elution with 2.3M HCl. Elution peaks as determined by titration with eriochrome black solution and by radiotracer experiment are shown in Fig. 6la. The difference in elution peaks between the LREE (illustrated by La, Nd and Sm), and the HREE (illustrated by Lu), is due to a change in coordination number of the lanthanide ion from 9 to 8 at atomic number 64 (Gd).

The Sr-bearing eluate usually contained some iron particularly when the sample was loaded in over 2 ml 2.3M HCl. After evaporation to dryness, this fraction was further purified on a 7x0.4 cm column equilibrated with 1M HCl. After discarding 7x1 ml 2.3M HCl, Sr was collected in 4 ml 2.3M HCl.

Column 2

After evaporation to dryness the Sm-Nd containing fraction was loaded onto a 38x0.3 cm column in 1 drop 2.3M HCl, for separation of these elements using 0.2M methyllactic acid (pH adjusted to 4.43) (Dosso and Murthy 1980). Elution peaks determined by titration with eriochrome black solution are shown in Fig. 61b. Separation of Sm and Nd is complete and Sm was never observed as a significant contaminant during Nd analysis.

Column 3

Organics from the drying of the methyllactic acid eluates were removed by successive elutions of 5x1 ml 1M HCl, followed by 7 ml 2.3M HCl on a 7x0.4 cm column equilibrated with 1M HCl. Nd or Sm were stripped from the column in 20 ml 6M HCl. Only minor amounts of organic material, mostly from the ion-exchange resin , remained at this stage, and were treated with 2x1 ml 16M HNO_3 before loading onto the mass spectrometer filament.

Total blanks for the chemical procedures are presented in Table 18. All were significantly reduced following the move to new laboratory

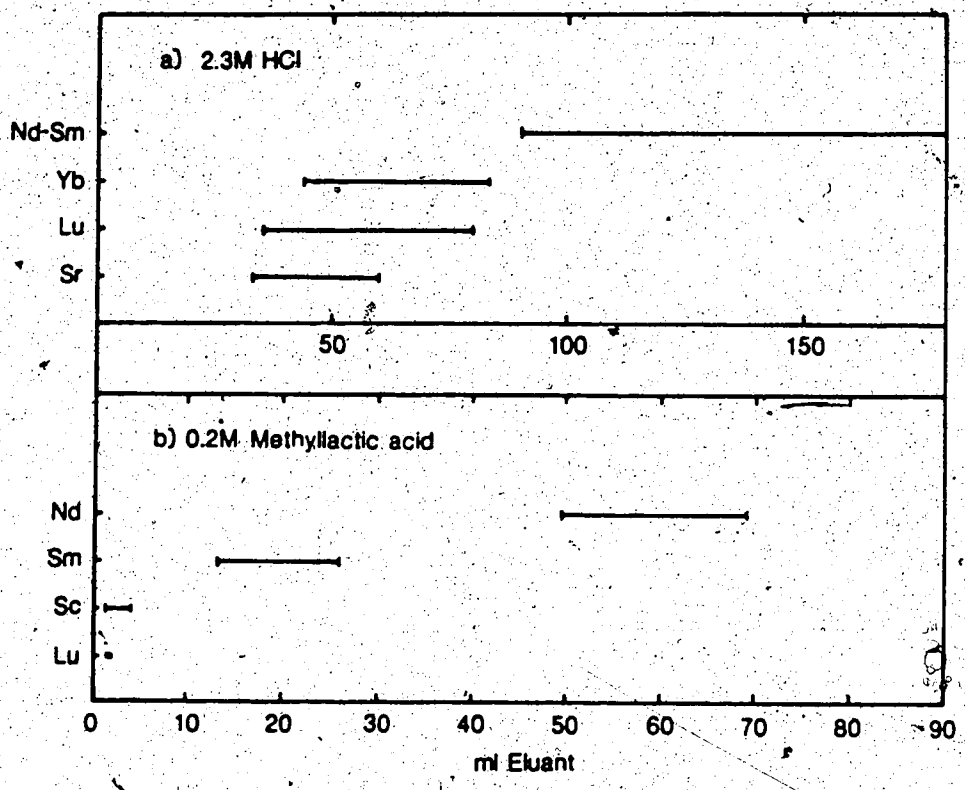

Fig. 6I. Ion exchange column elution sequences:
(a) Column 1 . 24x0.6 cm, AG1-X8, 100-200 mesh, eluant 2.3M HCl. Elution of Lu was determined using a ^{177}Lu (t1/2=6.75d) radiotracer, all others by titration with eriochrome black solution.
(b) Column 2 . 38x0.3 cm, AG1-X8, 100-200 mesh, eluant 0.2M methyllactic acid pH 4.43±0.01 . All peaks were determined by titration with eriochrome black solution. The elution with methyllactic acid at pH 4.43 produces good separation of Sm and Nd but poor separation of the HREE and other elements such as Sc.

Table 18.

Mass spectrometry blanks (in nanograms).

	Date	Rb	Sr	Sm	Nd	Sm/Nd
Blank 1	July 1984	0.38	36	0.75	3.87	0.194
Blank 2	July 1984		35	1.27	10.5	0.121
Blank 3	Sept.1984	0.15	6.6	3.51	9.56	0.367
Blank 4	Sept.1985		3.8	0.24	1.02	0.235
NaOH (per g)	Oct. 1983			14.1	70.4	0.200
MLA (per g soln)	July 1984			0.78	2.47	0.316

facilities in August 1984. A Nd-Sm blank was also performed on NaOH pellets which were considered for use in an alternative chemical procedure. Although only 0.1 to 0.3 g of NaOH would have been required, the use of this reagent would have increased the blank by at least a factor of two.

Mass Spectrometry

Nd and Sm were analysed as the metals using a triple filament (Re centre, Ta sides) in a Micromass MM30 mass spectrometer or using a double Re filament in a VG354 mass spectrometer. Samples were loaded onto the filaments in 1M HNO_3. Gentle heating of the filaments in air was found to be sufficient to remove any organics remaining from the third ion-exchange column . Analyses were performed on the MM30 with multiple measurements of background in each cycle and twice as many $^{143}Nd/^{144}Nd$ data sets as $^{146}Nd/^{144}Nd$. VG354 analyses were performed in peak switching mode with quintuple collector assembly. Sr was analysed as the chloride using a double Re filament in the MM30.

Nd isotopic ratios are reported normalised to $^{146}Nd/^{144}Nd=0.7219$, Sr analyses to $^{86}Sr/^{88}Sr=0.1194$. $^{143}Nd/^{144}Nd$ determined for the La Jolla standard was 0.511841±7 (one σ standard error) (n=21) for the MM30, and 0.511843±6 (n=4) for the VG354 . Similarly, $^{143}Nd/^{144}Nd$ measured on an in-lab standard prepared from neodymium oxide powder, was 0.511044±14 (n=14) for the MM30, 0.511057±6 (n=1) for the VG354. $^{87}Sr/^{86}Sr$ determined on the NBS SRM987 Sr standard was 0.710261±8 (n=13) over the same time period. Isotopic ratios determined for BCR1 were $^{143}Nd/^{144}Nd$ 0.512625±10 (n=4) and $^{87}Sr/^{86}Sr$ 0.70502 ±2 (n=1), also Nd, Sm concentrations 28.93, 6.637 ppm respectively, by mass spectrometry

isotope dilution.